DOC.20041012.0001

QA: QA

MDL-NBS-HS-000017 REV 01

October 2004

BECHTEL SAIC COMPANY LLC

Drift Scale THM Model

Prepared for:
U.S. Department of Energy
Office of Civilian Radioactive Waste Management
Office of Repository Development
1551 Hillshire Drive
Las Vegas, Nevada 89134-6321

Prepared by:
Bechtel SAIC Company, LLC
1180 Town Center Drive
Las Vegas, Nevada 89144

Under Contract Number
DE-AC28-01RW12101

DISCLAIMER

This report was prepared as an account of work sponsored by an agency of the United States Government. Neither the United States Government nor any agency thereof, nor any of their employees, nor any of their contractors, subcontractors or their employees, makes any warranty, express or implied, or assumes any legal liability or responsibility for the accuracy, completeness, or any third party's use or the results of such use of any information, apparatus, product, or process disclosed, or represents that its use would not infringe privately owned rights. Reference herein to any specific commercial product, process, or service by trade name, trademark, manufacturer, or otherwise, does not necessarily constitute or imply its endorsement, recommendation, or favoring by the United States Government or any agency thereof or its contractors or subcontractors. The views and opinions of authors expressed herein do not necessarily state or reflect those of the United States Government or any agency thereof.

QA: QA

Drift Scale THM Model

MDL-NBS-HS-000017 REV 01

October 2004

OCRWM	MODEL SIGNATURE PAGE/CHANGE HISTORY	Page iii
		1. Total Pages: 246

2. Type of Mathematical Model

☒ Process Model ☐ Abstraction Model ☐ System Model

Describe Intended Use of Model

The purpose of this model report is to document drift scale modeling of coupled thermal-hydrological-mechanical (THM) processes around a drift containing heat-releasing waste canisters, as well as to study the impact of THM processes on permeability and flow in this near-field rock.

3. Title

Drift Scale THM Model

4. DI (including Rev. No., if applicable):

MDL-NBS-HS-000017 REV 01

5. Total Appendices	6. No. of Pages in Each Appendix
Four (4)	A-6, B-6, C-4, D-6

	Printed Name	Signature	Date
7. Originator	J. Rutqvist	Jonny Rutqvist	10/7/04
8. Independent Technical Reviewer	R. Andrews	R. Andrews	10/7/04
9. Checker	Y. Sun	Yimeng Sun	10/7/04
10. QER	J. Gobhart	J. Gobhart	10/7/04
11. Responsible Manager/Lead	J. Birkholzer	J. Birkholzer	10/7/04
12. Responsible Manager	E. Hardin	E. Hardin	10/7/04

13. Remarks

This revision incorporates the change described in ERRATA 001 for REV00 ICN01 of this report.
Junghun Leem checked data, references and DIRS.

Change History

14. Revision No.	15. Description of Change
REV 00	Initial Issue.
REV 00/ICN01	Modifications were made to the text to address new results from the *Drift Degradation Analysis* report (BSC 2003 [DIRS 162711]) regarding poor quality rock in the lower lithophysal unit.
REV 01	Revised to address findings of the Regulatory Integration Team/Near-Field Environment Team. An additional simulation case was performed for an impact analysis of updated thermal properties, resulting in two additional output DTNs. This revision addresses the closure of condition reports CR-2063D, CR-2049B, and CR-2044B. Revisions to the document are too extensive to be shown with change bars.

CONTENTS

Page

CONTENTS (Continued)

Page

CONTENTS (Continued)

Page

INTENTIONALLY LEFT BLANK

FIGURES

Page

FIGURES (Continued)

Page

FIGURES (Continued)

Page

FIGURES (Continued)

Page

FIGURES (Continued)

Page

INTENTIONALLY LEFT BLANK

TABLES

Page

INTENTIONALLY LEFT BLANK

ACRONYMS AND ABBREVIATIONS

AFM	active fracture model
DKM	dual-permeability model
DST	Drift Scale Test
DTN	data tracking number
EBS	engineered barrier system
ECRB	enhanced characterization of the repository block
ESF	Exploratory Studies Facility
FEPs	features, events, and processes
GSI	Geological Strength Index
HM	hydrological-mechanical
MD	mean-difference
MPBX	multiple-point borehole extensometer
NAMD	normalized-absolute mean difference
QA	quality assurance
RMSD	root-mean-square-difference
SHT	Single Heater Test
TDMS	Technical Data Management System
TH	thermal-hydrological
THC	thermal-hydrological-chemical
THM	thermal-hydrological-mechanical
TM	thermal-mechanical
TSPA	total system performance assessment
TWP	technical work plan
UZ	unsaturated zone
UZ Model	unsaturated zone flow and transport model
YMP	Yucca Mountain Project
YMRP	*Yucca Mountain Review Plan, Final Report*

GEOLOGICAL ABBREVIATIONS

CHn	Calico Hills and Lower Paintbrush nonwelded thermal mechanical unit
PTn	Upper Paintbrush Tuff nowelded thermal mechanical unit
TCw	Tiva Canyon welded thermal mechanical unit
Tptpmn	Topopah Spring tuff middle nonlithophysal unit
Tptpll	Topopah Spring tuff lower lithophysal unit
Tptpul	Topopah Spring tuff upper lithophysal unit
TSw1	Topopah Spring lithophysal-rich thermal mechanical unit
TSw2	Topopah Spring lithophysal-poor thermal mechanical unit
TSw3	Topopah Spring vitrophyre thermal mechanical unit

1. PURPOSE

This model report documents the drift scale coupled thermal-hydrological-mechanical (THM) processes model development and presents simulations of the THM behavior in fractured rock close to emplacement drifts. The modeling and analyses are used to evaluate the impact of THM processes on permeability and flow in the near-field of the emplacement drifts. The results from this report are used to assess the importance of THM processes on seepage and support in the model reports *Seepage Model for PA Including Drift Collapse* and *Abstraction of Drift Seepage*, and to support arguments for exclusion of features, events, and processes (FEPs) in the analysis reports *Features, Events, and Processes in Unsaturated Zone Flow and Transport* and *Features, Events, and Processes: Disruptive Events*. The total system performance assessment (TSPA) calculations do not use any output from this report.

Specifically, the coupled THM process model is applied to simulate the impact of THM processes on hydrologic properties (permeability and capillary strength) and flow in the near-field rock around a heat-releasing emplacement drift. The heat generated by the decay of radioactive waste results in elevated rock temperatures for thousands of years after waste emplacement. Depending on the thermal load, these temperatures are high enough to cause boiling conditions in the rock, resulting in water redistribution and altered flow paths. These temperatures will also cause thermal expansion of the rock, with the potential of opening or closing fractures and thus changing fracture permeability in the near-field. Understanding the THM coupled processes is important for the performance of the repository because the thermally induced permeability changes potentially effect the magnitude and spatial distribution of percolation flux in the vicinity of the drift, and hence the seepage of water into the drift. This is important because a sufficient amount of water must be available within a drift to transport any exposed radionuclides out of the drift to the groundwater below, and eventually to people within the accessible environment. Absent sufficient water, radionuclides cannot be transported and there would be no significant health effect on people, even if radioactive waste containers were damaged or corroded to such an extent that radionuclides were exposed to water.

Inputs from other project reports to this model report include repository drift configuration, thermal line load, ventilation efficiency, infiltration rates and certain mechanical rock properties. The thermal line load of 1.45 kW/m and 50-year ventilation period used in this model report are described in the repository design drawing, *D&E/ PA/C IED Emplacement Drift Configuration and Environment* (BSC 2004 [DIRS 168489], effective date 3/26/2004). Time-dependent thermal-line-load values stem from the repository design drawing, *Repository Design, Repository/PA IED Subsurface Facilities Plan Sht. 5 of 5* (BSC 2002 [DIRS 159527], effective date 05/20/2002), and the ventilation efficiency of 86.3 percent is taken from *Ventilation Analysis and Model Report* (BSC 2002 [DIRS 160975], Table 6-6). Mean infiltration rates were taken from *Drift-Scale Coupled Processes (DST and TH Seepage) Models* (BSC 2004 [DIRS 170338], Appendix B). In addition, certain rock mechanical properties were taken from the recent *Drift Degradation Analysis* (BSC 2004 [DIRS 166107], Table E-10).

The main model outputs from this model report are the potential changes in key hydrologic properties (permeability and capillary strength). In addition, the impact of THM coupling on the flow field around the drift is assessed. The results supplement thermal seepage results from thermal-hydrological (TH) simulations reported in the model report entitled *Drift-Scale Coupled*

Processes (DST and TH Seepage) Models (BSC 2004 [DIRS 170338]), which feeds the model report *Abstraction of Drift Seepage* (BSC 2004 [DIRS 169131]), where probability distributions of ambient and thermal seepage are developed for use in the TSPA. To ensure consistency between the present model report and TH study (BSC 2004 [DIRS 170338], Section 6.2), the same conceptual model and TH properties are used.

The analyses documented in this report were initially conducted under the *Technical Work Plan for: Performance Assessment Unsaturated Zone* (BSC 2004 [DIRS 167969]). The relevant technical work plan (TWP) portions for this work are Section 1.12, "Coupled Effects on Flow & Seepage" (Work Package AUZM08), and Attachment I, "Model Validation Plans" (Section I-3-3-1). Note that this model report has a new ID, U0250. It was previously identified as N0030 within the TWP. In accordance with the TWP, the work scope of this model report includes the prediction of coupled THM effects on fracture permeability and flow field at the drift scale and validation against measurements from the ongoing Drift Scale Test (DST).

This model report has been further modified according to activities described in the more recent *Technical Work Plan for: Near-Field Environment and Transport: Near-Field Coupled Processes (TH Seepage and THM) Model Report Integration* (BSC 2004 [DIRS 170236]). The modifications include editing, partial rewriting, and reformatting to incorporate Regulatory Integration Team Phase 1 comments, performed under Work Package ARTM02. The primary tasks associated with these modifications for this model report are given in Section 1.2.2 of this TWP (BSC 2004 [DIRS 170236]). This TWP also reflects changes in the model validation strategy (BSC 2004 [DIRS 170236]) compared to the *Technical Work Plan for: Performance Assessment Unsaturated Zone* (BSC 2004 [DIRS 167969]). The details of the model validation plan and rationale for selecting the model validation for this model report can be found in Section 2.2.2 of this TWP (BSC 2004 [DIRS 170236]). The acceptance criteria identified in Section 4.2 differ from those identified in Section 3.2.2 of the TWP (BSC 2004 [DIRS 170236]), with the addition of discussion regarding model abstraction output. Also, this report supports excluded FEPS (Section 6), but no FEPs are included in the TSPA through this report. This represents a deviation from the list of FEPs in the TWP (BSC 2004 [DIRS 170236], Table 4). These deviations in the criteria and FEPs discussions reflect changes resulting from the integration of reports that refer to thermal-hydrological-mechanical processes, since the TWP was developed.

The detailed analysis of coupled THM processes and the excluded FEPs related to the effects of THM on permeability conducted in this model report is justified by a literature review on coupled processes performed by Manteufel et al. (1993 [DIRS 100776]) for the U.S. Nuclear Regulatory Commission. Manteufel et al. (1993 [DIRS 100776]) reviewed the importance of coupled processes for design and performance assessment of a geological repository. Recommendations for future work were summarized in (i) the continuing development of conceptual and mathematical models, (ii) the performance of well-documented coupled effects experiments, and (iii) the validation of models through comparison of model prediction and experimental observation. They concluded that coupled THM processes were among the coupled processes that warrant further investigations (Manteufel et al. 1993 [DIRS 100776], Executive Summary). The work presented in this model report includes the three recommended components (i, ii, iii) for further investigations on THM processes.

The coupled THM model presented in this model report builds upon insight obtained in earlier studies involving a sequential snapshot approach, in which thermal-mechanical (TM) analyses were made using the results of TH simulations to obtain thermal stresses, which, in turn, were used in an independent analysis to calculate fracture permeability changes. More specifically, in the analysis model report entitled *Calculation of Permeability Change Due to Coupled Thermal-Hydrological-Mechanical Effects* (CRWMS M&O 2000 [DIRS 149040]) and later updated in *Coupled Thermal-Hydrologic-Mechanical Effects on Permeability Analysis and Models Report* (BSC 2001 [DIRS 155957]), TM behavior in a region of fractured rock surrounding a section of a long, horizontal emplacement drift was simulated. The effects of drift excavation and of heating and cooling cycles associated with the radioactive waste packages on the directions and magnitudes of the principal stresses, were calculated using the distinct-element code 3DEC V2.0 (Itasca Consulting Group 1998 [DIRS 148865]) as documented in *Coupled Thermal-Hydrologic-Mechanical Effects on Permeability Analysis and Models Report* (BSC 2001 [DIRS 155957]). Results included rotation of the principal stress direction and separate changes in permeability values for the vertical and subvertical fractures and for horizontal fracture sets. Such changes appear to persist throughout the 1,000-year simulation period reported in that analysis model report.

The present model report involves development and application of a new coupled THM methodology, based on joining two well-established codes through carefully designed linkage routines. The first is the TOUGH2 V1.6 code (LBNL 2003 [DIRS 161491]), that calculates coupled TH processes, which in this case uses the dual-permeability continuum (fracture and matrix continua) approach. This code has proven successful in predicting the TH processes, including the temperature and moisture distribution, of field experiments at Yucca Mountain, including the Single Heater Test (SHT) (CRWMS M&O 1999 [DIRS 129261], Section 8.7) and the DST (BSC 2001 [DIRS 157330], Section 6). The second is the rock mechanics-standard FLAC3D V2.0 code (Itasca Consulting Group 1997 [DIRS 156788]), which can calculate fractured-rock mechanical processes in a continuum model. The two codes, TOUGH2 V1.6 and FLAC3D V2.0, are linked through two coupling functions, one that dictates TM coupling (TOUGH2 V1.6 to FLAC3D V2.0 coupling) and one that dictates hydrological-mechanical (HM) coupling (FLAC3D V2.0 to TOUGH2 V1.6 coupling), which provides a full THM loop.

The predictive simulations from the drift scale THM model are performed in two-dimensional vertical cross sections perpendicular to the axis of a representative waste emplacement drift. Different cross sections (model domains) are studied, depending on the location of the drifts. The Tptpmn model domain has the emplacement drift located in the Topopah Spring Tuff middle nonlithophysal unit (Tptpmn). The Tptpll model domain has the emplacement drift located in the Topopah Spring Tuff lower lithophysal unit (Tptpll). This model report considers a thermal load representative of the average thermal conditions for the current repository design, resulting in maximum rock temperatures close to emplacement drifts that are above the boiling point of water for several hundred years. A bounding analysis is conducted that brackets the potential impact of THM processes on hydrologic properties (including permeability) and the flow field. The bounding case is realized by adopting parameter values that emphasize the effect of coupling (Section 6.4.5). This includes a bounding estimate of the thermal expansion coefficient (that emphasizes thermal stress) and a bounding estimate of a stress-versus-permeability function (that emphasizes TM-induced permeability change). In addition, the results of THM analyses with maximum effect of coupling are compared to TH analyses with no effect of THM coupling.

Thus, the current analysis covers the entire sensitivity range, from minimum to maximum effect of THM coupling.

Simulation results from the drift scale THM model are given in Sections 6.5 (Tptpmn model domain), 6.6 (Tptpll model domain), and 6.7 (low quality lithophysal rock). The results include the distribution of calculated changes in hydraulic properties, in particular calculated changes in horizontal and vertical intrinsic permeability and their impact on the vertical percolation flux around the emplacement drift. In addition, Section 6.8 estimates potential changes in hydrologic properties around a degraded and collapsed drift in the Tptpll unit. The estimate of changes in hydrologic properties around a collapsed drift is based on mechanical analysis performed in the recent *Drift Degradation Analysis* (BSC 2004 [DIRS 166107], Section 6.4). Although the *Drift Degradation Analysis* (BSC 2004 [DIRS 166107], Sections 6.4.2.4 and 8.1) indicates that only partial rock fall is likely to occur for drifts located in the low quality lithophysal rocks, the extreme bounding case of a completely collapsed drift is also investigated in Section 6.8.

Measured data from the ongoing DST are used to evaluate and validate the drift scale THM model. The geometry of the DST Heated Drift is consistent with the current designs of the potential repository and can therefore, provide a test of the drift scale THM model at a relevant scale. The simulation of the DST is conducted with the drift scale THM model on a model domain constructed for the DST—the DST model domain. Validation results are provided in Section 7.

The limitations of the drift scale THM model, as for all predictive models, are defined by the conceptual model and by the uncertainties and validity ranges of input data. The following model limitations on user or application of the drift scale THM model are identified:

- The drift scale THM model is a continuum model, with average properties, and therefore is meant to represent overall changes in space and time. Hence, the analysis does not provide local changes occurring at the scale of an individual fracture, but rather their impact on the overall average changes.

- The coupled THM analysis is conducted in two-dimensional vertical sections rather than with a full three-dimensional representation. However, the two-dimensional approach has been tested by model validation against several three-dimensional field experiments (e.g. DST).

- Rather than a sensitivity study with variation of each input parameter over a wide range of values, a bounding analysis is conducted that brackets the potential impact of thermal-hydrological-mechanical processes on hydrologic properties (including permeability) and the flow field (Section 6.2.4).

- The drift scale THM analysis is conducted with homogenous properties that vary for different rock units. Therefore, the analysis provides mean changes in hydrological properties, but does not explicitly provide potential changes in spatial distribution (e.g. standard deviation) of hydrological properties.

- The existing main heater experiments used for model validation (SHT and DST) are both located in the Tptpmn repository unit. Because no heater test has been performed in the Tptpll unit, the calculated effects of THM processes (and estimated changes in permeability) are more uncertain for the Tptpll unit (Section 8.2).

In summary, the coupled THM process model provides a bounding estimate of TM-induced mean changes in hydrologic properties (permeability and capillary strength), a function of time and space at the drift scale. Such mean changes in permeability can be factored into seepage models as a correction factor for the permeability field.

INTENTIONALLY LEFT BLANK

2. QUALITY ASSURANCE

Development of this model report on drift scale THM processes and the supporting modeling activities have been determined to be subject to the Yucca Mountain Project's quality assurance (QA) program as documented in *Technical Work Plan for: Near-Field Environment and Transport: Near-Field Coupled Processes (TH Seepage and THM) Model Report Integration* (BSC 2004 [DIRS 170236], Section 8.1, Work Package ARTM02). Approved QA procedures identified in this technical work plan (TWP) (BSC 2004 [DIRS 170236], Section 4) have been used to conduct and document the activities described in this model report. Electronic management of information was evaluated in accordance with AP-SV.1Q, *Control of the Electronic Management of Information* and controlled under YMP-LBNL-QIP-SV.0, *Management of YMP-LBNL Electronic Data*, as planned in the TWP (BSC 2004 [DIRS 170236], Section 8.4).

This model report documents a drift scale model of THM processes in the unsaturated zone rocks, which are natural barriers that are classified in the *Q-List* (BSC 2004 [DIRS 168361], Table A-2), as "Safety Category" because they are important to waste isolation, as defined in AP-2.22Q, *Classification Analyses and Maintenance of the Q-List*. The report contributes to the analysis and modeling data used to support performance assessment.

INTENTIONALLY LEFT BLANK

3. USE OF SOFTWARE

A list of software codes and routines used in this model report is given in Table 3-1. The software codes and routines have been baselined in accordance with LP-SI.11Q-BSC, *Software Management*. All software used is considered appropriate for the intended use, has been applied in the range of the validation, and was obtained from Software Configuration Management.

Commercial off-the-shelf software applications, Tecplot Version 8.0 and Microsoft Excel 97 SR-2, were used for graphic visualization. In a few cases, computations were performed using these commercial off-the-shelf software programs, which are exempt from LP-SI.11Q-BSC. All information to reproduce these computations using the off-the-shelf software programs is included in this report within the specified reference (i.e., the Scientific Notebooks listed in Table 6-1).

TOUGH2 V1.6 was selected because it has been proven adequate for simulating coupled TH processes at Yucca Mountain Project, and because it is the major numerical simulator used for modeling of fluid flow and heat transport in the Yucca Mountain Project, and it is the code applied in *Drift-Scale Coupled Processes (DST and TH Seepage) Models* (BSC 2004 [DIRS 170338]) which the THM analysis provided in this model report supports. Thus, to be consistent with the hydrological and coupled TH models, the same numerical simulator (TOUGH2 V1.6) is selected for modeling of the TH part of the coupled THM analysis.

The FLAC3D V2.0 was selected because it is a widely used commercial code used in the soil-and rock mechanics community that adequately simulates mechanical processes in geological media, and has the capabilities of simulating TM and HM couplings. Furthermore, although FLAC3D V2.0 is a commercial code, with no availability to the source code for modifications, the code has built-in programming capabilities (called FISH). The FISH capabilities enable a coupled THM capability with interaction between FLAC3D V2.0 and TOUGH2 V1.6 using external qualified routines programmed in FISH. The routines Gpzones.dat V1.0, Tin V1.1 and Delb.dat V1.0 are such routines that have been developed and qualified for used with FLAC3D V2.0 and TOUGH2 V1.6 in a coupled THM analysis.

2KGRIDV1.F V1.0 and EXT V1.0 were selected for pre-processing the TOUGH2 V1.6 numerical grid and for post-processing the TOUGH2 V1.6 output data, because these software items are existing adequate software for their respective purpose.

There are no limitations on outputs to the selected software.

Table 3-1. Software Tracked by Configuration Management

Code Name	Version	STN Number	Platform	Operating System	Range of use	Brief Description
TOUGH2 [DIRS 161491]	V1.6	10007-1.6-01	PC	Windows 98 (DOS emulation)	Used for TOUGH2 TH simulations and for performing a joint execution with FLAC3D V2.0, for THM coupling simulations according to functional requirements listed in Table 1 (pp.6-8) of the *Software Validation Report (VTR) for TOUGH V1.6* (LBNL 2003 [DIRS 170764]). The software was used within an allowable range described in the *Users Manual (UM) for TOUGH V1.6* (LBNL 2002 [DIRS 170765], Attachment B).	A general purpose numerical simulator for nonisothermal, multiphase, and multicomponent fluid flow in porous and fractured geological media.
FLAC3D [DIRS 154783]	V2.0	10502-2.0-00	PC	Windows 98	Used for mechanical analysis with HM and TM couplings according to functions 1 through 5 and 8 of the functional requirements listed in the *Requirements Document (RD) for FLAC3D Version 2.0* (LBNL 2002 [DIRS 170766], Table 1). These have been validated as documented in the *Validation Test Report (VTR) for FLAC3D Version 2.0* (LBNL 2002 [DIRS 170767]). This software was used within the allowable ranges described in the *Users Manual (UM) for FLAC3D Version 2.0* (LBNL 2002 [DIRS 170769]).	A commercial numerical simulator designed for rock and soil mechanics with TM and HM interactions.
Gpzones.dat [DIRS 154792]	V1.0	10509-1.0-00	PC	Windows 98	Used within allowable limits described in the *Software Management Report (SMR) for Gpzones.dat V1.0* (LBNL 2002 [DIRS 170770]). That is, the FISH routine was used in the FLAC3D V2.0 environment and within the allowable number of element connections.	The software is developed to find out which zones are connected to each grid point and how much zone volumes are connected to each grid point to be used with routine Tin V1.1.
Tin [DIRS 162038]	V1.1	10899-1.1-00	PC	Windows 98	Used within allowable limits described in the *Software Management Report (SMR) for tin v1.1* (LBNL 2002 [DIRS 170771]). That is, the FISH routine was used in the FLAC3D V2.0 environment. No other limits applicable.	This software is developed to take temperature output from TOUGH2 and interpolate it into FLAC3D for coupled THM simulations.

Table 3-1. Software Tracked by Configuration Management (Continued)

Code Name	Version	STN Number	Platform	Operating System	Range of use	Brief Description
Delb.dat [DIRS 154791]	V1.0	10507-1.0-00	PC	Windows 98	Used within allowable limits described in the *Software Management Report (SMR) for Delb.dat v1.0*. (LBNL 2002 [DIRS 170772]). That is, the FISH routine was used in FLAC3D V2.0 environment and within the validated range of normal stress.	This software is developed to calculate changes in fracture aperture for joint TOUGH2 and FLAC3D coupled THM analyses.
2KGRIDV1.F [DIRS 147553]	V1.0	10244-1.0-00	SUN Ultra-Sparc	SunOS 5.5.1 (UNIX)	Used to convert a 3D single-continuum mesh to a DKM mesh for modeling of 3D drift scale problem with TOUGH2 as described in the *Software Baseline Request, 2KGRIDV1.F V1.0* (LBNL 2000 [DIRS 170773]).	This routine is developed to convert files for modeling of 3D drift scale problems with TOUGH2.
EXT [DIRS 147562]	V1.0	10047-1.0-00	SUN Ultra-Sparc	SunOS 5.5.1 (UNIX)	Used for post-processing of TOUGH2 output data within functional requirements described in LBNL (1998 [DIRS 170774]). Only regular rectangular mesh is used in the TOUGH2 analysis conducted in this model report.	This software is a post-processor for TOUGH2 accepting outputs from the code in one, two, or three dimensions to give an easy visualization of results graphically.

3D = three-dimensional; DKM = dual-permeability model; HM = hydrological-mechanical

INTENTIONALLY LEFT BLANK

4. INPUTS

4.1 DIRECT INPUTS

This section provides documentation for data inputs to the model report. Data inputs to the model report are referred to by Data Tracking Numbers (DTN) or references listed in Tables 4.1-1a, b, and c. Section 4.1.1 provides details about direct input references to the predictive analysis with the drift scale THM model. Table 4.1.2 and Section 4.1.2 provides indirect input references for the coupled THM analysis of the DST used as corroborative information for model validation, and Section 4.1.3 summarizes measured data from the DST and niches, which is indirect inputs used as corroborative information for model validation.

Note that this model report uses the nomenclature for lithostratigraphic units defined in *Geologic Framework Model (GFM2000)* (BSC 2004 [DIRS 170029]), while some DTNs refer to the same lithostratigraphic units using the nomenclature of the unsaturated zone (UZ) model reports. The relationship between these is given in several model reports (e.g., BSC 2004 [DIRS 169855], Table 6-5). In addition, some DTNs refer to thermal-mechanical units that are frequently used for mechanical and thermal-mechanical rock properties. The relationship among geological framework model units, UZ hydrological model units, and thermal-mechanical model units (TM units) is given in Figure 6.4-1.

4.1.1 Direct Input Data to Drift-Scale THM Model Used for Predictive Analysis

This subsection summarizes input data and provides references for input to the drift scale THM model used for predictive analysis of typical emplacement drifts located in the Tptpmn unit (Tptpmn model domain) and Tptpll unit (Tptpll model domain).

4.1.1.1 Rock Properties

The THM properties used as direct input into the drift scale THM model and their sources are summarized in this subsection. A more in-depth discussion of the appropriateness of the selected THM properties for the drift scale THM model is given in Section 6.4. Hydrological properties (such as permeability, van Genuchten parameters, residual saturation for both the fractures and the matrix, and the active fracture parameter for the fractures) used in the drift scale THM model are excerpted from the UZ drift-scale calibrated property set for the mean infiltration scenario (DTN: LB0208UZDSCPMI.002 [DIRS 161243]). The approach and method adopted in developing these properties can be found in *Calibrated Properties Model* (BSC 2004 [DIRS 169857], Section 6.3.2). Other sources used for hydrological, thermal, and mechanical properties are consistent with current UZ analyses and analyses of coupled processes. This includes other hydrological properties such as fracture porosity, frequency, aperture, and interface areas obtained from DTN: LB0205REVUZPRP.001 [DIRS 159525] and thermal properties and matrix porosity are taken from DTN: LB0210THRMLPRP.001 [DIRS 160799]. Together, these hydrological and thermal properties are referred to as the DS/AFM-UZ02-Mean property set in this model report. During preparation of this model report, new estimates of thermal properties for nonrepository units have been developed and are summarized in DTN: LB0402THRMLPRP.001 [DIRS 168481]. The differences in the thermal properties between DTN: LB0210THRMLPRP.001 [DIRS 160799] and DTN: LB0402THRMLPRP.001

[DIRS 168481] only apply to rock units located away from the repository. A detailed comparison of the thermal properties of the two sets provided in Table C-1 of *Drift-Scale Coupled Processes (DST and TH Seepage) Models* (BSC 2004 [DIRS 170338]) shows that the differences are generally within a few percent but is substantial for some of the units. The largest difference occurs in the tsw31 unit where revised bulk thermal conductivity is about 40 percent higher in the revised data. However, a sensitivity analysis documented in Appendix D of this model report shows that these differences in thermal properties do not significantly impact the results and conclusions presented in this model report, which addresses the effects in the near-field rock. Although a 40 percent increase in thermal conductivity in tsw31 may appear significant, it is not because the tsw31 layer is located more than 100 meters away from the emplacement drift where there is small effect from the repository thermal load. In addition, this layer is only a few meters thick (see Table 4.1-3c for location and thickness).

The basic mechanical properties of the rock mass (Young's Modulus and Poisson's ratio) are developed using an established engineering geological rock mass quality classification system with associated empirical relationships (Section 6.4.2). These properties are derived within this model report from qualified sources of laboratory measurements and field mapping in the Exploratory Studies Facility (ESF). The properties are derived (from the qualified input sources) in a Microsoft Excel spreadsheet: THM rock mass modulus v1.xls, which has been submitted to the Technical Data Management System (TDMS) under output DTN: LB0306DRSCLTHM.001. For a base case of mechanical properties, the Young's modulus and Poisson's ratio for TCw, PTn, TSw1, and TSw2 TM units are developed in: THM rock mass modulus v1.xls. The mechanical properties of TSw3 are assumed to be equal to TSw2 (see Assumption 3 in Section 5), and the mechanical properties of the CHn TM unit are extracted from mean of intact rock values extracted from DTN: SNL02030193001.026 [DIRS 108436], Table S99119_002 (see Assumption 4 in Section 5). For a sensitivity case of a low quality lithophysal rock—rocks with a high percentage of lithophysal porosity with relatively low bulk and shear modulus, and relatively low rock strength—the mechanical properties of the Tptpll unit is extracted from properties developed in the recent *Drift Degradation Analysis* (BSC 2004 [DIRS 166107], Table E-10, Category 1). Further justification for the adopted mechanical properties is given in Section 6.4.2.

Source DTNs and references for hydrological, thermal, and mechanical properties are given in Tables 4.1-1a and b. For quick reference, values of these properties are listed in Tables 4.1-3a and b for the Topopah Spring Tuff middle nonlithophysal (Tptpmn or tsw34) and lower lithophysal (Tptpll or tsw35) stratigraphic units, in which the main part of the repository will be located. For the sake of completeness, properties for the upper lithophysal (Tptpul or tsw33) unit are also provided. The values for the low quality lithophysal properties, which are used in the above mentioned sensitivity study, are listed in Table 4.1-3b. The tensile strength of 0.8 Mpa, given in Table 4.1-3b, was obtained from the x-intercept of Figure 7-21 in *Drift Degradation Analysis* (BSC 2004 [DIRS 166107]), to be consistent with that report.

In addition, properties for the rock mass stress-permeability relationship and rock mass thermal expansion coefficient are developed within this model report according to Sections 6.4.3 and 6.4.4. Source DTNs and references used for developing those data are given in Table 4.1-1b. The rock mass thermal expansion coefficient is derived from laboratory data in

DTN: SNL01B05059301.006 [DIRS 129168] with calculated mean values documented in Brodsky et al. (1997 [DIRS 100653], Table 4-4).

An estimate of the tortuosity parameter for vapor-air diffusion processes are derived by Jury et al. (1991 [DIRS 102010], p. 203). Because there are no direct measurements of the tortuosity parameter for the volcanic Tuff at Yucca Mountain, values from similar porous media are adopted according to Section 5, Assumption 5. Jury et al. (1991 [DIRS 102010], p. 203) presents results of diffusion tests through packed soil core samples with a recommended average value of 0.66 (≈0.7) for the tortuosity parameter. Jury et al. (1991 [DIRS 102010]), which was initially published in 1972 and the references source from 1991, is the fifth edition of the textbook. The authors of this source, W.A. Jury, W.R. Gardner, and W.H. Gardner, have published extensively on these subjects as evidenced by their appearance in the bibliography of Hillel, D. (1998 [DIRS 165404]). W.A Jury is cited seven times, W.R. Gardner is cited 18 times, and W.H. Gardner is cited three times. Therefore, the qualifications of the personnel generating the source of information are considered adequate through extensive publication over 30 years (from 1972), and thus the information from the source by Jury et al. (1991 [DIRS 102010]) is considered reliable for the intended uses. The extent to which this source of information addresses the topics noted here is considered adequate because these topics are well known, as documented here. Justification for adopting values of the tortuosity parameter derived from diffusion tests on packed soil by Jury et al. (1991 DIRS 102010], p. 203) to Yucca Mountain rock is given in Section 5, Assumption 5.

The open space of the emplacement drift is represented by an element of high permeability, high porosity, and small capillarity. The drift element is also assigned a large heat conductivity to simulate the effective radiative heat transfer within the drift. Since flow and transport processes within the drift (including the waste packages) are not explicitly modeled in this model report, these input properties of the drift elements are part of the conceptual model for the simulation analyses; they are not direct inputs to this model report.

4.1.1.2 Boundary and Initial Conditions

Boundary conditions and initial conditions before excavation of an emplacement drift are required (Figure 6.3-1). Hydraulic and thermal boundary conditions on the top and bottom boundary of the model are used to calculate vertical profiles of initial temperature, pressure, and saturation. The hydraulic and thermal boundary conditions include infiltration rate, temperature, and gas pressure at the ground surface (top of Tptpmn and Tptpll model domains), and temperature and liquid pressure at the groundwater table (bottom of Tptpmn and Tptpll model domains).

The infiltration rates applied at the top of Tptpmn and Tptpll model domains are adopted from the mean infiltration scenario that includes present day (0 to 600 years), monsoon (600 to 2,000 years), and glacial transition climates (more than 2,000 years), as described in the analysis model report, *Simulation of Net Infiltration for Modern and Potential Future Climates* (BSC 2004 [DIRS 170007], Sections 6.9 and 6.11). The specific infiltration values of 6, 16, and 25 mm/year for the present day, monsoon, and glacial transition periods, respectively, represent repository-wide averages. These values have been calculated as the arithmetic average of the 31 repository locations considered in the *Multiscale Thermohydrologic Model* (BSC 2001

[DIRS 158204], Section 6.3.1). Infiltration values at these 31 repository locations are provided in DTN: LL000114004242.090 ([DIRS 142884], file chimney_infiltration_fluxes). The calculation for deriving the repository-wide averages is given in *Drift-Scale Coupled Processes (DST and TH Seepage) Models* (BSC 2004 [DIRS 170338], Appendix B).

More recent estimates of the average infiltration rates under different climatic conditions are available at present. For example, Table 6.1-2 in *UZ Flow Models and Submodels* (BSC 2004 [DIRS 169861]) provides the mean infiltration values at the top of the UZ model domain as 4, 12, and 17 mm/yr under present-day, monsoonal, and glacial-transition climatic conditions. These numbers are obtained by averaging infiltration data in DTN: GS000308311221.005 [DIRS 147613]. Note that average percolation rates at the ptn-tsw interface have also been developed based on the average infiltration rates given in Table 6.1-2 of *UZ Flow Models and Submodels* (BSC 2004 [DIRS 169861]). These average rates are summarized in Table 6.6-11 of *Abstraction of Drift Seepage* (BSC 2004 [DIRS 169131]). It is evident that the average percolation fluxes (6, 16, and 25 mm/yr for the present-day, monsoon, and glacial-transition climatic conditions, respectively) used in this model report are larger than the most recent estimates of 4, 12, and 17 mm/yr. Moreover, the range of timing of climatic change was recently updated (BSC 2004 [DIRS 170007]). This includes a range of 400–600 years for duration of the present day climate and 900–1400 years for the duration of the monsoon climate. Thus, revised climatic changes may occur earlier than in the previous infiltration scheme adopted in this analysis. However, since the objective of this model report is to determine the impact of THM processes on permeability and flow field, the precise magnitude of the infiltration does not impact the conclusion of this study significantly. Because this analysis also aims at investigating the impact of THM processes by comparing the THM results to the TH results, it is important that the infiltration rate used in this model report is consistent with the infiltration rate used in *Drift-Scale Coupled Processes (DST and TH Seepage) Models* (BSC 2004 [DIRS 170338], Section 4.1.1.4), which this analysis supplements. The infiltration rates used are justified in *Drift-Scale Coupled Processes (DST and TH Seepage) Models* (BSC 2004 [DIRS 170338], Section 4.1.1.4) as being conservative from TSPA perspectives, because the infiltration rates used are generally higher and therefore overestimate the amount of seepage under thermal conditions. The slightly updated infiltration rates are not expected to have any significant impact on the main output of this model report, which is THM induced changes in hydrological properties. Thus, the adopted infiltration rates (6, 16, and 25 mm/yr with durations of 0–600, 600–2,000, and greater than 2,000 yr, respectively) are adequate for the purpose and intended use of this model report.

The top and bottom boundary conditions for the drift scale THM model represent the conditions at the USW SD-9 borehole, at column “I64” (E171234, N234074) of the unsaturated zone flow and transport model (UZ model) grid (for the Tptpmn model domain), and the conditions at the center of the repository, at column “j34” (E170572, N233195) of the UZ model grid (for the Tptpll model domain), respectively. The values are given in DTN: LB991131233129.004 ([DIRS 162183], filename: pa99cal_ecm.out). Elements with names “Tpi64” and “Bti64” provide pressure, saturation, and temperature conditions at the top and bottom of the Tptpmn model domain, respectively. Elements with names “Tpj34” and “Btj34” provide pressure, saturation, and temperature conditions at the top and bottom of the Tptpll model domain, respectively. Further information on developing these boundary conditions can be found in *UZ Flow Models and Submodels* (BSC 2001 [DIRS 158726], Sections 6.5.2 and 6.7.2).

The boundary conditions in the UZ model grid have since been updated, details of which can be found in *UZ Flow Models and Submodels* (BSC 2004 [DIRS 169861]). The new boundary conditions can be found in DTN: LB0303THERMSIM.001 [DIRS 165167]. In the new UZ model grid (DTN: LB03023DKMGRID.001 [DIRS 162354], filename SAVE_2_20_03_as_final_calibrated), Column 'h28' (E171210, N234050) is closest to the location of Column 'I64' in the earlier model grid (DTN: LB990501233129.004 [DIRS 111475]). Thus, the boundary conditions at the top and the bottom of the Tptpmn model domain in this report should be those of Column 'h28' as given in DTN: LB0303THERMSIM.001 [DIRS 165167]. In Table 4.1-3e, a comparison is given of the top and bottom boundary conditions (in terms of pressure, temperature, and gas saturation) in Column 'h28' of the updated UZ numerical grid (DTN: LB03023DKMGRID.001 [DIRS 162354]) and those in Column 'I64' of the older numerical grid (DTN: LB990501233129.004 [DIRS 111475]). The details on extracting these boundary conditions from the cited DTNs can be found in *Drift-Scale Coupled Processes (DST and TH Seepage) Models* (BSC 2004 [DIRS 170338], Appendix D). There are only minor differences in the boundary conditions between the revised values and the adopted values for the Tptpmn model domain (Table 4.1-3e). These differences are partly caused by the slightly different gridding with slightly different locations (elevation) of the top and bottom boundaries according to Tables 4.1-3c and d. The minor difference in pressure and temperature boundary conditions at the top and bottom is unlikely to have any impact on the coupled THM simulations presented in this report. The small difference in the boundary temperature (maximum about 2 and 5°C, respectively, at the top and bottom of the Tptpmn unit) results in a slightly different temperature field. This small difference in the temperature field will not impact the calculated THM changes significantly. Thus, it is justified to continue using boundary conditions for Column 'I64' from DTN: LB991131233129.004 [DIRS 162183] for the Tptpmn model domain.

For the Tptpll model domain, the column closest to Column 'j34' of DTN: LB990501233129.004 [DIRS 111475] is Column 'h74' (E170600, N23170) in DTN: LB03023DKMGRID.001 [DIRS 162354]. Thus, the boundary conditions at the top and the bottom of the Tptpll model domain should be those of Column 'h74' as given in DTN: LB0303THERMSIM.001 [DIRS 165167]. In Table 4.1-3e, a comparison is also given of the top and bottom boundary conditions (in terms of pressure, temperature, and gas saturation) in Column 'h74' of the updated UZ numerical grid (DTN: LB03023DKMGRID.001 [DIRS 162354]) and those in Column 'j34' of the older numerical grid (DTN: LB990501233129.004 [DIRS 111475]). The extraction of these boundary conditions from the cited DTNs can also be found in Appendix D of *Drift-Scale Coupled Processes (DST and TH Seepage) Models* (BSC 2004 [DIRS 170338]). There are only minor differences in the boundary conditions between the revised values and the adopted values for the Tptpll model domain (Table 4.1-3e). The minor differences in pressure and temperature boundary conditions at the top and bottom are unlikely to have any impact on the THM simulations presented in this report. Thus, it is all justified to continue using boundary conditions for Column 'j34' from DTN: LB991131233129.004 [DIRS 162183] for the Tptpll model domain.

The infiltration rates and TH model boundary conditions used in this model report are identical to the ones used in the drift scale TH modeling described in *Drift-Scale Coupled Processes (DST and TH Seepage) Models* (BSC 2004 [DIRS 170338], Table 4.1-6), and in the drift scale thermal-hydrological-chemical (THC) modeling described in *Drift-Scale THC Seepage Model*

(BSC 2004 [DIRS 169856], Tables 6.5-2 and 6.7-2). The specific values used in this model report are presented in Tables 4.1-3e and 6.3-1, and Figure 6.3-1. Source DTNs for hydraulic and thermal boundary conditions are given in Table 4.1-1a.

The mechanical boundary conditions are zero displacement restrictions on displacements normal to the bottom and the lateral (vertical side of the model) boundaries and the top of the model (ground surface) is free to move. Thus, there are no data sources needed for mechanical boundary conditions. The mechanical boundary conditions are justified in Section 6.3.

Initial stress (before excavation) for all the model domains of the drift scale THM model is estimated according to Assumption 2, Section 5, using sources of saturated density given in Table 4.1-1b.

4.1.1.3 Thermal Load

The thermal output of individual waste packages placed into drifts is represented by an average thermal line load, which is 1.45 kW/m according to current designs. A 50-year ventilation period is considered, in which a significant fraction of the heat is removed from the repository. The thermal line load of 1.45 kW/m and 50-year ventilation period are described in repository-design drawing, *D&E/ PA/C IED Emplacement Drift Configuration and Environment* (BSC 2004 [DIRS 168489], effective date 3/26/2004). Note that the value of 1.45 kW/m refers to the initial thermal line load at emplacement time. This value decreases with time as a result of radioactive decay. The time-dependent thermal-line-load values used in this report stems from the repository design drawing, *Repository Design, Repository/PA IED Subsurface Facilities Plan Sht. 5 of 5* (BSC 2002 [DIRS 159527], effective date 05/20/2002). More recent time-dependent thermal-line-load values are available in the repository design drawing *D&E/PA/C IED Typical Waste Package Components Assembly* (BSC 2004 [DIRS 167369], effective date 01/30/2004). The time-dependent thermal-line-load values are virtually identical in the two sources, and hence no impact is expected on the TH simulations in this model report.

Ventilation efficiency denotes the fraction of heat removed from the repository as a result of ventilation during the 50-year preclosure period. The ventilation efficiency is time-dependent and average values of the integrated ventilation efficiency are used for simplification. The integrated ventilation efficiency provided by current Yucca Mountain Project (YMP) reports is 88 percent (DTN: MO0306MWDASLCV.001 2003 [DIRS 165695]) when the emplacement drift is 600 m in length. When the emplacement drift is 800-m long, integrated ventilation efficiency is calculated to be 86 percent (DTN: MO0307MWDAC8MV.000 2003 [DIRS 165395]). Further details on the calculation of these ventilation efficiencies are provided in *Ventilation Analysis and Model Report* (BSC 2004 [DIRS 169862], Equation 6-6). Uncertainties in calculated integrated ventilation efficiencies have also been addressed (BSC 2004 [DIRS 169862], Section 8.2.1). For both 600 m and 800 m long drifts, the standard deviation of the calculated ventilation efficiency is 3 percent (BSC 2004 [DIRS 169862], Table 8-2). Thus, the ventilation efficiency can be in the range 85 to 91 percent for a 600 m long drift. For 800 m long drifts, the range of ventilation efficiency is 83 to 89 percent.

The ventilation efficiency value used in this model report is 86.3 percent. The 86.3 percent value was reported in an earlier version of *Ventilation Analysis and Model Report* (BSC 2002

[DIRS 160975], Table 6-6), which has subsequently been revised to address repository design changes and to replace calculations that utilized unqualified software. The ventilation efficiency of 86.3 percent, which was the best estimate available at the time that the majority of the analysis in this report was conducted, is qualified for use in this report by corroboration with the more recent, qualified data presented above (the data qualification plan is included in Appendix H of BSC 2004 [DIRS 170338]). This adopted ventilation efficiency value (= 86.3 percent) is almost in the middle of the suggested range of ventilation efficiency values as defined by the range of standard deviations (see the paragraph immediately above), and actually is very close to the mean ventilation efficiency for 800-m long emplacement drifts. The choice of ventilation efficiency value is also consistent with the choice of ventilation efficiency in other UZ coupled-processes model reports including the *Drift-Scale Coupled Processes (DST and TH Seepage) Models* report (BSC 2004 [DIRS 170338], Sections 4.1.1.3 and, 6.2.1.3.3), which this model report supplements.

All source DTNs and references for thermal load are given in Table 4.1-1a.

4.1.1.4 Grid Design Data

The data needed for grid design are the stratigraphy at the respective locations of the Tptpmn and Tptpll model domain, and the data related to the configuration of emplacement drifts.

The geologic data for the Tptpmn and Tptpll model domains were derived from the UZ model grid in DTN: LB990501233129.004 [DIRS 111475]. The stratigraphy in a one-dimensional column close to Borehole USW SD-9 is chosen as representative for the vertical profile of geologic contacts into the Tptpmn model domain. Geologic data for this location are best represented by column "I64" in DTN: LB990501233129.004 [DIRS 111475] at approximately Nevada State Plane coordinates E171234, N233194. The elevations of the contacts between various geological layers as implemented in the Tptpmn model domain are shown in Table 4.1-3c. The stratigraphy of the Tptpll model domain is extracted at a location near the center of the potential repository (at approximately Nevada State Plane coordinates E170572, N233194). Geologic data from column "j34" of the UZ model grid (DTN: LB990501233129.004 [DIRS 111475]) are used to map geologic contacts into the two-dimensional mesh. The elevations of the contacts between various geological layers as implemented in the Tptpll model domain are shown in Table 4.1-3d.

DTN: LB990501233129.004 [DIRS 111475] represents the UZ model grid that was current at the time that the thermal seepage modeling was performed; however, a more recent numerical grid for the UZ is now available (DTN: LB03023DKMGRID.001 [DIRS 162354]). For the Tptpmn model domain, the one-dimensional column closest to Borehole USW SD-9 in the new UZ numerical grid (DTN: LB03023DKMGRID.001 [DIRS 162354]) is Column 'h28.' The elevations of the various geological layers in Column 'h28' are shown (and compared with) those in Column 'I64' (from DTN: LB990501233129.004 [DIRS 111475]). A comparison of the adopted (Column 'I64' from DTN: LB990501233129.004 [DIRS 111475]) and revised (Column 'h28' from DTN: LB03023DKMGRID.001 [DIRS 162354]) is also shown in Table 4.1-3c. The thicknesses of the respective layers in these two columns ('I64' and 'h28') are very close except for layers far away from the heat sources. For example, the thicknesses of layers 'tsw33,' 'tsw34,' 'tsw35,' and 'tsw36' in Column 'I64' (the adopted thickness values in

the TH seepage model) are 85.3, 35.3, 102.5, and 35.7 m, respectively (see Table 4.1-3c, third column). The revised thicknesses for these same layers, in the same order, are 85.6, 34.8, 102.5, and 35.5 m. Thus, the differences between adopted and revised thicknesses for the geological units in which the impact of heating is expected to be maximum are about or less than one percent. Thus, implementing geological data in the Tptpmn model domain from an older DTN (LB990501233129.004 [DIRS 111475]) in this model report is justified because the difference in thicknesses of the repository units ('tsw33,' 'tsw34,' 'tsw35,' and 'tsw36') is less than one percent, no additional sensitivity analyses are required. The procedures followed to calculate the elevations and thicknesses can be found in *Drift-Scale Coupled Processes (DST and TH Seepage) Models* (BSC 2004 [DIRS 170338], Appendix E).

For the Tptpll model domain, as has been noted earlier, geological data were adopted from Column 'j34' in DTN: LB990501233129.004 [DIRS 111475]. The elevations at the top of each geological layer in Column 'j34' are given in Table 4.1-3d. Table 4.1-3d also gives the thickness of each geological layer in Column 'j34' (see the third column in Table 4.1-3d). These thickness values have been adopted for the Tptpll model domain. The column closest to the location of Column 'j34' in the revised UZ numerical grid (DTN: LB03023DKMGRID.001 [DIRS 162354]) is Column 'h74.' The elevations and thicknesses of each geological layer in Column 'h74' in LB03023DKMGRID.001 [DIRS 162354] are also shown in Table 4.1-3d (see the fourth and fifth columns). The procedures followed to obtain the numbers in Table 4.1-3d can be found in *Drift-Scale Coupled Processes (DST and TH Seepage) Models* (BSC 2004 [DIRS 170338], Appendix E). Again, though not as close as those for the Tptpmn model domain, the top elevations and thicknesses of the geological layers in Column 'h74' (revised) are comparable with those of Column 'j34' (adopted), particularly, for the geological layers closest to the sources of heat. For example, for the 'tsw33,' 'tsw34,' 'tsw35,' and 'tsw36' layers, the (adopted) thicknesses in Column 'j34' are 80.1, 37.2, 101.4, and 33.2 m, respectively. The respective (revised) values in Column 'h74' are 80.3, 34.5, 102.5, and 32.7 m. In the Tptpll model domain, the waste emplacement drift (and the source of heat) is located in the 'tsw35' geological layer. For this layer, the difference between adopted and revised thicknesses is only 1.1 m (or about one percent). The thickness of the 'tsw34' layer differs by about 2.7 m (or less than eight percent). However, the 'tsw34' layer is situated about 50 meters away from the source of heat in the Tptpll model domain (The emplacement drift is located at an elevation of 1082.8 m (see Section 6.3) and therefore according to Table 4.1-3d, tsw34 is located at a distance of 49.2 m from the center of the emplacement drift.). Thus, the difference in thickness in the tsw34 layer between the adopted and revised values is unlikely to have any impact on THM simulations in the Tptpll model domain. The differences in thickness between adopted and revised values for the units far away (both top and bottom) from the source of heat in the Tptpll model domain are similarly not expected to have any significant impact on the thermal seepage simulations. It is thus justified to use geological data from the older DTN (LB990501233129.004 [DIRS 111475]). Also, no sensitivity analysis is considered necessary for this adaptation. Furthermore, the adopted layering is consistent with the TH seepage model applied in *Drift-Scale Coupled Processes (DST and TH Seepage) Models* (BSC 2004 [DIRS 170338], Section 6.2), which this analysis supplements. The current drift configuration, as given in repository design drawing, *D&E/ PA/C IED Emplacement Drift Configuration and Environment* (BSC 2004 [DIRS 168489], effective date 3/26/2004), calls for a drift diameter of 5.5 m and a drift spacing of 81 m. There is no backfill in the drifts. The in-drift geometry for waste package and drip-shield configuration is not explicitly accounted for in the drift scale

THM, and the heat transfer between the waste package and the drift wall is simulated with an effective radiative heat exchange within the open drift. The radiative heat exchange within the drift is rapid, so that the temperature difference within the drift should effectively equilibrate. Since the focus of this model report is the quantification of THM processes in the rock outside the drift, the details of the heat transfer within the drift is of secondary importance. This simulation approach (of effective radiative heat exchange within the open drift) is applied, and hence tested, in the modeling of the DST in Section 7. It is shown in Section 7.4.1, that temperature evolution in the rock is accurately simulated and agrees very well with measured values, and hence the adopted approach is sufficiently accurate for the purpose of this model report. Source DTNs and references for grid design data are given in Table 4.1-1a.

4.1.1.5 Input Data for Estimation of Changes in Hydrological Properties Around a Collapsed Drift in the Tptpll Unit

Drift Degradation Analysis (BSC 2004 [DIRS 166107], Appendix R) provides predictions of drift profiles and mechanical responses in the rock mass in the vicinity of degraded drifts in lithophysal units. In this model report, results of drift profiles, stress and volumetric strain were used as input for estimation of changes in hydrological properties around a collapsed drift in the Tptpll unit. The drift-profiles, stress and volumetric strain are extracted from DTN: MO0306MWDDPPDR.000 [DIRS 164736], Scenarios 7, 2 and 1, from file names *_profile.eps, *_stress.dat and *_volstrain.dat, respectively. The DTNs for these inputs are given in Table 4.1-1c.

4.1.2 Indirect Input Data to DST Model Domain Used for Model Validation

This subsection summarizes indirect input data and references for the drift scale THM model applied to the DST model domain and used as corroborative information for model validation against measurements at the DST. The values in Table 4.1-4 are properties used in the DST model domain. The validation method between the drift scale THM model simulation results and measured values in the DST includes (Section 7):

1. Checking that the simulated temperature field is in reasonable agreement with the observed temperature field to ensure that the THM model is properly implemented in terms of thermal behavior.

2. Checking that simulated rock mass displacements capture the general trends and average magnitudes of observed displacements (validation of TM processes).

3. Checking that the simulated changes in air permeability capture the general trends and magnitudes observed in the field (validation of THM processes).

TM and HM properties of the rock mass developed in this analysis are used in the validation (i.e., initial hydraulic aperture, parameters for the stress-aperture function, and thermal expansion coefficient). Sections 4.1.2.4 through 4.1.3.4 describe observed measurements associated with DST. The DST measurements shown in Table 4.1-5 include data acquired for validation of the THM model. Source DTNs and references for all inputs related to the model validation are given in Table 4.1-2.

4.1.2.1 Rock Properties

The DST model domain is designed for comparative model analysis with the measured data from the DST, utilizing a TH property set partially based on a site-specific characterization of the DST test block. This data set, referred to as DKM-TT99, is described in the previous *Thermal Tests Thermal-Hydrological Analyses/Model Report* (BSC 2001 [DIRS 157330], Section 4.1, Table 5). The DKM-TT99 property set is selected because it is more representative of the rock at the DST than the alternative DS/AFM-UZ02-Mean property set. DKM-TT99 is considered more representative since it captures TH responses at the DST better than the alternative (BSC 2004 [DIRS 170338], Section 7.3.1). A comparison of simulation results against measurements at the DST using these two property sets shows only minor differences, and both property sets produced results that were within the acceptable limit around measured data (BSC 2004 [DIRS 170338], Section 7.5). However, as will be discussed in Sections 6.4.4 and 6.10.4, the DKM-TT99 property set with a fracture permeability of 1e-13 m^2 is the appropriate property set to be used for calibration and validation of the stress-versus-permeability relationship developed in Section 6.4.4 of this model report. The local permeability at the DST is slightly lower (by a factor of 3.3) than for the permeability of the Tptpmn unit as a whole defined in the DS/AFM-UZ02-Mean property set. This is a small difference in fracture permeability (compared to the general variability of fracture permeability) but is relevant for the calibration and validation of the stress-versus-permeability relationship. As will be pointed out in Sections 6.4.4 and 6.10.4, the calibration and validation of the stress-versus-permeability relationship should be conducted at the appropriate local permeability value. The fracture frequency, noted as N/A in the *Thermal Tests Thermal-Hydrological Analyses/Model Report* (BSC 2001 [DIRS 157330], Section 4.1, Table 5 for the DKM-TT99), is extracted from the current estimates given in DTN: LB0205REVUZPRP.001 [DIRS 159525]. Mechanical properties, Young's modulus and Poisson's ratio for TSw1 and TSw2 TM units, are identical to those in the predictive drift scale THM analysis (Section 4.1.1.1). These properties were derived in the Microsoft Excel spreadsheet entitled: THM rock mass modulus v1.xls (submitted to TDMS under DTN: LB0306DRSCLTHM.001) based on intact rock properties and field mapping in the ESF. TH properties of the DKM-TT99 property set and mechanical properties are summarized in Table 4.1-4 for the three geological units comprising the DST model domain, namely the Tptpul, the Tptpmn, and the Tptpll. Fracture frequency and other hydrological properties are obtained from other sources given in Table 4.1-4, but are consistent with mean input values used in the UZ and other coupled process models, including predictive analyses.

4.1.2.2 Boundary and Initial Conditions

Boundary conditions and initial conditions at the start of heating are required (Figure 7.3-1). The top and bottom thermal and hydrological boundary conditions are identical to the ones used in the *Thermal Tests Thermal-Hydrological Analyses/Model Report* (BSC 2001 [DIRS 157330], Section 6.1.2). The boundary condition values are given in DTN: LB000300123142.001 ([DIRS 148120], filename: Incon.heat in directory /LBNL_DST_AMR_DKMTT99). Elements with names "Tt001" and "tt001" provide pressure, saturation, and temperature conditions at the top, while elements with names "Bb001" and "bb001" provide pressure, saturation, and temperature conditions at the bottom of the model domain (for both fracture and matrix continua) (Table 4.1-2). These boundary values were developed from simulations of a one-dimensional column extending from the land surface to the water table, mapped to the location of the top and

bottom of the model domain. Stress initial and boundary conditions are estimated according to Assumption 2, Section 5.

4.1.2.3 Thermal Load

In the DST, heat is provided by nine canister heaters located on the floor of the Heated Drift. Additional heating is provided by 50 wing heaters (Section 7.2.1). The total output power from both the canister and the wing heaters has been continuously collected. Average values of this total power over certain time periods have been used in the DST model domain (see Section 7.3 for more details.). Table 4.1-2 provides source reference for the average total canister and wing heater power at various times.

4.1.2.4 Borehole and Sensor Location Data

Passive monitoring of THM data (such as temperature, pressure, and displacement) from the DST is carried out with measurement sensors located in a number of boreholes (Figure 7.2.1-2). Active monitoring of data (such as periodic air-injection tests) is carried out in boreholes specifically designed for such purposes. Results from the model simulation are compared directly against these measured data from the DST. Though the boreholes and sensors have not been explicitly modeled in the DST model domain, the three-dimensional numerical grid has been developed in such a way that simulated THM data can be easily interpolated to specific sensor location. The DTN containing these design parameters of the DST is listed in Table 4.1-2.

4.1.3 Measurements at the DST and Niches

The data presented in this subsection are considered as corroborative information (indirect input) since it is used for model validation purposes. In Section 7, the drift scale THM model is validated by comparison to measured data at DST and niches. The input information on measurement data used for validation is explained below and summarized in Table 4.1-5.

4.1.3.1 Temperature Measurements at DST

Temperature data, similar to heater power in Section 4.1.2.3, have been continuously collected from the DST. For model validation, these measured temperatures are directly compared against simulated temperatures. The DTN for the measured temperature data is given in Table 4.1-5.

4.1.3.2 Air-Permeability Measurements at DST

Periodic air-permeability-measurement testing has been carried out at the DST. The air permeability at the DST also includes a pretest baseline test to capture the ambient condition in the fractures. Subsequent air-permeability measurements during heating and cooling at the DST are used to determine fractional changes in air permeability. These measured air-permeability ratios are compared against simulated air-permeability ratios. The DTN for measured air-permeability ratios is given in Table 4.1-5.

4.1.3.3 Displacement Measurements at DST

Displacement data have been continuously collected from multiple-point borehole extensometers (MPBX) at the DST. For model validation, these measured displacements are directly compared against simulated displacements from the model simulation. The DTN for the measured displacement data is given in Table 4.1-5.

4.1.3.4 Air-Permeability Measurements at Niches

Air-permeability measurements were conducted at several excavated niches to study permeability changes near a drift wall caused by excavation effects (i.e., mechanical unloading of the rock mass near the drift wall, causing fracture opening and consequently permeability increase). These types of tests were conducted at three excavated niches located in the Tptpmn unit and one excavated niche located in the Tptpll unit (BSC 2004 [DIRS 170004], Section 6.1). For model validation, the measured changes in permeability induced by the excavation of the niches (air-permeability ratio) are compared to model simulations. The DTN for measured air-permeability ratios is given in Table 4.1-5.

Table 4.1-1a. Data Tracking Numbers for Sources of Data Input to the Drift Scale THM Model Used for Predictive Analysis

DTN/Reference	Description	TDMS Input	Design Input	Other Analyses
Rock Properties (Section 4.1.1.1)				
LB0205REVUZPRP.001 [DIRS 159525]	Fracture porosity, frequency, and surface area (Table 4.1-3a)	X		
LB0208UZDSCPMI.002 [DIRS 161243]	Fracture and matrix calibrated parameters—mean infiltration (Table 4.1-3a)	X		
LB0210THRMLPRP.001 [DIRS 160799][1]	Matrix thermal data and porosity	X		
BSC 2004 [DIRS 166107], Table E-10, Category 1, and Figure 7-21	Rock mass mechanical properties for low quality lithophysal rock in Tptpll (Table 4.1-3b, Section 6.7)			X
Boundary Conditions (Section 4.1.1.2)				
BSC 2004 [DIRS 170338], Appendix B	Infiltration rates for present day, monsoon, and glacial periods (Table 6.3-1 and Figure 6.3-1). The median infiltration case is used in this report for both Tptpmn and Tptpll model domains.			X
LB991131233129.004 [DIRS 162183] File "pa99cal_ecm.out" : Elements Tpi64 and Bti64 for top and bottom of Tptpmn model domain Elements Tpj34 and Btj34 for top and bottom of Tptpll model domain	Top and bottom boundary temperatures, pressure, liquid/gas saturations (Table 6.3-1 and Figure 6.3-1). At borehole USW SD-9 for Tptpmn model domain (Nevada State Plane coord. E171234, N234074). At center of the repository for Tptpll model domain (Nevada State Plane coord. E170572, N233195).	X		

Table 4.1-1a. Data Tracking Numbers for Sources of Data Input to the Drift Scale THM Model Used for Predictive Analysis (Continued)

DTN/Reference	Description	TDMS Input	Design Input	Other Analyses
Thermal Load (Section 4.1.1.3)				
DWG-MGR-MD-000003 (BSC 2002 [DIRS 159527])	Thermal decay (Figure 6.5.2-1)		X	
800-IED-MGR0-00201-000-00B BSC 2004 [DIRS 168489]	Heat load (1.45 kW/m)		X	
BSC 2002 [DIRS 160975], Table 6-6	Ventilation efficiency (86.3%)			X
Grid Design Data (Section 4.1.1.4)				
LB990501233129.004 [DIRS 111475] File primary.mesh Column I64 for Tptpmn domain Column j34 for Tptpll domain	Stratigraphy taken from UZ model grid At borehole USW SD-9 for Tptpmn model domain (Nevada State Plane coord. E171234, N234074) At center of the repository for Tptpll model domain (Nevada State Plane coord. E170572, N233195)	X		
800-IED-MGR0-00201-000-00B BSC 2004 [DIRS 168489]	Drift geometry (diameter and spacing)		X	

[1] Note thermal properties of non-repository units have been updated in DTN: LB0402THRMLPRP.001 [DIRS 168481]. There is no significant impact of these changes on the results of This model report (Appendix D).

Table 4.1-1b. Data Tracking Numbers for Sources for Data Developed or Estimated in this Model Report Used as Input to the Drift Scale THM Model for Predictive Analysis

DTN/Reference	Description	TDMS Input	Design Input	Other Analyses
Rock Properties (Section 4.1.1.1)				
SNL02030193001.001 [DIRS 120572] SNL02030193001.002 [DIRS 120575] SNL02030193001.003 [DIRS 120578] SNL02030193001.004 [DIRS 108415] SNL02030193001.005 [DIRS 122545] SNL02030193001.006 [DIRS 120579] SNL02030193001.007 [DIRS 120582] SNL02030193001.008 [DIRS 120597] SNL02030193001.012 [DIRS 108416] SNL02030193001.013 [DIRS 120614] SNL02030193001.014 [DIRS 109609] SNL02030193001.015 [DIRS 120617] SNL02030193001.016 [DIRS 120619] SNL02030193001.018 [DIRS 109611] SNL02030193001.019 [DIRS 108431]				

Table 4.1-1b. Data Tracking Numbers for Sources for Data Developed or Estimated in this Model Report Used as Input to the Drift Scale THM Model for Predictive Analysis (Continued)

DTN/Reference	Description	TDMS Input	Design Input	Other Analyses
Rock Properties (Section 4.1.1.1) (Continued)				
SNL02030193001.020 [DIRS 108432] SNL02030193001.021 [DIRS 108433] SNL02030193001.022 [DIRS 109613] SNL02030193001.023 [DIRS 108435] SNL02030193001.024 [DIRS 122530] SNL02030193001.026 [DIRS 108436]	Intact rock properties from laboratory tests for development of rock mass mechanical properties (Young's modulus and Poisson's ratio in Table 4.1-3a) using Excel spreadsheet entitled *THM rock mass modulus v1.xls* (Section 6.4.2; Section 5, Assumptions 3 and 4).	X		
GS950508314224.003 [DIRS 107488] GS960908314224.020 [DIRS 106059] GS000608314224.006 [DIRS 152572] GS960908314224.015 [DIRS 108372] GS960908314224.016 [DIRS 108373] GS960908314224.017 [DIRS 108376] GS970108314224.002 [DIRS 107490] GS970208314224.004 [DIRS 107492] GS970808314224.009 [DIRS 107494] GS970808314224.011 [DIRS 107495] GS970808314224.013 [DIRS 107497]	Field mapping of rock quality parameters along ESF for development of rock mass mechanical properties (Young's modulus and Poisson's ratio in Table 4.1-3a) using Excel spreadsheet entitled *THM rock mass modulus v1.xls* (Section 6.4.2; Section 5, Assumptions 3 and 4). Note that this table only lists ESF data since only ESF data was used to derive the adopted rock mass properties. *THM rock mass modulus V1.xls* lists sources from both ESF and ECRB Cross Drift used for comparison.	X		
LB970600123142.001 [DIRS 105589] LB980120123142.004 [DIRS 105590] LB980120123142.005 [DIRS 114134], with calculated mean value documented in BSC (2004 [DIRS 170038]), Figure 6-2.	Fracture permeability of Tptpmn unit around the DST for development of a rock mass stress-permeability relationship (Section 6.4.4, Figure 6.4.4-2, Appendix A).	X		
LB0205REVUZPRP.001 [DIRS 159525]	Fracture frequency of the Tptpmn unit for development of a rock mass stress-permeability relationship (Section 6.4.4, Appendix A).	X		
LB0208AIRKDSTH.001 [DIRS 160897]	Permeability change factor at the DST used for development of a rock mass stress-permeability relationship (Section 6.4.4, Figure 6.4.4-2, Appendix A).	X		
LB0310AIRK0015.001 [DIRS 168564], BSC (2004 [DIRS 170004], Figures 6.1.2-12 to 6.1.2-16).	Pre to post excavation permeability ratio at Niche Tests used for development of a rock mass stress-permeability relationship (Section 6.4.4, Figure 6.4.4-2, Appendix A).	X		
SNL01B05059301.006 [DIRS 129168], with calculation of mean values documented in Brodsky et al. (1997 [DIRS 100653], Table 4-4).	Laboratory thermal expansion coefficient for development of a temperature dependent thermal expansion coefficient (Section 6.4.3, Figure 6.4.3-1).	X		

Table 4.1-1b. Data Tracking Numbers for Sources for Data Developed or Estimated in this Model Report Used as Input to the Drift Scale THM Model for Predictive Analysis (Continued)

DTN/Reference	Description	TDMS Input	Design Input	Other Analyses
Rock Properties (Section 4.1.1.1) (Continued)				
Jury et al. (1991 [DIRS 102010], p. 203).	Tortuosity factor for diffusion in a porous media applied to rock matrix and rock fractures (Section 5, Assumption 5).			X
Initial Stress Field (Section 4.1.1.2)				
SNL02030193001.027 [DIRS 108410]	Laboratory values of saturated bulk rock density for derivation of an average overburden bulk density at the repository horizon (using Excel spreadsheet entitled *THM saturated density v1.xls*) applied in Section 5, Assumption 2 for estimation of initial stress field.	X		

ESF = Exploratory Studies Facility

ECRB = enhanced characterization of the repository block

Table 4.1-1c. Data Tracking Numbers for Sources of Drift Profiles and Degraded Rock Mass Characteristics in Lithophysal Units Used for Predictive Analysis of Changes in Hydrologic Properties around a Collapsed Drift in the Tptpll Unit

DTN	Description
MO0306MWDDPPDR.000 [DIRS 164736] files *_profile.eps for Scenarios 7, 2, 1.	Drift Profiles after excavation and seismic loading (Section 6.8).
MO0306MWDDPPDR.000 [DIRS 164736] files *_stress.dat for Scenarios 7, 2, 1.	Calculated rock stress after excavation and seismic loading (Section 6.8).
MO0306MWDDPPDR.000 [DIRS 164736] files *_volstrain.dat for Scenarios 7, 2, 1.	Calculated rock volumetric strain after excavation and seismic loading (Section 6.8).

Table 4.1-2. Data Tracking Numbers for Sources of Data Input to the Drift Scale THM Model Used for Corroborative Information in Model Validation

DTN/Reference	Description	TDMS Input	Design Input	Other Analyses
Rock Properties (Section 4.1.2.1)				
ANL-NBS-TH-000001 REV 00 ICN 02 (BSC 2001 [DIRS 157330], Section 4.1, Table 5).	Matrix and fracture thermal and hydrological properties for simulations with the DKM-TT99 property set (Table 4.1-4).			X
LB0205REVUZPRP.001 [DIRS 159525].	Fracture frequency (Table 4.1-4).	X		
See list of 21 DTNs given under the same item in Table 4.1-1b (Starting with SNL02030193001.001 [DIRS 120572] and ending with SNL02030193001.026 [DIRS 108436]).	Intact rock properties from laboratory tests for development of rock mass mechanical properties (Young's modulus and Poisson's ratio in Table 4.1-4) using Excel spreadsheet entitled *THM rock mass modulus v1.xls* (See Sections 6.4.2 and 7.4).	X		

Table 4.1-2. Data Tracking Numbers for Sources of Data Input to the Drift Scale THM Model Used for Corroborative Information in Model Validation (Continued)

DTN/Reference	Description	TDMS Input	Design Input	Other Analyses
See list of 11 DTNs given under the same item in Table 4.1-1b (Starting with GS950508314224.003 [DIRS 107488] and ending with GS970808314224.013 [DIRS 107497].	Field mapping of rock quality parameters along ESF for development of rock mass mechanical properties (Young's modulus and Poisson's ratio in Table 4.1-4) using Excel spreadsheet entitled *THM rock mass modulus v1.xls* (See Sections 6.4.2 and 7.4).	X		
Boundary Conditions (Section 4.1.2.2)				
LB000300123142.001 [DIRS 148120] File "Incon.heat" in directory /LBNL_DST_AMR_DKMTT99) Elements Tt001 and tt001 for top Elements Bb001 and bb001 for bottom	Top and bottom boundary temperature, pressure, and saturation (Figure 7.3-1).	X		
Thermal Load (Section 4.1.2.3)				
BSC 2004 [DIRS 170338], Table 7.3.4-1	DST average heating phase power (Table 7.3-1)			X
DST Borehole and Sensor Locations (Section 4.1.2.4)				
MO0002ABBLSLDS.000 [DIRS 147304]	Coordinates of borehole collar and bottom; coordinates of sensor locations (Figures 7.4.1-1, 7.4.2-1, and 7.4.3-1).	X		

DKM = dual-permeability model

Table 4.1-3a. Summary of Rock Properties of Geologic Units Tptpul, Tptpmn, and Tptpll in the Drift Scale THM Model Applied to the Tptpll and Tptpmn Model Domains for Predictive Analysis

Geologic Framework Model Unit >		Tptpul	Tptpmn	Tptpll	Source
Matrix Thermal and Hydrological Properties					
Hydrogeological Unit > (Label for matrix properties)>		**Tsw33 (TswM3)**	**Tsw34 (TswM4)**	**Tsw35 (TswM5)**	
Permeability	k_m (m^2)	6.57E-18	1.77E-19	4.48E-18	LB0208UZDSCPMI.002 [DIRS 161243]
Porosity	f_m (-)	0.1425	0.1287	0.1486	LB0210THRMLPRP.001 [DIRS 160799]
Van Genuchten α	α_m (1/Pa)	6.17E-6	8.45E-6	1.08E-5	LB0208UZDSCPMI.002 [DIRS 161243]
Van Genuchten m (or λ)	m_m (-)	0.283	0.317	0.216	LB0208UZDSCPMI.002 [DIRS 161243]
Residual saturation	S_{lrm} (-)	0.12	0.19	0.12	LB0208UZDSCPMI.002 [DIRS 161243]
Rock grain density	ρ (kg/m3)	2358	2466	2325	LB0210THRMLPRP.001 [DIRS 160799]
Specific heat Capacity	C_p (J/kg K)	985	985	985	LB0210THRMLPRP.001 [DIRS 160799]
Bulk Dry thermal conductivity	λ_{dry} (W/m K)	1.164	1.419	1.278	LB0210THRMLPRP.001 [DIRS 160799]
Bulk Wet thermal conductivity	λ_{wet} (W/m K)	1.675	2.074	1.890	LB0210THRMLPRP.001 [DIRS 160799]

Table 4.1-3a. Summary of Rock Properties of Geologic Units Tptpul, Tptpmn, and Tptpll in the Drift Scale THM Model Applied to the Tptpll and Tptpmn Model Domains for Predictive Analysis (Continued)

Geologic Framework Model Unit >		Tptpul	Tptpmn	Tptpll	Source
Fracture Hydrological Properties					
Hydrogeological Unit > (Label for fracture properties)>		**TSw33 (TswF3)**	**TSw34 (TswF4)**	**TSw35 (TswF5)**	
Permeability	k_f (m^2)	7.80E-13	3.30E-13	9.10E-13	LB0205REVUZPRP.001 [DIRS 159525]
Porosity	f_f (-)	5.8E-3	8.5E-3	9.6E-3	LB0208UZDSCPMI.002 [DIRS 161243]
Van Genuchten α	α_f (1/Pa)	1.59E-3	1.04E-4	1.02E-4	LB0208UZDSCPMI.002 [DIRS 161243]
Van Genuchten m (or λ)	m_f (-)	0.633	0.633	0.633	LB0208UZDSCPMI.002 [DIRS 161243]
Residual saturation	S_{lrf} (-)	0.01	0.01	0.01	LB0208UZDSCPMI.002 [DIRS 161243]
Fracture frequency	f (m^{-1})	0.81	4.32	3.16	LB0205REVUZPRP.001 [DIRS 159525]
Fracture surface area	A_f (m^2/m^3)	4.44	13.54	9.68	LB0205REVUZPRP.001 [DIRS 159525]
Active fracture coefficient	γ (-)	0.600	0.569	0.569	LB0208UZDSCPMI.002 [DIRS 161243]
Rock Mass Mechanical Properties					
Thermal Mechanical Unit >		**TSw1**	**TSw2**	**TSw2**	
Young's Modulus	E (GPa)	19.40[1]	14.77[1]	14.77[1]	These properties were derived in Excel spreadsheet entitled *THM rock mass modulus v1.xls* from the qualified sources listed in Table 4.1-1b under items about intact rock properties and field mapping.
Poisson's Ratio	ν (-)	0.23[1]	0.21[1]	0.21[1]	

[1] The listed values can be found in the Microsoft Excel spreadsheet entitled *THM rock mass modulus v1.xls* in output DTN: LB0306DRSCLTHM.001.

Table 4.1-3b. Low Quality Lithophysal Rock Properties Applied to the Tptpll Model Domain as a Sensitivity Case of Predictive Analysis

Property		Value	Source
Young's Modulus	E (GPa)	1.9	BSC 2004 [DIRS 166107], Table E-10, Category 1
Bulk Modulus	K (GPa)	1.07	BSC 2004 [DIRS 166107], Table E-10, Category 1
Shear Modulus	G (GPa)	0.8	BSC 2004 [DIRS 166107], Table E-10, Category 1
Cohesion for $\phi = 40°$	C (MPa)	2.33	BSC 2004 [DIRS 166107], Table E-10, Category 1
Tensile Strength	T (MPa)	0.8	BSC 2004 [DIRS 166107], Figure 7-21

Table 4.1-3c. Comparison of Adopted and Revised Values of Elevation and Thickness of Stratigraphic Layers for the Tptpmn Model Domain

Model Layer	Adopted Elevation for Top of Layer, Column 'i64' in LB990501233129.004 (m)	Adopted Thickness, Column 'i64' in LB990501233129.004 (m)	Revised Elevation for Top of Layer, Column 'h28' in LB03023DKMGRID.001 (m)	Revised Thickness, Column 'h28' in LB03023DKMGRID.001 (m)
Top	1,302.5	—	1,308.8	—
tcw12	1,302.5	17.1	1,308.8	21.3
tcw13	1,285.4	5.8	1,287.5	6.0
ptn21	1,279.6	4.6	1,281.5	4.4
ptn22	1,275.0	5.9	1,277.1	6.3
ptn23	1,269.1	4.6	1,270.8	3.0
ptn24	1,264.5	9.0	1,267.8	9.5
ptn25	1,255.5	21.7	1,258.3	21.0
ptn26	1,233.8	12.8	1,237.3	12.8
tsw31	1,221.0	2.0	1,224.5	0.1
tsw32	1,219.0	53.3	1,222.4	52.8
tsw33	1,165.7	85.3	1,169.6	85.6
tsw34	1,080.4	35.3	1,084.0	34.8
tsw35	1,045.1	102.5	1,049.2	102.5
tsw36	942.6	35.7	946.7	35.5
tsw37	906.9	17.8	911.2	26.2
tsw38	889.1	20.7	884.9	29.2
ch2z	868.4	138.4	855.7	123.7
Bottom	730.0	—	732.0	—

DTN: LB990501233129.004 [DIRS 111475], LB03023DKMGRID.001 [DIRS 162354].

NOTE: In the actual numerical grid for the Tptpmn model domain, tcw12 was not modeled and the top of the grid was fixed at 1286.0 m. Also, the stratigraphy was simplified under the ch2z layer. These simplifications, as they occur far away from the source of heat, are not expected to impact the TH results of the Tptpmn model domain in the vicinity of the emplacement drifts.

Table 4.1-3d. Comparison of Adopted and Revised Values of Elevation and Thickness of Stratigraphic Layers for the Tptpll Model Domain

Model Layer	Adopted Elevation for Top of Layer, Column 'j34' in LB990501233129.004 (m)	Adopted Thickness, Column 'j34' in LB990501233129.004 (m)	Revised Elevation for Top of Layer, Column 'h74' in LB03023DKMGRID.001 (m)	Revised Thickness, Column 'h74' in LB03023DKMGRID.001 (m)
Top	1,446.6	—	1,424.4	—
tcw11	1,446.6	27.4	1,424.4	3.6
tcw12	1,419.2	77.1	1,420.8	96.7
tcw13	1,342.1	15.6	1,324.1	5.3
ptn21	1,326.5	3.4	1,318.8	2.3
ptn22	1,323.1	2.1	1,316.5	5.1
ptn23	1,321.0	2.8	—	—
ptn24	1,318.2	5.5	1,311.4	4.3

Table 4.1-3d. Comparison of Adopted and Revised Values of Elevation and Thickness of Stratigraphic Layers for the Tptpll Model Domain (Continued)

Model Layer	Adopted Elevation for Top of Layer, Column 'j34' in LB990501233129.004 (m)	Adopted Thickness, Column 'j34' in LB990501233129.004 (m)	Revised Elevation for Top of Layer, Column 'h74' in LB03023DKMGRID.001 (m)	Revised Thickness, Column 'h74' in LB03023DKMGRID.001 (m)
ptn25	1,312.7	9.1	1,307.1	7.9
ptn26	1,303.6	9.5	1,299.2	13.6
tsw31	1,294.1	14.4	1,285.6	2.0
tsw32	1,279.7	30.4	1,283.6	39.1
tsw33	1,249.3	80.1	1,244.5	80.3
tsw34	1169.2	37.2	1164.2	34.5
tsw35	1132.0	101.4	1129.7	102.5
tsw36	1030.6	33.2	1026.2	32.7
tsw37	997.4	16.6	993.5	23.1
tsw38	980.8	13.8	970.4	9.2
tsw39	967.0	10.1	961.2	4.1
ch1v	956.9	21.7	957.1	14.4
ch2v	945.2	13.3	942.7	12.9
ch3v	931.9	12.7	929.8	12.8
ch4z	919.2	12.8	917.0	10.3
ch5z	906.4	14.0	906.7	20.3
ch6	892.4	13.9	886.4	7.8
pp4	878.5	12.6	878.6	13.3
pp3	865.9	32.7	865.3	50.3
pp2	833.2	15.0	—	—
pp1	818.2	61.5	815.0	64.1
bf3	756.7	33.7	—	—
Bottom	730.0	—	751.9	—

DTNs: LB990501233129.004 [DIRS 111475], LB03023DKMGRID.001 [DIRS 162354].

NOTE: The elevations in the second column above have been calculated by taking an average of the elevations at nodes of respective elements in the vertical column 'j34.' Note also that in Column 'h74' of DTN: LB03023DKMGRID.001 [DIRS 162354], there is no ptn23 geologic layer. Also, geologic layers pp2 and bf3 are absent in this column. The water table is located at 751.9 m at this column.

Table 4.1-3e. Top and Bottom Boundary Conditions for the Tptpmn and Tptpll Model Domains

Boundary	Boundary Condition Used in this Model Report	Revised Boundary Conditions
Top, Tptpmn Model Domain	T = 17.68°C S_g = 0.99 P = 86339 Pa	T =15.73°C S_g = 0.99 P = 84512 Pa
Bottom, Tptpmn Model Domain	T = 31.68°C S_L = 0.99999 P = 92000 Pa	T = 26.45°C S_L = 0.9999 P = 90842 Pa

Table 4.1-3e. Top and Bottom Boundary Conditions for the Tptpmn and Tptpll Model Domains (Continued)

Boundary	Boundary Condition Used in this Model Report	Revised Boundary Conditions
Top, Tptpll Model Domain	T = 16.13°C S_g = 0.99 P = 84725 Pa	T =17.33°C S_g = 0.99 P = 86304 Pa
Bottom, Tptpll Model Domain	T = 32.62°C S_L = 0.99999 P = 92000 Pa	T = 29.28°C S_L = 0.9999 P = 91998 Pa

NOTES: Extraction of values in this table from DTN LB991131233129.004 [DIRS 162183] and DTN: LB0303THERMSIM.001 [DIRS 165167] is described in detail in BSC 2004 [DIRS 170338], Appendix D.

The boundary conditions used in this report are taken from DTN: LB991131233129.004 [DIRS 162183] (Temperature and pressure for Tpj34 corresponding to the top of the Tptpll Model Domain are given as 16.08°C and 84765 Pa, respectively, in DTN: LB991131233129.004 [DIRS 162183]).

Revised boundary conditions are presented in DTN: LB0303THERMSIM.001 [DIRS 165167].

Table 4.1-4. Summary of Rock Properties of Geologic Units Tptpul, Tptpmn and Tptpll in the Drift Scale THM Model Applied to the DST Model Domain Used for Model Validation

Geologic Framework Model Unit >		Tptpul	Tptpmn	Tptpll	Source
Matrix Thermal and Hydrological Properties					
Hydrogeological Unit > (Label for matrix properties)>		**TSw33 (TswM3)**	**TSw34 (TswM4)**	**TSw35 (TswM5)**	
Permeability	k_m (m^2)	5.25E-18	1.24E-17	2.47E-16	ANL-NBS-TH-000001 REV 00 ICN 02 (BSC 2001 [DIRS 157330], Table 5)
Porosity	f_m (-)	0.154	0.11	0.13	ANL-NBS-TH-000001 REV 00 ICN 02 (BSC 2001 [DIRS 157330], Table 5)
van Genuchten α	α_m (1/Pa)	1.06E-5	2.25E-6	2.82E-6	ANL-NBS-TH-000001 REV 00 ICN 02 (BSC 2001 [DIRS 157330], Table 5)
van Genuchten m^2 (or λ)	M_m (-)	0.243^2	0.247^2	0.207^2	ANL-NBS-TH-000001 REV 00 ICN 02 (BSC 2001 [DIRS 157330], Table 5)
Residual saturation	S_{lrm} (-)	0.06	0.18	0.13	ANL-NBS-TH-000001 REV 00 ICN 02 (BSC 2001 [DIRS 157330], Table 5)
Rock grain density	ρ (kg/m^3)	2510	2530	2540	ANL-NBS-TH-000001 REV 00 ICN 02 (BSC 2001 [DIRS 157330], Table 5)
Specific heat capacity	C_p (J/kg•K)	917	953	953	ANL-NBS-TH-000001 REV 00 ICN 02 (BSC 2001 [DIRS 157330], Table 5)
Dry thermal conductivity	λ_{dry} (W/m•K)	1.15	1.67	1.59	ANL-NBS-TH-000001 REV 00 ICN 02 (BSC 2001 [DIRS 157330], Table 5)
Wet thermal conductivity	λ_{wet} (W/m•K)	1.7	2.0	2.29	ANL-NBS-TH-000001 REV 00 ICN 02 (BSC 2001 [DIRS 157330], Table 5)

Table 4.1-4. Summary of Rock Properties of Geologic Units Tptpul, Tptpmn and Tptpll in the Drift Scale THM Model Applied to the DST Model Domain Used for Model Validation (Continued)

Geologic Framework Model Unit >		Tptpul	Tptpmn	Tptpll	Source
Fracture Hydraulic Properties					
Hydrogeological Unit > (Label for fracture properties)>		**TSw33 (TswF3)**	**TSw34 (TswF4)**	**TSw35 (TswF5)**	
Permeability	k_f (m^2)	6.353E-13	1.00E-13	1.87E-12	ANL-NBS-TH-000001 REV 00 ICN 02 (BSC 2001 [DIRS 157330], Table 5)
Porosity	f_f (-)	0.171E-3	0.263E-3	0.392E-3	ANL-NBS-TH-000001 REV 00 ICN 02 (BSC 2001 [DIRS 157330], Table 5)
van Genuchten α	α_f (1/Pa)	1.57E-4	9.73E-5	1.66E-5	ANL-NBS-TH-000001 REV 00 ICN 02 (BSC 2001 [DIRS 157330], Table 5)
van Genuchten m^2 (or λ)	m_f (-)	0.492[2]	0.492[2]	0.492[2]	ANL-NBS-TH-000001 REV 00 ICN 02 (BSC 2001 [DIRS 157330], Table 5)
Residual saturation	S_{lrf} (-)	0.01	0.01	0.01	ANL-NBS-TH-000001 REV 00 ICN 02 (BSC 2001 [DIRS 157330], Table 5)
Fracture frequency	f (m^{-1})	0.81	4.32	3.16	LB0205REVUZPRP.001 [DIRS 159525]
Rock Mass Mechanical Properties					
Thermal Mechanical Unit >		**TSw1**	**TSw2**	**TSw2**	
Young's Modulus	E (GPa)	19.40[3]	14.77[3]	14.77[3]	These properties were derived in Excel spreadsheet entitled *THM rock mass modulus v1.xls* from the qualified sources listed in Table 4.1-1b under items about intact rock properties and field mapping.
Poisson's Ratio	ν (-)	0.23[3]	0.21[3]	0.21[3]	

[1] Section 4.1.2.1 explains the differences between these TH properties and those in Table 4.1-3a.
[2] Denoted β_m and β_f in ANL-NBS-TH-000001 REV 00 ICN 02 (BSC 2001 [DIRS 157330], Table 5).
[3] The listed values can be found in Excel spreadsheet entitled *THM rock mass modulus v1.xls* in output DTN: LB0306DRSCLTHM.001.

Table 4.1-5. Data Tracking Numbers for Sources of Measured Data at DST and Niches Used for Model Validation

DTNs	Description
Temperature Measurements at DST (Section 4.1.3.1)	
MO0208RESTRDST.002 [DIRS 161129]	Restructured Drift Scale Test (DST) heating phase temperature measurements
Air-Permeability Measurements at DST (Section 4.1.3.2)	
LB0208AIRKDSTH.001 [DIRS 160897]	Measured air-permeability data during heating at the DST
MPBX Displacement Measurements at DST (Section 4.1.3.3)	
SN0207F3912298.037 [DIRS 162046]	Smoothed measurements of displacement during heating at the DST
Air-Permeability Measurements at Niches (Section 4.1.3.4)	
LB0310AIRK0015.001 [DIRS 168564]	Measured air-permeability change ratio during excavation of Niche 3107, Niche 3650, Niche 4788, and Niche CD 1620

4.2 CRITERIA

Technical requirements to be satisfied by performance assessment (PA) are based on 10 CFR 63.114 [DIRS 156605] and identified in the *Project Requirements Document* (Canori and Leitner 2003 [DIRS 166275]). The acceptance criteria that will be used by the U.S. Nuclear Regulatory Commission (NRC) to determine whether the technical requirements have been met are identified in the *Yucca Mountain Review Plan, Final Report* (YMRP) (NRC 2003 [DIRS 163274]). Pertinent requirements and acceptance criteria for this model report are summarized in Table 4.2-1.

Table 4.2-1. Project Requirements and YMRP Acceptance Criteria Applicable to This Model Report

Requirement Number[a]	Requirement Title[a]	10 CFR 63 Link	YMRP Acceptance Criteria
PRD-002/T-015	Requirements for Performance Assessment	10 CFR 63.114(a-c) [DIRS 156605]	Criteria 1 to 5 for Quantity and Chemistry of Water Contacting Engineered Barriers and Waste Forms [b].

[a] Canori and Leitner 2003 [DIRS 166275], Table 5-4.
[b] NRC 2003 [DIRS 163274], Section 2.2.1.3.3.3.

The acceptance criteria for *Quantity and Chemistry of Water Contacting Engineered Barriers* are:

Acceptance Criterion 1, **System Description and Model Integration Are Adequate:**

AC1(1) Total system performance assessment adequately incorporates important design features, physical phenomena, and couplings, and uses consistent and appropriate assumptions throughout the quantity and chemistry of water contacting engineered barriers and waste forms abstraction process.

AC1(2) The abstraction of the quantity and chemistry of water contacting engineered barriers and waste forms uses assumptions, technical bases, data, and models, that are appropriate and consistent with other related U.S. Department of Energy abstractions. For example, the assumptions used for the quantity and chemistry of water contacting engineered barriers and waste forms are consistent with the abstractions of "Degradation of Engineered Barriers" (Section 2.2.1.3.1); "Mechanical Disruption of Engineered Barriers (Section 2.2.1.3.2); "Radionuclide Release Rates and Solubility Limits" (Section 2.2.1.3.4); "Climate and Infiltration" (Section 2.2.1.3.5); and "Flow Paths in the Unsaturated Zone" (Section 2.2.1.3.6). The descriptions and technical bases provide transparent and traceable support for the abstraction of quantity and chemistry of water contacting engineered barriers and waste forms.

AC1(3) Important design features, such as waste package design and material selection, backfill, drip shield, ground support, thermal loading strategy, and degradation processes, are adequate to determine the initial and boundary conditions for calculations of the quantity and chemistry of water contacting engineered barriers and waste forms.

AC1(4) Spatial and temporal abstractions appropriately address physical couplings (thermal-hydrologic-mechanical-chemical). For example, the U.S. Department of Energy evaluates the potential for focusing of water flow into drifts, caused by coupled thermal-hydrologic-mechanical-chemical processes.

AC1(8) Adequate technical bases are provided, including activities such as independent modeling, laboratory or field data, or sensitivity studies, for inclusion of any thermal-hydrologic-mechanical-chemical couplings and features, events, and processes.

AC1(12) Guidance in NUREG–1297 and NUREG–1298 (Altman, et al., 1988 [DIRS 103597], [DIRS 103750]), or other acceptable approaches, is followed.

Acceptance Criterion 2, Data Are Sufficient for Model Justification:

AC2(2) Sufficient data were collected on the characteristics of the natural system and engineered materials to establish initial and boundary conditions for conceptual models of thermal-hydrologic-mechanical-chemical coupled processes, that affect seepage and flow and the engineered barrier chemical environment.

AC2(3) Thermo-hydrologic tests were designed and conducted with the explicit objectives of observing thermal-hydrologic processes for the temperature ranges expected for repository conditions and making measurements for mathematical models. Data are sufficient to verify that thermal-hydrologic conceptual models address important thermal-hydrologic phenomena.

AC2(4) Sufficient information to formulate the conceptual approach(es) for analyzing water contact with the drip shield, engineered barriers, and waste forms is provided.

Acceptance Criterion 3, **Data Uncertainty Is Characterized and Propagated Through the Model Abstraction:**

AC3(1) Models use parameter values, assumed ranges, probability distributions, and bounding assumptions that are technically defensible, reasonably account for uncertainties and variabilities, and do not result in an under-representation of the risk estimate;

AC3(4) Adequate representation of uncertainties in the characteristics of the natural system and engineered materials is provided in parameter development for conceptual models, process-level models, and alternative conceptual models. The U.S. Department of Energy may constrain these uncertainties using sensitivity analyses or conservative limits. For example, the U.S. Department of Energy demonstrates how parameters used to describe flow through the engineered barrier system bound the effects of backfill and excavation-induced changes;

Acceptance Criterion 4, Model Uncertainty Is Characterized and Propagated Through the Model Abstraction:

AC4(1) Alternative modeling approaches of features, events, and processes are considered and are consistent with available data and current scientific understanding, and the results and limitations are appropriately considered in the abstraction.

AC4(2) Alternative modeling approaches are considered and the selected modeling approach is consistent with available data and current scientific understanding. A description that includes a discussion of alternative modeling approaches not considered in the final analysis and the limitations and uncertainties of the chosen model is provided.

AC4(3) Consideration of conceptual model uncertainty is consistent with available site characterization data, laboratory experiments, field measurements, natural analog information and process-level modeling studies; and the treatment of conceptual model uncertainty does not result in an under-representation of the risk estimate.

AC4(5) If the U.S. Department of Energy uses an equivalent continuum model for the total system performance assessment abstraction, the models produce conservative estimates of the effects of coupled thermal-hydrologic-mechanical-chemical processes on calculated compliance with the postclosure public health and environmental standards.

Acceptance Criterion 5, Model Abstraction Output is Supported by Objective Comparison:

AC5(2) Abstracted models for coupled thermal-hydrologic-mechanical-chemical effects on seepage and flow and the engineered barrier chemical environment, as well as on the chemical environment for radionuclide release, are based on the same assumptions and approximations demonstrated to be appropriate for process-level models or closely analogous natural or experimental systems. For example, abstractions of processes, such as thermally induced changes in hydrological properties, or estimated diversion of percolation away from the drifts, are adequately justified by comparison to results of process-level modeling, that are consistent with direct observations and field studies.

AC5(3) Accepted and well-documented procedures are used to construct and test the numerical models that simulate coupled thermal-hydrologic-mechanical-chemical effects on seepage and flow, engineered barrier chemical environment, and the chemical environment for radionuclide release. Analytical and numerical models are appropriately supported. Abstracted model results are compared with different mathematical models, to judge robustness of results.

How these criteria are met is documented in Section 8.4.

4.3 CODES, STANDARDS, AND REGULATIONS

No specific formally established standards have been identified as applying to this modeling activity.

5. ASSUMPTIONS

This section contains the basic assumptions of the drift scale THM model used in this model report. Each statement of an assumption is followed by the rationale for why the assumption is considered valid or reasonable.

1. The stratigraphy layers represented in the Tptpmn and Tptpll model domains in Section 6.3 follow an earlier revision of the geologic framework model (DTN: MO9901MWDGFM31.000 [DIRS 103769]), corresponding to an earlier revision of the geologic framework model as described in *Geologic Framework Model (GFM3.1)* (CRWMS M&O 2000 [DIRS 138860]). The modifications presented in the most current revision, as described in the *Geologic Framework Model (GFM2000)* (BSC 2004 [DIRS 170029]), have not been implemented in order to use layering consistent with the TH seepage model applied in *Drift-Scale Coupled Processes (DST and TH Seepage) Models* (BSC 2004 [DIRS 170338], Section 6.2), which this analysis supplements.

   Basis:
   The stratigraphy modifications in the current revision of the geologic framework model are small for the repository units. It is noted in *Geologic Framework Model (GFM 2000)* (BSC 2004 [DIRS 170029], Section 6.1) that the changes between the earlier and the new revisions of the geologic framework model relating to the elevations in geologic layers are relatively small in magnitude, rarely as large as 25 feet (7.6 m), and are primarily near the edges of the GFM boundary. Detailed comparisons of the geological layering between the two versions of the geologic framework model for the two model domains (Tptpmn and Tptpll model domains) are provided in Tables 4.1-3c and d. The tables show that changes in thickness and contact elevations in the repository are minor, much smaller than the extent of the host rock units considered in Section 6. Since this study is focused on THM in the repository unit around an emplacement drift, the results of this model report are not affected by these changes. This assumption is considered adequate and requires no further confirmation.

2. The initial vertical stress field is assumed to be $\sigma_v = -\rho g z_d = -2.2 \cdot 10^3 \times 9.81 \times z_d = -21{,}582 \times z_d$ Pa, where z_d is depth in meter. Horizontal stresses are assumed to be $\sigma_H = 0.6 \times \sigma_v$ (max compressive horizontal stress) and $\sigma_h = 0.5 \times \sigma_v$ (min compressive horizontal stress), with the maximum compressive stress oriented perpendicular to the drifts. This assumption is consistently used for all simulation cases in the model report, including the Tptpmn and Tptpll model domains (Section 6.3), and for the simulation of the DST (Section 7.3). It is also used in Appendix A and Section 6.4.4 for development of a rock mass stress-permeability relationship.

   Basis:
   The assumed magnitude of the initial stress field represents the best estimate of the stress field at the repository horizon. Vertical stress is estimated based on the weight of the overburden rock with an average density of $2.2 \cdot 10^3$ kg/m^3. The average density of $2.2 \cdot 10^3$ kg/m^3 was calculated for the overburden rock at the repository horizon using

a Microsoft Excel spreadsheet entitled *THM saturated density v1.xls* (submitted to TDMS under DTN: LB0306DRSCLTHM.001). The horizontal stresses represent the best estimate at the repository horizon (CRWMS M&O 1997 [DIRS 103564], Table 3-2, pp. 3–23). The orientation of the maximum principal stress was estimated at N32°E in CRWMS M&O (1997 [DIRS 103564], Table 3-2, pp. 3-23) not exactly perpendicular to the axes of the emplacement drifts, but rather at an angle of about 45°. However, because the initial horizontal stress field is almost isotropic (a factor of 0.5 and 0.6 of the vertical stress field) the exact orientation of the initial horizontal stress field has no significant impact. This estimate of the initial stress is considered sufficiently accurate because this model report concerns itself with thermally induced stresses, which are largely independent of the initial stress field. This assumption is considered adequate and requires no further confirmation.

3. The TSw3 TM unit is assigned rock mass mechanical properties (Young's modulus and Poisson's ratio) that are equal to that of the TSw2 TM unit. This assumption is needed for complete definition of mechanical material properties in the Tptpmn and Tptpll subdomains (Section 6.4.2). The relation between TM and lithostratigraphic units is given in Figure 6.4-1. Although qualified mechanical properties for intact rock from this lithostratigraphic unit exist, such property data do not account for the effect of fracturing and should, in general, not be used directly for representing in situ rock mass properties.

   Basis:
   Rock mass properties of the TSw3 TM unit cannot be derived solely from intact rock properties and field mapping of rock quality in the ESF because the ESF does not penetrate the TSw3 TM unit. Although qualified mechanical properties for intact rock from this lithostratigraphic unit exist, such property data do not account for the effect of fracturing and should, in general, not be used directly for representing in situ rock mass properties. Assigning the TSw3 TM unit mechanical properties equivalent to the TSw2 TM unit is considered to be a good estimate for the following reasons: (1) the Young's modulus measured on intact rock samples from TSw3 and TSw2 TM units is similar—mean values of intact rock Young's modulus are 37.43 GPa for the TSw3 TM unit (mean of three values in DTN: SNL02030193001.023 [DIRS 108435]) and 33.03 GPa for the TSw2 TM unit (Microsoft Excel file *THM rock mass modulus v1.xls* DTN: LB0306DRSCLTHM.001); and (2) the mean fracture spacing of the two TM units is similar (about 4 fractures per meter according to DTN: LB0205REVUZPRP.001 [DIRS 159525]). This estimate is considered sufficiently accurate, considering that the TSw3 TM unit is located below and away from the repository units. For the THM analysis conducted in this model report, concerns are focused on THM processes primarily in the repository units and secondarily on units located above the repository. This assumption is considered adequate and requires no further confirmation.

4. The rock mass mechanical properties (Young's modulus and Poisson's ratio) of the CHn TM unit are assumed to be equivalent to the intact-rock mechanical properties (Young's modulus and Poisson's ratio). This assumption is needed for complete definition of mechanical material properties in the Tptpmn and Tptpll subdomains

(Section 6.4.2). The relation between TM and lithostratigraphic units is given in Figure 6.4-1.

Basis:
Rock mass properties of the CHn TM unit cannot be derived solely from intact rock properties and field mapping in the ESF because the ESF does not penetrate the CHn TM unit. Although qualified mechanical properties for intact rock from this lithostratigraphic unit exist, such property data do not account for the effect of fracturing and should, in general, not be used directly for representing in situ rock mass properties. Assuming the rock properties of the CHn TM unit to be equal to its intact rock properties is justified in this particular case, because: (a) for the CHn TM unit, the measured values of Young's modulus of intact rock samples are very low—three values of Young's modulus and Poisson's ratio for CHn (Table S99119_002, DTN: SNL02030193001.026 [DIRS 108436]) yield mean values of 5.63 GPa and 0.17, respectively. The low Young's modulus indicates that the rock mass deformability is controlled by the deformability of the intact rock matrix rather than by the deformability of rock fractures; (b) The intact rock modulus provides an upper limit for the rock mass modulus of deformation, which can be considered a bounding estimate giving the maximum possible TM impact: A higher elastic modulus results in a higher thermal stress, and the in situ elastic modulus for fractured rock cannot be higher than the modulus of intact rock. This estimate is considered sufficient, considering that the CHn TM unit is located far below the repository units. For the THM analysis, concern is focused on THM processes primarily in the repository units and secondarily in units located above the repository. This assumption is considered adequate and requires no further confirmation.

5. Appropriate values of the tortuosity parameter are selected based on Jury et al. (1991 [DIRS 102010], p. 203). Jury et al. (1991 [DIRS 102010], p. 203) presents results of diffusion tests through packed soil core samples with recommended average value of 0.66 (≈0.7) for the tortuosity parameter. A tortuosity factor of 0.7 is adopted for rock matrix and fractures in both the Tptpmn and Tptpll subdomains, as well as for the DST model domain (Sections 6.2 and 7).

   Basis:
   This assumption is needed because there are no available direct measurements of tortuosity factor for the Yucca Mountain volcanic tuff. Therefore, values of tortuosity factor from the literature for similar porous media are utilized and assumed to be valid for the volcanic tuff at Yucca Mountain. The tortuosity parameter is used for calculating vapor-air diffusion processes. These processes are of minor importance to modeling results because their impact on TH conditions in the rock is very small compared to conductive and convective processes. Thus, exact quantification or even calibration of this parameter is not needed; instead, appropriate tortuosity values are taken from the literature. The value 0.7, selected based on the results of Jury et al. (1991 [DIRS 102010], p. 203), is further supported by being within the range of values given in de Marsily (1986 [DIRS 100439], p. 233) for various geological materials. A tortuosity factor of 0.7 is a sufficiently accurate estimate for its intended use in this

model report. This assumption is considered adequate and requires no further confirmation.

6. The same values for parameters (b_{max} and α) defining the exponential relationship between fracture aperture and normal stress, which in turn are used to define the stress-versus-permeability relationship, are adopted for all rock units in the drift scale THM model. The adopted estimates for these parameters (b_{max} = 200 μm and $\alpha = 0.52\ MPa^{-1}$) derived from in situ experiments in the Tptpmn unit (Section 6.4.4) are adopted for all rock units. This assumption is needed for estimation of TM-induced changes in hydrologic properties for nonrepository units located above and below the repository units.

   Basis:
   Laboratory tests of fractures from different units indicate that fracture stiffness varies from fracture to fracture, but the average stiffness value for each unit does not vary more than a factor of two (CRWMS M&O 1997 [DIRS 103564], Table 5-39). While these laboratory tests indicate a relatively small variability of joint normal stiffness, the magnitude of laboratory values is not the best representation for in situ values of joint stiffness because of scale effects (Section 6.4.4). Thus, the calibrated in situ values developed in Section 6.4.4 are considered to be the best estimates for an in situ stress-permeability relationship that emphasizes the effect of stress on permeability for all rock units in the drift scale THM model. This assumption is considered adequate and requires no further confirmation.

6. MODEL DISCUSSION

In this section, a fully coupled thermal-hydrological-mechanical (THM) analysis is conducted to investigate the impact of THM processes on the drift-scale flow field of a repository at Yucca Mountain.

A model denoted the drift scale THM model is developed in Sections 6.3 and 6.4, based on the coupled THM simulator TOUGH2-FLAC3D (Rutqvist et al. 2002 [DIRS 162048]), which is presented in Section 6.2. This model is applied to predict coupled THM processes around an emplacement drift, first for an emplacement drift located in the Tptpmn unit (Tptpmn model domain) presented in Section 6.5, and then for an emplacement drift located in the Tptpll unit (Tptpll model domain) presented in Section 6.6. For both cases, the fully coupled THM analysis is complemented by a partially coupled TH analysis, leading to a total of four simulations. In addition, one simulation is conducted for a sensitivity case of low quality (low bulk and shear modulus and low-strength rock properties) lithophysal rock in the Tptpll unit (Section 6.7). The above-mentioned simulations in Sections 6.5 to 6.7 investigate the impact of THM coupling on hydrological properties and flow fields around an intact emplacement drift. Section 6.8 investigates potential changes in hydrologic properties around a collapsed drift. All simulation results are summarized in Section 6.9, followed by a discussion of uncertainties and an alternative conceptual model in Sections 6.10 and 6.11, respectively. The key scientific notebooks (with relevant page numbers) used in the study are presented in Table 6-1.

Table 6-1. Scientific Notebooks Used in This Model Report

Scientific Notebook ID	Relevant Pages	Citation
SN-LBNL-SCI-204-V1	14–18, 104–148	Rutqvist 2002 [DIRS 162047]
SN-LBNL-SCI-204-V2	9–184, 237–293	Rutqvist 2004 [DIRS 170509]
SN-LBNL-SCI-204-V3	9–37	Wang 2004 [DIRS 170508]

Arguments to support the exclusion of FEPs in *Features, Events, and Processes in Unsaturated Zone Flow and Transport* (BSC 2004 [DIRS 170012]) and *Features, Events, and Processes: Disruptive Events* (BSC 2004 [DIRS 170017]) are based upon the results from this model report. The TSPA calculations do not use any output from this report.

6.1 COUPLED THM PROCESSES IN GEOLOGICAL MEDIA AND THEIR POTENTIAL IMPACT ON REPOSITORY PERFORMANCE

In general, geological disposal of heat-releasing nuclear waste leads to an increased temperature of the rock mass for several thousands of years. This increased temperature will give rise to thermally driven coupled THM processes that may impact the performance of the repository. Figure 6.1-1 presents examples of expected couplings between thermal, hydrological and mechanical processes in geological media. The fact that these processes are coupled implies one process affects the initiation and progress of another and, therefore, the repository behavior may not be predicted with confidence considering each process independently. However, as discussed below, some of the couplings can be neglected if their effects on the repository performance are negligible.

In a geological medium, thermal processes affect the mechanics through thermal expansion of the rock mass (Figure 6.1-1). When rock is heated, rock material expands, leading to thermal strain. However, in a confined rock mass environment, the rock material cannot expand freely and thermal stress will occur. Conversely, the mechanical processes can affect thermal processes through mechanical energy conversion into heat. In addition, the thermal conductivity could be impacted by mechanically induced changes in porosity. However, neither mechanical energy conversion nor mechanically induced changes in thermal conductivity are important to geological disposal of nuclear waste. Mechanical energy conversion is only significant in very special cases, for example, as a result of large-scale fault slip during major earthquakes, whereas, heat generated during thermally induced mechanical responses in rocks around a nuclear waste disposal is negligible. The thermal conductivity of rock is mainly dominated by the thermal conductivity of matrix rock and in lithophysal rich rock units, there is a significant impact of lithophysal porosity. The porosity of matrix rock and the lithophysal porosity will not be significantly changed by the magnitudes of thermally-induced stresses expected at a geological nuclear waste disposal. Thus, the coupling from mechanical to thermal processes (marked with a dashed arrow in Figure 6.1-1) can be neglected.

The hydrological processes can affect mechanical processes through fluid-pressure-induced changes in effective stress or through moisture-induced swelling of the geological material (Figure 6.1-1). Conversely, the mechanical processes can impact the hydrological processes through mechanically induced changes in porosity and permeability. In the case of Yucca Mountain, coupling from hydrological to mechanical processes through pressure-induced changes in effective stress can be neglected because fractures are generally dry with an inherent capillary pressure of less than 0.01 MPa. This implies that any change in saturation in the fractured system may give rise to fluid-pressure changes on the order of 0.01 MPa. This is very low pressure for a system exposed to in situ stresses and thermal compressive stresses on the order of 10 MPa. Thus, the fluid-pressure-induced changes could be 1 percent or less compared to the in situ stresses and thermally induced stresses. Consequently, the coupling from hydrological processes to mechanical processes is neglected in this analysis. On the other hand, the coupling from mechanical processes to hydrological processes is not neglected, but is rather one of the main issues investigated in this model report. This coupling is important to estimated thermo-mechanically induced changes in hydrological properties and their impact on the flow field and drift seepage.

Hydrological and thermal processes are coupled through, for example, heat convection, and changes in saturation-dependent thermal conductivity and temperature-dependent thermal and hydrological properties. The coupled TH processes are considered in *Drift-Scale Coupled Processes (DST and TH Seepage) Models* (BSC 2004 [DIRS 170338]), which this model report supplements. The coupled TH processes are also considered in this analysis in the same manner as in the *Drift-Scale Coupled Processes (DST and TH Seepage) Models* (BSC 2004 [DIRS 170338]). As discussed in the previous paragraph, one of the main issues investigated in this model report is TM-induced changes in hydrological properties and their impact on the flow field. This model report seeks to determine whether the full THM coupling needs to be considered for the TSPA, or if a simpler, partially coupled TH analysis is sufficient.

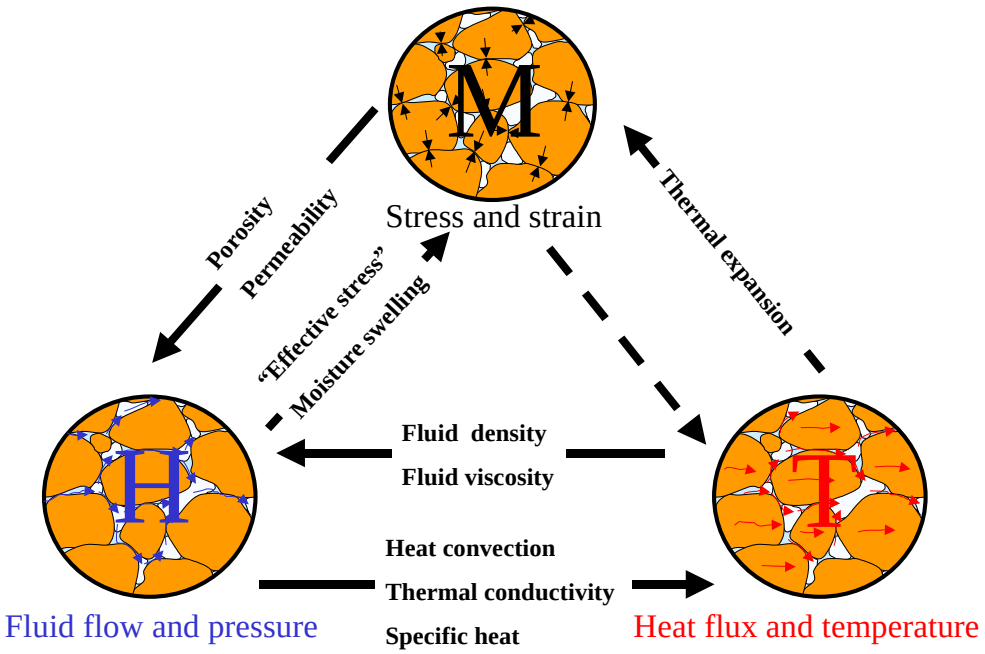

NOTE: The coupling from M to T is marked with dashed line because it is negligible in this particular application.

Figure 6.1-1. Examples of Couplings between Thermal (T), Hydrological (H), and Mechanical (M) Processes in Geological Media

Key TH processes occurring around a drift are shown schematically in Figure 6.1-2. The figure indicates that heating of the rock causes pore water in the rock matrix to boil and vaporize. The vapor moves away from the drift through the permeable fracture network, driven primarily by pressure increase caused by boiling. In cooler regions away from the drift, the vapor condenses in the fractures, where it can drain either toward the heat source above or away from the drift into the zone below the heat source. Condensed water can also imbibe from fractures into the matrix, leading to increased liquid saturation in the rock matrix. With continuous heating, a hot dryout zone will develop closest to the heat source, separated from the condensation zone by a nearly isothermal zone maintained at about the boiling temperature. This nearly isothermal zone is characterized by a continuous process of boiling, vapor transport, condensation, and migration of water back towards the heat source (either by capillary forces or gravity drainage), and is often referred to as a heat pipe (Pruess et al. 1990 [DIRS 100819]). For the current repository design at Yucca Mountain, the dryout zone around drifts extends to a maximum distance of approximately 5 to 10 m from the drift wall (BSC 2004 [DIRS 170338], Sections 6.2.2 and 6.2.3). The current repository design has parallel emplacement drifts separated by 81 m from center to center and a drift radius of 2.75 m, adopted from repository design drawing. The current drift configuration is given in repository design drawing *D&E/ PA/C IED Emplacement Drift Configuration and Environment* (BSC 2004 [DIRS 168489], effective date 3/26/2004). The drift spacing is large compared to the dryout zone, indicating that water above the emplacement drifts may drain between drifts where the rock remains below boiling. This process of pillar drainage is important for repository performance because it reduces the potential amount of water buildup above drifts.

Figure 6.1-3 illustrates the coupled THM processes occurring near a drift and their potential impact on long-term repository performance. As for drift-scale TH processes, most coupled THM processes will occur during the first 1,000 years after emplacement. Stress-induced changes can occur as a result of tunneling excavation, as well as heating and long-term strength degradation of the rock mass surrounding the waste emplacement drifts. Tunneling excavation can affect permeability through opening or closing of existing fractures and potentially through formation of new fractures near the drift wall. After waste emplacement, the heating of the rock mass will induce thermal expansion and thermal stresses that will tend to strain existing fractures, leading to a change in fracture permeability. Permeability changes that occur during the thermal period could be fully reversible under some circumstances, meaning that the permeability could recover to pre-emplacement conditions after the temperature has declined to ambient. However, given the general nonelastic behavior of fractures, some residual change in permeability would be expected following the thermal period. In addition, long-term time-dependent rock strength degradation and seismic loading of the rock surrounding an open drift may lead to additional irreversible mechanical changes and rock blocks falling out from the drift wall (BSC 2004 [DIRS 166107], Section 8.1). TM-induced changes in hydrological properties, in the near-field of a drift and in the pillar region between drifts, can impact the vertical flow in the near-field and may also impact the drainage of liquid water through the pillar region. The drift itself provides a capillary barrier that tends to prevent water from entering the drift leading to a diversion of vertical flow around the drift (Figure 6.1-3b). Changes in hydrological properties in the rock above the crown of the drift may impact the potential for water seeping into the drift. For example, changes in permeability may either tend to prevent or promote flow diversion around the drift opening. In addition, mechanically induced changes in porosity may change the capillary strength for retaining water in the rock mass and thereby impact the capillary barrier function (Figure 6.1-3b). Through the fully coupled THM analysis conducted in this model report, an assessment is made regarding the magnitude of changes in hydrological properties around an emplacement drift and its potential impact on the flow field and drift seepage.

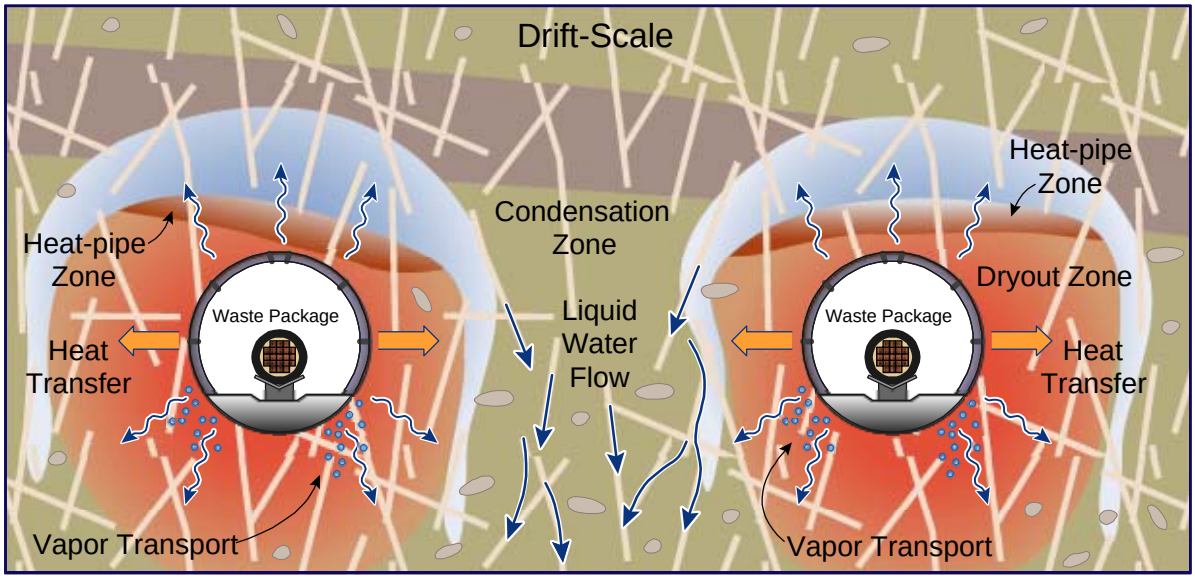

Source: BSC 2004 [DIRS 170338], Figure 6.1-1.

Figure 6.1-2. Schematic of TH processes at the Drift Scale

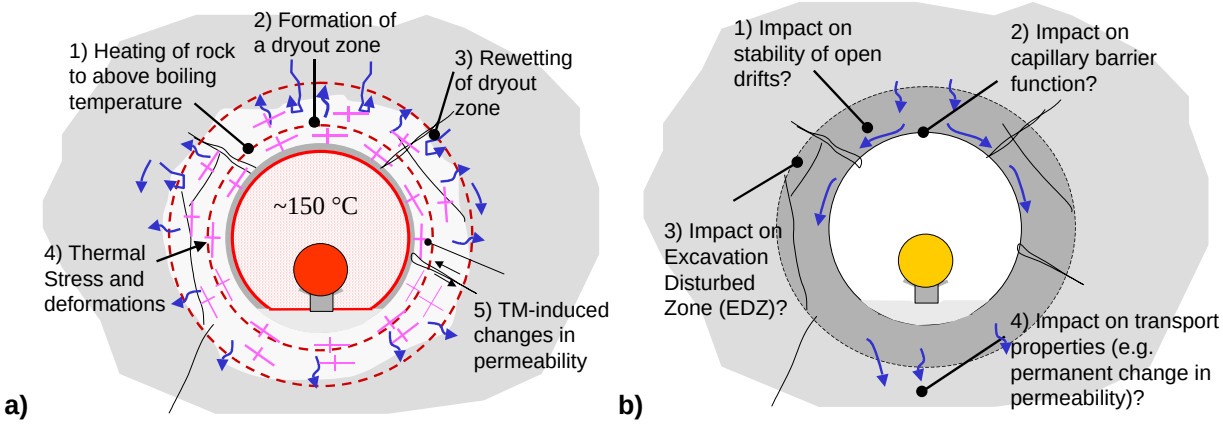

Figure 6.1-3. Schematic (a) THM Processes and (b) Potential Consequences

6.2 COUPLED THM MODEL

This section describes the coupled THM model. This includes the conceptual model for coupled THM processes at Yucca Mountain, the computer code for simulation of coupled THM processes, justification for the THM model, and finally, the general strategy of a bounding analysis of the impact of coupled THM processes.

6.2.1 Conceptual Model for Analysis of Coupled THM Processes at Yucca Mountain

Because of the high density and connectivity of the fracture network, the conceptual model used is a dual-permeability continuum model with interacting fracture and matrix continua, consistent with the UZ flow model and other YMP coupled models. For mechanical analysis, the fractured porous medium is always in a static equilibrium, and the three-dimensional stress is equivalent in the fracture and matrix continua. Therefore, the mechanical dual-continuum model reduces to a lumped fracture-matrix continuum model (equivalent continuum model). A homogeneous, isotropic, elastic or elasto-plastic constitutive mechanical model is applied. This is consistent with fluid and heat transport, the dual continuum stills exists, but with fracture and matrix continua that may not be in equilibrium, and hence can have different fluid pressure and temperature. In the following section, justification for the conceptual model and continuum model approach is provided. Further justification of the adopted THM model is provided in Section 6.2.4, and justification for adopted equivalent properties for the continuum model is provided in Section 6.4.

Continuum Representation for THM Processes

Fractures are modeled as an effective continuum, using averaged parameters for simulating unsaturated flow, heat transport, and mechanical processes. A continuum representation of unsaturated fracture flow is appropriate when fracture density is high and a well-connected fracture network can form at the scale of interest (the drift-scale in this case). The appropriateness of this representation for the flow conditions in the UZ at Yucca Mountain has been discussed in detail in *Conceptual and Numerical Models for UZ Flow and Transport*

(BSC 2004 [DIRS 170035], Section 6.3). The appropriateness of the continuum approach to simulate flow through fractured rock at Yucca Mountain was also demonstrated by Jackson et al. (2000 [DIRS 141523]), using synthetic and actual field data. It is mainly supported by the dispersive nature of fracture water flow in the densely fractured, welded-tuff repository units. Based on this assessment, continuum approaches are the main modeling method for the UZ at Yucca Mountain, applied in simulations for water flow, heat transfer, and contaminant transport (BSC 2004 [DIRS 170035], Section 6.3). In some welded-tuff repository units there is an abundance of lithophysal cavities, which were formed during welding from accumulation of gases. The lithophysal cavities may vary in size from less than a centimeter to over a meter, and the total lithophysal porosity be up to 40 percent (BSC 2004 [DIRS 166107], Section 6.1.4.2). Like fractures, the lithophysal cavities are not explicitly included in the numerical model (as discrete features), but are implicitly accounted in the equivalent continuum model. Thus, the thermal and hydrological properties derived for the underlying continuum model account, in an average sense, for lithophysal cavities. For example, thermal conductivity of the rock accounts for the effect of lithophysal porosity. Hydrological properties are generally developed and calibrated using in situ measurements (conducted in rock units that contain lithophysal cavities), and the material properties implicitly account for the effect of lithophysal cavities.

For mechanical processes, the use of a continuum model is also justified by intensively fractured rock with a mean fracture spacing much smaller than the characteristic scale of the problem, which in this case, is the diameter of the emplacement drift. The appropriateness of a continuum analysis is supported by previous TM analyses of in situ experiments at the Yucca Mountain. Previous analyses of TM-induced displacements at two major heater tests at Yucca Mountain (Single Heater Test [SHT] and DST) have shown that mechanical deformations in the Tptpmn unit can be reasonably well captured with linear-elastic or nonlinear-elastic continuum mechanical models (Sobolik et al. 1998 [DIRS 162049]; BSC 2001 [DIRS 155957]; pp. 115-125; and Sobolik et al. 1999 [DIRS 163202], p. 735). Furthermore, previous comparisons of the discrete-fracture approach and continuum approach for the modeling of mechanical displacements in the DST show minor differences, indicating that the continuum approach is sufficient for accurately representing the average drift-scale in situ TM behavior at Yucca Mountain (BSC 2001 [DIRS 155957], p. 125). This indicates that the drift-scale bulk-rock mass behavior is essentially elastic, although locally a small slip may occur on fracture planes. A small slip along fracture planes can also be implicitly represented in the continuum model as an equivalent shear strain. The effect of lithophysal cavities on the mechanical behavior of the rock is a general reduction in modulus and strength, which can be implicitly accounted for by an underlying continuum model in an average sense.

For studies of THM induced changes in hydrologic properties at the drift scale and its impact on drift seepage, the changes in hydrologic properties occurring next to the drift wall, especially in the rock above the crown of the drift, is most important. Next to the drift wall, more significant inelastic shear slip or tensile fracturing may occur because of the strong stress redistribution and lack of confinement in that region (Figure 6.2-1a). Inelastic mechanical behavior is most likely to occur near a drift located in low quality (low bulk and shear modulus and low-strength rock properties) lithophysal rock of the Tptpll unit during excavation and during a strong postclosure earthquake event (BSC 2004 [DIRS 166107], Section 8.1). In the case of strong earthquakes or long term drift degradation, more substantial inelastic behavior may occur near the drift wall with loads causing instability of the rock by movement (slip or opening) on the joints,

movements of rock blocks, and eventually complete collapse of the drift. In those special cases, a detailed analysis at the scale of individual fractures may be necessary, which a continuum model cannot resolve, and hence, a distinct-element model may more appropriate. For example, in the *Drift Degradation Analysis* (BSC 2004 [DIRS 166107], Section 6.4), the impact of rock fall on the drift shield is calculated using a distinct element model. For such a purpose, a distinct element model is clearly required because a continuum model cannot simulate movements and fall of rock block. As will be shown in Sections 6.7 and 6.8 of this model report, for the purpose of calculating THM induced changes in hydrologic properties and its impact on drift-seepage, a continuum model is adequate as long as the drift stays intact. In the unlikely and extreme case of completely collapsed drift, the distinct element model may be more appropriate for estimating change in hydrologic properties near the drift. In this report, the continuum model is adequately adopted for the case of intact drift, whereas the results from the distinct element analysis of the *Drift Degradation Analysis* (BSC 2004 [DIRS 166107], Section 6.4) are utilized in cases of a completely collapsed drift.

Dual-Permeability Method for Fluid Flow

A key issue for simulating fluid and heat flow in the fractured-porous rock of Yucca Mountain is how to address fracture and matrix flow and interactions under multiphase, multicomponent, and nonisothermal conditions. For the work documented in this model report, the dual-permeability method (DKM) is applied to evaluate fluid, heat flow, and transport in the fracture rock. This methodology is based on the modeling framework of so-called dual-continuum models (BSC 2004 [DIRS 170035], Section 6.3.1.1.3). Such models are often applied to fractured porous rock, where one component (fractures) typically has a large permeability, but small porosity, while the other component (rock matrix) has a larger porosity, but small permeability. The dual-permeability method accounts for these differences by assuming two separate, but interacting continua that overlap each other in space, one describing flow and transport in the fractures, the other describing flow and transport in the matrix. Each continuum is simulated with a separate numerical grid, separate TH properties, and separate variables (pressure, saturation, and temperature). Thus, at each location in space, there is a fracture gridblock and an overlapping matrix gridblock. The two gridblocks at each location are connected to model the interaction between the two continua. Global flow and transport occur within the fracture continuum and the matrix continuum, while local interflow occurs between the two continua as a result of the local pressure and temperature differences. The interflow between fractures and matrix is handled using a quasi-steady transfer, estimating the exchange of fluid, gas, and heat between the two components by a linear gradient approximation. Details have been well documented by Doughty (1999 [DIRS 135997], Section 2) and are not reproduced here. Again, the effects of lithophysal cavities are implicitly accounted for in an average sense in the average properties derived for the fracture and matrix continua of the dual-permeability model.

Active Fracture Model for Fluid Flow

The DKM, as introduced above, typically considers flow to occur through all the connected fractures and to be uniformly distributed over the entire fracture area. In this case, the entire fracture-matrix interface area is available for coupling flow between the matrix and fractures, implying relatively large fracture-matrix interactions. In natural systems, however, unsaturated fracture flow is not uniformly distributed because (a) flow channels may form within a fracture, and (b) only a subset of all fractures may be actively contributing to the flow processes. To account for this reduced coupling between the fracture and the matrix continua, the active fracture model (AFM) was developed to modify fracture-matrix interface areas for flow and transport between fracture and matrix systems (Liu et al. 1998 [DIRS 105729]). The AFM proposes to use a fracture-matrix reduction factor proportional to a power function of liquid saturation, with the power function coefficient calibrated from measured data. In this model report, the AFM was chosen as the primary conceptual model for predictive simulation of the TH processes in both fully coupled THM analyses and partially coupled TH analyses. This choice was based mainly on consistency considerations since the AFM has been implemented in other models for unsaturated flow and transport at Yucca Mountain, e.g., *Conceptual and Numerical Models for UZ Flow and Transport* (BSC 2004 [DIRS 170035], Section 6.3.7); *UZ Flow Models and Submodels* (BSC 2004 [DIRS 169861], Section 6.1); and *Calibrated Properties Model* (BSC 2004 [DIRS 169857], Section 6.1).

Stress-versus-Permeability Model

To couple changes in the three-dimensional stress field to rock mass permeability, a cubic-block conceptual model is utilized (Figure 6.2-1b). This model is justified by the fracture mapping that has been conducted at the Yucca Mountain. At Yucca Mountain, the two main stratigraphic units in which the emplacement drifts may be located (middle nonlithophysal [Tptpmn] and the lower lithophysal [Tptpll] units of the Topopah Spring Tuff) are both highly fractured, and the fractures are well connected. In these rock units, three major sets of fractures are oriented almost orthogonal to each other (CRWMS M&O 1998 [DIRS 102679], Section 7.4.5; BSC 2004 [DIRS 166107], Section 6.1.4.1), two subvertical and one subhorizontal. The average fracture spacing mapped along the ESF for the TSw2 TM unit is about 0.33 m (CRWMS M&O 1998 [DIRS 102679], Table 4), and the mean spacing developed in LB0205REVUZPRP.001 [DIRS 159525] is 1/4.32 = 0.23 m and 1/3.16 = 0.32 m, for the Tptpmn and Tptpll units, respectively. However, if one only looks at the fractures belonging to the identified three main fracture sets, the fracture spacing may be larger (CRWMS M&O 1998 [DIRS 102679], Table 4), which indicates that a significant proportion of the fracture network belongs to the randomly oriented fractures. In the Tptpll unit, there is also a significant amount of densely spaced small-scale (short tracelength) fractures that connect with lithophysal cavities. The hydraulic significance of these small-scale fractures in relation to the large-scale fractures is unclear. In this study, these small-scale fractures can be considered part of the rock matrix continuum rather than the fracture continuum.

The fracture orientation in the cubic-block model with orthogonal fractures and uniform spacing is a simplified representation of the in situ fracture network at Yucca Mountain. For example, in some rock units, the subhorizontal fracture set may be less frequent, and as mentioned above, there may also be randomly oriented fractures. Furthermore, trace distributions of fractures mapped for the Tptpmn unit make them discontinuous in nature, with fractures frequently terminating against intersecting fractures (BSC 2004 [DIRS 166107], Section 6.1.4.1). However, the conceptual model shown in Figure 6.2-1b is consistent with established hydrological and TH process models for the Yucca Mountain UZ. The hydrological properties of those models are largely derived directly from in situ permeability measurements and through model calibration against in situ hydrological data, such as liquid saturation profiles along vertical boreholes and air-permeability measurements (e.g., BSC 2004 [DIRS 169857], Section 6.3.2). The fracture density is basically used for deriving parameters for the fracture-matrix interaction behavior, such as interface area and connection length between fracture elements and matrix blocks in the underlying conceptual model (BSC 2004 [DIRS 169857], Sections 6.2.1). Using this underlying conceptual model, the hydraulic properties (such as the water retention curve) are calibrated against field measurements. Thus, for deriving hydrological properties and for analysis of hydrological and TH processes in the unsaturated zone of Yucca Mountain, detailed information indicating distribution of fracture length, orientation, and aperture is not explicitly incorporated, except for a generic value of mean fracture spacing (or frequency) in each rock unit (BSC 2004 [DIRS 169857], Section 6.2.1).

The underlying conceptual model for stress-versus-permeability coupling shown in Figure 6.2-1b is justified as being consistent with the established hydrological models of the Yucca Mountain unsaturated zone (BSC 2004 [DIRS 170035], Section 6.1). In these hydrological models, the permeability field is heterogeneous, but isotropic (BSC 2004 [DIRS 169857], Section 6.1.1), leading to an underlying conceptual model with equal fracture spacing and properties for vertical and horizontal fractures. Isotropic permeability is an idealization because the anisotropic in situ stress field and different genesis of the joint sets (i.e., the subvertical joints are relatively smooth, cooling joints; the subhorizontal joints are rough vapor-phase partings with mineral filling) probably affect permeabilities in different directions. However, as will be discussed below, analogous to the derivation of hydrological properties, the resulting continuum hydromechanical properties (e.g., stress-versus-permeability function) are not critically dependent on the precise underlying conceptual model. This is because the relationship is calibrated for the underlying conceptual model, and thus is only valid for the underlying conceptual model. Similarly, the calibrated hydrological properties are only valid when using the same appropriate conceptual model. It is therefore, important that the same conceptual model is used for both model calibration and predictions.

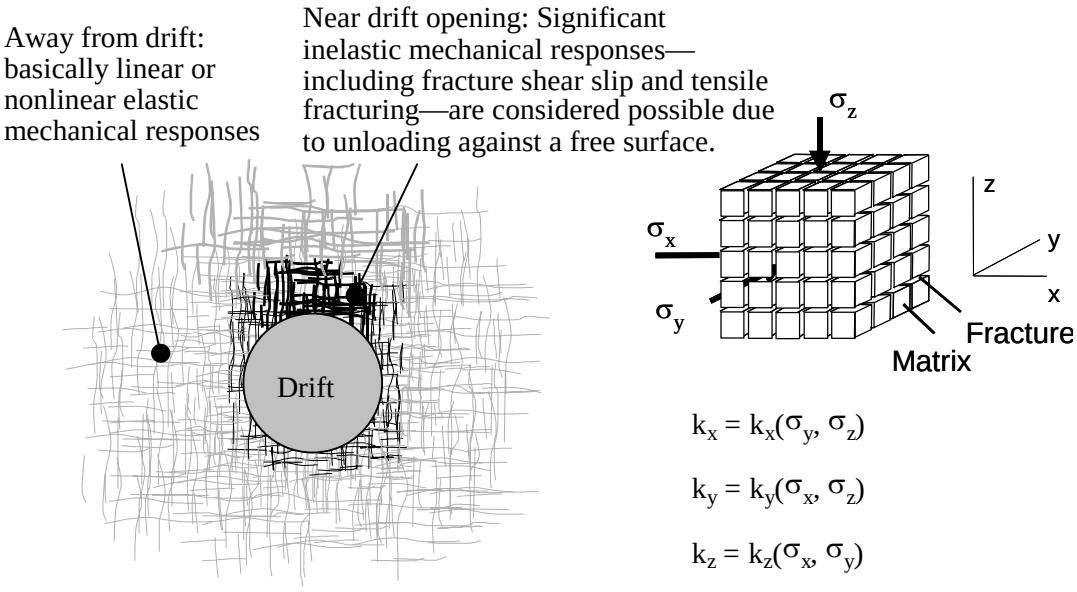

(a) Fractured rock mass system **(b) Conceptual stress-permeability model**

NOTE: σ_x, σ_y, σ_z and k_x, k_y, k_z are stresses and permeabilities in x, y and z directions, respectively. The illustrated inelastic zone near the drift wall may or may not exist depending on rock mass strength properties.

Figure 6.2-1. Schematic of the Fractured Rock Mass System Near a Drift and the Conceptual Model Used for Stress Permeability Coupling

6.2.2 The TOUGH-FLAC Coupled THM Simulator

The two computer codes, TOUGH2 V1.6 and FLAC3D V2.0, have been coupled for the analysis of coupled multiphase flow, heat transport, and rock deformations in fractured porous media (Rutqvist et al. 2002 [DIRS 162048]). The TOUGH2 (Pruess et al. 1999 [DIRS 160778]) code is designed for hydrological analysis of multiphase, multicomponent fluid, and heat transport, while FLAC3D (Itasca Consulting Group 1997 [DIRS 156788]) is designed for rock and soil mechanics. TOUGH2 has been successfully applied in the Yucca Mountain Project (YMP) to predict the temperature and moisture distribution of field experiments, including the SHT (Tsang and Birkholzer 1999 [DIRS 137577]) and the DST (BSC 2001 [DIRS 157330], Section 6). TOUGH2 is used to simulate relevant coupled TH processes, including evaporation of liquid water to vapor with the transfer of latent heat during boiling, advection of moisture and dissolved air with gas and liquid-phase flow, heat convection with water transport, vapor diffusion, and condensation of vapor to liquid water upon cooling. With these capabilities, the TOUGH2 code is applied to simulate the evolution of temperature and moisture around an emplacement drift, including the formation and resaturation of a dryout zone. FLAC3D has the capability to analyze coupled HM and TM responses of soil, rock, or other types of materials that may undergo plastic flow when their yield limit is reached. It contains various constitutive models suitable for mechanical analysis of geological materials. This includes Mohr-Coulomb elasto-plastic and ubiquitous joint models. In this model report, the FLAC3D code is applied using an elastic or elasto-plastic constitutive mechanical model to simulate relevant rock mechanical aspects, including stress and strain redistribution, and the possibility of rock mass failure around an emplacement drift.

In this analysis, FLAC3D and TOUGH2 are coupled through external modules: one that calculates changes in effective stress as a function of multiphase pore pressure and thermal expansion, and one that corrects porosity, permeability, and capillary pressure as a function of stress (Figure 6.2.2-1). Because these coupling parameters are material specific, specially designed coupling modules have been constructed and qualified for Yucca Mountain. The coupling modules are contained in the qualified software routines Tin V1.1 (STN: 10899-1.1-00; LBNL 2002 [DIRS 162038]), Delb.dat V1.0 (STN: 10507-1.0-0.0; LBNL 2002 [DIRS 154791]), and Gpzones.dat V1.0 (STN: 10509-1.0-00; LBNL 2002 [DIRS 154792]), the functions of which are described in more detail below.

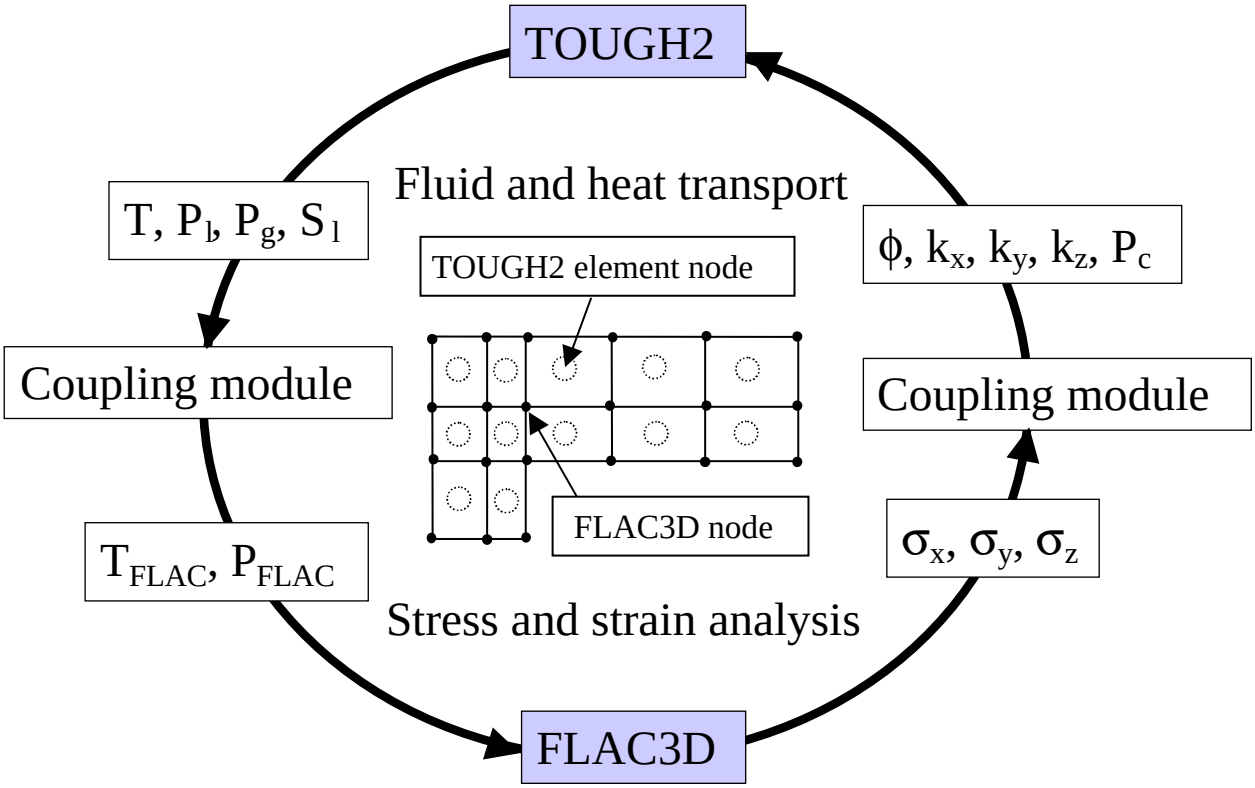

NOTE: T = Temperature; P_l = liquid fluid pressure; P_g = gas pressure; S_l = liquid saturation; T_{Flac} = temperature at FLAC3D node; P_{FLAC} = pressure at FLAC3D node; ϕ = porosity; k_x, k_y, and k_z are permeabilities in x, y and z directions, respectively, P_c is capillary pressure and σ_x, σ_y, and σ_z are stresses in x, y and z directions, respectively. For the unsaturated fractured hard rock zone at Yucca Mountain, the illustrated transfer of P_l, P_g and S_l from TOUGH2 to FLAC3D is not significant and therefore neglected. The fluid pressure in fractures of the unsaturated rock is very small and does not induce any significant mechanical changes. Therefore, only temperature has to be transferred from TOUGH2 to FLAC3D.

Figure 6.2.2-1. Schematic of Coupling between TOUGH2 and FLAC3D

For modeling of the unsaturated zone at Yucca Mountain, the linkage function from TOUGH2 to FLAC3D considers only the effect of thermally induced strain and stresses. The changes in effective stress and bulk density caused by the multiphase fluid pressure and saturation changes are neglected. As mentioned in Section 6.1, this is defensible considering that the fracture system is unsaturated, with a capillary pressure (air-entry pressure) of less than 0.01 MPa, which is a very small pressure for a system that has in situ stresses and compressive thermal stresses with magnitudes on the order of 10 MPa. Thus, the coupling module for the link from TOUGH2 to FLAC3D transfers the temperature field from TOUGH2 nodes to FLAC3D nodes. This coupling is provided by the FLAC3D FISH routine Tin V1.1 (LBNL 2002 [DIRS 162038]) and with volume interpolation factors calculated by Gpzones.dat V1.0 (LBNL 2002 [DIRS 154792]).

The simulation is conducted in a two-dimensional cross-section using a one-layer thick three-dimensional numerical grid, which is consistent in both FLAC3D and TOUGH2. A 2-D plane strain condition is simulated in FLAC3D by fixing the displacements in the plane perpendicular to the two-dimensional cross-section. Note that the permeability field in the plane of the model (k_x and k_z) depends on the three-dimensional stress field (Figure 6.2-1b). Using the conceptual model in Figure 6.2-1b, the porosity, permeability, and capillary pressure in the fractured continuum are corrected for any change in the stress field according to:

$$\phi = F_{\phi} \times \phi_i \qquad \text{(Eq. 6.2-1)}$$

$$k_x = F_{kx} \times k_{ix},\ k_y = F_{ky} \times k_{iy},\ k_z = F_{kz} \times k_{iz} \qquad \text{(Eq. 6.2-2)}$$

$$P_c = F_{Pc} \times P_{ci} \qquad \text{(Eq. 6.2-3)}$$

where F denotes various correction factors and subscript i denotes initial conditions. Porosity and permeability correction factors are calculated from the initial and current apertures, b, in Fracture Sets 1, 2, and 3 according to:

$$F_{\phi} = \frac{b_1 + b_2 + b_3}{b_{1i} + b_{2i} + b_{3i}} \qquad \text{(Eq. 6.2-4)}$$

$$F_{kx} = \frac{b_2^3 + b_3^3}{b_{2i}^3 + b_{3i}^3},\ F_{ky} = \frac{b_1^3 + b_3^3}{b_{1i}^3 + b_{3i}^3},\ F_{kz} = \frac{b_1^3 + b_2^3}{b_{1i}^3 + b_{2i}^3} \qquad \text{(Eq. 6.2-5)}$$

where fractures in Fracture Sets 1, 2, and 3 are equally spaced and oriented normal to x, y, and z directions, respectively, and a parallel-plate fracture flow model (Witherspoon et al. 1980 [DIRS 123506]) is adopted. The capillary pressure is corrected with porosity and permeability changes according to the Leverett (1941 [DIRS 100588]) function:

$$F_{Pc} = \sqrt{\frac{F_{\phi}}{F_k}} \qquad \text{(Eq. 6.2-6)}$$

where

$$F_k = \sqrt[3]{F_{kx} \times F_{ky} \times F_{kz}} \quad \text{(Eq. 6.2-7)}$$

Thus, in areas where permeability increases by fracture opening, the capillary pressure tends to decrease. In this study, the current fracture aperture b depends on the current effective normal stress σ'_n, according to the following exponential function (Rutqvist and Tsang 2003 [DIRS 162584]):

$$b = b_r + b_m = b_r + b_{\max}\left[\exp\left(\alpha\sigma'_n\right)\right] \quad \text{(Eq. 6.2-8)}$$

where b_r is a residual aperture, b_m is a mechanical aperture, b_{max} is the mechanical aperture corresponding to zero normal stress, and α is a parameter related to the curvature of the function (Figure 6.2.2-2). This relationship can also be expressed in terms of an initial aperture, b_i, and changes in aperture, Δb, as:

$$b = b_i + \Delta b = b_i + b_{\max}\left[\exp\left(\alpha\sigma_n\right) - \exp\left(\alpha\sigma_{ni}\right)\right] \quad \text{(Eq. 6.2-9)}$$

where σ_{ni} is the initial stress normal to the fractures. The engineering sign convention is used for effective normal stress in Equation 6.2-9 implying that tensile stresses have positive values and compressive stresses have negative values. This expression can be inserted into Equation 6.2-5 to derive expressions for rock mass permeability correction factors in x, y, and z directions. In this formulation, the permeability changes as a function of normal stress across each fracture set, while no shear-induced permeability changes are considered. It is sufficient because closure of vertical fractures caused by thermally induced horizontal stresses dominates impact on permeability changes (Section 8.1). Furthermore, the potential for shear-induced permeability changes can be evaluated indirectly from the results of the stress analysis. The calculation of fracture aperture changes is conducted in the qualified software routine Delb.dat V1.0 (LBNL 2002 [DIRS 154791]), which is then transferred into the TOUGH2 code for the correction of hydrological properties

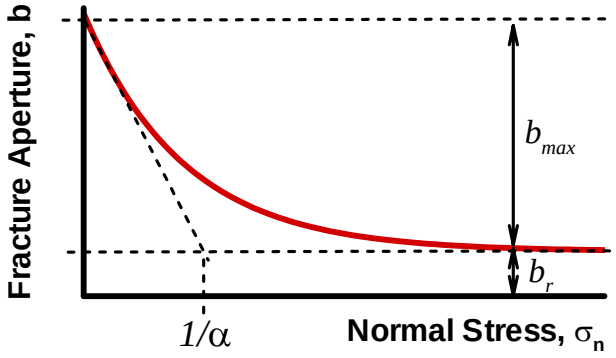

NOTE: b_{max} and α are parameters that determine the shape of the exponential function, and b_r is the residual aperture when the fracture is completely compressed from a mechanical point of view at a high normal stress.

Figure 6.2.2-2. Schematic for Normal Stress Versus Fracture Aperture Relation

6.2.3 Further Justification of the Adopted THM Model

The modeling choice was made, simplifying the approach, consistent with the intended use. The conceptual model in Figure 6.2-1 is sufficient for estimating the impact of mechanical processes on the established hydrological models at Yucca Mountain. This model can capture relevant THM processes observed at several in situ experiments conducted at Yucca Mountain (Section 7). The simplified conceptual model can capture relevant THM processes because the rock at Yucca Mountain is highly fractured, forming a network that is well connected for fluid flow. For the Tptpmn and Tptpll units, a mean fracture spacing of less than 0.4 m (Table 4.1-3a) has been derived, using mappings of fractures with a trace length larger than one meter. However, as pointed out in the *Drift Degradation Analysis* (BSC 2004 [DIRS 166107], Section 6.3.3), 80 percent of the fractures have a trace length of less than one meter and therefore, counting small-scale fractures, the fracture spacing should be less than 0.4 m. The concept of a well-connected fracture network for fluid flow is confirmed by air-permeability measurements conducted in boreholes with short (about 0.3 m) packer intervals at several excavated niches at Yucca Mountain (BSC 2004 [DIRS 170004], Section 6.1). In these tests, the permeability at each 0.3-meter interval of the boreholes is several orders larger than the matrix permeability, indicating that at least one hydraulic conductive fracture intersects (about 0.3 m) and is connected to a network of hydraulic conducting fractures. For such intensively fractured rock, the detailed fracture geometry does not impact the coupled THM behavior significantly, and hence, the adopted conceptual model is appropriate. Effects of lithophysal cavities can, as discussed in Section 6.2.1, be accounted for in an average sense by modifying the equivalent continuum properties and by model calibration against field measurements conducted in lithophysal rocks.

The most important parameter for estimating stress-induced changes in hydraulic properties is the relationship between fracture aperture and stress (which controls changes in both permeability and capillarity) defined in Equation 6.2-8. For a well-connected fracture network, fracture spacing and fracture orientation have little importance for the stress-versus-permeability relationship in comparison with the fracture-aperture-versus-stress function. In the literature, determinations of the relationship between fracture hydraulic aperture and stress have been reported, both from laboratory samples and in the field for various types of rock. This relationship depends on fracture characteristics such as roughness and degree of mineral filling (Rutqvist and Stephansson 2003 [DIRS 162583]). However, aperture versus normal stress relationships derived from small-scale laboratory samples are generally not applicable in the field. A size effect on the permeability and normal stiffness of fractures has been confirmed in both theoretical and experimental studies (Rutqvist and Stephansson 2003 [DIRS 162583]). Because of the potential effects of size and nonrepresentative sampling, it is important to determine the stress-versus-aperture relationship in situ (Rutqvist and Stephansson 2003 [DIRS 162583]). An in situ determination of the stress-aperture relationship for Yucca Mountain is performed in Section 6.4.4 of this model report. Such an in situ determination constrains the basic parameters b_{max} and α for fractures in the underlying conceptual model.

The adopted cubic relationship between aperture and permeability in Equation 6.2-5 is the well-known cubic law for fracture flow. Fairly recent reinterpretations of literature data suggest that a cubic relationship generally holds as long as a modified version of the cubic law is adopted (Boitnott 1991 [DIRS 170529] Chapter 3; Alvarez et al. 1995 [DIRS 170495]). The modified

cubic law includes a factor, f, between normal deformation and changes in hydraulic conducing aperture. Boitnott (1991 [DIRS 170529], Chapter 3) conducted a careful analysis of published literature data of fracture flow experiments. He concluded that the cubic law, and especially the modified cubic law, commonly holds for a variety of fractures. In many cases, the cubic law breaks down as closure is increased, with these cases typically exhibiting a progressive decrease in the sensitivity of hydraulic aperture to further closure. Therefore, the residual aperture, b_r, is an important feature of the relationship between normal stress, aperture and permeability of a natural fracture. During the 1990s, these observations were confirmed in several studies (Zhao and Brown 1992 [DIRS 170499]; Alvarez et al. 1995 [DIRS 170495]). In these studies, the modified cubic law was adopted, together with the exponential function described in Equation 6.2-8. The exponential relationship shows a typical nonlinear normal closure behavior frequently observed in laboratory experiments. The other bound to applicability of the cubic law to fracture flow occurs when the joint aperture becomes relatively large. In most simulations discussed in this model report the dominant mode of deformation is joint closure caused by increased compressive stress. Significant joint opening is predicted in the cases of total drift collapse (Section 6.8) for strong ground motion and the extreme case of time-dependent strength degradation. In these cases, the drift outline is modified to include all joints with relatively large aperture. This approximation is extreme because it implies that the permeability of the joints with large aperture (included into the drift outline) is infinite. It is concluded that the modified cubic law is the best available, and a good representation of fluid flow in the repository host rock.

It should be pointed out that because the stress-versus-aperture function is calibrated against in situ measurements of permeability, the resulting stress-versus-permeability function would be similar for a slightly different underlying relationship between stress and aperture. That is, if an exponent different from 3 (e.g., 2.8) were chosen in Equation 6.2-5, and if a slightly different functional relationship were chosen in Equation 6.2-8, a model calibration against field measurements would result in a similar stress-versus-permeability function (of course, the underlying relationships could not be completely different from the ones used). Furthermore, the uncertainty (with a factor f) between normal displacement and changes in hydraulic aperture is bypassed because the calibration provides a direct measure of changes in permeability (and hence the hydraulic aperture). Thus, the in situ calibrated stress-versus-aperture relationship is a relationship between hydraulic aperture and stress. Determination of the stress-versus-permeability relationship by in situ calibration is analogous to the development of the hydrological properties used for all UZ models. An underlying conceptual model with estimated fracture spacing and fracture-matrix interface areas is used to calibrate water-retention curves using an assumed van Genuchten type of function (BSC 2004 [DIRS 169857], Section 6.3.2), and the effect of lithophysal cavities on flow is implicitly accounted for in an average sense. It is important that the same underlying conceptual model and the same functions are used for both model calibration and predictions. Consequently, the same conceptual model with the corresponding calibrated parameters b_{max} and α is used in the predictive analysis of coupled THM processes around an emplacement drift in Sections 6.5 through 6.8. Finally, the conceptual model shown in Figure 6.2-1 and the adopted stress-versus-aperture function are validated against field measurements in Section 7.

An alternative to a stress-versus-permeability model would be a model that relates either volumetric strain or fracture strain to permeability. A model that relates permeability to strain rather than stress is more general (than a stress-versus-permeability relation) because:

1. It would account for inelastic deformation (caused by both slip induced dilation and tension-induced joint opening).

2. It would be independent of mechanical properties of rock mass. The change in stiffness of the rock mass would not lead to a change in the strain-versus-permeability relation.

Most of the analyses for this model report were carried out for thermally induced stresses. Deformation of the rock mass around the emplacement drifts is predominantly elastic for those loads. Localized yielding (approximately 0.5 m) of rock in the drift wall takes place after excavation of the emplacement drifts in the low quality lithophysal rock mass only (BSC 2004 [DIRS 166107], Executive Summary). For those conditions, the stress-versus-permeability relation is adequate. As long as the rock behaves elastically, there is a reversible relationship between stress and strain, and it does not matter whether a strain-versus-permeability or stress-versus-permeability model is used. Significant inelastic deformation of the rock mass (and collapse of the emplacement drift) is expected for the strong ground motions and extreme conditions of time-dependent strength degradation. In those cases, as discussed in Section 6.8, the strain-permeability relation is used to account for the effect of mechanically induced changes in permeability on seepage.

In the Tptpll unit, lithophysal porosity is the primary factor affecting rock quality (and consequently the stiffness), whereas the contribution of jointing to overall compliance of the rock mass does not significantly change as the quality of the rock mass changes. Therefore, the calibrated stress-versus-permeability relation does not need to be changed when applied to a rock mass with different stiffness (e.g., the low quality lithophysal tuff discussed in Section 6.7).

6.2.4 Bounding Analysis of the Impact of Coupled THM Processes

This section describes the strategy for a bounding analysis to be conducted by adopting material properties that will bracket the potential impact of THM processes on hydrologic properties and the flow field. As discussed in Sections 1, 6, and 6.1, the analysis performed in this model report aims to assess coupled THM processes and their impact on fracture permeability, percolation flux around a waste emplacement drift, and the potential for drift seepage. Drift seepage is analyzed in other model reports dedicated solely to predicting the probability for seepage into drifts by using hydrological models or TH models, and stochastic modeling with multiple realizations of heterogeneous rock properties (BSC 2004 [DIRS 169131]; BSC 2004 [DIRS 170338], Section 6.2). The seepage analysis considers the changes in hydrologic properties due to excavation effects but neglects any post-closure THM-induced changes in hydrologic properties caused by elevated temperatures. The excavation effects are considered in the seepage models because the seepage threshold is determined from in situ tests performed at excavated drifts. The effect of THM-induced changes on hydrologic properties (including permeability and capillarity) is an excluded FEPs and is thus considered negligible in the seepage analysis. The bounding analysis is conducted to evaluate THM-induced changes in hydrologic

properties and its impact on the flow field for a bounding case. The bounding case is realized by adopting parameter values that emphasize the effect of THM coupling on hydrologic properties.

The approach for bounding analysis of the impact of coupled THM processes is illustrated in Figure 6.2.4-1. Figure 6.2.4-1a shows the basic TH coupled analysis, omitting couplings through mechanical processes. This is how the problem is analyzed in the *Drift-Scale Coupled Processes (DST and TH Seepage) Models* (BSC 2004 [DIRS 170338]). Figures 6.2.4-1b and c illustrate that coupled THM processes can impact hydrological process via couplings (T to M and M to H) through mechanical processes. First, temperature changes give rise to thermal strain and stress, of which magnitude depends on the magnitude of the temperature changes (ΔT) and the thermal expansion coefficient (α_T). Secondly, for a given stress and strain change, the permeability of the fractured media will change, in this case depending on the relationship between stress and permeability $k(\sigma)$. Figure 6.2.4-1c illustrates the bounding case of relatively strong THM-induced changes in hydrological properties realized by adopting parameter values that emphasize the effect of coupling. This includes a bounding estimate of the thermal expansion coefficient (that emphasizes thermal stress) and a bounding estimate of a stress-versus-permeability function (that emphasizes TM-induced permeability change). The output, in the form of THM-induced changes in mean permeability, can be input to the above-mentioned hydrological or coupled TH multiple realization analyses as a correction factor for permeability. The bounding case of the maximum THM-induced changes in mean permeability calculated in this model report is considered in the *Abstraction of Drift Seepage* (BSC 2004 [DIRS 169131]), where the overall impact of the variability of hydrological properties on drift seepage is abstracted. Furthermore, the comparison of the flow field obtained for the fully coupled THM analysis, with the flow field from partially coupled TH analysis is used to assess the impact of THM processes on the flow field.

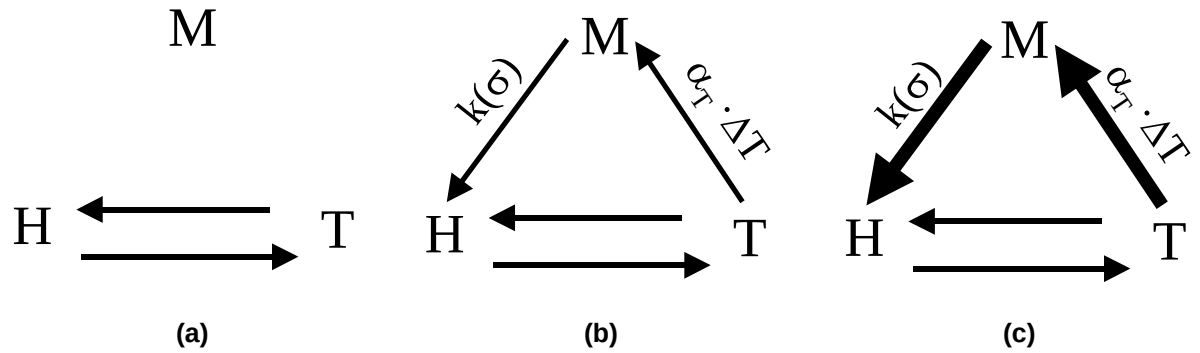

NOTE: (a) conventional TH analysis with couplings through M neglected, (b) THM analysis using weak T to M and M to H coupling parameters, and (c) THM analysis with parameters that emphasized the effect of THM coupling.

Figure 6.2.4-1. Illustration of the Bounding Analysis Concerning the Impact of THM Processes by Adopting Parameters that Emphasize the Effect of T to M and M to H Couplings

6.3 TPTPMN AND TPTPLL MODEL DOMAINS

The drift scale THM model is a two-dimensional model that extends from the ground surface down to the groundwater table. It includes one-half of the emplacement drift as a result of lateral symmetry (Figure 6.3-1a). Coupled THM simulations were conducted on two model domains, representing two different vertical two-dimensional cross sections through the interior of the repository at Yucca Mountain. The first one, the Tptpmn model domain, considers a waste emplacement drift located in the Topopah Spring Tuff middle nonlithophysal unit (Tptpmn unit). The second one, the Tptpll model domain, has a drift located in the Topopah Spring lower lithophysal unit (Tptpll unit). The two sections are selected to account for the two main host rock units of the repository and are the same sections being considered in both the *Drift-Scale Coupled Processes (DST and TH Seepage) Models* report (BSC 2004 [DIRS 170338], Section 6.2) and *Drift-Scale Coupled Processes (DST and THC Seepage) Models* (BSC 2004 [DIRS 169856], Sections 6.5 and 6.7). TOUGH2 dual-permeability meshes of both the Tptpmn and Tptpll model domains were constructed using the qualified software 2KGRIDV1.F V1.0 (STN: 10244-1.0-00; LBNL 2000 [DIRS 147553]). As mentioned in Section 6.2.1, in the repository units, three major sets of fractures are oriented almost orthogonal to each other (CRWMS M&O 1998 [DIRS 102679], Section 7.4.5; BSC 2004 [DIRS 166107], Section 6.1.4.1), two subvertical and one subhorizontal. More specifically, in the TSw2 TM unit, these major fracture sets (Tptpmn unit) are (CRWMS M&O 1998 [DIRS 102679], Section 7.4.5):

1. One prominent vertical, southeast trending
2. One less-prominent vertical, southwest trending
3. One less-prominent subhorizontal.

In addition, there are also fractures labeled as randomly oriented that account for a significant portion of all fractures measured in the ESF (CRWMS M&O 1998 [DIRS 102679], p. 37). At Yucca Mountain, the repository is designed with emplacement drift oriented with their axes approximately normal to the southeast trending fracture set. As already discussed in Section 6.2.1, in the Tptpll unit there is also a significant amount of densely spaced small-scale (short tracelength) fractures that connect with lithophysal cavities. The hydraulic significance of these small-scale fractures in relation to the large-scale fractures is unclear. In this study, these small-scale fractures can be considered part of the rock matrix continuum rather than the fracture continuum.

The Tptpmn model domain is a multiple-layered column extending 555.4 m vertically from the top of the tcw13 model layer near the ground surface down to the water table (Table 4.1-3c), with the repository located in the Tptpmn. The vertical layering for the model was chosen to correspond to the vertical contacts at borehole USW SD-9 at about Nevada State Plane Coordinates 171,234 (Easting) and 234,074 (Northing), as implemented in the three-dimensional Yucca Mountain UZ model grid (DTN: LB990501233129.004 [DIRS 111475]) (see Table 4.1.3c for layering dimensions). In the Tptpmn model domain, the emplacement drift is located at an elevation of about 1,065.3 m corresponding to a depth of 220.1 m (1,285.4-1,065.3 = 220.1 m with elevation 1,285.4 extracted from Table 4.1-3c). The elevation 1,065.3 m of the repository corresponds to the location of the repository in UZ model grid

(DTN: LB990501233129.004 [DIRS 111475], filename primary.mesh, element 3Ei64, with z-coordinate shown in the rightmost column).

The Tptpll model domain extends 716.6 m vertically from the top of the tcw11 model layer at the ground surface down to the water table (Table 4.1-3d), with the repository located in the Tptpll. The stratigraphy of the Tptpll model domain was taken at a location near the center of the repository at about Nevada State Plane coordinates 170572 m (Easting) and 233195 m (Northing). The geological data are derived from the "j34"column of three-dimensional Yucca Mountain UZ model grid (DTN: LB990501233129.004 [DIRS 111475]) as described in detail in Section 4.1.1.4 (see Table 4.1.3d for layering dimensions). In the Tptpll model domain, the emplacement drift is located at an elevation of about 1082.8 m corresponding to a depth of 363.8 m (1,446.6-1,082.8 = 363.8 m, with elevation 1,446.6 m extracted from Table 4.1-3d). The elevation 1082.8 m of the repository corresponds to the location of the repository in UZ model grid (DTN: LB990501233129.004 [DIRS 111475], filename: primary.mesh, at an average elevation [z = {1085.2863+1080.2863}/2 = 1,082.8 m] of elements 3EJ34 [at z = 1085.2863] and 3FJ34 [at z = 1080.2863], with z-coordinate shown in the rightmost column).

The ground-surface boundary was set at a constant temperature and atmospheric pressure, mechanically free, and the water table boundary was set at a constant temperature and mechanically fixed (Figure 6.3-1 and Table 6.3-1). Specific boundary values used for the Tptpmn model domain represent observations at the locations of the USW SD-9 borehole. The Tptpll model domain uses values representative of the center of the repository at column "j34" of the UZ model grid (DTN: LB9905012331329.004 [DIRS 111475]), as described in detail in Section 4.1.1.4. A varying infiltration rate was applied at the ground surface according to the mean infiltration scenario described in *Simulation of Net Infiltration for Modern and Potential Future Climates* (BSC 2004 [DIRS 170007], Sections 6.9 and 6.11) (Table 6.3-1). The specific infiltration values, 6, 16, and 25 mm/year for the present-day, monsoon, and glacial transition periods, respectively, represent repository-wide averages as calculated in *Drift-Scale Coupled Processes (DST and TH Seepage) Models* (BSC 2004 [DIRS 170338], Appendix B). The mean infiltration scenario is one of three scenarios that represent uncertainties in present-day infiltration and the uncertainty in undisturbed hydrologic properties that arise as a result. The variation of undisturbed hydrological properties does not impact the outcome of this analysis. Thus, for this study, which aims at estimating the impact of any THM-induced disturbance in hydrological properties, it is sufficient to conduct the analysis for the mean-infiltration scenario.

Horizontally, by symmetry, only half of the distance between two adjacent drifts (40.5 m) was modeled because the drift spacing is 81 m. Thus, the left boundary was at the middle plane vertically through a drift, and the right boundary was mid-distance between two adjacent drifts. Both lateral boundaries of the model were mechanically constrained for displacements normal to the boundary and closed for heat and fluid flow by symmetry (Figure 6.3-1). This boundary condition is certainly appropriate for the drifts located in the middle of the repository and for large time after emplacement of the waste compared to the time lag between waste emplacement into two neighboring drifts. The simulation of stress evolution conducted in this analysis and its comparison to other simulations conducted with mountain-scale models, confirm the appropriateness of the fixed mechanical boundary conditions (Section 6.5.3).

The preexcavation ambient thermal and hydrological conditions were derived by running a TH model to steady state, using the prescribed boundary conditions at the ground surface and water table, and the present-day infiltration rate of 6 mm/year. The initial stress field represents the best estimate of the stress field at the repository horizon (Section 5, Assumption 2). The initial vertical stress was estimated based on the weight of the overburden rock mass, with an average saturated bulk rock density of $2.2 \cdot 10^3$ kg/m^3. The magnitude of maximum and minimum principal compressive horizontal stresses are a factor of 0.6 and 0.5 of the vertical stress, with the maximum stress oriented perpendicular to the emplacement drift (CRWMS M&O 1997 [DIRS 103564], Table 3-2, pp. 3–23). As mentioned in Section 5, Assumption 2, the in situ stress field at Yucca Mountain rather oriented with the maximum stress at an angle about 45° to the emplacement drift. However, with an approximately isotropic horizontal stress field (horizontal stresses a factor of 0.5 and 0.6 of the vertical stress) this deviation will have no significant impact on the model results. Furthermore, the estimate of the initial stress is considered sufficiently accurate because this model report concerns itself with thermally induced stresses, which are largely independent of the initial stress field.

An emplacement drift of 5.5 m diameter was simulated as being excavated in both the Tptpmn and Tptpll model domains and the waste emplacement was designed for a heat load of 1.45 kW (initial heat power) per meter emplacement drift (BSC 2004 [DIRS 168489]). Consistently with the reference-mode heat load studied in *Drift-Scale Coupled Processes (DST and TH Seepage) Models* (BSC 2004 [DIRS 170338], Sections 1, 4.1.1.3, 6.2.1.3), the emplacement is set to occur all at once followed by a ventilation period of 50 years with a ventilation efficiency of 86.3 percent (see Section 4.1.1.3 for details and sources). The condition that emplacement of all waste occurs at once leads to the highest possible heat load and therefore the highest possible thermal stress. In reality, all the waste cannot be emplaced at once but is rather planned over a period of 23 years, followed by 50 more years of continuous ventilation. The differences in the THM responses between the case of emplacing all canisters at once and the case of a 23 years emplacement period can only be significant in the early time (less than about 500 years). At a longer time period, the relative difference in time after emplacement in each emplacement drift becomes smaller (e.g. at 500 years the relative difference could be maximum 500/523 = 0.96).

The in-drift geometry for waste package and drip-shield configuration is not explicitly accounted for in the drift scale THM, and the heat transfer between the waste package and the drift wall is simulated with an effective radiative heat exchange within the open drift. The radiative heat exchange within the drift is rapid, so that the temperature difference within the drift should effectively equilibrate. Because the focus of this model report is the quantification of THM processes in the rock outside the drift, the details of the heat transfer within the drift are of secondary importance. This simulation approach (of effective radiative heat exchange within the open drift) is demonstrated to be applicable in the modeling of the DST in Section 7. It is shown in Section 7.4.1, that temperature evolution in the rock agrees well with measured values, and hence the adopted approach is sufficiently accurate for the purpose of this model report.

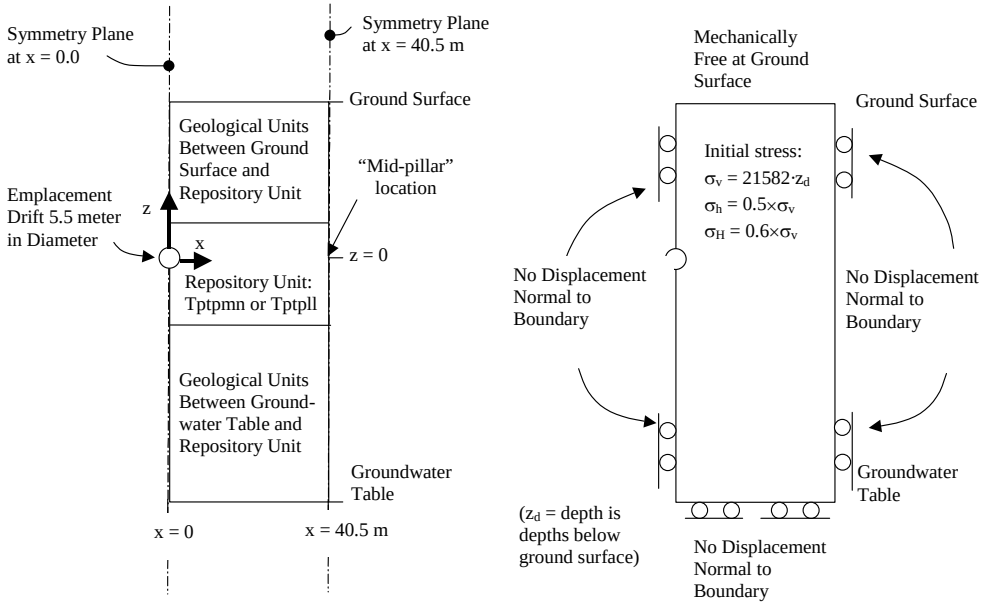

(a) Geometry

(b) Mechanical boundary conditions

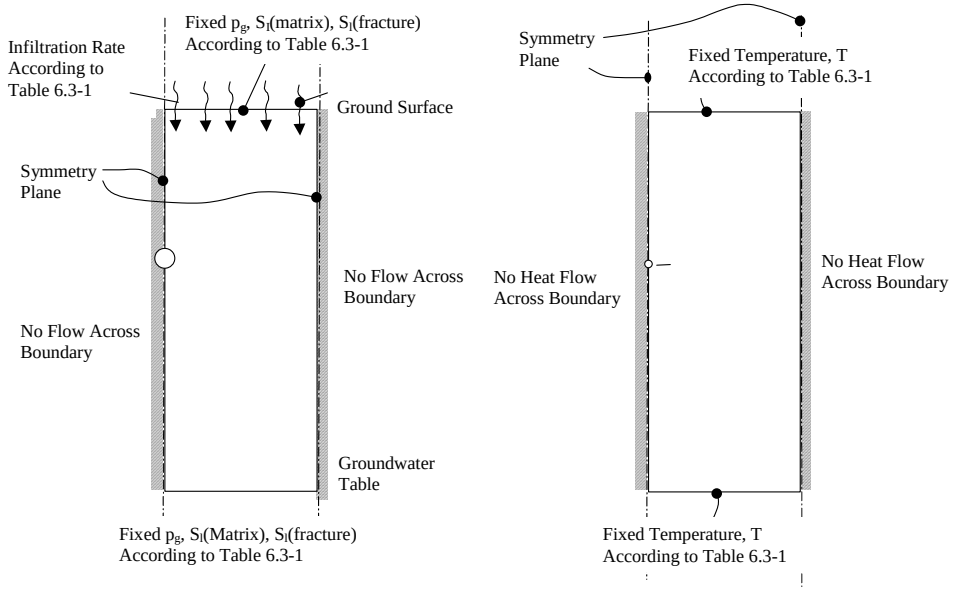

(c) Hydrological boundary conditions

(d) Thermal boundary conditions

Figure 6.3-1. Domain and Boundary Conditions for the Drift Scale THM Model

Table 6.3-1. THM Model Boundary Conditions

Boundary	Boundary Condition	Reference
Top of Tptpmn model domain that represents the ground surface near borehole USW SD-9	T = 17.68 °C Sl = 0.01 P = 86339 Pa Infiltration rate: 6 mm/year 0-600 years 16 mm/year 600-2000 years 25 mm/year >2000 years	Tables 4.1-1a and 4.1-3e Tables 4.1-1a and 4.1-3e Tables 4.1-1a and 4.1-3e Tables 4.1-1a
Bottom of Tptpmn model domain that represents the groundwater table near borehole USW SD-9	T = 31.68 °C Sl = 0.99999 P = 92000 Pa	Tables 4.1-1a and 4.1-3e Tables 4.1-1a and 4.1-3e Tables 4.1-1a and 4.1-3e
Top of Tptpll mode domain that represents the ground surface near the center of the repository	T = 16.13 °C Sl = 0.01 P = 84725 Pa Infiltration rate: 6 mm/year 0-600 years 16 mm/year 600-2000 years 25 mm/year >2000 years	Tables 4.1-1a and 4.1-3e Tables 4.1-1a and 4.1-3e Tables 4.1-1a and 4.1-3e Tables 4.1-1a
Bottom of Tptpll model domain that represents the groundwater table near the center of the repository	T = 32.62 °C Sl = 0.99999 P = 92000 Pa	Tables 4.1-1a and 4.1-3e Tables 4.1-1a and 4.1-3e Tables 4.1-1a and 4.1-3e
Sides	No flux of water, gas, and heat Mechanically fixed for normal displacement	Not Applicable Not Applicable
Drift Wall	Open boundary for water, gas, and heat Mechanically free	Not Applicable Not Applicable
Waste Package Thermal Load	Initial heat of 1.45 kW/m decreasing with time (due to radioactive decay), and reduced by 86.3% during the first 50 years (due to removal by ventilation)	Table 4.1-1a

T = temperature, S_l = liquid saturation, P = pressure

6.4 MATERIAL PROPERTIES

The THM properties used as direct input into the drift scale THM model and their sources are summarized in Section 4. Note that this model report uses the nomenclature for lithostratigraphic units defined in *Geologic Framework Model (GFM2000)* (BSC 2004 [DIRS 170029]), while some properties refer to the same lithostratigraphic units using the nomenclature of the UZ model reports. In addition, TM units are frequently used for mechanical and thermal-mechanical rock properties. The relationship between Geologic Framework Model units, UZ hydrological model units, and TM units are given in Figure 6.4-1.

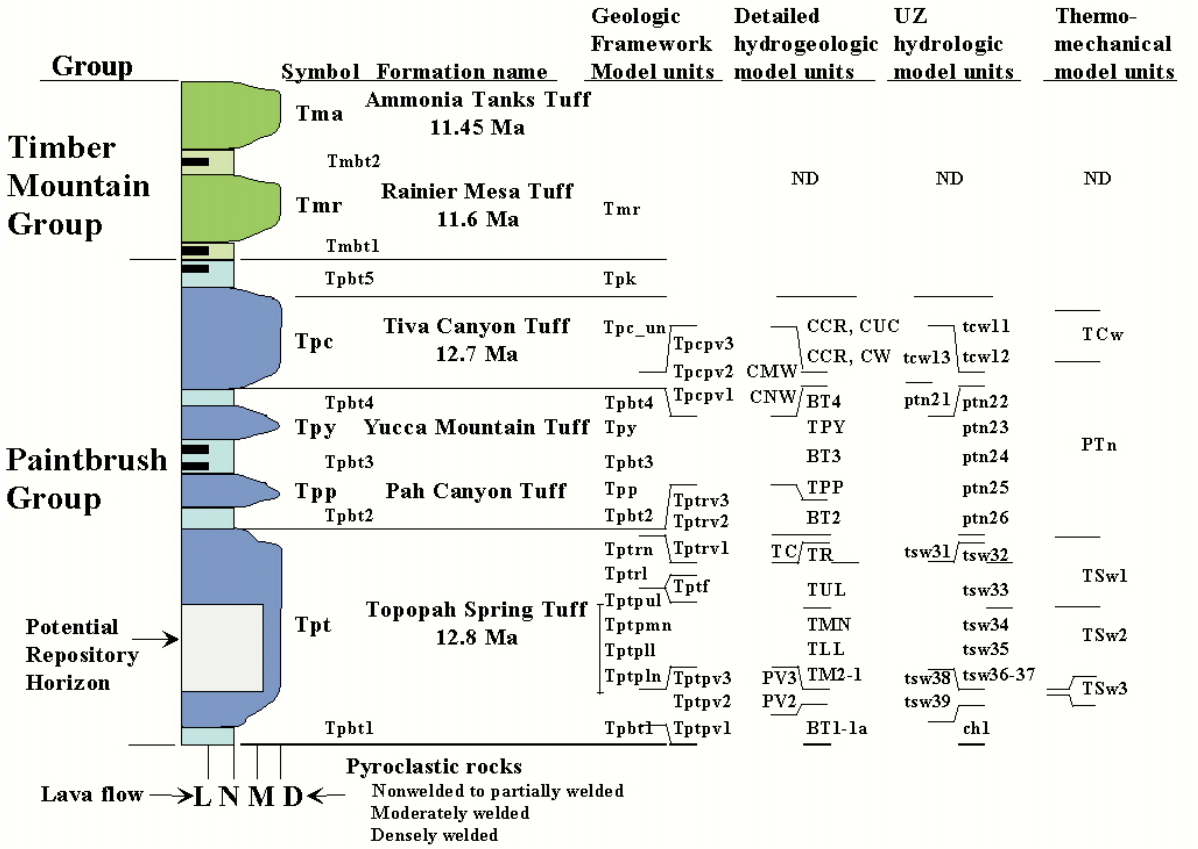

Source: BSC 2004 [DIRS 166107], Figure 6-1.

Figure 6.4-1. Simplified Lithostratigraphic Column of Paintbrush Group and the Rock Units That Form the Repository Horizon

6.4.1 Hydrological and Thermal Properties

The hydrological property set was developed in the mountain-scale calibration runs for the present day ambient conditions at Yucca Mountain (BSC 2004 [DIRS 169857], Section 6.3.2, Table 4). Together with adopted thermal properties, this property set is referred to in this model report as the DS/AFM-UZ02-Mean Property set. It is the same property set considered in both the *Drift-Scale Coupled Processes (DST and TH Seepage) Models* report (BSC 2004 [DIRS 170338], Section 6.2) and *Drift-Scale Coupled Processes (DST and THC Seepage) Models* (BSC 2004 [DIRS 169856], Sections 6.5 and 6.7). The properties implicitly account for the effects of lithophysal cavities because they are calibrated against in situ measurements. For an in-depth discussion on the appropriateness of the TH properties, the reader is referred to the *Drift-Scale Coupled Processes (DST and TH Seepage) Models* report (BSC 2004 [DIRS 170338], Section 6.2) and *Calibrated Properties Model* (BSC 2004 [DIRS 169857], Section 6.3.2).

6.4.2 Mechanical Properties

The basic mechanical properties of the rock mass (Young's Modulus and Poisson's ratio) are developed using an established engineering geological rock mass quality classification system

with associated empirical relationships. These properties are derived within this model report from qualified sources of laboratory measurements and field mapping in the ESF (Table 4.1-1b). The properties are derived in an Microsoft Excel spreadsheet entitled *THM rock mass modulus v1.xls*, which has been submitted to the TDMS under DTN: LB0306DRSCLTHM.001. As a base case, the Young's modulus and Poisson's ratio for the TCw, PTn, TSw1, and TSw2 TM units are developed in *THM rock mass modulus v1.xls*. The mechanical properties of TSw3 are assumed to be equal to TSw2 (Assumption 3, Section 5), and the mechanical properties of the CHn TM unit are set equal to mean values of intact rock properties extracted from DTN: SNL02030193001.026 ([DIRS 108436], Table S99120_002) (Assumption 4, Section 5). The rock mass deformation modulus (Young's modulus of the rock mass) is derived in *THM rock mass modulus v1.xls* using the Geological Strength Index (GSI) according to Hoek and Brown (1997 [DIRS 170501]). The GSI is calculated as:

$$GSI = 9\ln Q' + 44 \qquad \text{(Eq. 6.4-1)}$$

where,

$$Q' = \left(\frac{RQD}{J_n}\right) \times \left(\frac{J_r}{J_a}\right) \qquad \text{(Eq. 6.4-2)}$$

RQD = rock quality designation

Jn = joint set number

Jr = joint roughness number

Ja = joints alteration number.

Following the approach by Hoek and Brown (1997 [DIRS 170501]), the rock mass modulus of deformation is given a formula derived based on the work by Serafim and Pereira (1983 [DIRS 101711]) as (Hoek et al. 2002 [DIRS 162204]):

$$E_m = \left(1 - \frac{D}{2}\right) \cdot 10^{(GSI-10)/40} \qquad \text{(Eq. 6.4-3)}$$

where *D* is a factor that depends on the degree of disturbance to which the rock mass has been subjected by blast damage and stress relaxation (In this case D = 0 because tunnels are mechanically excavated rather than by drill and blast).

The field mapping of the walls along the ESF provides *RQD*, J_n, J_r and J_a sampled for five meters intervals. In the calculation file *THM rock mass modulus v1.xls*, the data from the field mapping are first sorted according to lithostratigraphy and second according to its rock mass quality index (Q'). Thereafter, the location of each five-meter section in the cumulative frequency distribution is calculated and the rock mass modulus is calculated according to Equation 6.4-3. The adopted rock mass Young's modulus for the rock in the main repository units derived by this method is 14.77 GPa for RMQ category 3, which is about 50 percent lower

than the Young's modulus of intact rock determined on core samples from the site (the mean value of Young's modulus for intact rock core samples from TSw2 TM unit is calculated in *THM rock mass modulus v1.xls* to be 33.03 GPa). A reduction of the rock mass modulus on the order of 50 percent is in agreement with other estimates reported by Lin et al. (1993 [DIRS 104585], Table 6-1), and CRWMS M&O (2000 [DIRS 168569], pp. I-2 through I-10). A reduced in situ modulus of elasticity (compared to its value for intact rock) has also been measured in various in situ tests at Yucca Mountain:

1) Field rock mass moduli from borehole jack testing in the SHT block ranged from 3 to 23 GPa (CRWMS M&O 1999 [DIRS 129261], Section 9.6).

2) Plate loading tests conducted at the DST suggested a rock mass modulus ranging from 11.5 to 29.7 GPa (CRWMS M&O 1998 [DIRS 108306], Table 6-7).

3) Previous in situ experiments in welded tuff in the G-tunnel indicated modulus values from 14.7 GPa to 17.6 GPa, about half of the intact rock values (CRWMS M&O 1999 [DIRS 129261], pp. 9-19).

These results are in agreement with in situ measured values of deformation modulus reported in the literature. Typically, the in situ deformation modulus in various types of rocks exhibits a variability and mean values that typically decrease with sample size (da Cunha 1993 [DIRS 168515], Section 3; da Cunha 1993 [DIRS 168514], Figure 10). However, the mean values of deformation modulus typically become constant for a measurement scales above one cubic meter. He (1993 [DIRS 168516]) reviewed 53 references with 258 deformation modulus entries for various rock types (igneous, metamorphic, and sedimentary) for which he calculated a mean value of 16.43 GPa. This value is close to the mean value adopted for the repository units in this study.

The values of the rock mass deformation modulus derived in this study are also consistent with values used in related geomechanical analyses at Yucca Mountain, including analyses of engineered barrier system design and ground control (BSC 2001 [DIRS 155187], Table 4-5a) as well as the *Drift Degradation Analysis* (BSC 2004 [DIRS 166107], Table E-16). In *Ground Control for Emplacement Drifts for SR* (BSC 2001 [DIRS 155187]), a Young's modulus of 15.21 GPa was calculated for a consistent 40 percent cumulative frequency (for the Tptpmn unit in BSC 2001 [DIRS 155187], Table 4-5a, Category 3). In the *Drift Degradation Analysis*, a value of 15.8 GPa was calculated for the TSw2 TM unit (BSC 2004 [DIRS 166107], Table E-16, Category 3). The value 15.8 GPa is calculated based on field mapping both in the ESF and ECRB Cross Drift, whereas the value 14.77 GPa, adopted in this study, is derived based on field mapping in ESF only. A comparison of values derived using data from both ESF and the enhanced characterization of the repository block (ECRB) Cross Drift versus values derived using data from ESF only is provided in the above mentioned calculation file *THM rock mass modulus v1.xls* (DTN: LB0306DRSCLTHM.001). This comparison of mechanical properties using both ESF and ECRB data versus using only ESF data and using a different version of Equation (6.4-3) shows that the Young's moduli for various rock units are almost identical except for the Tptpul unit. For the Tptpul unit, a Young's modulus of 17.3 GPa was used in *Drift Degradation Analysis* unit (BSC 2004 [DIRS 166107], Table E-16, Category 3) based on the alternative version of Equation (6.4-3) and data from both ESF and ECRB, whereas a value

of 19.40 GPa is used in this model report, derived using Equation 6.4-3 and data from ESF only. Using a slightly higher Young's modulus results in a slightly higher thermal stress in the Tptpul unit. This difference does not significantly impact the mechanical behavior near the emplacement drifts, which in this study are considered to be located in the Tptpll and Tptpmn units.

In the newly updated *Subsurface Geotechnical Parameters Report* (BSC 2003 [DIRS 166660]), cumulative probability for Young's modulus for the Tptpmn unit is provided (BSC 2003 [DIRS 166660], Figure 8-55). Linearly interpolating the data (25 percent probability equals 12.986 and 50 percent probability equals 16.743) yields a value of 15.24 GPa at 40 percent a cumulative probability. This is also close to the mean value adopted in this study.

The values given in the above studies for the TSw2 TM unit (15.21, 15.8 and 15.24 GPa) all compare favorable with the values 14.77 GPa adopted in this study. Thus, it can be concluded that a value of Young's modulus around 15 GPa (which is about 50 percent of the value for intact rock) is appropriate for nonlithophysal rock of the repository units and is consistent with values used for average quality rock in other related analyses at Yucca Mountain. Adopting a mean value for the rock mass deformation modulus representing an average rock quality is most appropriate for this analysis, since repository-wide thermally induced stresses are sought. In general, thermally-induced stresses are determined by temperature change, thermal expansion coefficient and deformation modulus. Although the deformation modulus varies spatially in the rock mass depending on the local rock quality, the thermally-induced stresses during the thermal period depend on the repository-wide mean temperature and the repository-wide deformation modulus. Therefore, adopting a repository-wide mean value is appropriate for the purpose of this model report.

As concluded in the previous paragraph, the value of a rock mass deformation modulus of around 15 GPa, derived using the GSI system, is appropriate for a nonlithophysal rock or for a lithophysal rock with relatively low percentage of lithophysal porosity. However, the GSI system does not consider the effect of lithophysal abundance and may therefore not be appropriate for estimating the rock mass deformation modulus in rocks with higher lithophysal porosity. Therefore, a sensitivity analysis is conducted in which mechanical properties for lithophysal rocks were taken from the recent *Drift Degradation Analysis* (BSC 2004 [DIRS 166107], Table E-10). In the *Drift Degradation Analysis*, the mechanical properties of lithophysal rocks are derived from laboratory tests of large-scale samples and from evidence of in situ plate loading tests. In the *Drift Degradation Analysis*, the mechanical properties (deformability and strength) are derived for six rock-quality categories related to the percentage of lithophysal porosity. In the sensitivity case discussed in this report, Category 1 rock properties are adopted, representing a low quality lithophysal rock with relatively high lithophysal porosity. Category 1 rock has a Young's modulus of 1.9 GPa (Table 4.1-3b) compared to 14.77 GPa for the base case properties (Table 4.1-3a, TSw2). A Young's modulus of 14.77 GPa roughly represents a Category 4 rock in the *Drift Degradation Analysis* (BSC 2004 [DIRS 166107], Table E-10), which is a relatively high quality lithophysal rock (high bulk and shear modulus, and high rock strength properties). Thus, for an emplacement drift in the Tptpll unit (Tptpll model domain), the mechanical properties of the rock mass are varied over a sensitivity range spanning from low quality lithophysal rock (Category 1) to relatively high quality lithophysal rock (Category 4). Finally, the adopted strength properties for lithophysal

rock are validated in Section 7.6 against observations of sidewall fracturing in drifts through lithophysal rock at Yucca Mountain.

Assumptions 3 and 4, in Section 5, justify the choice of mechanical properties for TSw3 and CHn TM units located below the emplacement drift. The elastic properties of the CHn are taken from measurements on intact core samples (DTN: SNL02030193001.026 [DIRS 108436]). The three values of Young's Modulus and Poisson's Ratio for the CHn (Table S99119_002, DTN: SNL02030193001.026 [DIRS 108436]) yield mean values of 5.63 GPa and 0.17, respectively.

6.4.3 Thermal Expansion Coefficient

The thermal expansion coefficient adopted for the drift scale THM model is derived from laboratory measurements on intact rock samples (Figure 6.4.3-1). The thermal expansion coefficient in the field could theoretically be equal to or lower than the intact value because of the presence of fractures. At the SHT, the in situ thermal expansion coefficient was determined to be slightly lower than the corresponding values for intact rock (CRWMS M&O 1999 [DIRS 129261], pp. 9-10). On the other hand, analysis of MPBX displacements at the early part of the DST by Sobolik et al. (1999 [DIRS 163202], p. 741) and *Coupled Thermal-Hydrologic-Mechanical Effects on Permeability Analysis and Models Report* (BSC 2001 [DIRS 155957], pp. 21 and 115–125) indicate that the displacements are well predicted if the intact rock thermal expansion coefficient is used. In addition, both laboratory and field measurements have shown that the thermal expansion coefficient increases with temperature (Brodsky et al. 1997 [DIRS 100653], Tables 4-4 through 4-7, pp. 37–40; DTN: SNL01B05059301.006 [DIRS 129168]). Adopting a thermal expansion coefficient that closely represents the intact rock values can be considered as a reasonable upper bound estimate for the purpose of this model report. The intact rock value is a reasonable upper bound of the possible in situ thermal expansion coefficient, which should give a reasonable upper bound of TM impact in the drift scale THM model. Figure 6.4.3-1 shows that the adopted function closely represents maximum intact-rock thermal expansion coefficients for various rock units at Yucca Mountain. Therefore, the linear function shown in Figure 6.4.3-1 is adopted for all rock units in the drift scale THM model. Figure 6.4.3-1 presents the intact values of the thermal expansion coefficient for saturated and dry samples. In general, the thermal expansion coefficients for these rock units (for the expected temperature ranges for each unit) are similar, though the saturated thermal expansion coefficient for the TSw1 TM unit is lower at a temperature range of 75 to 125°C. The lower values of saturated thermal expansion coefficient from the same source were adopted in the *Drift Degradation Analysis* (BSC 2003 [DIRS 166107], Table E-20). Because the in situ rock conditions at Yucca Mountain are neither fully saturated nor dry, a value inbetween dry and saturated could be expected. Again, in this study, a bounding estimate of the thermal expansion is adopted that will emphasize thermal stress and hence emphasize the effect of THM coupling on permeability and fluid flow. The coefficient of thermal expansion as a function of temperature is set to be homogeneous throughout the model. Variation of the coefficient between different layers could potentially induce slip along the interfaces between the layers. However, this is not expected to occur, because the coefficients of thermal expansion measured from intact rock samples from different units at and near the repository level are similar (Figure 6.4.3-1). The unit with lowest coefficient of thermal expansion is PTn, which is located more than 150 m from the repository level and therefore does not have a significant

effect on the coupled THM behavior at the repository level. Hence, use of the same coefficient of thermal expansion for all rock units is adequate for predicting of changes in permeability in the vicinity of the emplacement drifts, which is the main objective of the analyses presented here.

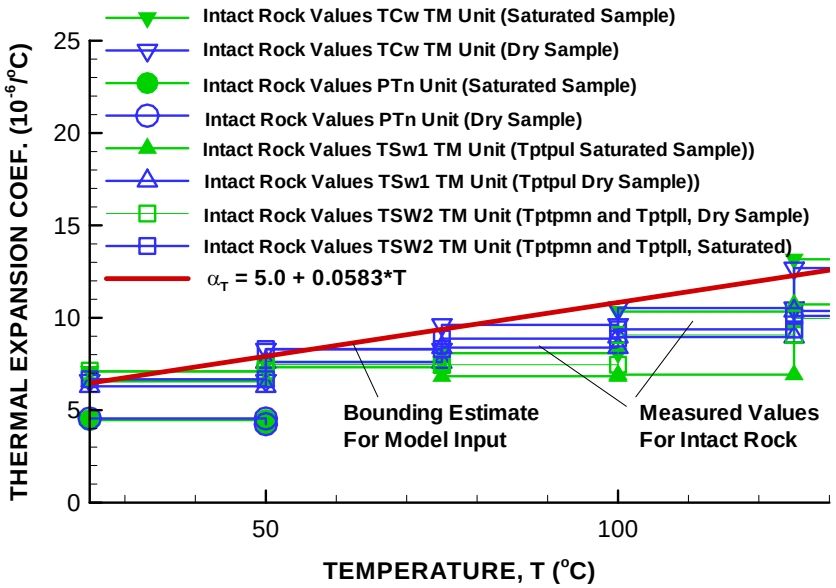

NOTE: Laboratory values are from source data DTN: SNL01B0505931.006 [DIRS 129168], with the calculation of mean data documented in Brodsky et al. (1997 [DIRS 100653]), and represent values determined during heat-up on specimens from NRG boreholes. The red line is matched visually to be close to the maximum values of thermal expansion coefficient at each temperature. The line was matched to maximum values of intact-rock thermal expansion because maximum thermal expansion represents a bounding estimate of maximum thermal-mechanical impact in a THM analysis.

Figure 6.4.3-1. Temperature-Dependent Thermal Expansion Coefficient in the Drift Scale THM Model with Comparison to Values of Intact Rock Samples for Various TM Units

6.4.4 Stress-versus-Permeability Relationship

In this section, the parameters, b_{max} and α, that define the stress-versus-aperture function for fractures (and hence the stress-versus-permeability relationship of the fractured rock mass), are derived. The aim is to derive a bounding estimate of a stress-versus-permeability function leading to maximum possible permeability change in the following THM analysis. The parameters b_{max} and α in the stress-aperture function (Equation 6.2-9) are estimated through model calibration against air-permeability measurements conducted at several field experiments at Yucca Mountain. It is essential that these parameters are determined in situ, at a relevant scale, because of the possible size dependency of the coupled HM properties of rock fractures (Rutqvist and Stephansson 2003 [DIRS 162583]). The parameters b_{max} and α are uniquely determined from three air-permeability measurements, conducted at different stress levels, that represent three points on the stress-aperture function (Figure 6.4.4-1). The first data point on the stress-aperture function is defined by the initial aperture (back-calculated from the measured initial permeability) and the initial stress (estimated from in situ stress measurements). The initial aperture is estimated from the mean fracture frequency, f = 4.32 m^{-1}, and isotropic initial

permeability, k_i = 1 x 10^{-13} m^2 for an ideal cubic block model with equal initial aperture and fracture spacing for three orthogonal fracture sets as shown in Figure 6.2-1b. The permeability for such a system is given by van Golf-Racht (1982 [DIRS 170723], Table 4.6 and Figure 4.20, model 6) as $k_i = (1/18)\times b_i^2\phi_f$, where ϕ_f is fracture porosity given as $3b_i/a$, where $a = 1/f$, leading to $k_i = (1/6)\times b_i^3\times f$. Thus, the initial aperture can be calculated as (Appendix A):

$$b_i = \sqrt[3]{6 \times k_i / f} \qquad \text{(Eq. 6.4-4)}$$

It should be noted that the initial permeability $k_i = 1 \times 10^{-13}$ m^2 represents the mean value measured locally at the DST, whereas the permeability for the Tptpmn unit as a whole is estimated at $k_i = 3.3 \times 10^{-13}$ m^2, i.e a factor of 3.3 higher. However, as will be discussed in Section 6.10.4, it is important that the stress-versus-permeability function be calibrated using consistent and actual local permeability at the field experiments (DST and niches). Therefore, it is appropriate to calibrate the stress-versus-permeability function using the actual mean permeability at the DST, which is $1 \cdot 10^{-13}$ m^2.

The second point on the stress-aperture function represents the conditions at high stress, when fractures are completely closed from a mechanical standpoint but still open to conduct water due to their residual aperture. This point is abstracted from observed air-permeability changes at the DST (Figure 6.4.4-1). In the DST, the temperature in the rock increases up to 200°C, inducing strong thermal stresses expected to compress fractures to a smaller aperture. At the end of a four-year heating phase, the thermal stresses are expected to be substantial around the heated drift, and the fractures are expected to be compressed close to their residual value.

Laboratory experiments on core samples of welded tuff from Yucca Mountain indicate that fractures would be closed to a residual permeability at about 15 MPa compressive normal stress (Peters et al. 1984 [DIRS 121957], Figures E4 through E10). Whereas these laboratory tests cannot be directly used to derive the in situ stress versus permeability function they indicate at which stress level a residual permeability is achieved. Moreover, a comparison between small scale laboratory and large block in situ tests shown in Figure 5 of Rutqvist and Stephansson (2003 [DIRS 162583]), indicates that the residual permeability is reached at a lower stress level for large block in situ tests than for small scale laboratory tests. This evidence supports the argument that residual permeability is reached at a compressive stress of about 15 MPa or even at a compressive stress lower than 15 MPa. At the DST, the compressive thermal stresses at the drift wall are estimated to increase to over 60 MPa (Figure 6.10.2-1) and to over 20 MPa a few meters away from the drift (horizontal stress at the end of the heating is plotted in Rutqvist (2004 [DIRS 170509], Figure 65, p. 169)). Thus, fractures near the DST drift would likely be compressed to a value close to their residual value well before the end of the four-year heating period. At early times, during an aggressive heating regime (as conducted during the DST), the significant temperature change is localized to a relatively small volume of the rock mass around the heat source. The remaining rock mass, where temperature change is still relatively small, provides confinement and resistance to expansion of the heated rock mass. Consequently, the stress increase inside the heated region is fairly isotropic (irrespective of the presence of stress-free ground surface above the DST). It is expected that to some distance from the drift, all joint sets, two subvertical and one subhorizontal, will close during the heating phase of the DST.

Air-permeability measurements at the DST show that the permeability decreases at most by a factor of about 0.15 at the end of the heating period (DTN: LB0208AIRKDSTH.001 [DIRS 160897], borehole Section 59-4 at 1/10/02 8:11 PM) and *Drift-Scale Coupled Processes (DST and TH Seepage) Models* (BSC 2004 [DIRS 170338], Figure 7.4.3.3-2a). The value of 0.15 from Section 59-4 is chosen because this section exhibits the strongest permeability reduction out of all measurements at the DST. At the SHT, air permeability measured in five boreholes sections decreased at most by a factor of 0.24 to its original value at the end of the nine months heating period (CRWMS M&O 1999 [DIRS 129261], Table 8-3 and Figure 8-4). Thus, the adopted value of 0.15 is the strongest decrease in permeability observed in SHT and DST combined. Thus, a bounding value of the maximum permeability reductions is abstracted to derive a bounding estimate of the in situ stress-versus-permeability relationship that emphasizes THM-induced changes in permeability. The factor of 0.15 includes the effects of both TH-induced permeability changes (caused by changes in fracture moisture content) and TM-induced permeability changes (caused by mechanical closure of fractures). The report *Drift-Scale Coupled Processes (DST and TH Seepage) Models* (BSC 2004 [DIRS 170338], Figure 7.4.3.3-2a) shows that TH-induced changes in permeability result in a permeability correction factor of 1.2. The TM-induced permeability correction factor is estimated to be 0.15/1.2 = 0.125. Hence, a residual permeability correction factor, F_{kr} = 0.125, is used for calibration of the stress-aperture function in this model report.

No numerical analysis is required for matching the stress-aperture function to the residual aperture. Applying a very high normal stress, σ_n to Equation 6.2-9, the residual aperture in each of the three fracture sets can be calculated directly. In this calculation, the initial aperture, b_i, is estimated to be 51.8 μm, using Equation 6.4-4, an initial hydraulic permeability of 1×10^{-13} m^2, and a mean fracture frequency of 4.32 m^{-1}, both taken from Table 4.1-4. The initial stresses are calculated as described in Section 5, Assumption 2, for a depth of about 260 m. The calculated residual aperture is then inserted into Equation 6.2-5 to calculate the residual permeability-correction factors F_{kxr}, F_{kyr}, and F_{kzr} in the x, y, and z directions, respectively. Finally, the geometric mean of the residual permeability correction factors is calculated as:

$$F_{kr} = \sqrt[3]{F_{kxr} \times F_{kyr} \times F_{kzr}} \qquad \text{(Eq. 6.4-5)}$$

A third data point on the stress-aperture curve (Figure 6.4.4-1) is obtained from numerical back-analyses of air-permeability measurements, conducted at three excavated niches in the Tptpmn unit and one excavated niche in the Tptpll unit. These tests were conducted to study permeability changes near a drift wall caused by excavation effects (i.e., mechanical unloading of the rock mass near the drift wall, causing a fracture opening and consequent permeability increase). In the Tptpmn unit, the air permeability was measured before and after excavation in 0.3-meter packer-isolated sections along three boreholes located about 0.65 m above the niches (BSC 2004 [DIRS 170004], Section 6.1). Although it results in significant stress relaxation, the deformation of the rock mass above the niche, due to excavation of the niche, is elastic. That is clear from the stresses listed in Appendix A and the fact that the rock mass compressive strength of Tptpmn is over 70 MPa (BSC 2004 [DIRS 166107]; Table E-15 derives a mean rock mass compressive strength of 75.25 MPa for the TSw2 TM unit at the DST). In general, the permeability at the niche tests was found to increase by a factor of about 1 (no change) to

1,000 (an increase by three orders of magnitude), averaging about one order of magnitude (BSC 2004 [DIRS 170004], Section 6.1). It was also found that permeability generally changes more in initially lower-permeability sections.

In this study, the niche excavations were modeled using the FLAC3D V2.0 code to calculate changes in the stress field (Figure 6.4.4-1) using the mechanical properties of the rock mass given in Table 4.1.4. The FLAC3D V2.0 model of the niches is described in Rutqvist (2002 [DIRS 162047], pp. 14 through 18). Based on the calculated stress field, new fracture apertures for each fracture set can be calculated from Equation 6.2-9. The new apertures are then inserted into Equation 6.2-5 to calculate the excavation permeability correction factors F_{kxe}, F_{kye}, and F_{kze} in the x, y, and z direction. Finally, the geometric mean of the excavation permeability correction factors are calculated as:

$$F_{ke} = \sqrt[3]{F_{kxe} \times F_{kye} \times F_{kze}} \qquad \text{(Eq. 6.4-6)}$$

As a matching point, a permeability correction factor of $F_{ke} = 9$ is abstracted from *In-Situ Field Testing of Processes* (BSC 2004 [DIRS 170004], Figures 6.1.2-12 to 6.1.2-16). In these figures, a permeability correction factor of $F_{ke} = 9$ is in good agreement with the observed trend lines for the measured data at Niches 3107, 4788, and CD 1620 at an initial permeability of 1×10^{-13} m^2. A permeability correction factor of $F_{ke} = 9$ represents the mean change in permeability from a large number of measurements taken in 0.3 meter-long borehole intervals. As will be discussed in Section 6.10, it is appropriate to calibrate the model against the mean permeability change in this case because the coupled THM analysis aims at predicting changes in the mean permeability, whereas the permeability distribution remains constant. As shown in Figure 6.10.5-1, the results of the niche-excavation experiments, to which this calibration is made, indicate that the excavation-induced changes in permeability result in a shift in the permeability distribution, while the spread (standard deviation of log permeability) remains approximately constant. Moreover, it is appropriate to calibrate the stress-versus-permeability function against the mean permeability changes caused by the excavation effect because excavation effects are already considered in the seepage analysis (BSC 2004 [DIRS 170338], Section 6.2) as discussed in Section 6.2.4. Thus, the calibrated stress-versus-permeability function provides the best estimate of changes in mean permeability caused by excavation, and a bounding estimate of permeability changes caused by thermally induced stresses.

Figure 6.4.4-2 presents the results of calibrating the parameters b_{max} and α. The two curves in Figure 6.4.4-2 show different combinations of b_{max} and α that satisfy the condition of $F_{kr} = 0.125$ (red curve) and $F_{ke} = 9$ (blue curve). The red curve is determined by a trial-and-error iterative calculation, in which b_{max} is kept fixed at different discrete values between 100 to 400 μm, and for each b_{max}, α is adjusted until the condition $F_{kr} = 0.125$ is satisfied. Similarly, the blue curve is determined by keeping b_{max} fixed and then adjusting α until the condition $F_{ke} = 9$ is satisfied. This calculation, resulting in the red and blue lines of Figure 6.4.4-2, was conducted using an MS Excel spreadsheet as described in Appendix A. A unique solution, satisfying both the condition of $F_{kr} = 0.125$ and $F_{ke} = 9$, is obtained for $b_{max} = 200$ μm and $\alpha = 0.52$ MPa^{-1} (Figure 6.4.4-2). The back-calculated values of $b_{max} = 200$ μm and $\alpha = 0.52$ MPa^{-1} are adopted for all rock units in the drift scale THM model (Section 5, Assumption 6).

To be consistent with other UZ flow and seepage models for the Yucca Mountain, an initial isotropic permeability was adopted when calibrating the stress-versus-permeability function. An alternative method would be to allow for an initially anisotropic permeability field with different initial apertures for fractures belonging to different fracture sets (as a result of the initially anisotropic stress field). A calibration can then be conducted restricting the residual aperture to be the same for all three fracture sets. Such alternative model calibration has been performed and is discussed in detail in Section 6.10.4. It is shown that the method of calibration adopted in this model report, with an initially isotropic permeability field, provides a bounding estimate of the stress-versus-permeability function for vertical fractures that will emphasize the effect of THM coupling on permeability (Section 6.10.4).

The consistency between the normal stress-versus-aperture relationship derived for the stress-versus-permeability function and the mechanical deformation modulus derived from empirical methods in Section 6.4.2 can be checked analytically. The conceptual model cubic block model shown in Figure 6.2-1b is only used for stress-versus-permeability coupling whereas for the stress analysis, a homogeneous, isotropic constitutive material model is used. In the stress analysis, the rock mass deformation modulus is set to be constant and do not vary with normal stress. For example, for the Tptpmn unit a constant deformation modulus of 14.77 GPa was adopted. An analytic expression for the deformation modulus, E_{RM}, of a fractured rock mass with uniform fracture spacing can be derived from (Rutqvist and Stephansson 2003 [DIRS 162583], Equation 68):

$$\frac{1}{E_{RM}} = \frac{1}{E_i} + \frac{f}{k_n} \qquad \text{(Eq. 6.4-7)}$$

where E_i is the Young's modulus of intact rock, f is fracture frequency, and k_n is fracture normal stiffness. The fracture normal stiffness resulting from the slope of the stress-versus-aperture relationship shown in Figure 6.2.2-2 can be calculated from Equation 6.2-8 as

$$k_n = \frac{\partial \sigma_n}{\partial b} = \frac{\exp(-\alpha \sigma_n)}{b_{\max} \alpha} \qquad \text{(Eq. 6.4-8)}$$

For an average in situ stress of -4 MPa (calculated as an average from stress values of -2.89, -3.46 and –5.77 GPa, at the DST, given in Appendix A), and for b_{max} = 200 μm and $\alpha = 0.52\ \text{MPa}^{-1}$, Equation 6.4-8 gives a fracture normal stiffness, $k_n \approx 76.7$ GPa/m. Using this value of the normal stiffness, a fracture frequency of 4.32 m^{-1} (Table 4.1-3a), and an intact rock Young's Modulus of 33.03 GPa (Section 6.4.2), the rock mass modulus estimated from Equation 6.4-7 is $E_{RM} \approx 11.5$ GPa. This compares favorably to the value of 14.77 GPa derived from empirical rock classification methods in Section 6.4.2, but is slightly lower. The slightly lower value of the E_{RM} is expected because b_{max} = 200 μm and $\alpha = 0.52\ \text{MPa}^{-1}$ were derived as a bounding estimate that emphasized the effect of stress on permeability. In Section 7.4.3, an alternative average estimate of b_{max} = 150 μm and $\alpha = 0.6\ \text{MPa}^{-1}$ is derived. Inserting those values into Equation 6.4-8 results in $k_n \approx 122.5$ GPa/m at -4 MPa stress. This in turn gives a rock mass modulus of $E_{RM} \approx 15.3$ GPa, which is very close to the adopted value of 14.77 GPa. It can be concluded that the fracture normal stiffness derived from the stress-versus-aperture relationship in this section results in a rock mass modulus that is consistent with the adopted rock mass modulus derived in Section 6.4.2.

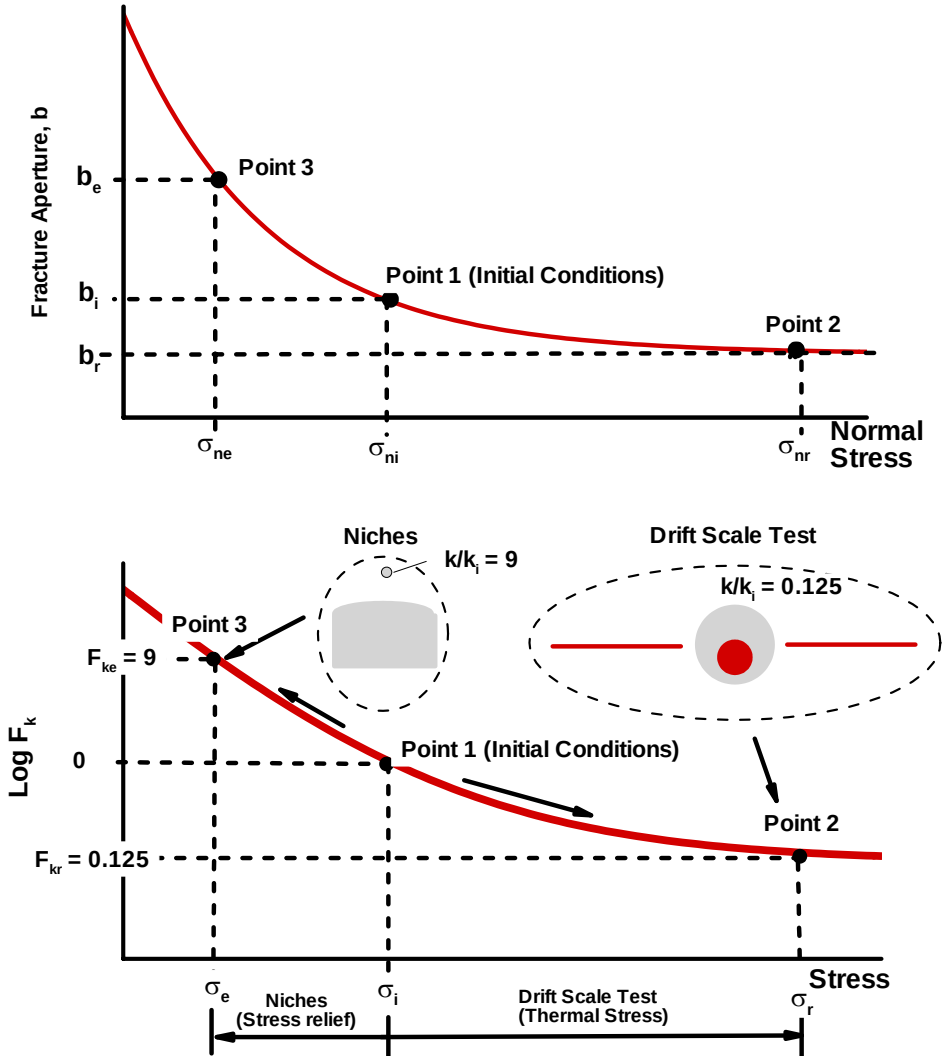

NOTE: The three data points can uniquely constrain the stress-aperture function resulting in the determination of parameters b_{max} and α.

Subscripts n = normal, i = initial conditions, e = conditions after excavation, and subscript r represents conditions at high stress when fracture aperture and fracture permeability as close to their residual values. Hence, F_{ke} is permeability correction factor after excavation and F_{kr} is permeability factor at high stress when fracture aperture and fracture permeability are close to their residual values.

Figure 6.4.4-1. Schematic of Calibration of Stress-Aperture Function Using Three Air-Permeability Measurements Conducted at Three Different Stress Levels

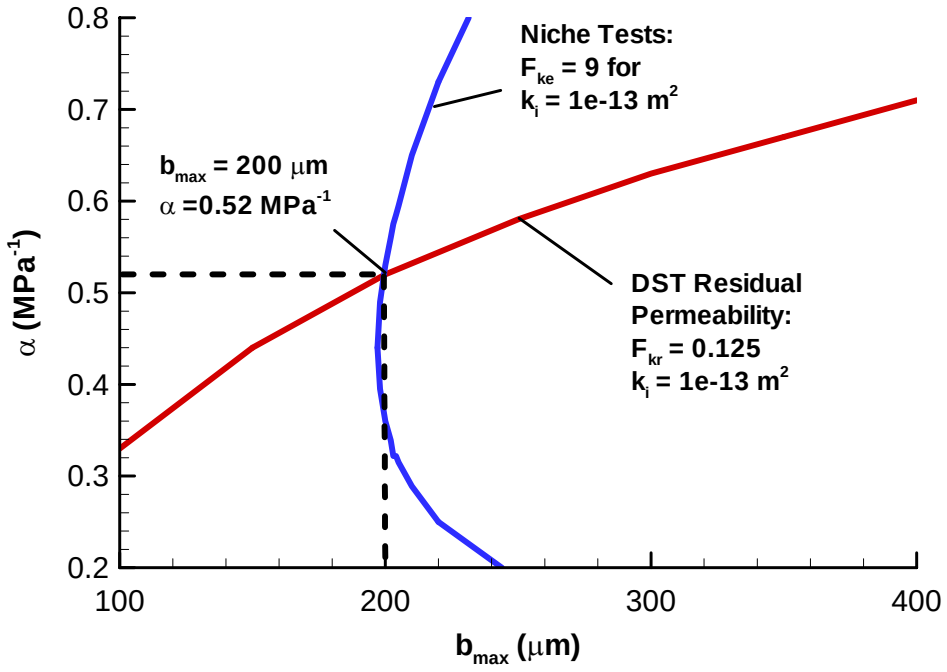

Output DTN: (calculation of red and blue lines) LB0306DSTTHMVL.002.

NOTE: F_{ke} = Permeability correction factor (ke/kI) as a result of stress relief after excavation of a niche.

F_{kr} = Permeability correction factor (kr/kI) as a result of stress increase caused by thermal stress at the DST.

k_i = Initial fracture permeability.

The red and blue lines show combinations of b_{max} and α that satisfy the conditions of F_{ke} = 9 and F_{kr} = 0.125, respectively. The calculations leading to the red and blue lines are described in detail in Appendix A. Both conditions of F_{ke} = 9 and F_{kr} = 0.125 are only satisfied at the intersection of the blue and red lines for b_{max} = 200 μm and α = 0.52 MPa–1.

Figure 6.4.4-2. Determination of Parameters b_{max} and α by Model Calibration Against Air-Permeability Measurements from the DST and Niche Tests

6.4.5 Summary of Developed Parameters

Table 6.4.5-1 summarizes the model parameters developed in this section of the model report. As described in Sections 6.2.4 and 6.4.4, to assess the impact of the THM processes on the flow field, it is sufficient to calculate changes in the mean value of the permeability for a bounding case of relatively strong THM-induced changes in permeability. The bounding case is realized by adopting parameters that emphasize the effect of THM coupling on hydrologic properties and flow field. This includes a reasonable bounding estimate of the thermal expansion coefficient (that emphasizes thermal stress) and a bounding estimate of a stress-versus-permeability function (that emphasizes THM-induced permeability change). The parameters listed in Table 6.4.5-1 provide such bounding estimates of the TM and HM properties, which are adopted in the analysis of THM processes at Yucca Mountain in Sections 6.5 through 6.7.

Table 6.4.5-1. Summary of TM and HM Parameters and Mechanical Properties of the Rock Mass Developed in This Model Report for the Drift Scale THM Model

Geologic. Unit >		Tptpul	Tptpmn	Tptpll	Source
Initial hydraulic fracture aperture	b_i (μm)	179	77	120	Calculated using Equation 6.4-4 using values of frequency and permeability given in Table 4.1-3a
Maximum joint closure for Equation 6.2-9	b_{max} (μm)	200	200	200	Developed by model calibration against field experiments (Figure 6.4.4-2)
Exponent for α for Equation 6.2-9	α (1/Pa)	5.2E-7	5.2E-7	5.2E-7	Developed by model calibration against field experiments (Figure 6.4.4-2)
Thermal expansion coefficient	α_T (10^{-6}/°C)	5.0+0.0583×T	5.0+0.0583×T	5.0+0.0583×T	Derived from laboratory tests (Figure 6.4.3-1)
Young's Modulus	E (GPa)	19.40	14.77	14.77	Extracted from Excel spreadsheet entitled *THM rock mass modulus v1.xls* (Submitted to TDMS under DTN: LB0306DRSCLTHM.001) in which these properties were derived from the qualified sources listed in Table 4.1-1b under items about intact rock properties and field mapping.
Poisson's Ratio	ν (-)	0.23	0.21	0.21	

T = Temperature in °C.

6.5 SIMULATION RESULTS FOR THE Tptpmn MODEL DOMAIN

This subsection presents modeling results for a representative drift located in the Tptpmn unit. Discussion is focused on permeability changes in the vicinity of the emplacement drift and its impact on the flow field. The impact on the flow field is evaluated by a comparison of fully coupled THM simulation results with partially coupled TH simulation results.

6.5.1 Excavation of the Emplacement Drift

The simulation was conducted by first excavating the drift and then implementing a thermal line load into the drift opening. Excavation of the drift causes stress and permeability changes in the rock mass immediately around the drift (Figures 6.5.1-1a and b). Most changes occur near the top and bottom of the drift, where the horizontal permeability increases by about one order of magnitude. Near the springline of the drift, vertical permeability increases while horizontal permeability decreases, resulting in much smaller changes in mean permeability. The increased permeability at the top of the drift is consistent with measured permeability changes at three excavated niches located in the Tptpmn unit (BSC 2004 [DIRS 170004], Table 6.1.2-1).

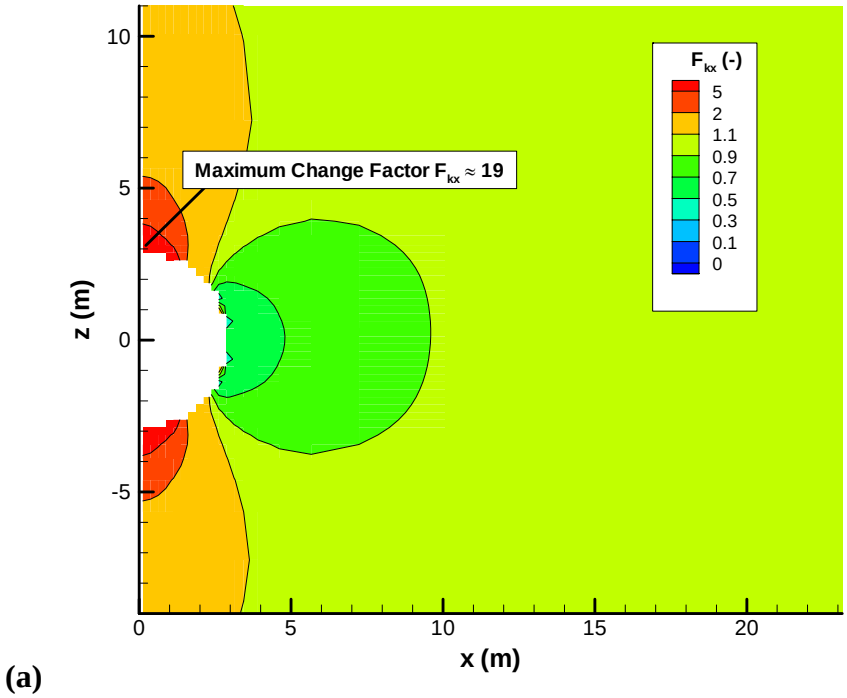

(a)

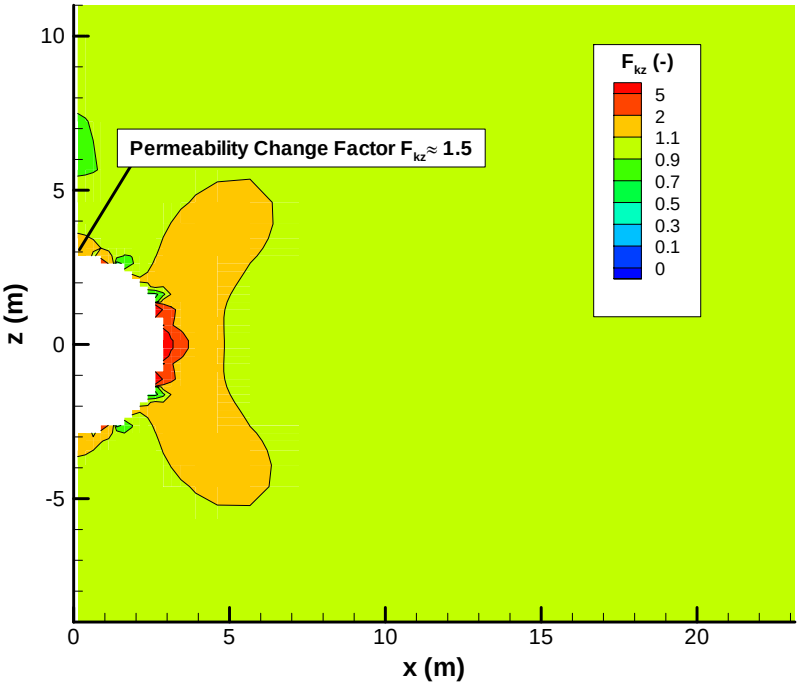

(b)

Output DTN: LB0306DRSCLTHM.002.

NOTE: (a) Correction Factor ($F_{kx} = k_x/k_i$) for Horizontal Permeability; (b) Correction Factor ($F_{kz} = k_z/k_i$) for Vertical Permeability (Tptpmn Model Domain).

Figure 6.5.1-1. Permeability Correction Factor Caused by Stress Redistribution During Excavation of the Emplacement Drift

6.5.2 Evolution of Temperature

After emplacement of the waste in the excavated drift (at time zero), the temperature in the drift wall rises rapidly and peaks at about 80 years (Figure 6.5.2-1). As explained in Section 6.3, the emplacement is conditioned to take place all at once in the entire repository. As shown in Figure 6.5.2-1, the simulated temperature in the rock mass away from the drift continues to rise, and the mid-pillar temperature peaks at about 89°C after 800 years (see location of mid-pillar in Figure 6.3-1a). After about 1,000 years, a general decline in temperature at the repository level takes place. At the same time, the thermal gradient around the repository becomes smaller with the declining temperature difference between the drift wall and mid-pillar. However, at 10,000 years, the temperature is about 45 to 50°C, which is still significantly higher than the initial temperature of about 24°C. The calculated evolution of temperature and peak-temperature is consistent and almost identical for a partially coupled TH and fully coupled THM analysis. Thus, the THM coupling does not significantly impact the temperature evolution.

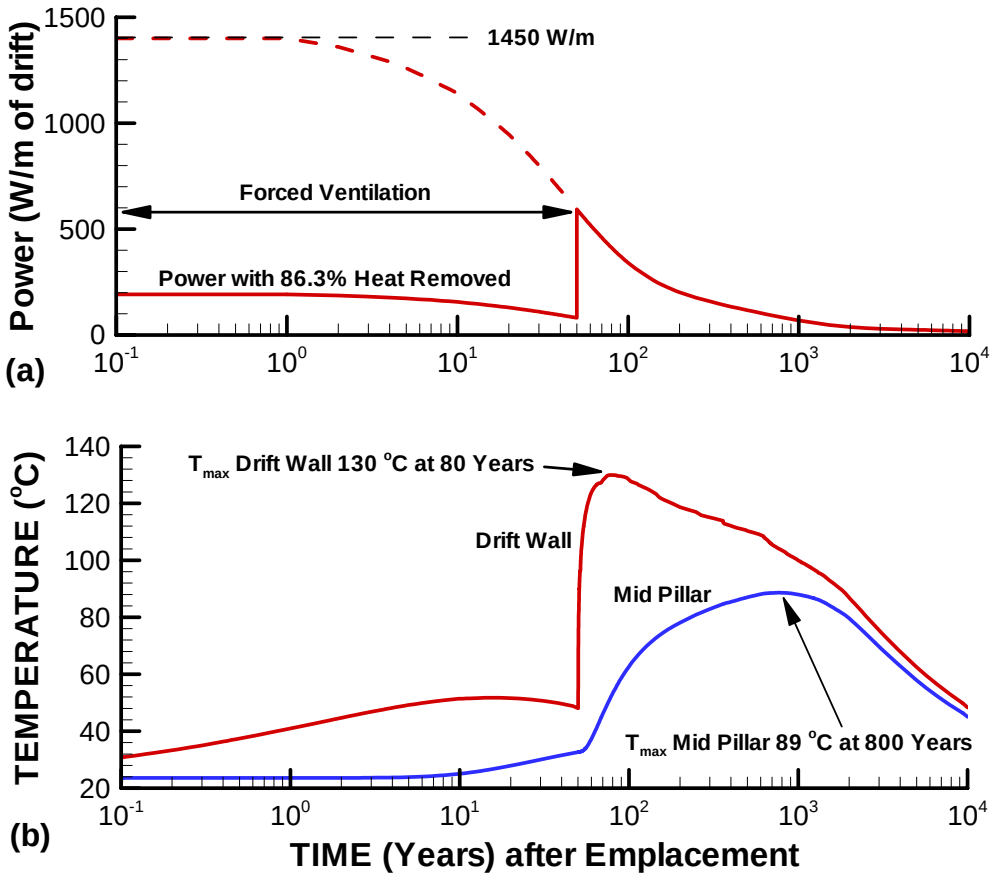

Output DTN: LB0306DRSCLTHM.002.

NOTE: Mid-pillar is a point located at the mid-distance between neighboring emplacement drifts as defined in Figure 6.3-1a. Time 0 is at emplacement of the waste package into the drift, which is assumed to take place all at once for the entire repository.

Figure 6.5.2-1. Evolution of Thermal Power from Waste Package (a) and Temperature at Two Points on the Level of the Emplacement Drifts (b) (Tptpmn Model Domain)

6.5.3 Evolution of Thermal Stress

Large differences between principal stresses can occur near the drift wall because of lack of confinement in the direction normal to the drift wall. Also, redistribution of compressive stresses around the drift implies that concentration of tangential compressive stress will occur near the drift wall. Changes in permeability caused by thermal stresses can occur both near the drift wall and away from the drift wall. It is therefore important to evaluate the thermal stresses near the drift wall as well as in the rock mass away from the drift wall.

Figures 6.5.3-1 and 6.5.3-2 show that the increased rock temperature causes thermal expansion of the rock mass with accompanying deformations and increased compressive stresses. The magnitude of thermally induced stress generally depends on the thermal expansion coefficient, modulus of elasticity, and degree of confinement. Consequently, the highest thermal stresses are created in the horizontal direction as a result of symmetry conditions with fixed lateral boundaries (see mechanical boundary conditions in Figure 6.3-1b). Note that the condition of fixed lateral boundaries result from the bounding condition that emplacement of all waste occurs at once, considering repository-center location.

The fixed lateral boundary conditions are certainly appropriate for the drifts located in the middle of the repository, and for a long time after emplacement of the waste compared to the time lag between waste emplacement into two neighboring drifts. Comparison of stresses around the drift calculated using a coupled regional and local-scale thermal-mechanical model (the local-scale model with several drifts is fed by boundary stress and temperature from the regional model) and a drift-scale model with symmetry boundary conditions (along the drift and halfway between the drifts) is presented in *Drift Degradation Analysis* (BSC 2004 [DIRS 166107], Section 6.2). The agreement between the results of those two models is excellent. The model with symmetry conditions predicts slightly greater horizontal stresses in the crown after 1,000 years of heating. Furthermore, the thermal-stress evolution computed with the drift scale THM model in this model report is consistent with the stress field calculated in the mountain-scale THM model in the *Mountain-Scale Coupled Processes (TH/THC/THM)* (BSC 2004 [DIRS 169866], Section 6.5). Both models (mountain-scale and drift scale THM models) consistently predict an increase in horizontal stress with a peak stress occurring at about 500 to 1,000 years. The magnitude of stress close to the drift is (as expected) higher in the drift scale THM model because of detailed discretization of the emplacement drift. The magnitude of maximum compressive stress at the mid-pillar in the mountain-scale THM model is 11 MPa; whereas the drift scale THM model predicts a maximum compressive stress of about 13 MPa. The slightly higher peak-stress (13 compared with 11 MPa) in the drift scale THM model is explained by a perfect confinement provided by lateral displacement boundary conditions. Thus, four different drift-scale and mountain-scale models, are consistent regarding thermally induced stresses around the emplacement drifts. This further confirms that the zero-displacement restrictions for normal displacement on the lateral boundaries are adequate. Use of the lateral fixed boundaries provides a bonding case for estimating the impact of THM processes because it leads to the highest possible thermal stress. Figure 6.5.3-1 shows that elevated horizontal stress develops at the repository level at 100 years (green contour level around z = 0). At 1,000 years, a zone of increased horizontal stress extends more than 100 m above and below the repository. This zone of increased thermal stress extends over the TSw1, TSw2, and TSw3 TM units, which have a relatively high moduli of elasticity. The thermal stresses are much smaller in the PTn and CHn

units because of the much smaller moduli of elasticity in these units. The zone of increased compressive stress contracts somewhat by 10,000 years. Figure 6.5.3-2 shows that smaller thermal stresses develop in the vertical direction. This is a result of the lack of mechanical confinement in the vertical direction. The maximum compressive stress occurs at the drift crown as a result of thermal stress in the horizontal direction and stress concentration around the drift opening (Figure 6.5.3-3a). Figure 6.5.3-4 shows that the maximum compressive horizontal stress is about 31 MPa at the drift crown and occurs at about 500 years after emplacement. The mid-pillar stress is lower than the stress at the drift crown, but is relevant for assessing the general permeability changes at the repository level in areas away from the immediate surroundings of the drift. This calculated stress evolution is in general agreement with the *Drift Degradation Analysis* (BSC 2004 [DIRS 166107], Section 6.2) with a maximum compressive horizontal stress of about 30 MPa at the drift wall.

The evolution of the hydraulic properties as a result of these thermally induced stress changes is presented in the next section. The potential for thermally induced rock failure at the drift crown is discussed in Section 6.10.2.

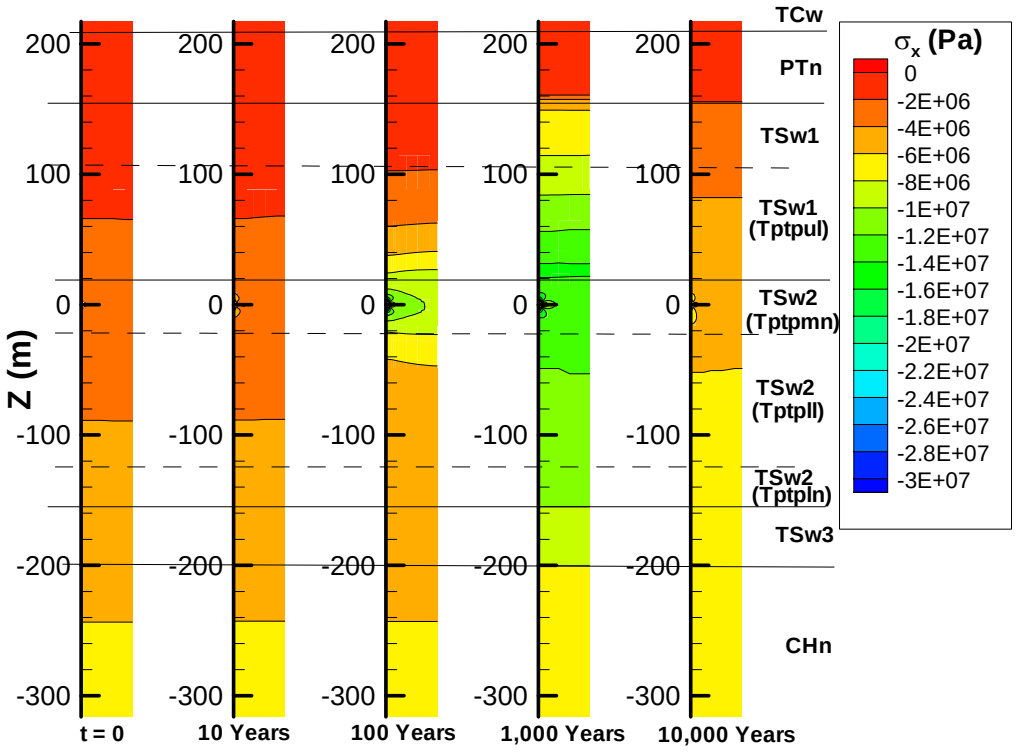

Output DTN: LB0306DRSCLTHM.002.

NOTE: The width of each column is 40.5 meters. The top is the ground surface and the bottom is the water table. In this figure, a negative stress value signifies compressive stress.

Figure 6.5.3-1. Evolution of Horizontal Stress (σ_x) in the Tptpmn Model Domain

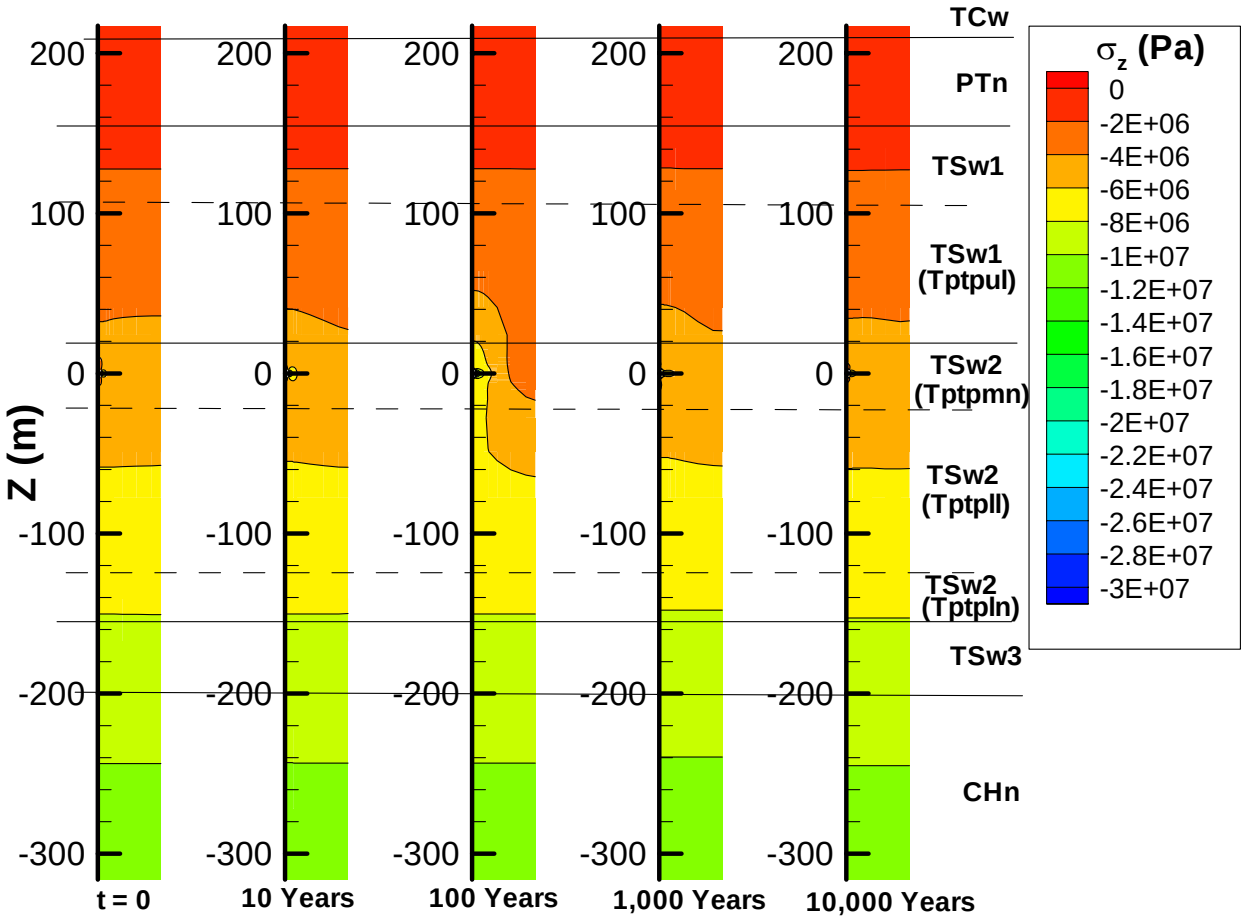

Output DTN: LB0306DRSCLTHM.002.

NOTE: The width of each column is 40.5 meters. The top is the ground surface and the bottom is the water table. In this figure, a negative stress value signifies compressive stress.

Figure 6.5.3-2. Evolution of Vertical Stress (σ_z) in the Tptpmn Model Domain

6.5.4 Evolution of Hydrologic Properties

Figures 6.5.4-1 to 6.5.4-6 present evolution of hydrologic properties at 10, 100, 1,000, and 10,000 years. These times are selected because they represent the following conditions: (1) preclosure conditions (10 years), (2) maximum drift-wall temperature (100 years), (3) maximum thermal-mechanical impact at the repository level (1,000 years), and (4) the end of the post-closure regulatory period (10,000 years).

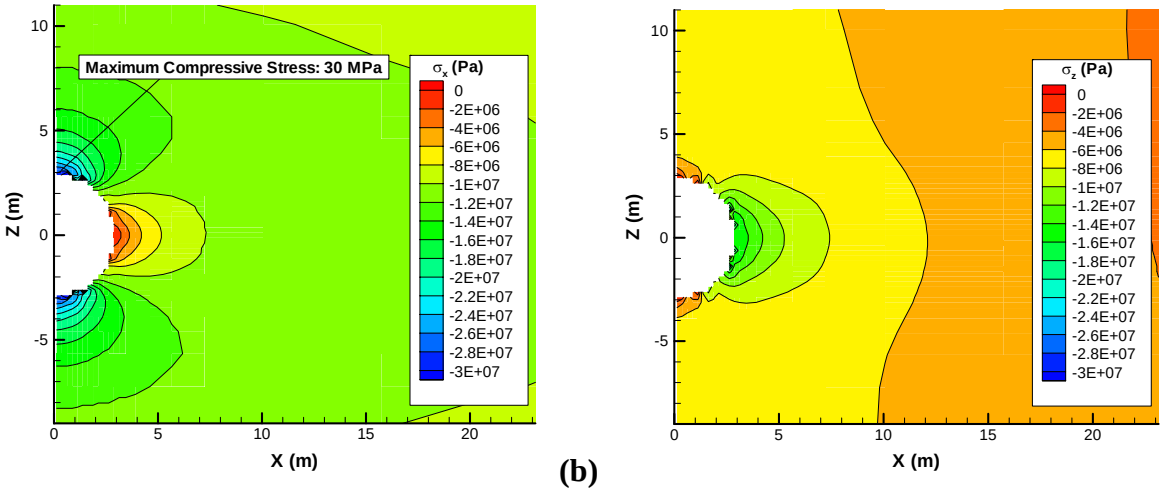

Output DTN: LB0306DRSCLTHM.002.

NOTE: In this figure, a negative stress value signifies compressive stress.

Figure 6.5.3-3. Distribution of (a) Horizontal Stress (σ_x) and (b) Vertical Stress (σ_z) at 100 Years after Emplacement (Tptpmn Model Domain)

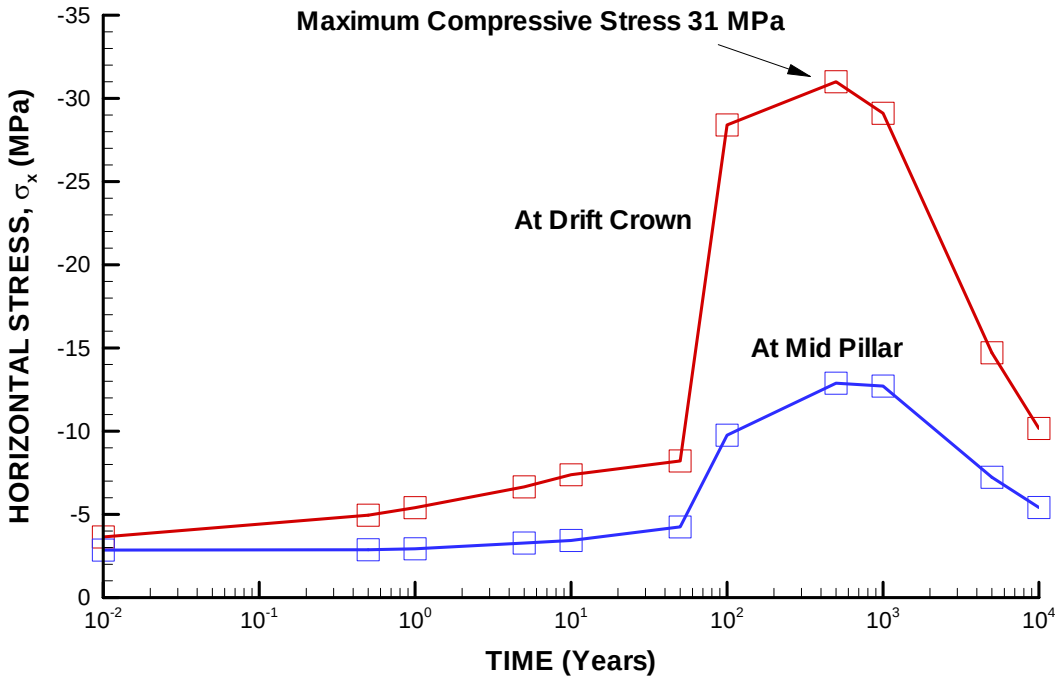

Output DTN: LB0306DRSCLTHM.002.

NOTE: Mid-pillar is a point located at the mid-distance between neighboring emplacement drifts as defined in Figure 6.3-1a. In this figure, a negative stress value signifies compressive stress.

Figure 6.5.3-4. Evolution of Horizontal Stress in the Drift Crown and at the Mid-Pillar Location

TM processes induce compressive stresses that act across fractures, closing them to a smaller aperture, with an associated decrease in permeability and an increase in capillary pressure. In general, the calculation shows that the vertical permeability (Figure 6.5.4-1) changes more than the horizontal (Figure 6.5.4-2), corresponding to the result that horizontal fractures stay open during the entire heating cycle, whereas vertical fractures undergo closure. The horizontal fractures remain open because no significant thermal stress can develop in the vertical direction, on account of the free-moving ground surface. Vertical fractures, on the other hand, close because thermal stresses develop in the horizontal direction as a result of the confinement (no displacement conditions) at lateral boundaries. For example, at 1,000 years, the results show that horizontal compressive stresses have generally increased from 2.9 to 14 MPa at drift level (stress at mid-pillar location in Figure 6.5.3-4), while vertical stresses remain almost unchanged.

Figures 6.5.4-1 and 6.5.4-2 show how the zone of decreased vertical permeability extends farther away from the repository over time. At 10 years, this zone extends about 20 m above and below the emplacement drift. At 1,000 years, permeability changes are observed several hundred meters below the drift and all the way up to the ground surface. The changes are relatively larger in the area above the repository, towards the ground surface, compared to regions below the repository. These trends are associated with different initial fracture permeability in different hydrological units and a small initial stress toward the ground surface. Furthermore, relatively strong permeability changes occur in the Tptpmn unit surrounding the repository ($z = \pm 20$ m) and in the tsw31–33 units ($z = 100$–160 m). The relatively stronger permeability changes in these units are also associated with a relatively small initial fracture aperture.

Figures 6.5.4-3 and 6.5.4-4 present the evolution of permeability around the drift in the Tptpmn unit. At 10 years, this decrease is able to overcome the initial excavation-induced permeability increases, except possibly in areas very close to the crown of the drift (Figure 6.5.4-4a). With time, the permeability decreases further and the zone of decreased permeability propagates farther from the drift. At 100 and 1,000 years, the vertical permeability has decreased to a residual value of around 0.03 to 0.07 of the original permeability because vertical fractures have closed to their residual aperture values. The horizontal permeability at 100 and 1,000 years shows a weaker reduction in permeability with a permeability correction factor of about 0.4. At 10,000 years, the declining rock temperature and thermal stresses cause permeability to recover somewhat. However, at the drift crown, the vertical permeability still remains at one order of magnitude below its original value. Figures 6.5.4-5 and 6.5.4-6 present the changes in fracture capillary pressure, that are calculated according to the Leverett correction function in Equations 6.2-3 and 6.2-6. In general, the capillary pressure increases because of fracture closure, except very close to the drift, where the capillary pressure decreases because of horizontal fracture opening. The calculated changes range between a factor of 0.6 to 2.

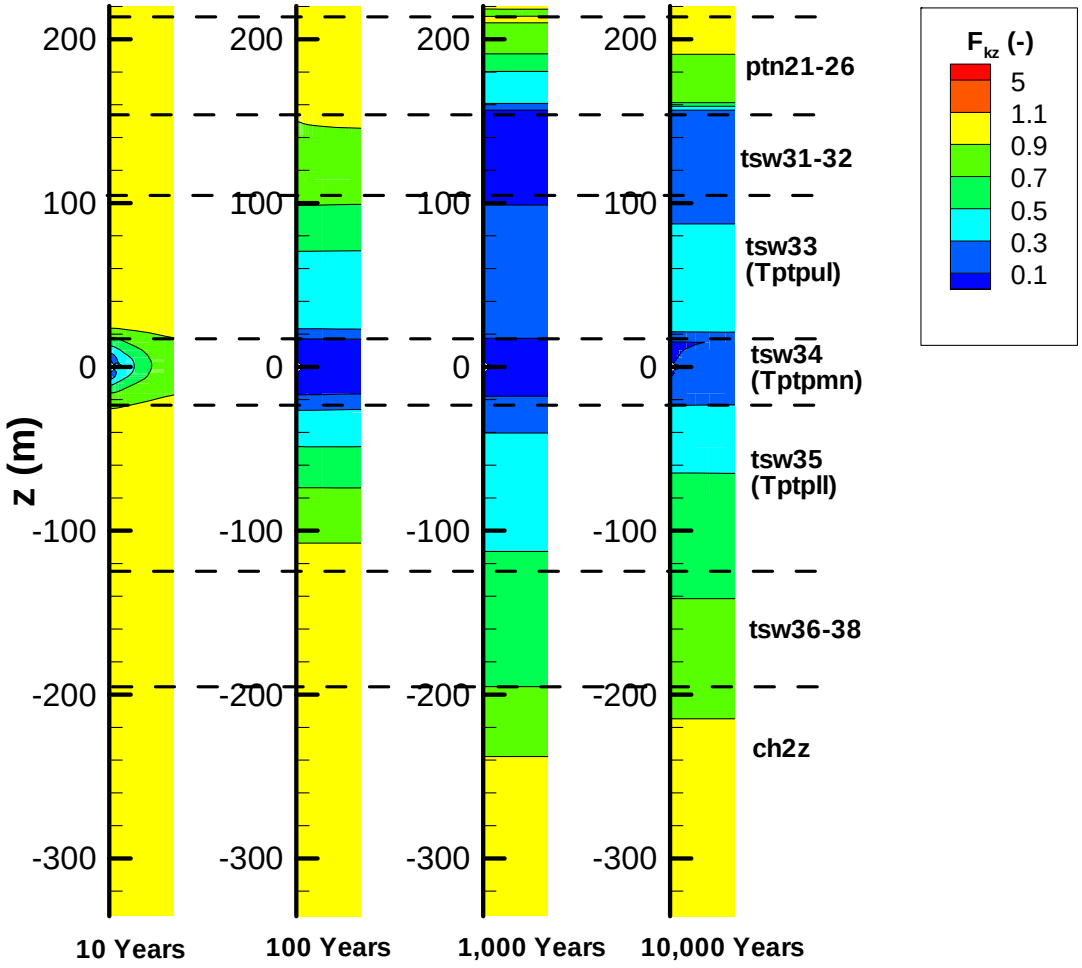

Output DTN: LB0306DRSCLTHM.002.

NOTE: The width of each column is 40.5 meters. The top is the ground surface and the bottom is the water table.

Figure 6.5.4-1. Evolution of Vertical Permeability Correction Factor ($F_{kz} = k_z/k_i$) Relative to Pre-Excavation Permeability in the Tptpmn Model Domain

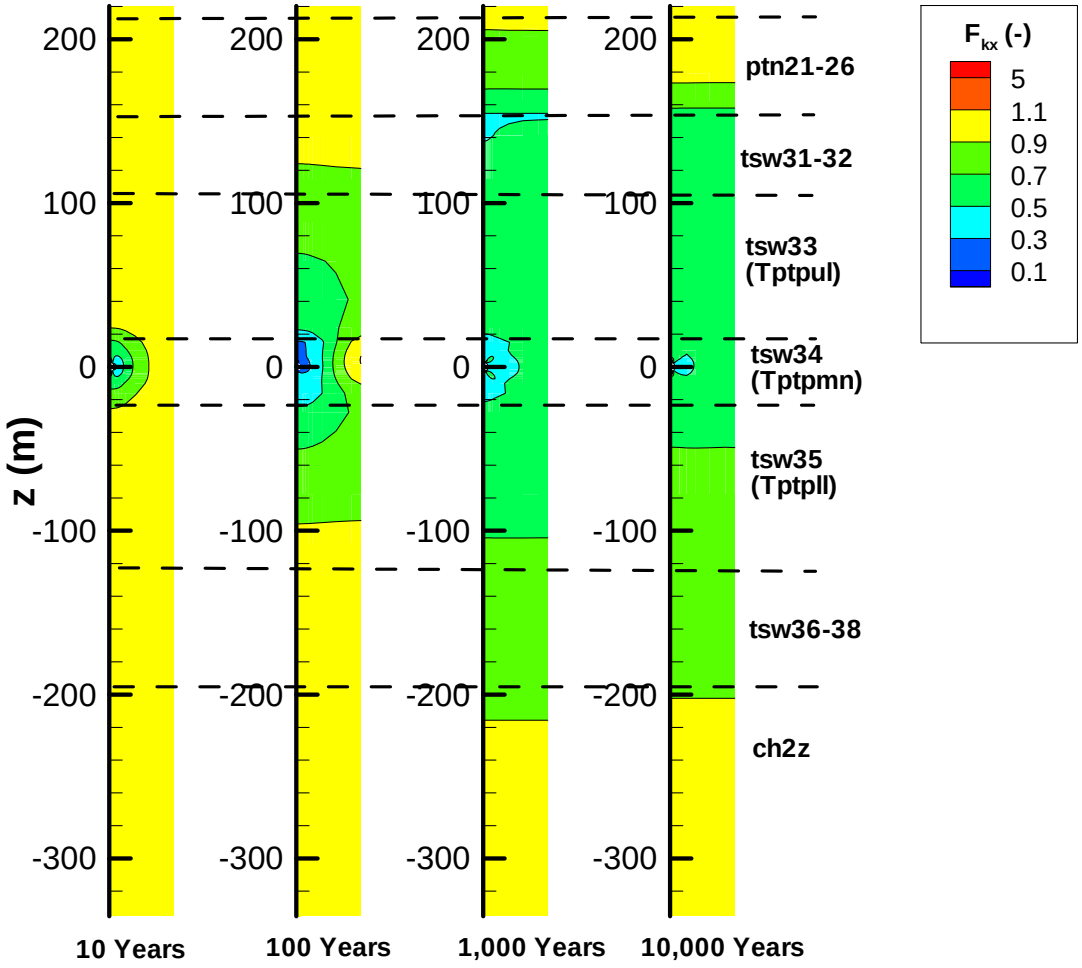

Output DTN: LB0306DRSCLTHM.002.

NOTE: The width of each column is 40.5 meters. The top is the ground surface and the bottom is the water table.

Figure 6.5.4-2. Evolution of Horizontal Permeability Correction Factor ($F_{kx} = k_x/k_l$) Relative to Pre-Excavation Permeability in the Tptpmn Model Domain

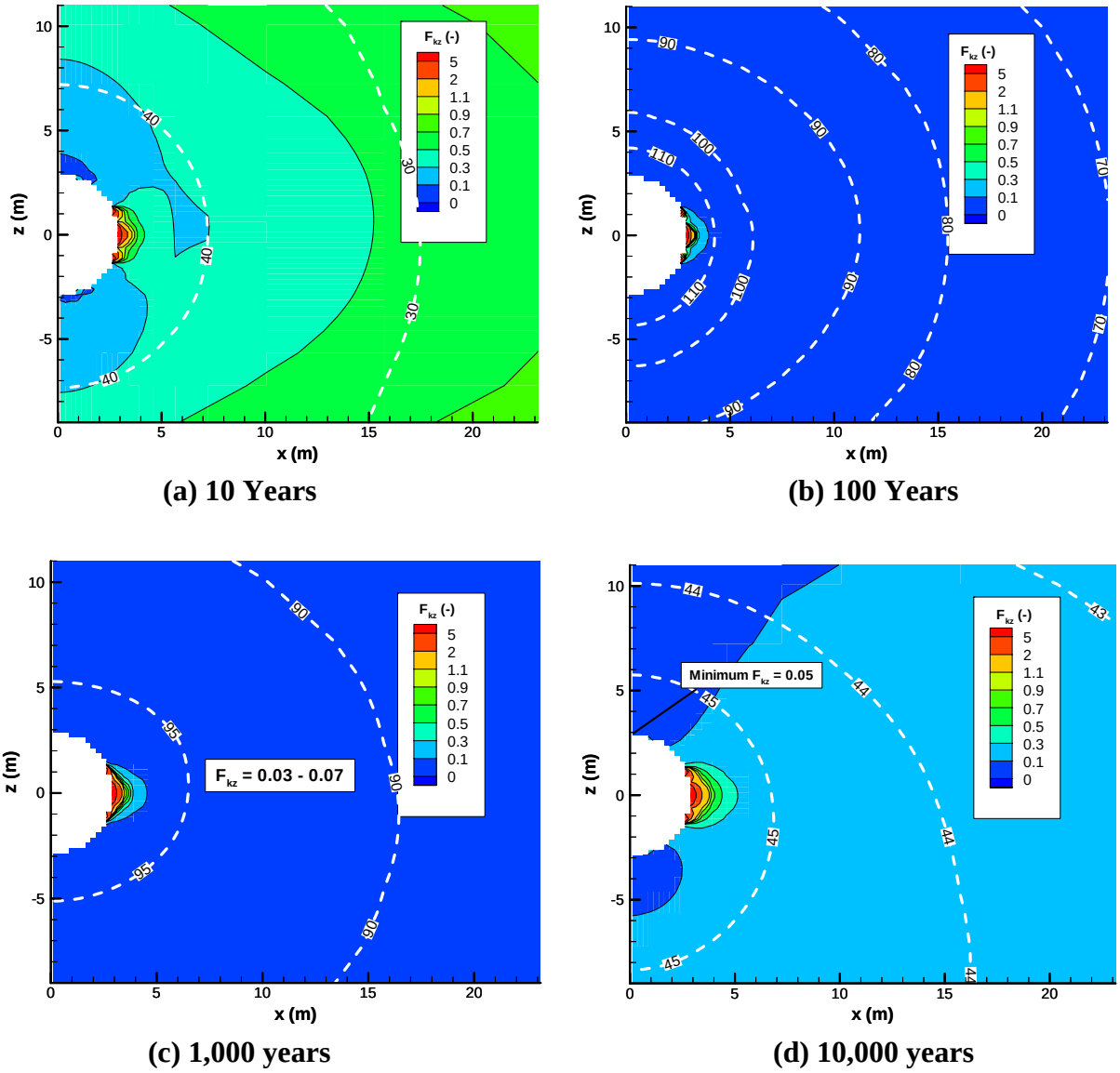

(a) 10 Years

(b) 100 Years

(c) 1,000 years

(d) 10,000 years

Output DTN: LB0306DRSCLTHM.002.

NOTE: Dashed contour shows temperature in °C.

Figure 6.5.4-3. Evolution of Vertical Permeability Correction Factor ($F_{kz} = k_z/k_l$) Relative to Pre-Excavation Permeability Around the Emplacement Drift in the Tptpmn Unit

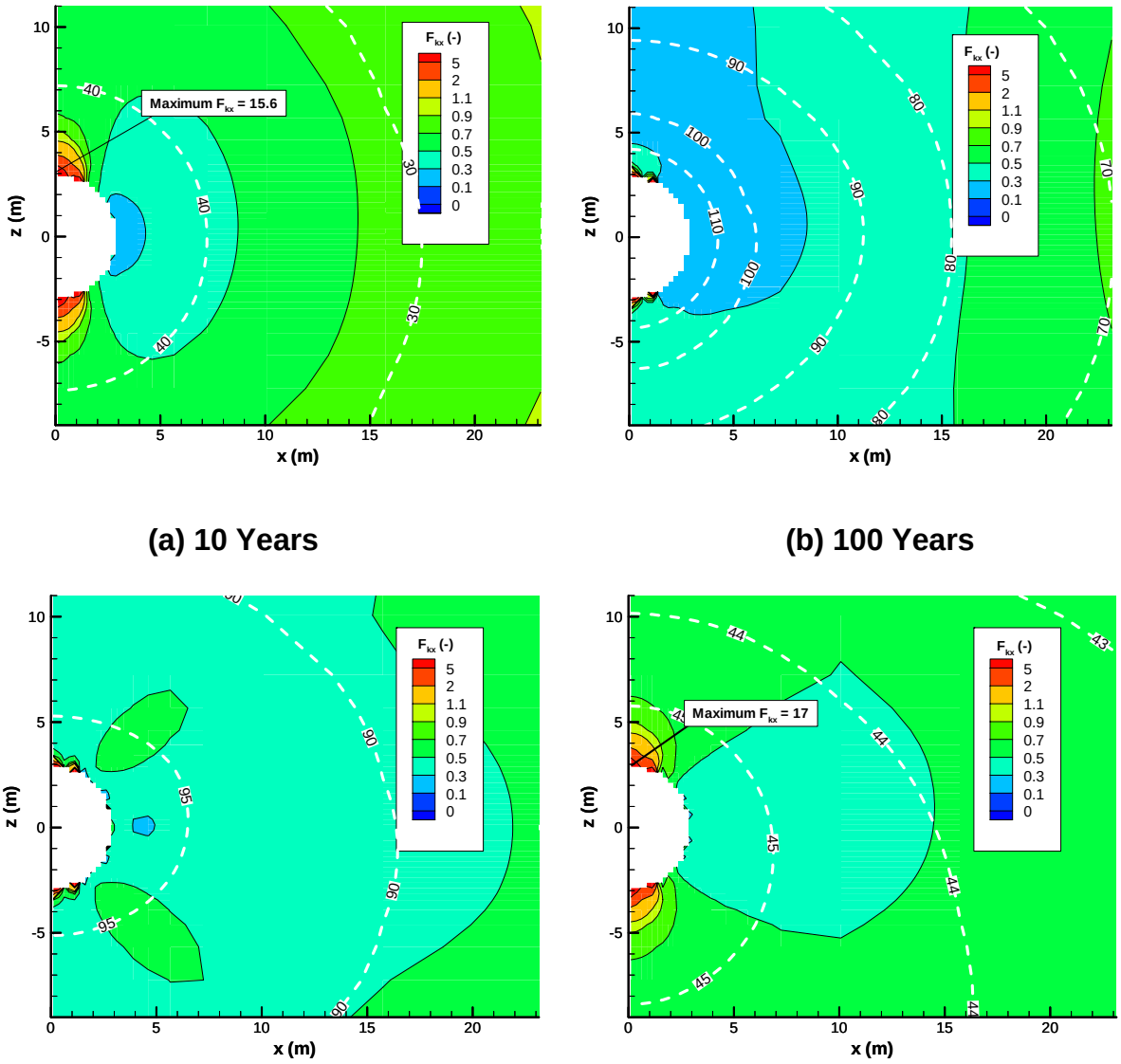

(a) 10 Years

(b) 100 Years

(c) 1,000 years

(d) 10,000 years

Output DTN: LB0306DRSCLTHM.002.

NOTE: Dashed contour shows temperature in °C.

Figure 6.5.4-4. Evolution of Horizontal Permeability Correction Factor ($F_{kx} = k_x/k_I$) Relative to Pre-Excavation Permeability Around the Emplacement Drift in the Tptpmn Unit

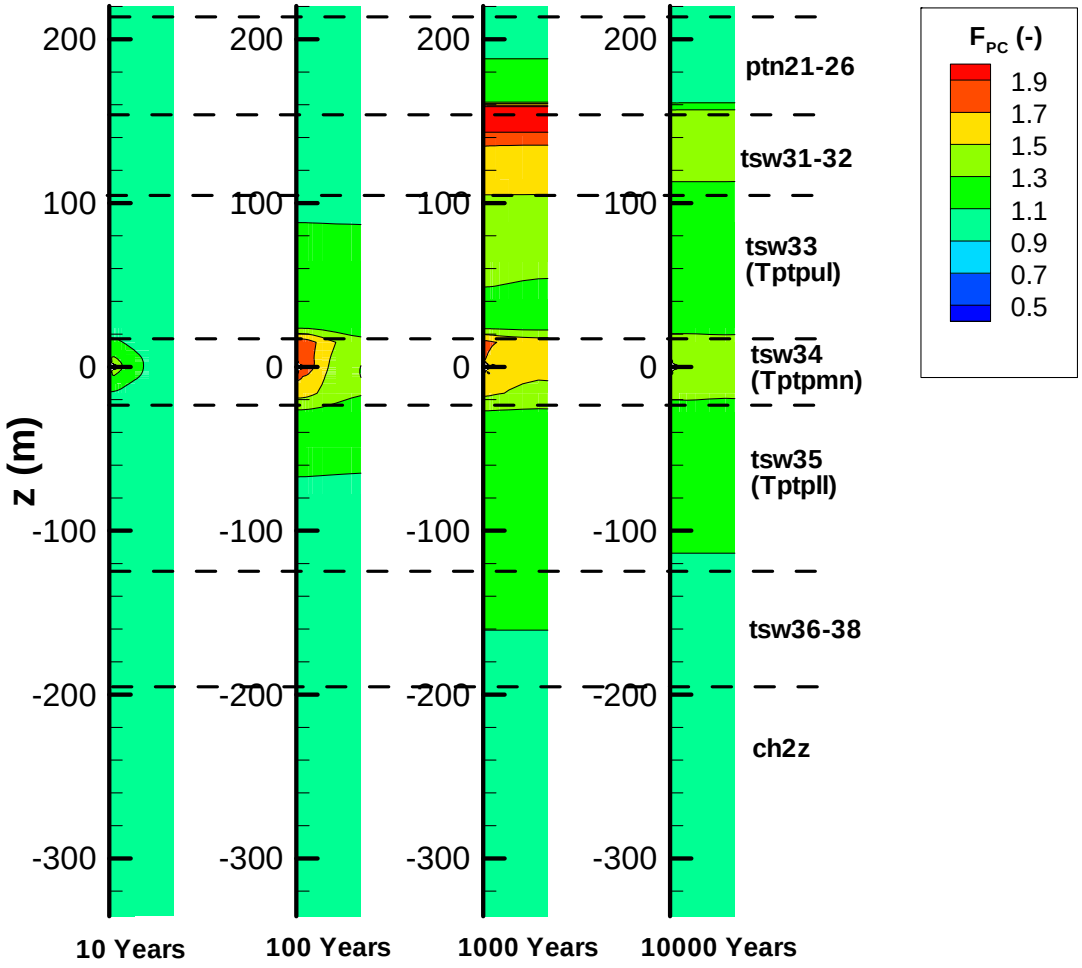

DTN: LB0306DRSCLTHM.002.

NOTE: The width of each column is 40.5 meters. The top is the ground surface and the bottom is the water table.

Figure 6.5.4-5. Evolution of Stress-Induced Capillary-Pressure Correction Factor ($F_{PC} = P_c/P_{ci}$) Relative to Pre-Excavation Value in the Tptpmn Model Domain

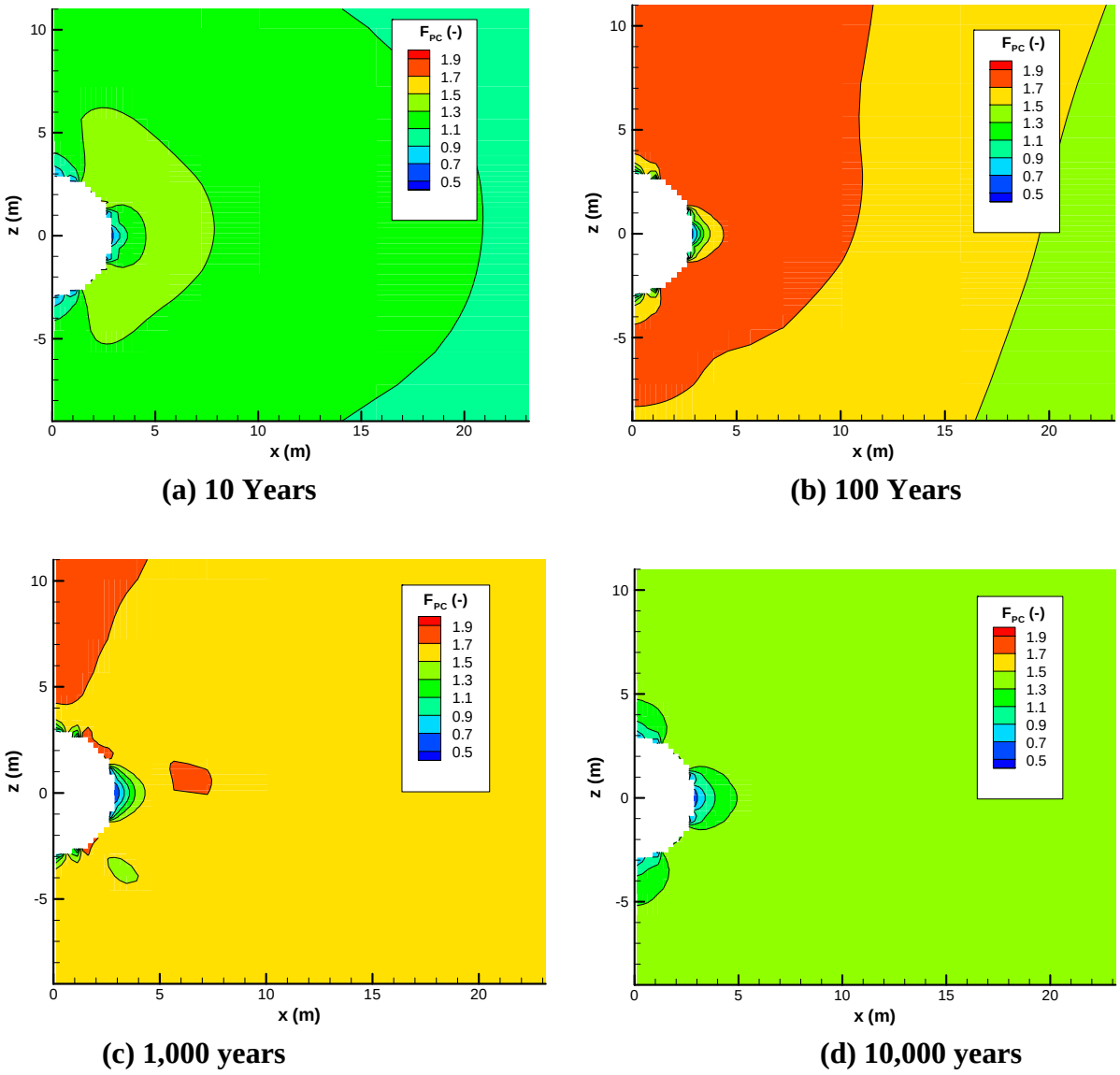

Output DTN: LB0306DRSCLTHM.002.

Figure 6.5.4-6. Evolution of Stress-Induced Capillary-Pressure Correction Factor ($F_{PC} = P_c/P_{ci}$) Relative to Pre-Excavation Values Around the Emplacement Drift in the Tptpmn Unit

6.5.5 Impact on Fluid Flow Field

The impact of HM coupling is investigated by comparing a fully coupled THM simulation with a TH simulation. In the TH simulation, the hydrological properties of the rock mass are constant in time, which means that the coupling between hydrologic and mechanical processes—the HM coupling, is neglected. The impact on the flow field is investigated by comparing vertical liquid flux in the fractured continuum and fracture liquid saturation. Saturation and vertical percolation flux distributions at 10, 100, 1,000, and 10,000 years, with and without HM coupling (TH and THM), are shown in Figures 6.5.5-1 and 6.5.5-2 for the entire Tptpmn model domain. The main difference in saturation profiles between TH and THM results is a slightly higher saturation in

the Tptpmn unit at z = -20 to 20 m (Figure 6.5.5-1) and in tsw31 and tsw32 at z = 100 to 140 m. These changes appear to be associated with changes in the capillary pressure function (Figure 6.5.4-5). The liquid flow patterns, on the other hand, are quite similar between the TH and THM cases (Figure 6.5.5-2). One reason for the similarity is that the reduced permeability is accompanied by a higher relative permeability from the increased liquid saturation, which compensates for part of its impact. Another reason is that permeability reduction is constant horizontally across the flow domain. Since the vertical downward flux cannot flow around regions of reduced permeability, it is thus forced to take the same flow pattern. Only in the area close to the repository does a noticeable change in the flow pattern occur.

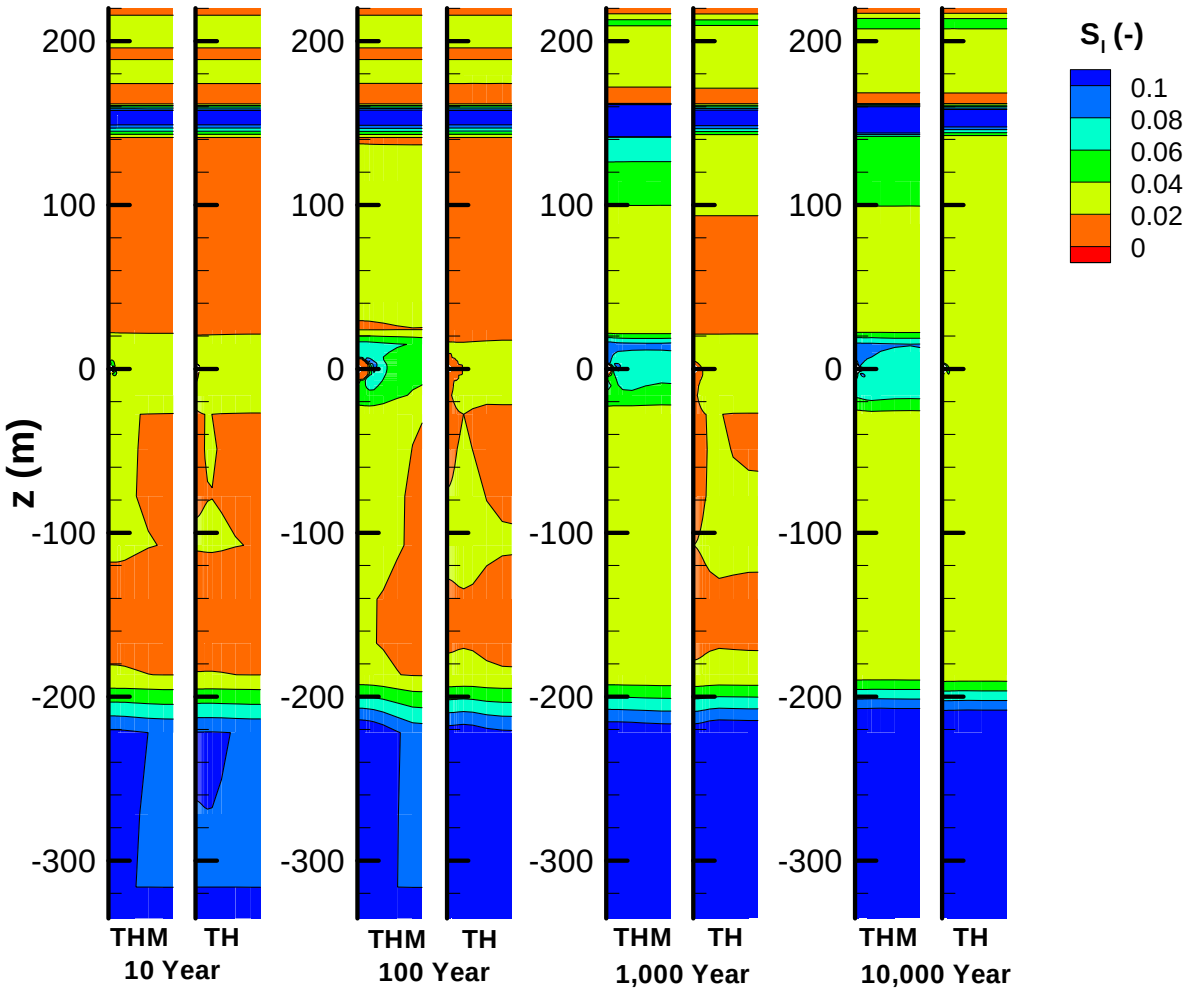

Output DTN: LB0306DRSCLTHM.002.

NOTE: The width of each column is 40.5 meters. The top is the ground surface and the bottom is the water table.

Figure 6.5.5-1. Comparison of the Distribution of Liquid Saturation (S_l) in the Fractures for a Fully Coupled THM Simulation and TH Simulation (Tptpmn Model Domain)

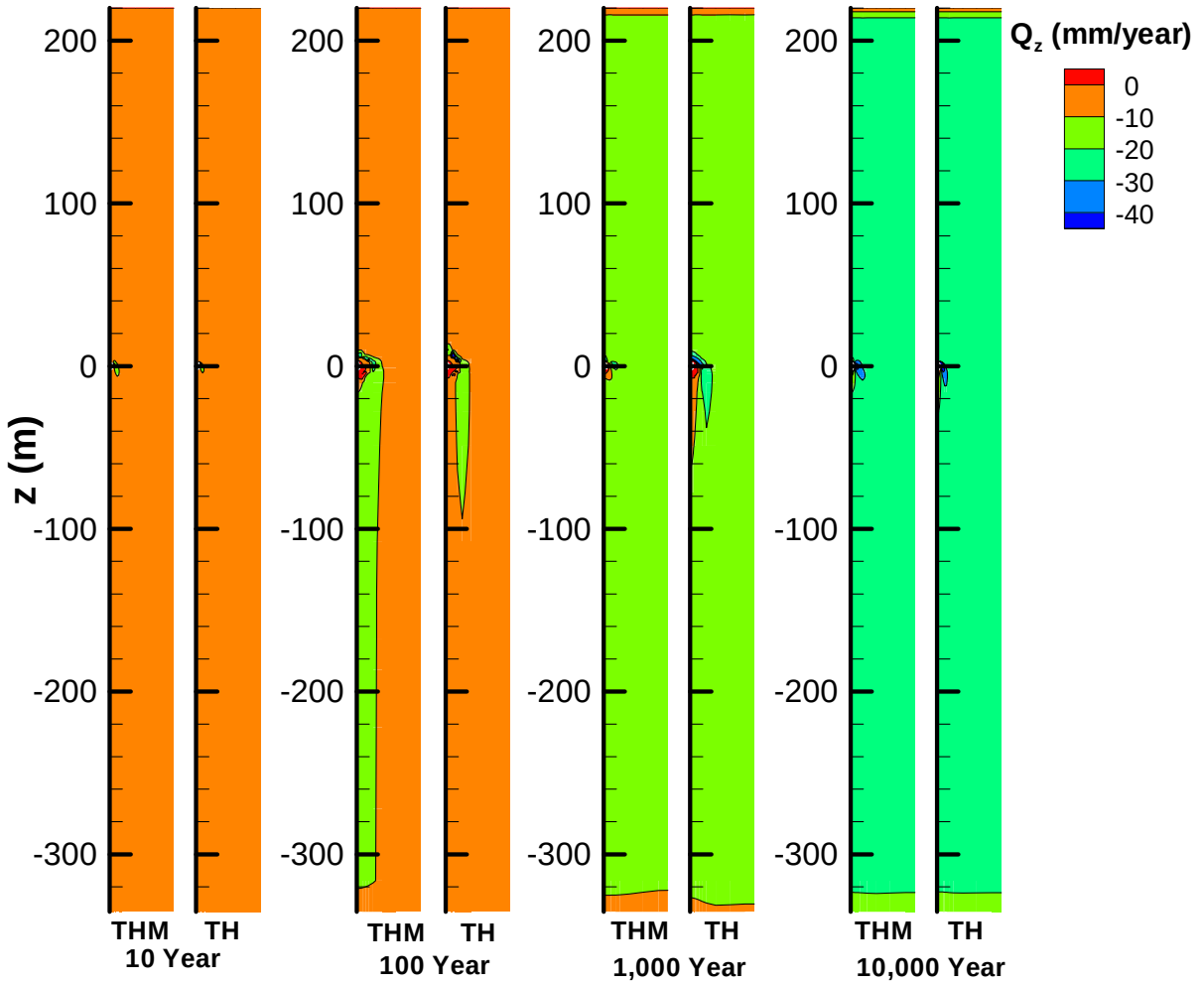

Output DTN: LB0306DRSCLTHM.002.

NOTE: The width of each column is 40.5 meters. The top is the ground surface and the bottom is the water table.

Figure 6.5.5-2. Comparison of the Distribution of Vertical Liquid Flux (Q_z) for a Fully Coupled THM Simulation and TH Simulation (Tptpmn Model Domain)

Figures 6.5.5-3 to 6.5.5-5 present a comparison between the TH and THM flow fields in the Tptpmn unit around the emplacement drift. At 100 years, the formation of a dryout zone and a condensation zone above the drift is apparent for both TH and THM results (Figure 6.5.5-3). It is shown that vertical liquid flow is redirected around the dryout zone. In Figures 6.5.5-3 to 6.5.5-5, there are some differences in the distribution of the vertical liquid flux between TH and THM results, which appear to be related to calculated changes in capillary pressure as shown in Figure 6.5.4-6. However, the main impact of the THM processes is that the dryout zone around the emplacement drift is smaller (Figure 6.5.5-4). In the THM modeling, the dryout zone has contracted to the drift wall at about 1,000 years. This smaller dryout zone is caused primarily by a significantly smaller fracture permeability, which reduces the convection of heat with gas flow and, thereby reduces the heat-pipe effect, leading to an accelerated rewetting of the dryout zone.

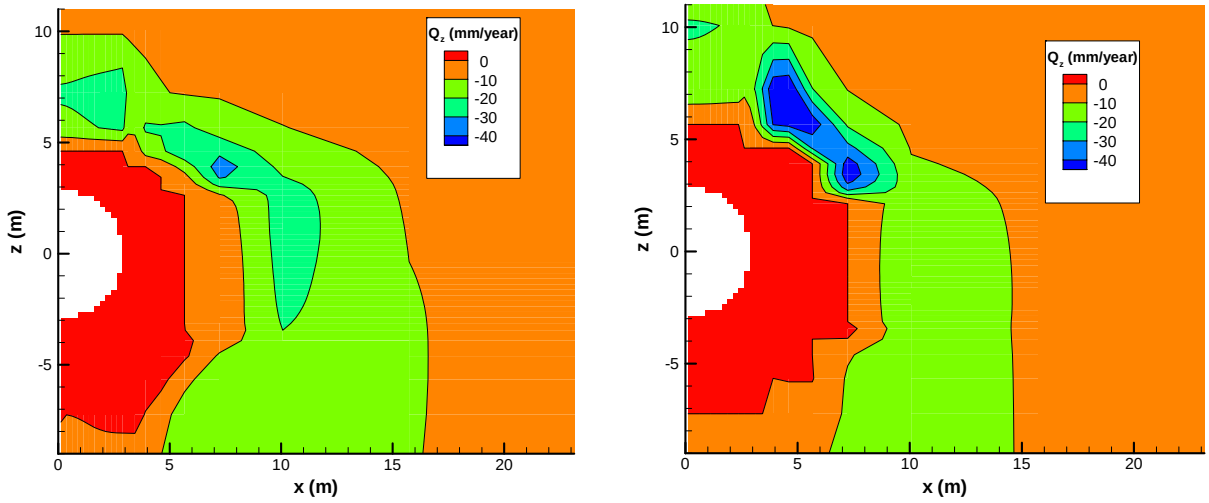

(a) THM **(b) TH**

Output DTN: LB0306DRSCLTHM.002.

Figure 6.5.5-3. Comparison of the Distribution of Vertical Percolation Flux (Q_z) in Fractures at 100 Years for a Fully Coupled THM Simulation and TH Simulation (Tptpmn Model Domain)

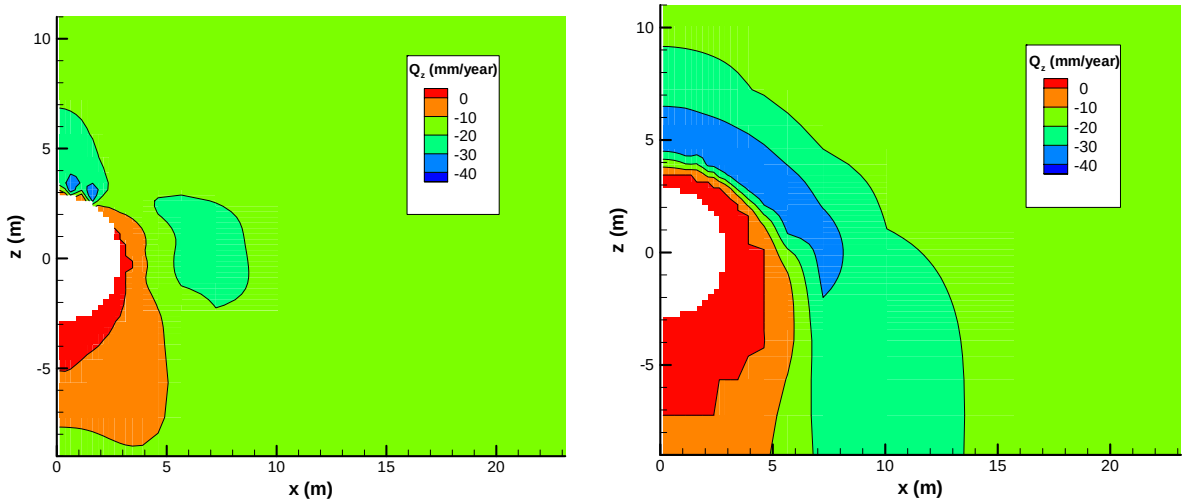

(a) THM **(b) TH**

Output DTN: LB0306DRSCLTHM.002.

Figure 6.5.5-4. Comparison of the Vertical Percolation Flux (Q_z) in Fractures at 1,000 Years for a Fully Coupled THM Simulation and TH Simulation (Tptpmn Model Domain)

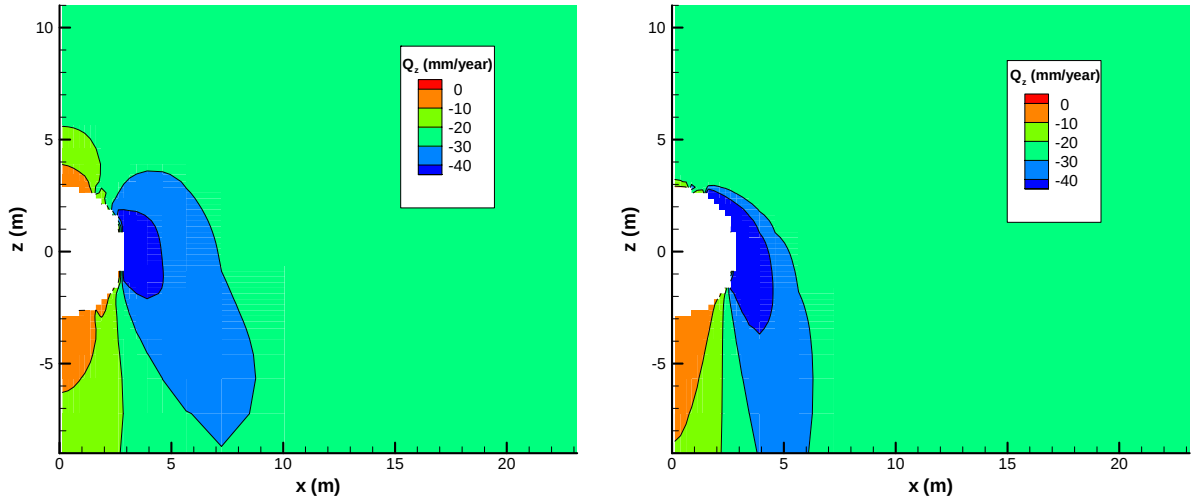

Output DTN: LB0306DRSCLTHM.002.

Figure 6.5.5-5. Comparison of the Distribution of Vertical Percolation Flux (Q_z) in Fractures at 10,000 Years for a Fully Coupled THM Simulation and TH Simulation (Tptpmn Model Domain)

6.6 SIMULATION RESULTS FOR THE Tptpll MODEL DOMAIN

This subsection of the model report presents modeling results for a representative drift located in the Tptpll unit. Modeling results of temperature and thermal-stress evolution for the Tptpll model domain are similar to those for the Tptpmn model domain and will, therefore not be repeated. The temperature at the emplacement drift is slightly higher in the Tptpll unit because the thermal conductivity of the Tptpll unit is lower (the thermal conductivity of the Tptpll unit is about 90 percent of that of the Tptpmn unit according to values in Table 4.1-3a). The near-peak temperature at 100 years is about 140 °C for an emplacement drift located in the Tptpll unit, which implies that the maximum temperature change is about 9 percent [(140-24)/(130-24) – 1 ≈ 0.09, where 24 is the initial temperature] higher than for an emplacement drift in the Tptpmn unit. At 1,000 years, which is near the time of peak temperature occurring, the temperature change is only about 3 percent higher for an emplacement drift in the Tptpll unit (102.1 – 24 °C for Tptpll versus 100.1 – 24 °C for Tptpmn). (The exact temperature values can be found in output DTN: LB0306DRSCLTHM.001 files Tmn1_th.out and Tll1_th.out for outputs at 100 and 1,000 years for element RP1 1). Thus, the temperature evolution is similar in the two cases and therefore the evolution of thermal stress is also similar. This section focuses on the difference between the impact of THM processes in the Tptpmn unit and Tptpll unit, and the reasons for these differences. Their impact on the evolution of hydraulic properties and vertical percolation flux is presented in Sections 6.6.1 and 6.6.2.

6.6.1 Evolution of Hydrologic Properties

Figure 6.6.1-1 presents the permeability changes induced by the excavation of the emplacement drift in the Tptpll unit. The permeability correction factor is about 8 for the horizontal permeability and about 1.3 for vertical permeability. These changes can be compared with corresponding results for a repository located in the Tptpmn unit, which are presented in

Figure 6.5.1-1. The maximum correction factor in the Tptpll repository unit (about 8 in Figure 6.6.1-1a) is roughly half of the maximum correction factor in the Tptpmn repository unit (about 19 in Figure 6.5.1-1a). This is explained by the fact that a higher initial permeability and, hence a larger initial fracture aperture in the Tptpll unit, leads to a relatively smaller change in permeability upon excavation. This is also consistent with the general trend of smaller changes in permeability for initially higher permeability values observed at the niche experiments (BSC 2004 [DIRS 170004], Figures 6.1.2-12 to 6.1.2-16).

The evolution of permeability changes in the Tptpll model domain is presented in Figures 6.6.1-2 and 6.6.1-3. A comparison of these results with corresponding results of permeability correction factors for the Tptpmn model domain in Figures 6.5.4-1 and 6.5.4-2 shows that the general pattern of permeability changes is similar, with early-time permeability changes occurring around the drift, and then gradually spreading away from the drift with time. However, the magnitudes are slightly smaller in the Tptpll model domain than in the Tptpmn model domain. For example, the blue area (F_{kz} < 0.5) extends up to 290 m in the Tptpmn model domain (z = -110 to z = +180 in Figure 6.5.4-1, 1,000 years), but only to about 180 m in the Tptpll model domain (z = +30 to z = +210 in Figure 6.6.1-2, 1,000 years). Furthermore, the minimum permeability correction factor is less than 0.1 in the Tptpmn model domain, whereas in the Tptpll model domain, it is between 0.3 and 0.5. The reason for the relatively smaller changes in permeability in the Tptpll model domain is that the overburden stress is larger, because of the additional geological layers (tcw11-12 and PTn units) on top of the vertical column. The additional geological layers provide about an additional 100 m of overburden, which in turn results in an increased in situ stress at the depth of corresponding geological units. For example, in the Tptpmn model domain, the Tptpmn unit is located at a depth of about 200 m (Table 4.1-3c), whereas in the Tptpll model domain, the Tptpmn unit is located at a depth of about 280 m (Table 4.1-3d). A higher initial stress implies that fractures are more closed, with a higher normal stiffness, and closer to their residual permeability values. All these factors contribute to a relatively smaller change in permeability during the heating of the rock mass.

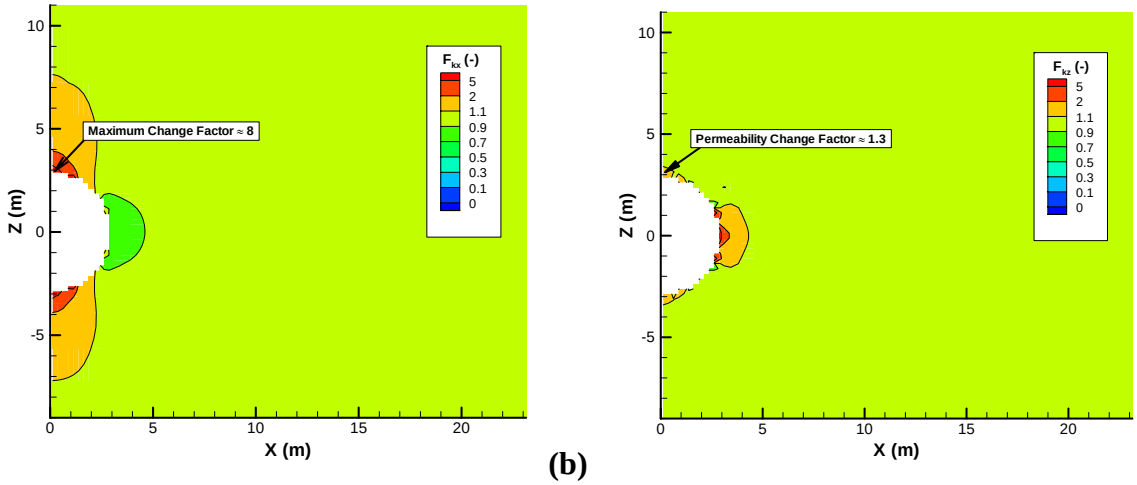

Output DTN: LB0306DRSCLTHM.002.

Figure 6.6.1-1. Permeability Correction Factor Caused by Stress Redistribution During Excavation of the Emplacement Drift: (a) Correction Factor (F_{kx} = k_x/k_i) for Horizontal Permeability, (b) Correction Factor (F_{kz} =k_z/k_i) for Vertical Permeability (Tptpll Model Domain)

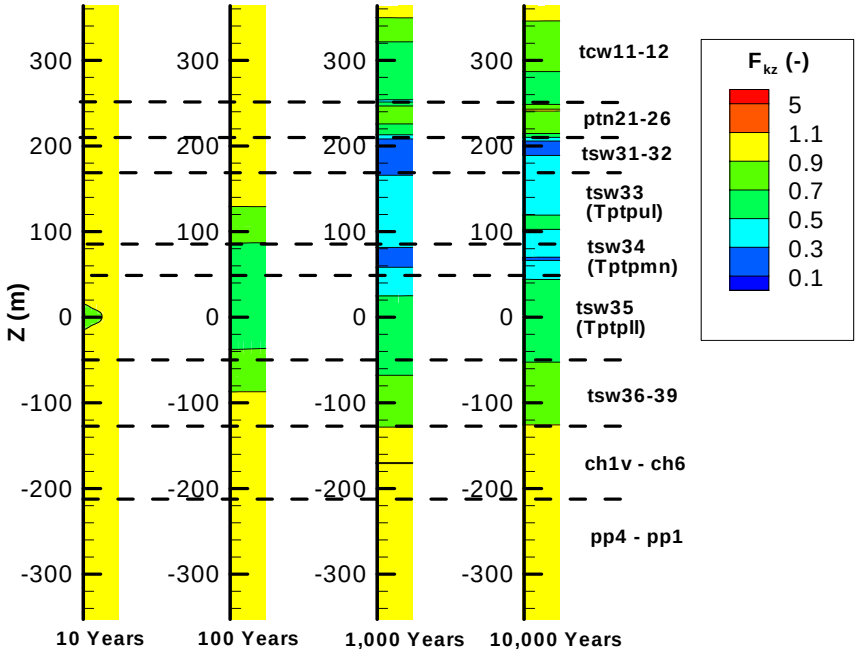

Output DTN: LB0306DRSCLTHM.002.

NOTE: The width of each column is 40.5 meters. The top is the ground surface and the bottom is the water table.

Figure 6.6.1-2. Evolution of the Vertical Permeability Correction Factor ($F_{kz} = k_z/k_i$) in the Tptpll Model Domain

Figures 6.6.1-4 and 6.6.1-5 present calculated permeability correction factors near a repository located in the Tptpll unit at 10 and 1,000 years. The corresponding results for a repository in the Tptpmn unit are presented in Figures 6.5.4-3 and 6.5.4-4. Again, the general pattern of permeability changes is similar, but the magnitude is very different. In the Tptpmn model domain, the permeability decreases to as low as 3 percent of its original value, while in the Tptpll model domain, the permeability stays above 50 percent of its original value.

Figure 6.6.1-6 shows the correction factor for capillary pressure at 10 and 1,000 years. Compared to corresponding results for a repository in the Tptpmn unit (Figures 6.5.4-6a and c), the stress-induced changes in capillary pressure are much smaller in the Tptpll unit. However, in both cases, capillary pressure strength decreases adjacent to the wall of the drift. This reduction results from the general unloading and opening of fractures oriented parallel to the drift wall.

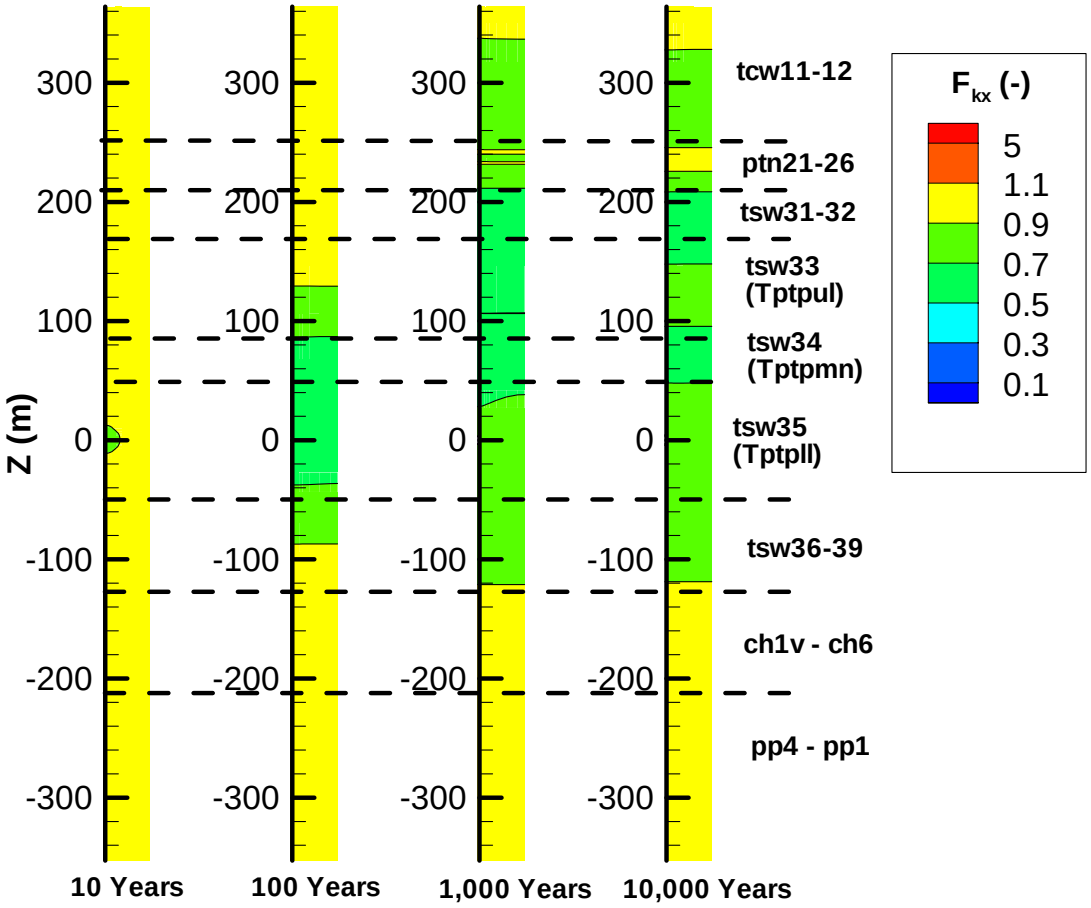

Output DTN: LB0306DRSCLTHM.002.

NOTE: The width of each column is 40.5 meters. The top is the ground surface and the bottom is the water table.

Figure 6.6.1-3. Evolution of the Horizontal Permeability Correction Factor ($F_{kx} = k_x/k_l$) in the Tptpll Model Domain

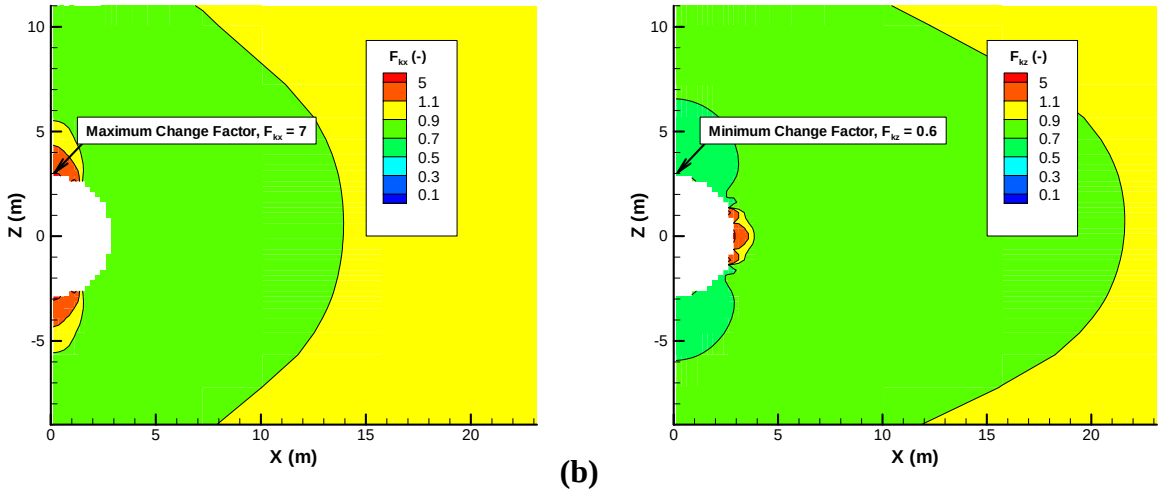

(a) **(b)**

Output DTN: LB0306DRSCLTHM.002.

Figure 6.6.1-4. Distribution of (a) Horizontal Permeability Correction Factor ($F_{kx} = k_x/k_i$) and (b) Vertical Permeability Correction Factor ($F_{kz} = k_z/k_i$) Around an Emplacement Drift in the Tptpll Unit at 10 years

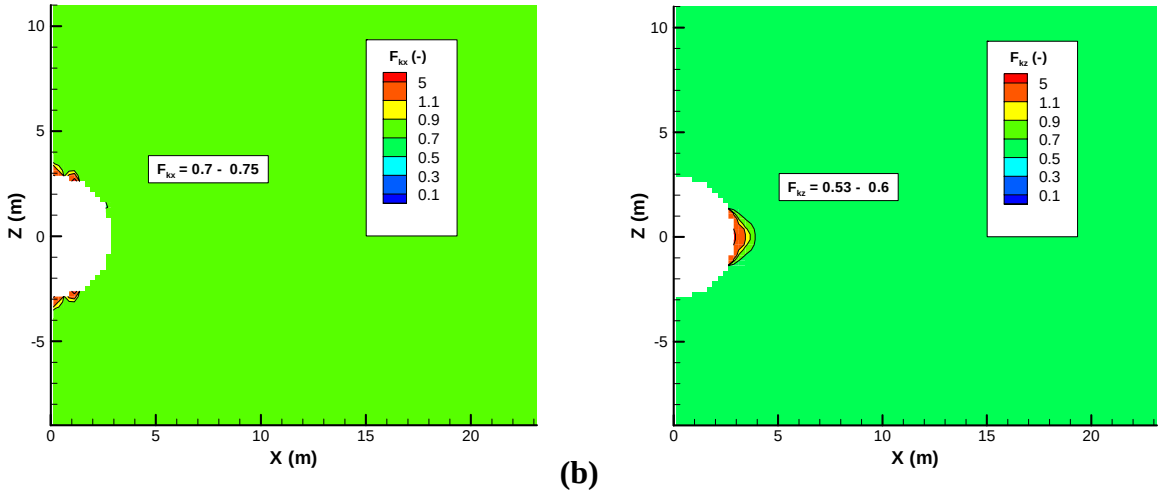

(a) **(b)**

Output DTN: LB0306DRSCLTHM.002.

Figure 6.6.1-5. Distribution of (a) Horizontal Permeability Correction Factor ($F_{kx} = k_x/k_i$) and (b) Vertical Permeability Correction Factor ($F_{kz} = k_z/k_i$) Around an Emplacement Drift in the Tptpll Unit at 1,000 Years

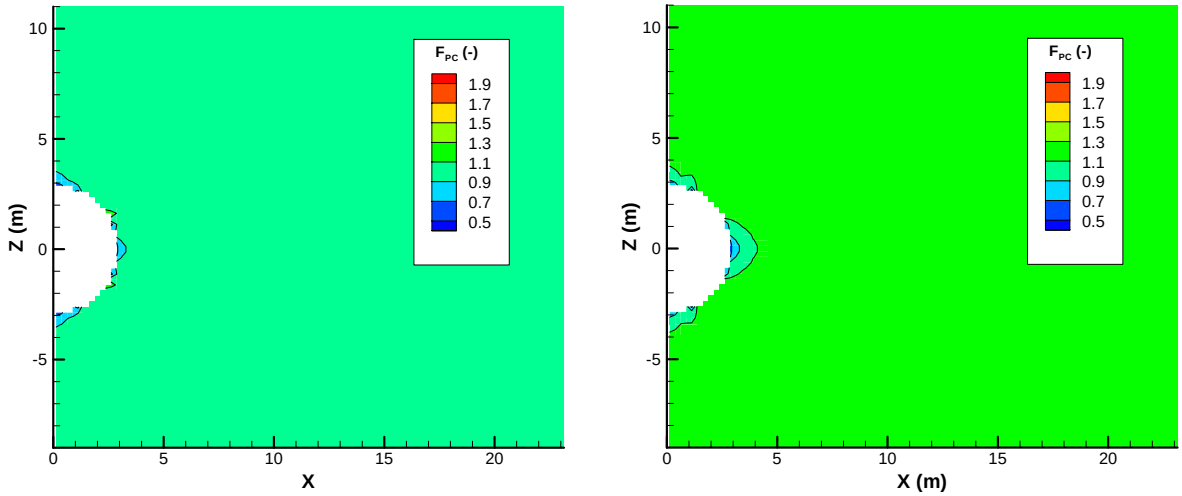

(a) 10 years **(b) 1,000 years**

Output DTN: LB0306DRSCLTHM.002.

Figure 6.6.1-6. Evolution of Stress-Induced Capillary-Pressure Correction Factor ($F_{PC} = P_c/P_{ci}$) Around an Emplacement Drift in the Tptpll Unit

6.6.2 Impact on the Fluid Flow Field

Figures 6.6.2-1 to 6.6.2-3 present calculated vertical percolation flux for a fully coupled THM analysis and partially coupled TH analysis. The results are qualitatively similar to the results for a repository in the Tptpmn unit, with the formation of a dryout zone and condensation zone above the drift, subsequent rewetting of the dryout zone, and slightly contracted dryout zone in the case of THM analysis. Figures 6.6.2-1 to 6.6.2-3 also show that the impact of THM processes is minimal for a repository in the Tptpll unit, with only a slight change in the flow pattern. As explained in Section 6.5.5, the impact of THM processes on the percolation flux is small, because a reduction in fracture intrinsic permeability can be compensated by a larger relative permeability, leading to an unchanged flow mobility. The impact of THM processes is relatively smaller in the Tptpll unit than in the Tptpmn unit because the permeability changes are less in the Tptpll unit than in the Tptpmn unit (for reasons explained in Section 6.6.1). However, while the analysis indicates that the impact of THM processes is smaller in the Tptpll unit, the prediction of THM changes in Tptpll units is more uncertain because of the lack of field experiments in the Tptpll unit (see discussion in Section 6.10.4). Moreover, the recent *Drift Degradation Analysis* (BSC 2004 [DIRS 166107], Section 6.4.2.2) indicates that for sections of low-rock quality in the Tptpll unit, more extensive inelastic behavior would occur near the drift, which could potentially lead to an increased permeability near the drift wall. Therefore, a sensitivity case is conducted in Section 6.7, using low quality lithophysal rocks, and the impact of severe inelastic deformations and drift collapse on hydrological properties are analyzed in Section 6.8.

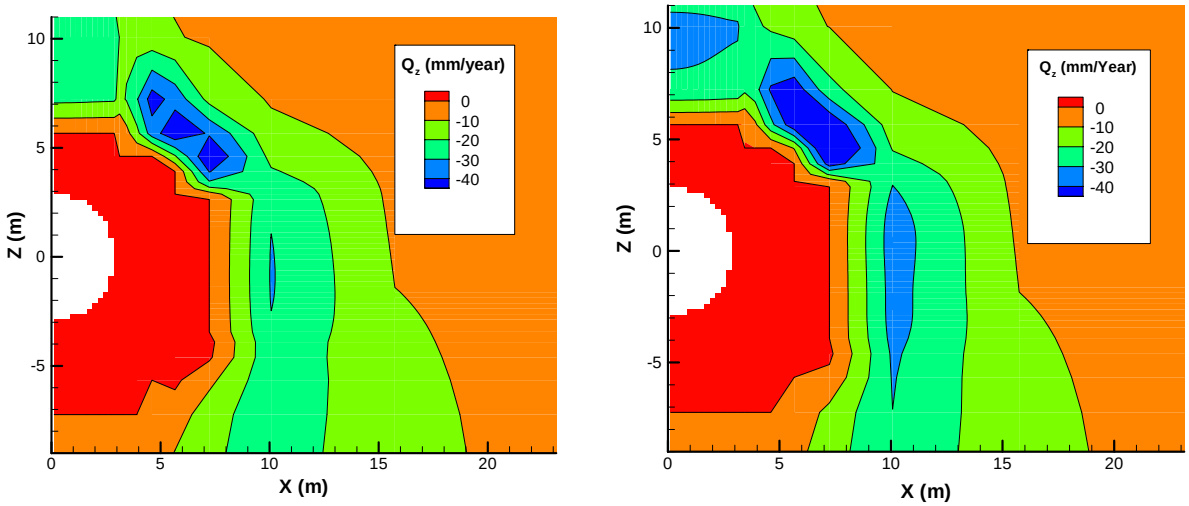

(a) THM **(b) TH**

Output DTN: LB0306DRSCLTHM.002.

Figure 6.6.2-1. Comparison of the Vertical Percolation Flux (Q_z) at 100 Years for a Fully Coupled THM Simulation and TH Simulation (Tptpll Model Domain)

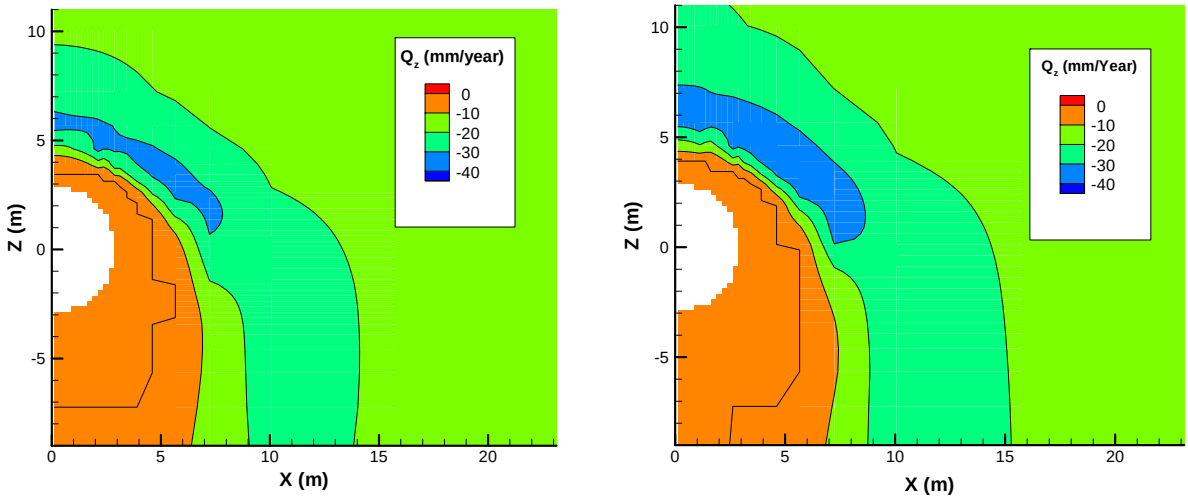

(a) THM **(b) TH**

Output DTN: LB0306DRSCLTHM.002.

Figure 6.6.2-2. Comparison of the Vertical Percolation Flux (Q_z) at 1,000 Years for a Fully Coupled THM Simulation and TH Simulation (Tptpll Model Domain)

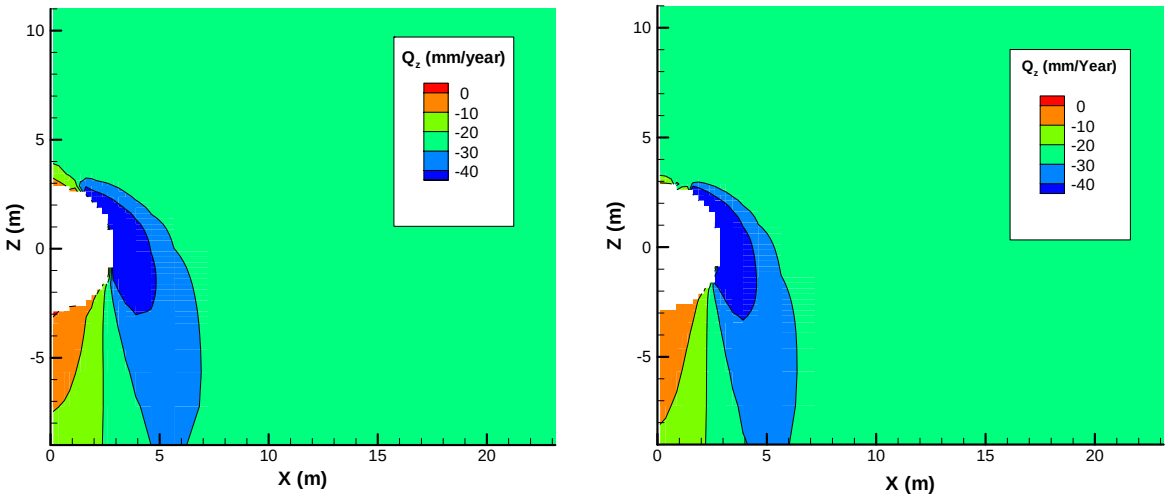

Output DTN: LB0306DRSCLTHM.002.

Figure 6.6.2-3. Comparison of the Vertical Percolation Flux (Q_z) at 10,000 Years for a Fully Coupled THM Simulation and TH Simulation (Tptpll Model Domain)

6.7 SENSITIVITY CASE FOR LOW QUALITY ROCK IN Tptpll UNIT

This subsection of the model report presents the modeling results of a sensitivity case for a drift located in low quality rock of the Tptpll unit. In the Tptpll unit, the rock mechanical properties (deformability and strengths) are clearly dependent on the lithophysal porosity (BSC 2004 [DIRS 166107], Figures 7-12 and 7-13), with lower bulk and shear modulus, and lower strength in rocks with high lithophysal porosity. The mechanical rock properties of low quality (low bulk and shear modulus, and low rock strength properties) lithophysal rock are extracted from a range of values given in the *Drift Degradation Analysis* (BSC 2004 [DIRS 166107], Appendix E, Table E-10, Category 1). In this type of low quality lithophysal rock, both the rock mass deformation modulus and strength are lower than in the base-case properties applied in Section 6.6. The low quality lithophysal rock has a Young's modulus of 1.9 GPa (Table 4.1-3b) compared to 14.77 GPa for the base-case properties (Table 4.1-3a, TSw2). A Young's modulus of 14.77 GPa roughly represents a Category 4 rock in the *Drift Degradation Analysis* (BSC 2004 [DIRS 166107], Table E-10 lists a value of 15.3 GPa, which is close to 14.77 GPa). This is a relatively high quality lithophysal rock (high bulk and shear modulus and high strength rock properties). The low quality rock has a relatively low cohesion of 2.33 MPa (for a friction angle of 40°) leading to an unconfined compressive strength of 10 MPa. The relatively low strength properties result in yielding near the drift wall during excavation of a drift in the Tptpll unit. The adopted strength properties for low quality lithophysal rock are given in Table 4.1-3b and are validated in Section 7.6 against observations of sidewall fracturing in drifts excavated through lithophysal rock at Yucca Mountain. The same stress-versus-aperture (and hence stress-versus-permeability) relationship is adopted in this sensitivity case for low quality lithophysal rock. It might seem inconsistent to adopt the same stress-versus-aperture

function (in effect the same joint stiffness) when rock mass modulus is substantially lower. However, as discussed above in this section, the lowering of the modulus of elasticity for the low quality rock is caused by the increased lithophysal porosity and not by differences in joint stiffness. Thus, it is reasonable to adopt the same stress-versus-permeability function for both the high- and low quality lithophysal rock.

6.7.1 Evolution of Stress and Yielding

The evolution of stress and deformation in low quality lithophysal rock is affected by both lower rock stiffness and lower rock strength. In general, a lower stiffness in the low quality lithophysal rock results in a lower thermal stress; whereas a lower strength can lead to rock yielding (inelastic deformation) near the drift wall.

The calculated evolution of thermal stress for low quality lithophysal rock is presented in Figure 6.7.1-1, with a comparison to thermal stress calculated for high quality rock (base-case) in Section 6.6. Figure 6.7.1-1 shows that the thermal stresses are much smaller for low quality rock. The thermal stress generally depends on the temperature change, thermal expansion coefficient and stiffness (e.g., Young's modulus) of the rock mass. In this case, the Young's modulus is reduced by a factor of 0.13 (1.9 GPa/14.77 GPa); consequently, the thermal stress is reduced roughly by a factor of 0.13. It should also be noted that due to the high porosity associated with the low quality rock, thermal conductivity may also be lower, which may lead to a relatively higher rock temperature and higher thermal stress than shown in these figures. However, such lithophysal-dependent thermal conductivity is expected to have only a minor impact on the calculated thermal stress. This can be confirmed by comparing Figure 6.7.1-1 (results for an emplacement drift located in lithophysal rock) with the Figure 6.5.3-4 (results for an emplacement drift located in nonlithophysal rock). The difference in calculated temperature changes for these two cases is about 9 percent at 100 years and about 3 percent at 1,000 years (see Section 6.6). The compressive peak-stress for the two cases occurs at about 1,000 years and is about 34 MPa in the lithophysal rock (Figure 6.7.1-1) and 31 MPa in the nonlithophysal rock (Figure 6.5.3-4). This difference in peak stress can be explained by the fact that the thermally-induced stresses are roughly proportional to the temperature change.

Figure 6.7.1-2 presents the evolution of rock yielding around a drift located in low quality lithophysal rock. The yielding zone presented in Figure 6.7.1-2 represents regions of the rock mass in which the stresses have exceeded the critical stress represented by the Mohr-Coulomb strength criterion. Although the rock mass has yielded in the drift wall, it can still sustain the mechanical load, and the drift is stable throughout the 10,000-year simulation period. Most of the yielding occurs during the excavation of the drift. A slight additional yielding takes place just after the steep temperature increase at around 50 years, leading to the slightly extended yield zone shown in Figure 6.7.1-2b. This yielding is a result of the slight increase in horizontal stress that can be observed in Figure 6.7.1-1a (solid line). At 1,000 and 10,000 years, there is no additional yielding compared to 100 years. As will be discussed in Section 6.9, the finding that the drift is stable and that there is no additional rock yielding throughout the 10,000-year period is significant to nominal drift-scale repository performance.

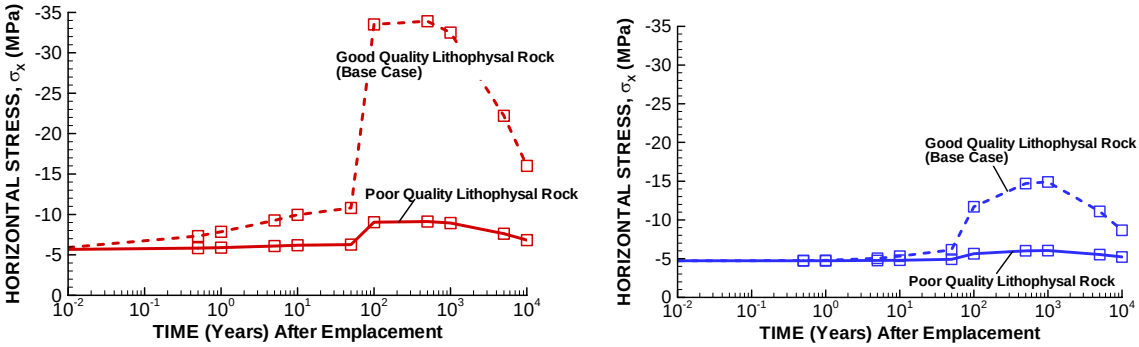

(a) In Drift Crown **(b) At Mid Pillar**

Output DTN: LB0308DRSCLTHM.002.

NOTE: In this figure, a negative stress value signifies compressive stress.

Figure 6.7.1-1. Evolution of Horizontal Stress at Drift Crown and Mid-Pillar Locations for Low Quality Lithophysal Rock (Solid Lines) Compared to High Quality Lithophysal Rock (Dashed Lines)

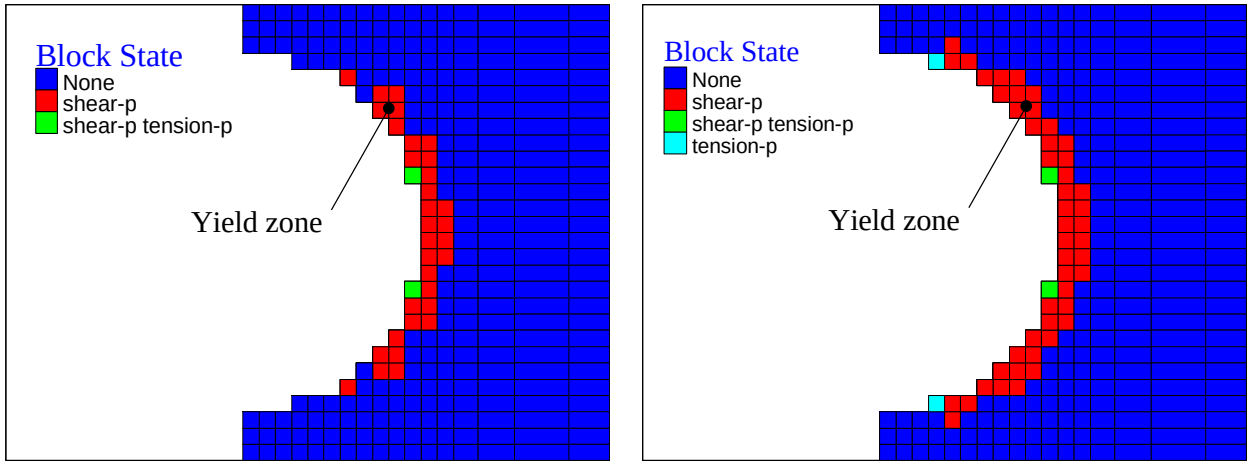

(a) After Excavation **(b) At 100, 1,000 and 10,000 years)**

Output DTN: LB0308DRSCLTHM.002.

NOTE: Shear-P and Tension-P denote that yielding has taken place previously.

Figure 6.7.1-2. Calculated Extent of Yield Zone for an Emplacement Drift Located in Low Quality Lithophysal Rock

The results of thermal stress and yielding around the drift calculated for a drift located in low quality lithophysal rock are consistent with the results of the *Drift Degradation Analysis* (BSC 2004 [DIRS 166107], Sections 6.4.2.3 and 8.1). Both the TM analysis conducted in this model report and the TM analysis conducted in the *Drift Degradation Analysis* (BSC 2004 [DIRS 166107], Sections 6.4.2.3 and 8.1) show a small impact of thermal stresses on the yield zone around the drift in the Tptpll unit. Thus, most of the yielding is expected to occur during the excavation with little or no additional yielding as a result of the TM-induced stresses during the thermal period.

6.7.2 Evolution of Hydrologic Properties

Figures 6.7.2-1 and 6.7.2-2 present the calculated permeability changes directly after excavation and at 1,000 years, respectively, for an emplacement drift located in low quality lithophysal rock. These results can be compared to corresponding results for the high quality lithophysal rock shown in Figures 6.6.1-1 and 6.6.1-5. The calculated permeability changes after excavation shown in Figure 6.7.2-1 are very similar to the corresponding results for high quality rock, with a factor of 8 maximum increase in horizontal permeability at the drift crown. The only exception is on the side of the drift, where an additional increase in permeability can be observed in the yield zone for the case of low quality rock. A comparison of the calculated permeability changes at 1,000 years, in Figures 6.7.2-2 and 6.6.1-5, shows that the thermal-mechanically induced permeability reduction is much smaller for the case of low quality rock, because the smaller deformation modulus results in a much lower thermal stress. For example, at 1,000 years, the vertical permeability has decreased to a factor of 0.53 of its original value at the drift crown for high quality lithophysal rock (Figure 6.6.1-5b). For low quality lithophysal rock, the vertical permeability has decreased to a factor of 0.7 at the same location (Figure 6.7.2-2b).

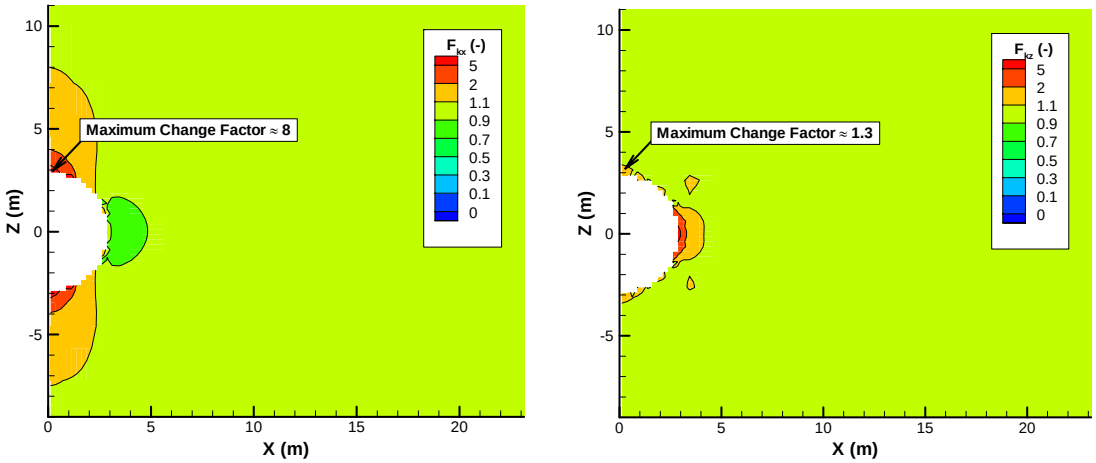

(a) **(b)**

Output DTN: LB0308DRSCLTHM.002.

NOTE: (a) Correction Factor ($F_{kx} = k_x/k_i$) for Horizontal Permeability, (b) Correction Factor ($F_{kz} = k_z/k_i$) for Vertical Permeability (Emplacement Drift Located in Low Quality Lithophysal Rock).

Figure 6.7.2-1. Permeability Correction Factor Caused by Stress Redistribution During Excavation of the Emplacement Drift

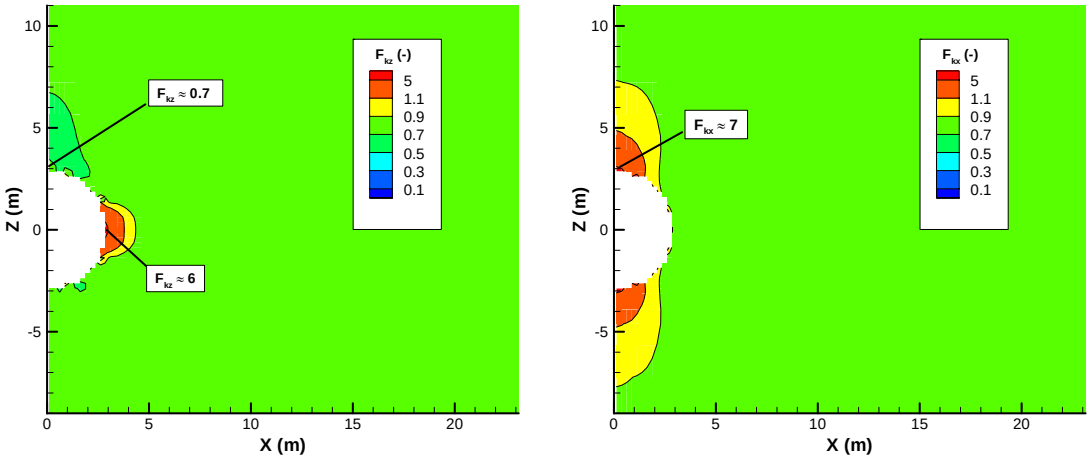

(a) **(b)**

Output DTN: LB0308DRSCLTHM.002.

Figure 6.7.2-2. Distribution of the (a) Horizontal Permeability Correction Factor ($F_{kx} = k_x/k_i$) and (b) Vertical Permeability Correction Factor ($F_{kz} = k_z/k_i$) Around an Emplacement Drift in the Tptpll Unit at 1,000 Years (Low Quality Lithophysal Rock)

6.7.3 Impact on the Fluid Flow Field

A comparison of the vertical percolation flux for a fully coupled THM and partially coupled TH analysis for low quality lithophysal rock shows that the impact of THM coupling on the flow field is small. As an example, Figure 6.7.3-1 shows the results at 1,000 years, which are very similar to the corresponding results for high quality lithophysal rock shown in Figure 6.6.2-2. The impact of THM processes is minimal for a repository in the Tptpll unit, with only a slight change in the flow pattern. Again, as explained in Sections 6.5.5 and 6.6.2, the impact of THM processes on the percolation flux is small because a reduction in fracture intrinsic permeability can be compensated by a larger relative permeability, leading to unchanged flow mobility. The impact of THM processes is relatively smaller in the Tptpll unit than in the Tptpmn unit because the permeability changes less in the Tptpll unit than in the Tptpmn unit (for reasons explained in Section 6.6.1). Note that these results were obtained for low quality lithophysal rock where the drift remains stable throughout the 10,000-year simulation period. As shown in the *Drift Degradation Analysis* (BSC 2004 [DIRS 166107], Sections 6.4.2.4 and 8.1), over a 10,000-year period a deterioration of the rock wall may occur with partially rock fall for the low quality lithophysal rocks (Section 6.8).

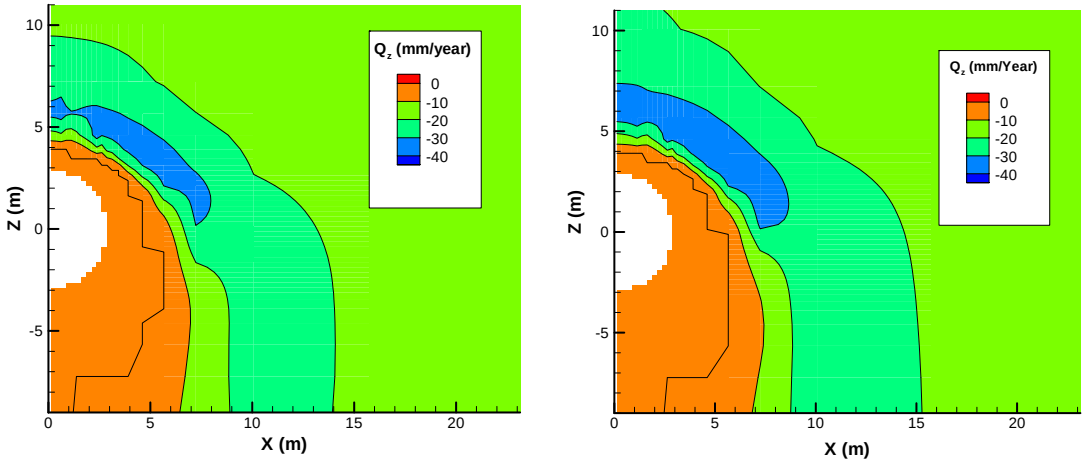

(a) THM **(b) TH**

Output DTN: LB0308DRSCLTHM.002.

Figure 6.7.3-1. Comparison of the Vertical Percolation Flux (Q_z) at 1,000 Years for a Fully-Coupled THM Simulation and TH Simulation (Poor Quality Lithophysal Rock)

6.8 ESTIMATE OF CHANGES IN HYDRAULIC PROPERTIES AROUND A COLLAPSED DRIFT IN THE Tptpll UNIT

As shown in the *Drift Degradation Analysis* (BSC 2004 [DIRS 166107], Sections 6.4.2.4 and 8.1), over a 10,0000-year period some deterioration of the rock wall will occur with partial rock fall for the low quality lithophysal rocks (Section 6.8). Furthermore, the *Degradation Analysis* (BSC 2004 [DIRS 166107], Section 8.1) indicates only minor damage from a preclosure earthquake, whereas only under the extreme and unlikely conditions of a severe postclosure earthquake, more extensive fall out of rocks can occur, effective increasing the size of the drift.

In the *Abstraction of Drift Seepage* (BSC 2004 [DIRS 169131]), predictions of changes in drift profile are considered when estimating seepage flux into emplacement drifts. The seepage flux is dependent on the diameter of the drift as well as the permeability and capillary strengths of the rock adjacent to the drift. Since the complete collapse of the drift in lithophysal rock provides a bounding estimate of the ultimate drift profile, it was determined that these post-collapse profiles would be used as a basis for drift conditions in the nominal (i.e. nonseismic) TSPA scenario (BSC 2004 [DIRS 166107], Section 6.4.2.4). In other words, for drift seepage estimates, the emplacement drifts are assumed to have the collapse profiles and to be rubble filled from the start of the postclosure period, even though this is not reasonable to occur at all under the nominal scenario.

A drift collapse may change the capillary barrier function around the drift and thereby impact the potential for seepage of groundwater into the drift. Thus, drift seepage can be impacted not only by the change in shape or size of the drift, but also by changes in hydraulic properties (permeability and capillarity) in the host rock surrounding the collapsed drift. Therefore, this section provides estimates of changes in hydrological properties around a collapsed drift to be used in the *Abstraction of Drift Seepage* (BSC 2004 [DIRS 169131]). The analysis is conducted

using outputs from the mechanical analysis conducted in the *Drift Degradation Analysis* (BSC 2004 [DIRS 166107], Section 6.4.2.2). DTN: MO0306MWDDPPDR.000 [DIRS 164736] of *Drift Degradation Analysis* provides output for about 30 different simulation cases, denoted Scenarios 1 to 30. For each scenario, DTN: MO0306MWDDPPDR.000 [DIRS 164736] provides drift geometry, distribution of stress, volumetric fracture strain, and aperture changes.

In this section, changes in hydrological properties for the rock around the drift are estimated using two alternative approaches:

1) Calculating the changes in permeability and capillarity resulting from changes in the stress field, using the stress-versus-permeability function developed in Section 6.4.4.

2) Calculating the changes in permeability and capillarity resulting from changes in volumetric strains, using a strain-versus-permeability function developed in Section 6.8.1.

The calculated changes in hydrologic properties using these two methods are compared and are also compared with results of the drift scale THM model in Section 6.7. The analysis is conducted by first studying the case of an intact drift unaffected by static fatigue or seismic effects. This case is important to assure that model results with the two approaches—using a stress-versus-permeability function and using a strain-versus-permeability function—correctly capture the typical one-order-of magnitude change in permeability that is observed near excavated drifts at Yucca Mountain (Section 6.4.4). This step includes a calibration of a strain-versus-permeability function in a similar way as the stress-versus-permeability function was calibrated in Section 6.4.4. After verifying the consistency of the two model approaches for the intact drift, the same models are then used for prediction of changes in hydrologic properties around a collapsed drift.

Changes in hydrological properties are evaluated for the following scenarios of DTN: MO0306MWDDPPDR.000 [DIRS 164736] (BSC 2004 [DIRS 166107], Table R-1):

- Scenario 7: Excavation without static fatigue or seismic effect (intact drift)
- Scenario 2: Severe seismic damage event (represented by a 1,000,000 year event)
- Scenario 1: Minor seismic damage event (represented by a 2,000 year event)

Scenario 7 is important for the derivation of strain-versus-permeability functions and for comparison for model comparison to the drift scale THM model results in Section 6.7. Scenario 2 represents a worst-case scenario of drift degradation, for which complete drift collapse is predicted by a severe seismic event in the *Drift Degradation Analysis* (BSC 2004 [DIRS 166107], Section 6.4.2.2). Scenario 1 represents one of the preclosure earthquake events for which minor damage is predicted in *Drift Degradation Analysis* (BSC 2004 [DIRS 166107], Section 6.4.2.2).

6.8.1 Scenario 7: Drift Excavation without Static Fatigue or Seismic Effect

This scenario represents the current conditions of an excavated drift in the Tptpll unit without strength degradation (static fatigue) or seismic effect. The *Drift Degradation Analysis*

(BSC 2004 [DIRS 166107], Figure 6-171a) predicts some fracturing in the sidewall of the drift, but the drift is predicted to remain stable, with no caving from the drift wall. Figure 6.8.1-1 shows mean stress and a volumetric strain distribution extracted from DTN: MO0306MWDDPPDR.000 [DIRS 164736] of the *Drift Degradation Analysis* (BSC 2004 [DIRS 166107]) for this scenario. The mean stress indicates a general unloading close to the drift wall, especially on top and on the sides, near the spring line of the drift. The volumetric strain is also largest at the top and on the side of the drift.

Permeability changes around the excavation are first estimated based on calculated changes in the stress field. Using this method, permeability changes are directly estimated from calculated changes of stresses in x and z directions, using the stress-versus-permeability function developed in Section 6.4.4 of this model report. The results presented in Figure 6.8.1-2 are consistent with the results of the drift scale THM model shown in Figure 6.7.2-1. Both analyses (shown in Figures 6.8.1-2 and 6.7.2-1) indicate that most changes occur in the horizontal permeability at the drift crown. The calculated permeability changes in Figure 6.8.1-2 are slightly larger than those in Figure 6.7.2-1 because the initial stress field is slightly different in the two cases. In the Tptpll model domain of the drift scale THM model, the initial vertical compressive stress is calculated from the weight of the overburden rock (363.8 m) to be 7.9 MPa, with the horizontal stress $0.6\times\sigma_v$, according to Assumption 2 in Section 5. In the *Drift Degradation Analysis* (BSC 2004 [DIRS 166107], Section 6.4.2.2), a vertical compressive stress is selected to be 7.0 MPa, with horizontal compressive stress of $0.5\times\sigma_v$, which would represent a slightly shallower location.

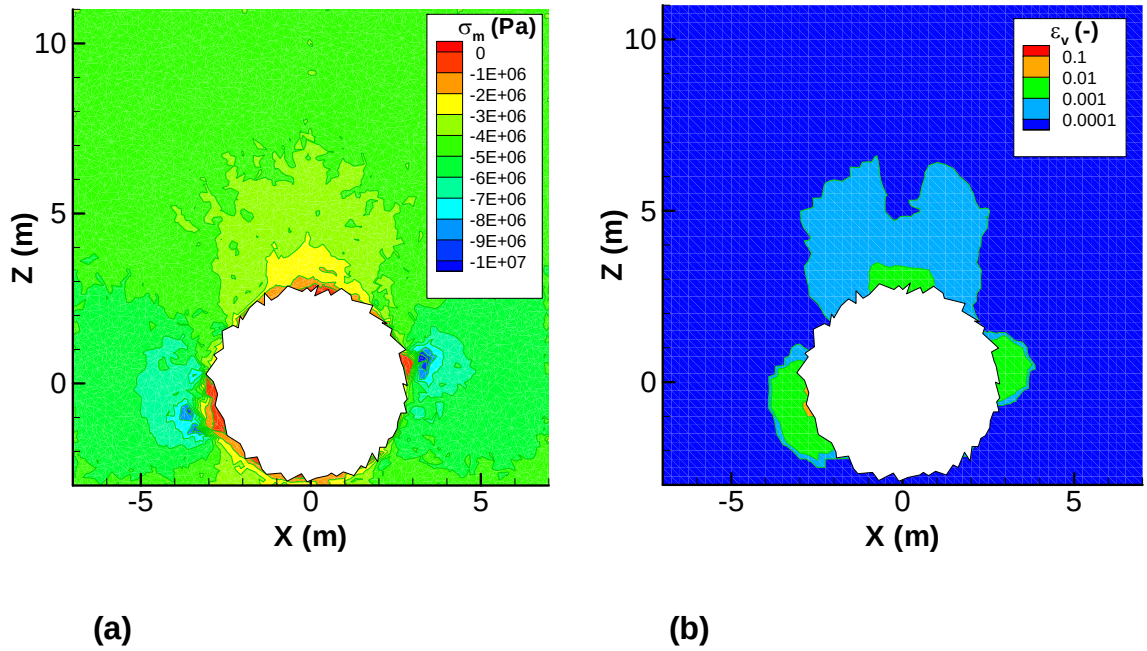

DTN: MO0306MWDDPPDR.000 [DIRS 164736].

NOTE: In this figure, a negative stress value signifies compressive stress and a positive strain value signifies expansion.

Figure 6.8.1-1. Results of (a) Mean Stress and (b) Fracture Volumetric Strain after Excavation of an Emplacement Drift (Scenario 7)

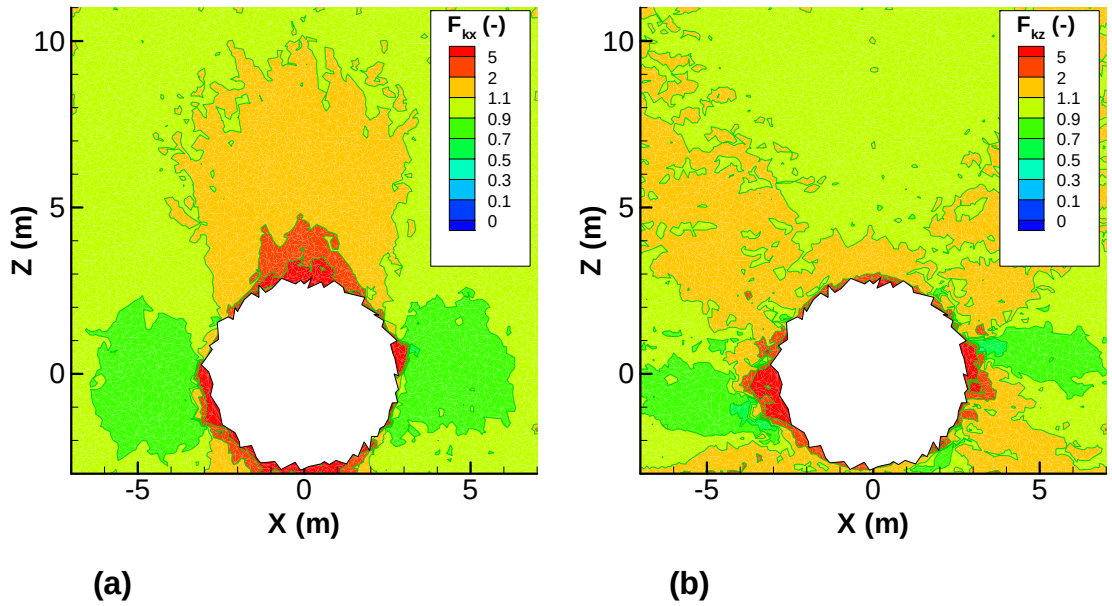

Source: Calculated from DTN: MO0306MWDDPPDR.000 [DIRS 164736] using algorithms from Rutqvist [DIRS 170509], pp. 262 to 266.

Figure 6.8.1-2. Permeability Correction Factor Caused by Stress Redistribution During Excavation of the Emplacement Drift: (a) Correction Factor (F_{kx} = k_x/k_i) for Horizontal Permeability, (b) Correction Factor (F_{kz} =k_z/k_i) for Vertical Permeability (Scenario 7)

Permeability changes can also be estimated using the calculated equivalent fracture volumetric strain shown in Figure 6.8.1-1b. The estimate of permeability changes caused by volumetric strain, a relationship between volumetric strain and permeability, needs to be derived. In this section, a linear strain versus permeability function is developed. The average fracture volumetric strain (ε_v) in Figure 6.8.1-1b is calculated from fracture aperture changes (Δb) using an averaging technique and can be interpreted as a change in fracture porosity, ϕ, according to:

$$\varepsilon_v = f(\Delta b) \approx \frac{\Delta\phi}{1-\phi_i} \qquad \text{(Eq. 6.8.1-1)}$$

The current fracture porosity, ϕ, can then be calculated as:

$$\phi = \phi_i + \Delta\phi \approx \phi_i + (1-\phi_i)\varepsilon_v \qquad \text{(Eq. 6.8.1-2)}$$

where ϕ_i is the initial permeability. For a medium in which the porosity consists of planar (fracture like) features, the permeability (k) is roughly proportional to the cube of the aperture (Witherspoon et al. 1980 [DIRS 123506]) and hence, to the cube of the fracture porosity according to:

$$k \approx a\phi^3 \qquad \text{(Eq. 6.8.1-3)}$$

or

$$k \approx a\left[\phi_i + (1-\phi_i)\varepsilon_v\right]^3 \qquad \text{(Eq. 6.8.1-4)}$$

where $\phi = \max[\phi_r, \phi_i + (1-\phi_i)\varepsilon_v]$ and ϕ_r is the irreducible porosity that results in residual permeability, when ϕ corresponds to closure stress. The permeability correction factor, F_k, and the porosity correction factor, F_ϕ, can now be calculated as:

$$F_k = \frac{k}{k_i} \approx \frac{a\left[\phi_i + (1-\phi_i)\varepsilon_v\right]^3}{a\left[\phi_i\right]^3} \approx \left[1 + \frac{1-\phi_i}{\phi_i}\varepsilon_v\right]^3 = \left[1 + A\varepsilon_v\right]^3 \qquad \text{(Eq. 6.8.1-5)}$$

$$F_\phi = \frac{\phi}{\phi_i} \approx \frac{\phi_i + (1-\phi_i)\varepsilon_v}{\phi_i} = 1 + A\varepsilon_v \qquad \text{(Eq. 6.8.1-6)}$$

The value of A could be estimated from the initial porosity fracture porosity according to

$$A = \frac{1-\phi_i}{\phi_i} \qquad \text{(Eq. 6.8.1-7)}$$

For example, using the porosity value of 9.6E-3 given in Table 4.1-3a, Equation 6.8.1-7, gives $A \approx 100$. However, there are many uncertainties in the above derivation of the strain-versus-permeability function, and a value of A has to be calibrated. In this study, the parameter A is calibrated to give a permeability correction factor, F_k, that is roughly consistent with the one calculated based on stress. Figure 6.8.1-3b shows the calculated permeability changes for A = 220, with an imposed residual permeability change of k_r/k_i = 0.15. The residual permeability change factor of 0.15 is implemented as a simple cut-off value, taking the maximum of 0.15 or F_k calculated from Equation 6.8.1-6. The cut-off value of 0.15 is selected to be the same as used in the model calibration of the exponential stress-versus-permeability function in Section 6.4.4, according to field observations from the DST. A comparison is also made with estimated stress-induced changes in mean permeability (Figure 6.8.1-3a). The figure shows that the estimated changes in mean permeability around the drift are roughly consistent between the two methods. For example, both methods show an increase by a factor of about 2 to 5 at the drift crown, and a larger increase at the sidewall of the drift. Because the two parameters in the strain-versus-permeability law, "A" and the cut-off value, were calibrated to obtain this result, it confirms that the calibration worked. The permeability changes at the side of the drift tend to be stronger in Figure 6.8.1-3b for the fracture-strain-based method. A relatively stronger permeability change at the sidewall for the fracture-strain-based method is probably associated with inelastic fracture strain caused by formation and opening of the fracture and sliding of loose blocks in the sidewall under almost uniaxial stress state. Furthermore, there is a region on the side of the drift extending about 1 to 3 meters outside the sidewall, in which the permeability changes based on volumetric strain predict a stronger reduction in permeability.

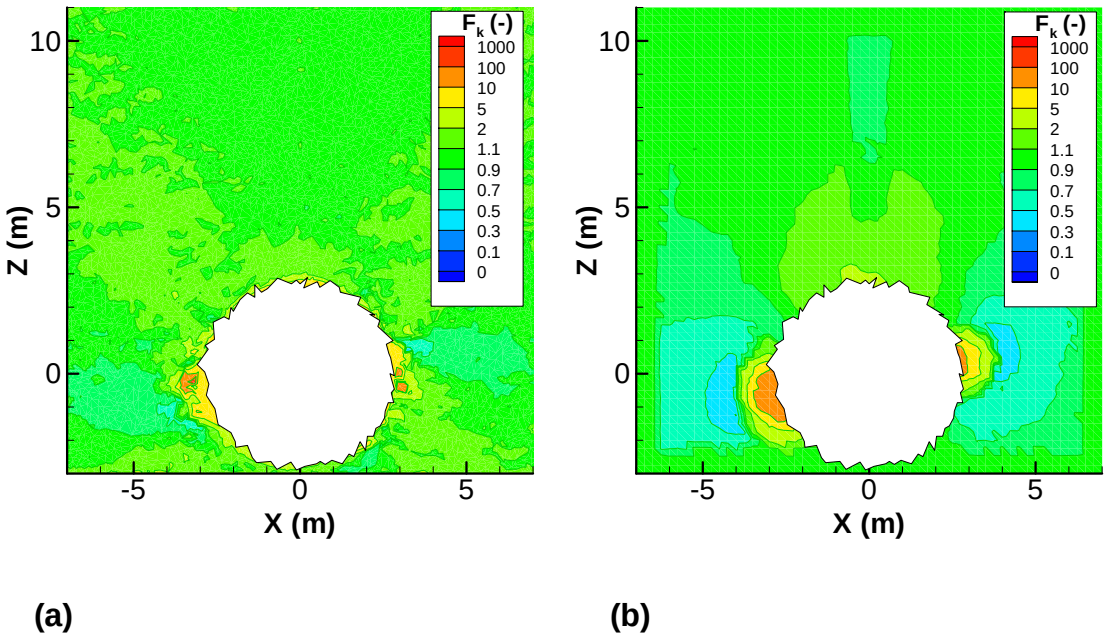

Source: Calculated from DTN: MO0306MWDDPPDR.000 [DIRS 164736] using algorithms from Rutqvist [DIRS 170509], pp. 262 to 266.

Figure 6.8.1-3. Permeability Correction Factor ($F_k = k/k_i$) Relative to Preexcavation Values: (a) Correction Factor Calculated from Changes in the Stress Field and (b) Correction Factor Calculated from Changes in Volumetric Fracture Strain (Scenario 7)

Figure 6.8.1-4 presents estimated changes in capillary pressure using Equation 6.2-6. Again, the results using stress-induced changes shown in Figure 6.8.1-4a are consistent with the results obtained in the Tptpll model domain for the drift scale THM model. The results using the strain-induced changes, show a reduction in capillary pressure by a factor of approximately 0.5 at the crown of the drift. On the side of the drift, near the springline, the capillary pressure is reduced to a factor of about 0.1 of its original value. This additional reduction of capillary pressure can be attributed to the inelastic fracture opening that is not fully captured in the stress-induced model.

6.8.2 Scenario 2: Severe Seismic Damage (Complete Drift Collapse)

Drift Degradation Analysis (BSC 2004 [DIRS 166107], Section 6.4.2.2) shows that for an extreme seismic event, a complete collapse of the drift could occur. The host rock caves in until the drift is completely filled with rubble, thereby preventing further caving. The size of the opening nearly doubles, and a zone of stress relief and large volumetric strain extends about 2 to 4 m (about 1 radius of the collapsed drift) into the host rock (Figure 6.8.2-1). Permeability is estimated to increase by 1 to 2 orders of magnitude just above the drift and about 3 orders of magnitude on the side of the drift (Figure 6.8.2-2). The corresponding changes in capillary pressure are a reduction to 0.5 of initial values all around the periphery of the drift; whereas the strain-induced prediction leads to a reduction to about 0.5 of initial values on the top of the drift and about 0.1 to 0.5 of initial values on the side of the drift (Figure 6.8.2-3).

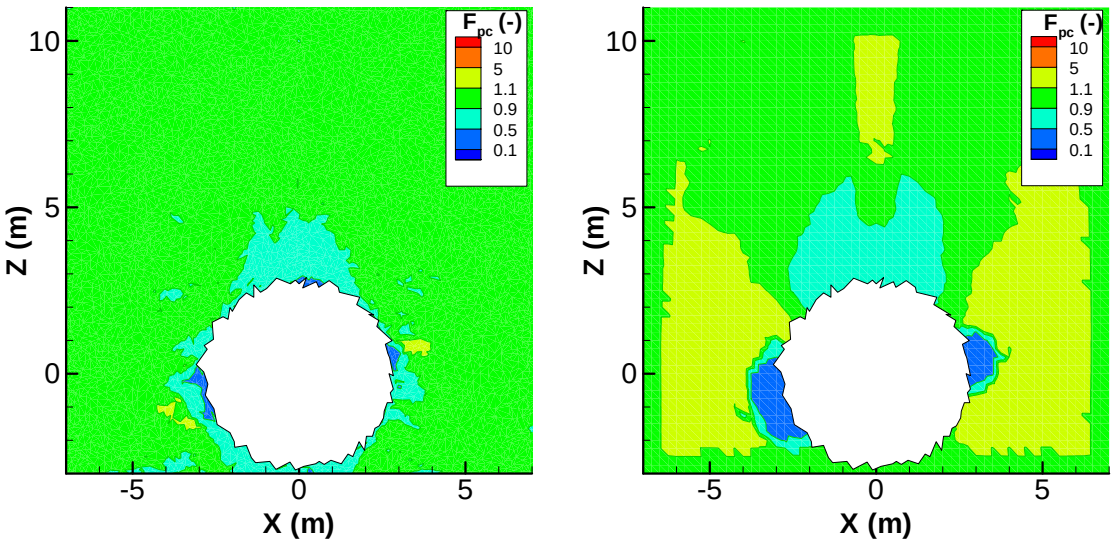

Source: Calculated from DTN: MO0306MWDDPPDR.000 [DIRS 164736] using algorithms from Rutqvist [DIRS 170509], pp. 262 to 266.

NOTES: (a) Correction Factor Calculated from Changes in the Stress Field and (b) Correction Factor Calculated from Changes in Volumetric Fracture Strain (Scenario 7).

Figure 6.8.1-4. Capillary-Pressure Correction Factor ($F_{PC} = P_c/P_{ci}$) Relative to Preexcavation Values

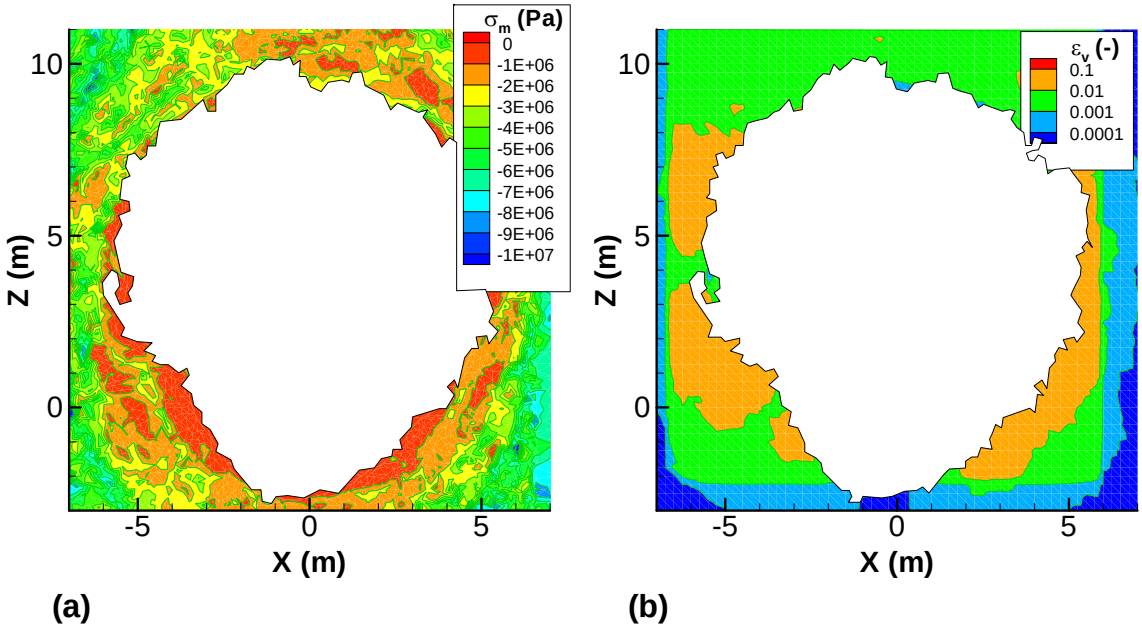

DTN: MO0306MWDDPPDR.000 [DIRS 164736].

NOTE: In this figure, a negative stress value signifies compressive stress and a positive strain value signifies expansion.

Figure 6.8.2-1. Results of (a) Mean Stress and (b) Fracture Volumetric Strain for the Rock Outside a Completely Collapsed Drift in the Scenario of Severe Seismic Damage (Scenario 2)

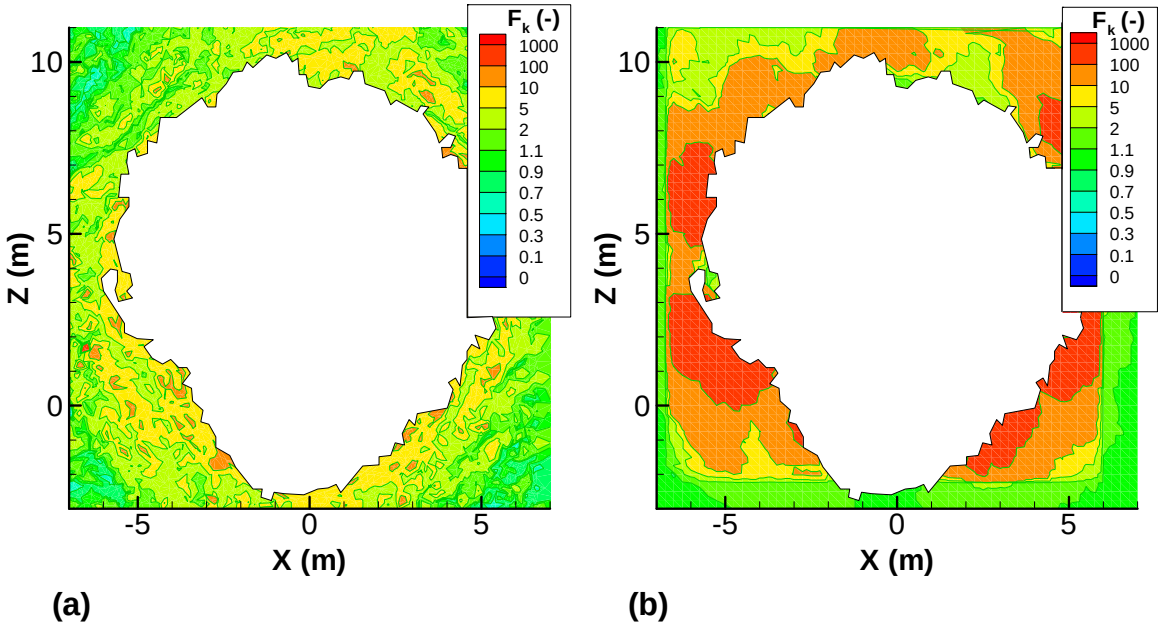

Source: Calculated from DTN: MO0306MWDDPPDR.000 [DIRS 164736] using algorithms from Rutqvist [DIRS 170509], pp. 262 to 266.

NOTE: (a) Correction Factor Calculated from Changes in the Stress Field and (b) Correction Factor Calculated from Changes in Volumetric Fracture Strain (Scenario 2).

Figure 6.8.2-2. Permeability Correction Factor (F_k = k/k_i) Relative to Pre-Excavation Values for a Completely Collapsed Drift in the Scenario of Severe Seismic Damage

6.8.3 Scenario 1: Minor Seismic Damage (Intact Drift)

Drift Degradation Analysis (BSC 2004 [DIRS 166107], Section 6.4.2.2) predicted only a relatively small amount of rock fall for minor seismic damage for low quality rock. The calculated rock fall takes place from the sidewall of the drift, where rock was already in a yield condition after excavation. That is, loosely attached blocks in the sidewall are shaken down, leading to a small extension of the drift shape near the sidewall. Figure 6.8.3-1 shows the calculated mean stress and volumetric strain after such an event. A comparison to the corresponding results after excavation of the drift (Figure 6.8.1-1) shows that the mean stress is almost unaffected by the minor seismic event. A significant increase in volumetric strain is calculated at the drift crown (compare Figures 6.8.1-1b and 6.8.3-1b). However, a close look at the calculated aperture changes in this area indicates that this localized increase in volumetric fracture strain is an artifact of a 9-cm opening of one fracture included in the data set.

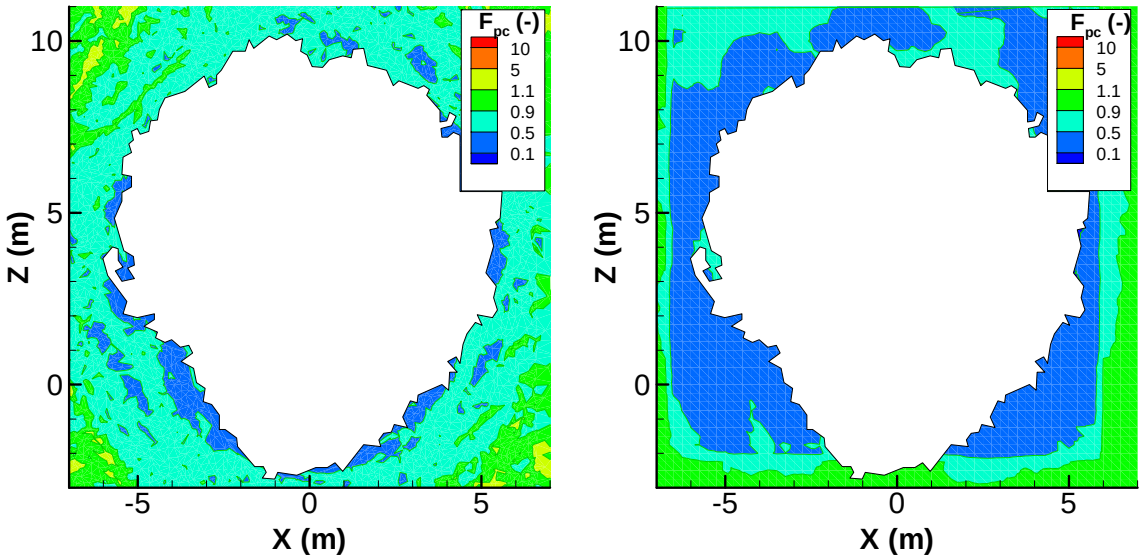

Source: Calculated from DTN: MO0306MWDDPPDR.000 [DIRS 164736] using algorithms from Rutqvist [DIRS 170509], pp. 262 to 266.

NOTE: (a) Correction Factor Calculated from Changes in the Stress Field and (b) Correction Factor Calculated from Changes in Volumetric Fracture Strain (Scenario 2).

Figure 6.8.2-3. Capillary Pressure Correction Factor ($F_{PC} = P_c/P_{ci}$) Relative to Preexcavation Values for a Completely Collapsed Drift in the Scenario of Severe Seismic Damage

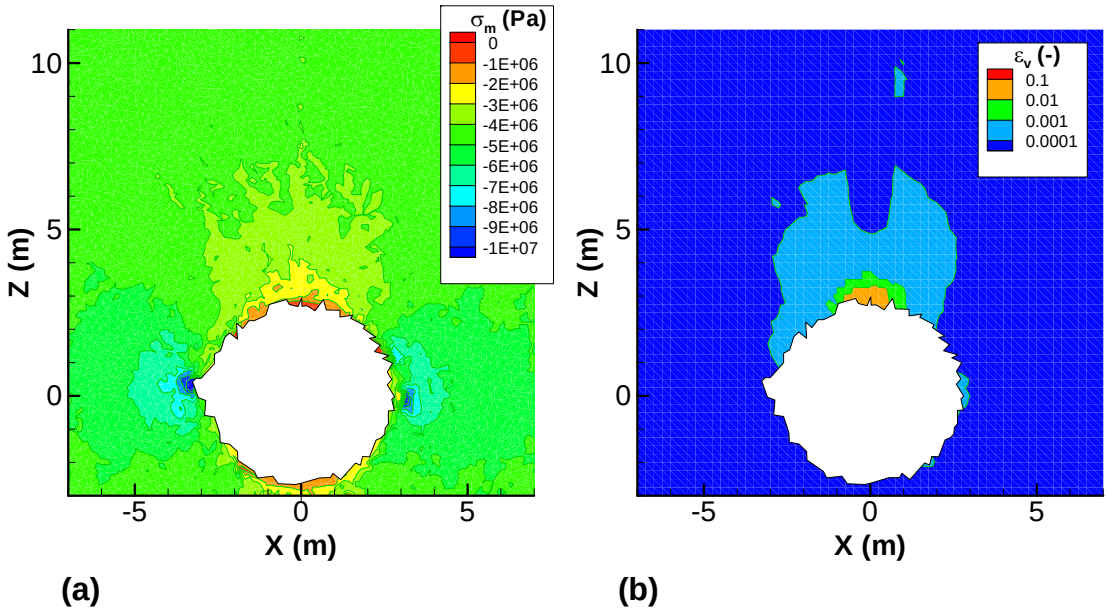

DTN: MO0306MWDDPPDR.000 [DIRS 164736].

NOTE: The localized increase in volumetric strain on top of the drift in (b) is an artifact caused by a 9 cm fracture opening in the data set (Scenario 1). In this figure, a negative stress value signifies compressive stress and a positive strain value signifies expansion.

Figure 6.8.3-1. Results of (a) Mean Stress and (b) Fracture Volumetric Strain for the Rock Outside a Drift in the Scenario of Minor Seismic Damage

Figures 6.8.3-2 and 6.8.3-3 present the estimated changes in permeability and capillarity around the drift. The permeability changes estimated using the stress-induced approach do not indicate any significant change in permeability as a result of minor seismic damage. The permeability changes estimated using the strain-induced approach show an increasing permeability in the region of increased volumetric strain at the drift crown. The corresponding stress-induced changes in capillary pressure are less than a factor of 0.5; whereas the strain-induced prediction shows a reduction to about 0.2 of its original value above the drift. The localized increases in permeability and reductions in capillarity shown on top of the drift in Figures 6.8.3-2b and 6.8.3-3b are artifacts of a 9-cm opening of one fracture included in the data set. Without this artificial change on top of the drift, the predicted changes in hydrologic properties for the minor seismic damage are small and comparable to changes predicted directly after excavation of the drifts. Thus, a minor seismic event is not expected to induce significant changes in hydrologic properties.

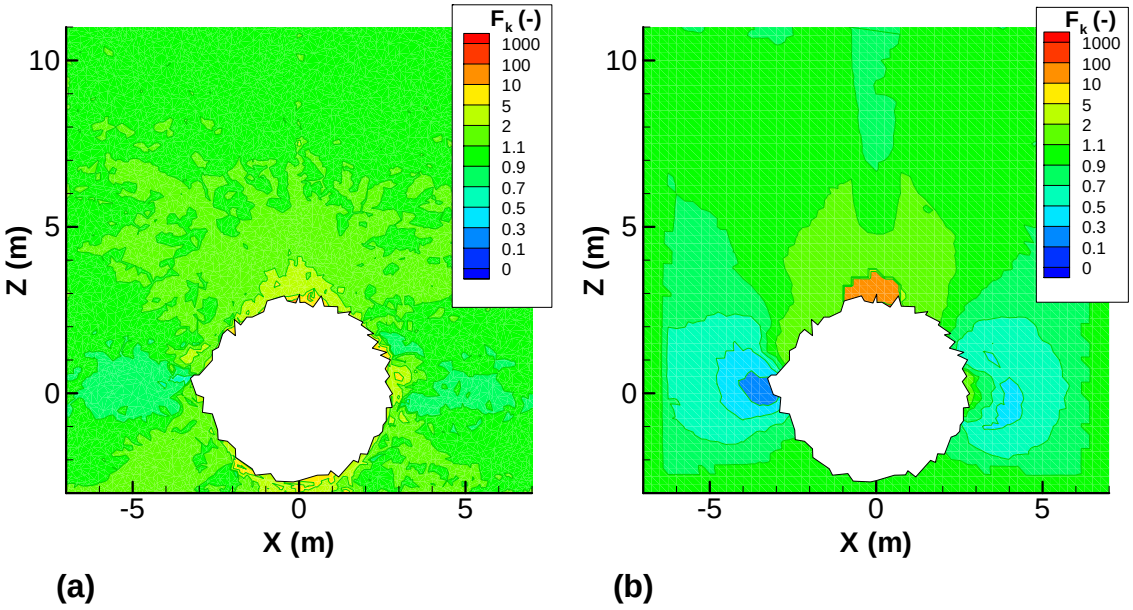

Source: Calculated from DTN: MO0306MWDDPPDR.000 [DIRS 164736] using algorithms from Rutqvist [DIRS 170509], pp. 262 to 266.

NOTES: (a) Correction Factor Calculated from Changes in the Stress Field and (b) Correction Factor Calculated from Changes in Volumetric Fracture Strain. The localized increase in permeability on top of drift in (b) is an artifact caused by a 9 cm fracture opening in the data set (Scenario 1).

Figure 6.8.3-2. Permeability Correction Factor ($F_k = k/k_i$) Relative to Preexcavation Values Drift in the Scenario of Minor Seismic Damage

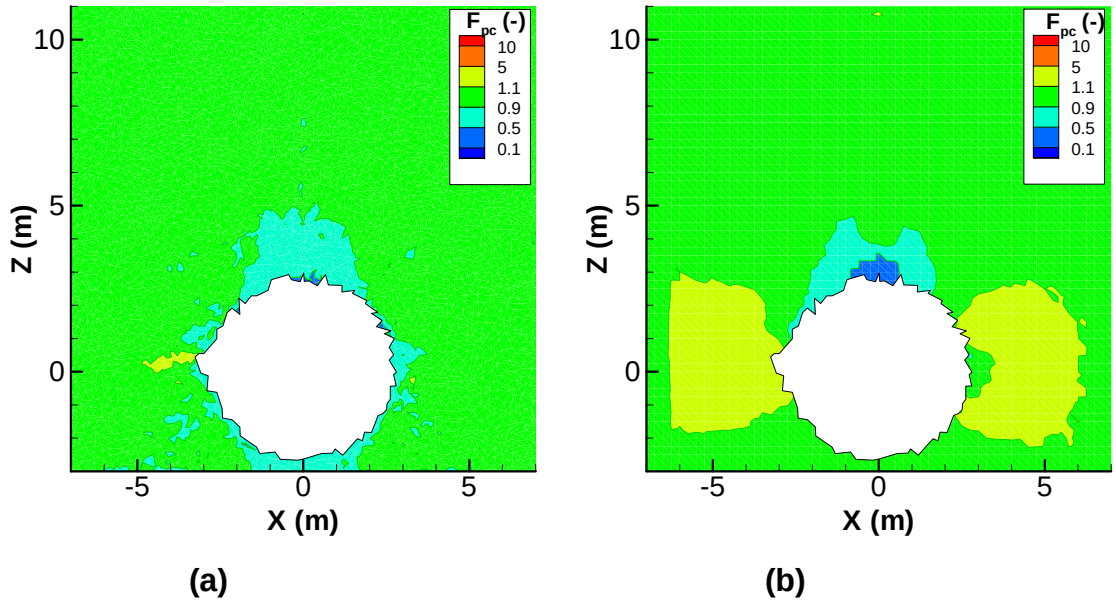

Source: Calculated from DTN: MO0306MWDDPPDR.000 [DIRS 164736] using algorithms from Rutqvist [DIRS 170509], pp. 262 to 266.

NOTES: (a) Correction Factor Calculated from Changes in the Stress Field and (b) Correction Factor Calculated from Changes in Volumetric Fracture Strain. The localized reduction in capillary pressure on top of the drift in (b) is an artifact caused by a 9 cm fracture opening in the data set (Scenario 1).

Figure 6.8.3-3 Capillary-Pressure Correction Factor ($F_{PC} = P_c/P_{ci}$) Relative to Preexcavation Values Drift in the Scenario of Minor Seismic Damage

6.8.4 Summary of Collapsed Drift Analysis and Possible Impact on Flow

The analysis in Sections 6.8.1 through 6.8.3 indicates that the changes in hydrological properties are consistent with the ones calculated for the drift scale THM model in Sections 6.6 and 6.7, as long as the drift remains intact. After excavation and after a minor seismic event, the drift is expected to remain intact, the permeability changes in the rock adjacent to the drift are within one order of magnitude, and the capillary pressure is estimated to change by less than a factor of 0.5. For a completely collapsed drift, the drift diameter is expected to nearly double, and larger changes in hydrological properties are also expected in a zone adjacent to the collapsed drift.

Figure 6.8.4-1 summarizes the estimated changes in hydrological properties around a completely collapsed drift. The changes shown in the figure reflect a complete collapse caused by severe seismic damage. It is estimated that the permeability could increase by about 1 to 2 orders of magnitude, and that capillary pressure could decrease to a factor of about 0.5 of initial values just above the drift; whereas larger changes are predicted to occur on the side of the drift. The larger changes occurring on the side of the drift are caused by a zone of loosening blocks partly detached from each other, creating larger openings. The cubic law is probably a rough approximation of fluid flow through such openings (aperture of the order of centimeters) between these blocks. The model predicts an increase in permeability up to 3 orders of magnitude compared to the initial permeability in this region (and permeability away from the damage zone). Thus, the calculated change in permeability provides an indication of large permeability increase.

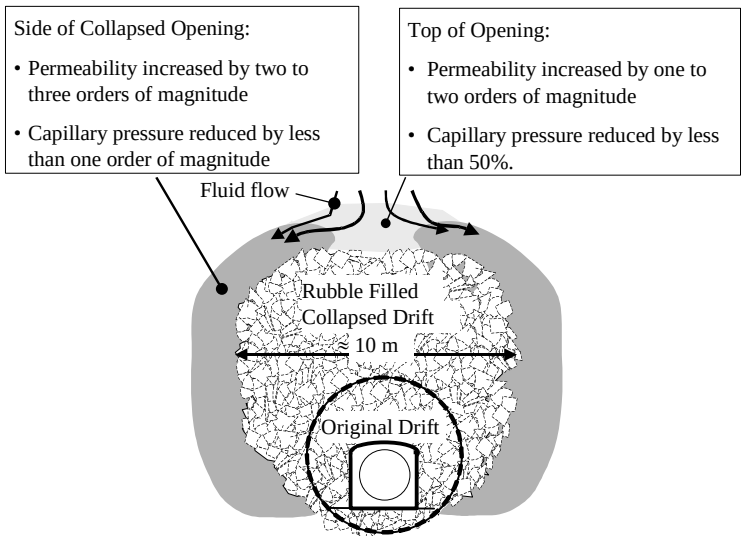

Figure 6.8.4-1. Summary of Estimated Changes in Hydrologic Properties Around a Completely Collapsed Drift (Illustrated for Information Purposes)

In general, the increase in permeability on top of the drift and the larger increase on the side of the drift will facilitate diversion of groundwater flow around the drift and thereby prevent water from seeping into the drift (BSC 2004 [DIRS 167652], Section 6.7). While most of the presented results in Sections 6.8.1 to 6.8.3 show permeability changes averaged over the horizontal and vertical directions, it is indicated that typically the horizontal increase at the drift crown is larger than the vertical increase. As discussed earlier, such anisotropic behavior would tend to increase the likelihood of flow diversion compared to isotropic conditions. On the other hand, increasing drift size while simultaneously reducing capillarity tends to weaken the capillary barrier thereby increasing the likelihood for drift seepage (BSC 2004 [DIRS 167652], Section 8; BSC 2004 [DIRS 169131], Section 6.8.2). The influence of drift collapse on seepage for the extreme case of a completely collapsed drift is evaluated in *Abstraction of Drift Seepage* (BSC 2004 [DIRS 169131]), where probability distributions of seepage are developed for use in TSPA.

6.9 SUMMARY OF RESULTS AND DISCUSSION OF PREDICTED THM EFFECTS AND THEIR IMPACT ON DRIFT SCALE PERFORMANCE

The results of the coupled drift scale THM model presented in Sections 6.5 (Tptpmn model domain), 6.6 (Tptpll model domain), and 6.7 (low quality lithophysal rock in Tptpll model domain) show that the effects of THM processes will last for well over 10,000 years, but that these processes have a negligible impact on temperature evolution and small impact on percolation flux. These model results were obtained for bounding estimates of input THM properties (including thermal expansion coefficient and stress-versus-permeability function that emphasizes the effect of THM coupling on hydrology), which are sufficient for bounding the maximum impact of the THM processes on permeability and percolation flux.

Away from the emplacement drift, increased horizontal thermal stresses tend to tighten vertical fractures toward their residual aperture values. As a result, the vertical intrinsic permeability will

decrease in a zone extending more than 100 m both above and below the repository (Figure 6.5.4-1). Using a bounding estimate of the stress-versus-permeability relationship that emphasized the effect of thermally induced stress on permeability, the vertical mean permeability in the Tptpmn unit decreases at most to 3 percent of its original permeability (Figure 6.5.4-3c). In the Tptpll unit, vertical mean permeability is estimated to decrease at most to 50 percent of its original value (Figure 6.1.1-5b).

At the drift crown, within one drift radius, horizontal fractures tend to stay open because they are oriented parallel to the stress-free open drift. Consequently, at the drift crown, the vertical permeability will decrease at the same time horizontal permeability tends to increase, leading to a pronounced anisotropy in the permeability field. As an example, Figures 6.5.4-3d and 6.5.4-4d show that at the drift crown, the horizontal permeability has increased most by a factor of 17, while the vertical permeability has decreased to 5 percent of its initial value.

The impact of these THM-induced changes in hydraulic properties is evaluated by a comparison of the liquid percolation flux for a partially coupled TH simulation and a fully coupled THM simulation. The comparison shows that away from the emplacement drift, where changes in permeability and capillary pressure are uniformly distributed horizontally, THM processes have no significant impact on the liquid flow field.

Close to the drift, where permeability changes are not uniform, some redistribution of the flow field is predicted. The dryout zone around the emplacement drift is smaller and contracts sooner toward the drift wall. A smaller dryout zone in the THM case may be related to changes in capillary pressure or to smaller air permeability, resulting in less effective heat convection in the boiling zone. A shorter dryout period could have an impact on the possibility for seepage of water into the drift. The small effect on the dryout time and overall results of this analysis indicate that THM processes have a minor impact on drift-scale repository performance including seepage of groundwater into the drift and its chemical composition. Moreover, the THM-induced changes in hydrological properties calculated in this model report are used for evaluation of the impact of THM processes on drift seepage in *Seepage Model for PA Including Drift Collapse* (BSC 2004 [DIRS 167652], Section 6.7). That analysis shows a slight reduction in drift seepage when THM coupling is considered.

In general, the findings in Section 6.7 of this model report is that the drifts (not exposed to strength degradation and seismic loading) will remain stable throughout the 10,000-year period although some yielding of the rock walls is expected for drift located in the low quality lithophysal rock during the first 100 years after closure. The finding that the drifts are stable throughout the 10,000-year period is significant to repository performance because intact drifts provide added confidence that capillarity will continue to divert significant amount of water around the drift, with little water available to seep into the drifts. With limited water available within the drift, there is little water available to transport exposed radionuclides, if any, out of the drift to the saturated zone below and ultimately to the accessible environment. In Section 6.8, changes in hydrological properties caused by a severe seismic event were estimated. For the extreme and unlikely case of a completely collapsed drift, changes in hydrological properties in the host rock adjacent to the collapsed drift would be larger than for an intact drift. In Section 6.8, it was estimated that the permeability could increase by about 1 to 2 orders of magnitude and that capillary pressure could decrease to about 50 percent of its initial value just

above the drift; whereas larger changes are predicted to occur on the side of the drift. The increase in permeability on top of the drift and the larger increase on the side of the drift will facilitate diversion of groundwater flow around the drift and, thereby prevent water from seeping into the drift. On the other hand, the reduced capillary pressure could reduce the strength of the capillary barrier and, thereby increase the likelihood for drift seepage. However, as discussed above the *Drift Degradation Analysis* (BSC 2004 [DIRS 166107], Sections 6.4.2.4 and 8.1) indicates that only partial rock fall is likely to occur for drifts located in the low quality lithophysal rocks. Furthermore, low quality rock representing a lithophysal porosity of about 25-30 percent represents an estimated less than 5 percent of the rock in the Tptpll unit (*Drift Degradation Analysis* (BSC 2004 [DIRS 166107], Figure E-10).

6.10 DISCUSSION OF UNCERTAINTIES

The model predictions in this analysis depend on a representation of TM-induced changes in hydraulic properties and in particular, changes in fracture permeability. In this context, a number of potential sources of uncertainty deserve further discussed below: (1) simplified conceptualization of the fracture network geometry, (2) drift-wall inelastic behavior, (3) possible fracture-shear-induced permeability enhancement, (4) fracture stress versus permeability relationship, (5) effects of heterogeneous rock properties, and (6) mechanical properties of the Tptpll unit.

6.10.1 Simplified Conceptualization of the Fracture Network

For correction of hydrologic properties, three orthogonal sets, two vertical and one horizontal, are used. These fracture sets reflect the three main fractures sets observed in the TSw2 TM unit (CRWMS M&O 1998 [DIRS 102679], Section 7.4.5):

1. One prominent vertical, southeast trending
2. One less-prominent vertical, southwest trending
3. One less-prominent subhorizontal.

In the field, there are also fractures labeled as randomly oriented that account for a significant portion of all fractures measured in the ESF (CRWMS M&O 1998 [DIRS 102679], p. 37). These randomly oriented fractures could impact the calculated changes in permeability in certain regions of the drift wall. For example, the calculated permeability correction factor presented in Figure 6.5.1-1 indicates that the fracture permeability increases preferably on top of the drift (red contour in Figure 6.5.1-1a) and at the spring line (red contour in Figure 6.5.1-1b). These increases in permeability are caused by the unloading of fractures that strike parallel to the drift opening, which are either horizontal or vertical. Figure 6.5.1-1 also shows that there are zones at the drift wall with little or no increase in permeability. These zones are located at the drift wall at an orientation about 45° above and below the horizontal. The fracture permeability increases less in this zone because no fractures dip 45°, hence, no fractures are oriented parallel to the drift in this area. If, on the other hand, randomly oriented fractures were considered in the model, the permeability would also increase in this area, giving a more uniform increase in permeability around the drift wall.

6.10.2 Drift Wall Inelastic Behavior and Drift Collapse

The possibility of inelastic deformation at the drift wall of an emplacement drift located in the Tptpmn unit can be assessed as using observations of inelastic drift wall deformation in the DST (Williams 2001 [DIRS 159516], pp. 4 to 7). At the DST, a limited scaling of rock at the drift crown was observed, first as small rock chips falling on the floor of the test drift after about 2 years of heating, then as larger pieces of loose rock appearing after 3 to 3.5 years of heating. A simulation of the DST is conducted in Section 7.4 for validation of the drift scale THM model. From this analysis, Figure 6.10.2-1 presents the calculated evolution of horizontal stress (maximum principal compressive stress) at the point of the DST drift crown, where limited scaling was observed. The figure shows that the calculated compressive stress is about 61 and 68 MPa at 2 and 3 years, respectively, which indicates that limited scaling at a drift wall could occur when the maximum compressive stress reaches about 60 MPa. This stress value is about one-third of the uniaxial compressive strength (187 MPa) of laboratory-scale intact rock (CRWMS M&O 1997 [DIRS 103564], Table 2-9, pp. 2-23).

The simulation results in Section 6.5 show that the maximum principal compressive stress at the crown for a drift located in the Tptpmn unit does not exceed 31 MPa (Figures 6.5.3-3 and 6.5.3-4). Thus, the expected maximum principal stress at the wall of the emplacement drift is roughly half the magnitude at which limited rock scaling was observed in the DST. It is reasonable that the thermal stress is much higher at the DST because of heating that is 6 to 12 times greater than the areal thermal loading for the current repository design (BSC 2004 [DIRS 169900], Section 6.3.1.1). Moreover, the uneven drift wall exacerbated the scaling at the DST; whereas emplacement drifts will be excavated with a tunnel boring machine, leading to smoother walls. The results of calculated thermal stress at the drift crown, as well as the estimated in situ rock compressive strength at the DST, are consistent with the results of the *Drift Degradation Analysis* (BSC 2004 [DIRS 166107], Sections 6.2 and 7.6.5.3). Overall, both the analysis conducted in this model report and the *Drift Degradation Analysis* (BSC 2004 [DIRS 166107]) show that inelastic drift wall behavior is not likely in the Tptpmn unit.

The results in Section 6.7 indicate that for a low quality lithophysal rock (with low bulk and shear modulus, and low-strength rock properties), drift wall inelastic behavior is initiated during the excavation of the drift. A yield zone develops and extends about 0.5 m into the sidewall of the drift. During the thermal period, this zone of yielding does not extend much further because of relatively low thermal stresses in the rock mass. Changes in hydrologic properties in the inelastic zone are expected to be within one order of magnitude as calculated in Sections 6.7.2 and 6.8.1. In the case of a drift collapse caused by seismic loading, the zone of yielding is more extensive, especially in the sidewall of the collapsed drift. The calculated permeability changes of 1 to 2 orders of magnitude on the top of a collapsed drift, and 2 to 3 orders of magnitude on the side of a collapsed drift, are the maximum changes calculated for the strain-based approach in Section 6.8. This is an extreme estimate of maximum changes, providing an upper bound of permeability increases around a collapsed drift.

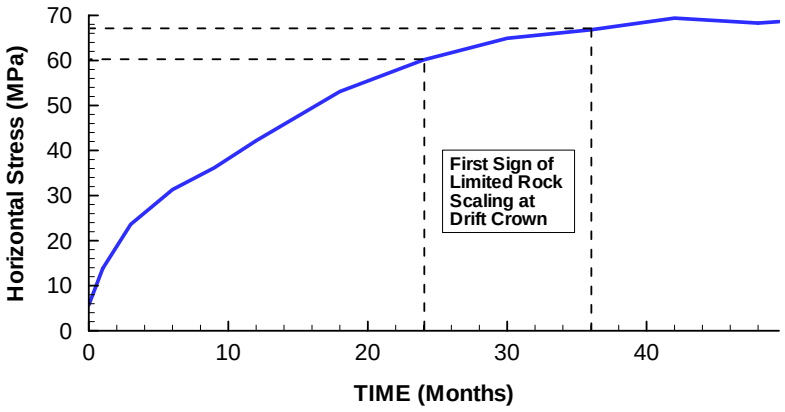

Output DTN: LB0306DSTTHMVL.002.

NOTE: From the analysis of the DST presented in Section 7.4 of this model report.

Figure 6.10.2-1. Calculated Evolution of Maximum Principal Compressive Stress (Horizontal Stress) at the Crown of the Heated Drift

6.10.3 Possible Fracture-Shear-Induced Permeability Enhancement

During heating of the rock mass, the horizontal stresses in the repository unit (away from the drift wall) increase with time, reaching a maximum at about 800 years when the average temperature at the repository level peaks (Figures 6.5.3-1 through 6.5.3-3), while the vertical stresses remain almost constant. This leads to increased differential stress, which could produce shear slip along favorably oriented discontinuities. Fracture shear slip would likely first occur near the drift wall, where the differential stresses are highest but could also occur in the rock mass away from the drift. The stress analysis presented in Figures 6.5.3-1 and 6.5.3-2 indicates that, except for the drift vicinity, the highest difference between vertical and horizontal stresses would occur above the repository and toward the ground surface. For example, at z = 40 m, the horizontal compressive stresses increase to about 13 MPa at 1,000 years; whereas the vertical stress is about 4 MPa. Using a Mohr-Coulomb failure criteria, it can be shown that if such a slip occurred, it would preferably take place along subhorizontal fractures, or fractures oriented at an angle of about 30° to the horizontal (maximum principal) stress. Vertical fractures, on the other hand, are not likely to slip during the thermal period because heating will increase the stress normal to these fractures and hence increase their shear strength. Furthermore, a potential fracture shear-induced enhancement of permeability along subvertical fractures is likely to be counteracted by the high compressive horizontal stresses that would tend to keep the fractures closed at a low permeability. This indicates that the vertical permeability is not likely to be enhanced by shear slip.

Furthermore, observations at the SHT and ongoing DST show little evidence of inelastic rock mass behavior (Sobolik et al. 1998 [DIRS 162049]; Sobolik et al. 1999 [DIRS 163202], p. 735) or shear-induced permeability enhancement. During heating, the permeability generally decreases (Section 7.10). Although these tests span, at most, several years and may, therefore not fully represent long-term behavior, the heating is generally more aggressive resulting in greater differential stress. However, as discussed in Section 6.10.2, fracture shear slip could

possibly occur very close to the drift wall; loose blocks could slip due to a lack of mechanical confinement near the drift wall. Such loosening of blocks and rock fall, which is studied in *Drift Degradation Analysis* (BSC 2004 [DIRS 166107], Sections 6.2 through 6.4), and changes in hydrologic properties for such cases are provided in Section 6.8 of this model report.

6.10.4 Fracture Stress versus Permeability Relationship

The model predictions in this model report depend on the relationship between stress and fracture permeability. The stress-versus-permeability function and the associated stress-versus-aperture function that also determines changes in capillarity were derived as a bounding estimate that emphasizes THM-induced changes in hydrologic properties. The function was calibrated against data from both niche experiments and the DST. The function was calibrated so that it gives the best estimate of mean permeability changes during excavation (for reducing stress), whereas it gives a bounding estimate THM-induced changes in hydrologic properties.

The adopted stress-versus-permeability function gives the best estimate for changes in mean permeability during excavation. As shown in Figure 6.10.5-1, the results of the niche-excavation experiments, to which this calibration is made, indicate that the excavation-induced changes in permeability result in a shift in the permeability distribution, while the spread (standard deviation of log permeability) remains approximately constant. Near the drift wall, the analysis shows that permeability can increase about one order of magnitude in a direction parallel to the drift wall (Figure 6.5.1-1). This magnitude of change is dictated by the fracture normal stress versus permeability function for reducing stress, which both have been calibrated against in situ tests in the Tptpmn and Tptpll units (Figure 6.4.4-1). The fact that mean permeability increases about one order of magnitude near the drift in the Tptpmn unit and less than one order of magnitude in the Tptpll unit is well established from observed permeability changes at excavated niches. *In-Situ Field Testing of Processes* (BSC 2004 [DIRS 170004], Table 6.1.2-1) shows that the geometric mean of the post/preratio varies between 9.42 to 25.38 for three niches in the Tptpmn unit; whereas Table 6.1-2-2 shows that the geometric mean of post/preratio is 2.37 for one niche in the Tptpll unit. Thus, the appropriateness of the fracture stress-permeability function to represent excavation effects is established from these field data.

In the longer term, at 1,000 to 10,000 years, the analysis in this model report shows that permeability decreases significantly in an area extending hundreds of meters above and below the drift (Figure 6.5.4-1). The model simulation shows that the permeability decreases most in the vertical direction, by closure of vertical fractures. Such closure of vertical fractures has also been predicted in calculations in *Coupled Thermal-Hydrologic-Mechanical Effects on Permeability Analysis and Models Report* (BSC 2001 [DIRS 155957], Section 7, bullet 2), using the alternative distinct-element model. In this same report (BSC 2001 [DIRS 155957], Section 6.3.3), permeability decreases of up to 6 orders of magnitude were calculated. This was a model artifact having no residual fracture aperture that could limit the amount of fracture closure. Our calculated lower limit of permeability decrease, a factor of 0.03 for vertical permeability in the Tptpmn unit (Figure 6.5.4-3c) and 0.5 in the Tptpll unit (Figure 6.6.1-5b), is strongly dependent on the residual fracture permeability, which was calibrated to field data. This residual permeability is a parameter constrained by the maximum observed decrease in permeability at the DST and SHT. The fact that the parameter is constrained from the maximum

observable change at DST and SHT implies that predicted change in permeability provides a bounding case that emphasizes the effects of THM-induced permeability changes at a future repository.

As pointed out in Section 6.4.4, an isotropic initial permeability is adopted to be consistent with other seepage models for Yucca Mountain. Setting the initial joint aperture and fracture spacing to be the same for all three joint sets results in an initially isotropic permeability. When calibrating the stress-versus-permeability function, different residual joint apertures were calculated (Appendix A) for each joint set due to different initial normal stresses acting on each set. The resulting residual hydraulic aperture of the subhorizontal set is approximately 2 to 5 times greater than the residual hydraulic apertures of the two subvertical joint sets. The subhorizontal joints are vapor-phase partings (BSC 2004 [DIRS 166107], Section 6.1.4.1) with rough surfaces on a small scale, and some mineral filling. The subvertical joints are cooling joints, relatively smooth, with large amplitude asperities, but wavelengths of meters. It is expected that the smooth fractures have smaller residual aperture. At the DST, the calibrated residual permeability correction factors in the horizontal directions are 0.26 and 0.29, while the residual permeability correction factor in the vertical direction is 0.025 (see Appendix A first table row 3 for where the calibrated values of $F_{krx,}$ F_{kry} and F_{krz} are listed for the case of b_{max} = 200 μm and α = 0.52 MPa^{-1}). In the Tptpmn model domain, this limits the permeability reduction to F_{kx} = 0.24, F_{ky} = 0.27 (at 100 years in Figure 6.5.4-4b), and F_{kz} = 0.04. (at 1,000 years in Figure 6.5.4-4c). The exact numbers for these changes can be extracted from the output DTN: LB0306DRSCLTHM.001 (filenames: Tmn1_100y.out and Tmn1_1ky.out) for elements located near the drift. The permeability correction factors in the Tptpmn model domain at the level of the repository are slightly different from those at the DST because the initial stress is lower and the initial permeability is higher. The initial stress is lower because the emplacement drift in the Tptpmn model domain is located at a shallower depth than the DST. The initial permeability is higher (by a factor 3.3) than at the DST, because the local mean permeability at the DST is slightly lower than the representative mean permeability over the entire Tptpmn unit. It is important that the stress-versus-permeability function is calibrated using consistent and actual local permeability at the field experiments (DST and niches). Therefore, it is appropriate to calibrate the stress-versus-permeability function using the actual mean permeability at the DST, which is $1 \cdot 10^{-13}$ m^2. This results in a stress-versus-permeability relation where the residual permeability depends on the initial permeability. Thus, in rock units where the initial permeability is higher, the residual permeability will also be higher, resulting in a less sensitive relationship between stress and permeability. This is in agreement with observations at the niche tests, and the current model can reproduce those observations (Section 7.5 and Figure 7.5-3).

It may be argued that since the initial stress field is anisotropic (by a factor of 2), the different fracture sets are subjected to different initial stress and therefore may have different initial aperture. Furthermore, it could be argued that the residual aperture would be an inherent property of the rock that may not vary substantially for different fracture sets. As an alternative approach, the stress-versus-permeability function can be calibrated assuming the same residual aperture for all fracture sets and a variable initial aperture, depending on the initial normal stress across each fracture set. Such calibration was performed and documented in Wang (2004 [DIRS 170508], pp. 25 to 34). In such a case, the calibrated parameters for the stress-versus-aperture function for each fracture set becomes b_{max} = 200 μm and α = 0.58 MPa^{-1}; that is, the

b_{max} is unchanged whereas α changes from 0.52 to 0.58 MPa^{-1}. The initial aperture for the different fracture sets would be b_{1i} = 53 μm, b_{2i} = 63 μm, and b_{3i} = 33 μm (compared to the isotropic condition of 51 μm for all fractures). Thus, the fractures in the horizontal fracture set (Set 3) would have smaller initial fracture aperture since the vertical stress is higher than the horizontal stresses. This results in a maximum anisotropy factor of 2.2 between horizontal and vertical permeability. The residual aperture for all fracture sets would be about 26 μm. The residual permeability correction factors would be F_{kx} = 0.12, F_{ky} = 0.19, and F_{kz} = 0.087.

For the predicting of changes in the repository rock, the vertical permeability correction factor is the most important, because the analysis showed that the thermal stresses increase mostly in the horizontal direction (Sections 6.5 to 6.7). The vertical permeability factor becomes F_{kz} = 0.087 for the alternative anisotropic initial permeability approach compared to F_{kz} = 0.025 for the adopted isotropic permeability approach. Thus, the adopted method of calibrating the stress-versus-permeability function results in a stronger reduction in permeability upon heating and will therefore result in stronger THM coupling than for the alternative method based on the calibration data available.

There currently are no in situ tests available to estimate residual permeability within the Tptpll unit. This means that the predicted changes in permeability for the Tptpll unit is more uncertain. However, considering the trend of relatively smaller changes in permeability for initially larger permeability values observed at the niche excavation experiments (BSC 2004 [DIRS 170004], Section 6.1.2.3), the impact of THM processes on fluid flow is likely to be smaller in the Tptpll unit than in the Tptpmn unit. This trend is also captured in the modeling results presented in Sections 6.5 and 6.6, which show a relatively smaller change in permeability for the Tptpmn unit than the Tptpll unit.

6.10.5 Effects of Heterogeneous Rock Properties

The analysis in this model report was conducted with initially homogeneous rock properties for each stratigraphic unit, based on calibrated mean hydrological properties, a bounding estimate of the thermal expansion coefficient that emphasizes the thermal stress, and a bounding fracture normal stress versus permeability relationship that emphasizes the effect of thermal stress on permeability.

Variability in the thermal expansion coefficient could cause uneven thermal expansion of the rock and, thereby, induce uneven deformation and shear. However, the variability of the thermal expansion coefficient in between various layers is small, as seen in Figure 6.4.3-1, and variability within each layer is not expected to induce any significant differential deformations. The standard deviation for the thermal expansion coefficient derived from laboratory measurements, at temperatures up to about 175°C, is generally less than $1 \cdot 10^{-6}$/°C (Brodsky et al. (1997 [DIRS 100653], Table 4-4). On the other hand, local fracturing could affect the in situ thermal expansion coefficient with larger expansion in relatively unfractured regions. The slight variability of TM-induced displacements at the DST may reflect variability in the in situ thermal expansion coefficient as a result of fracturing.

An initially heterogeneous permeability field would result in heterogeneous changes in permeability, with the largest changes occurring in a zone with an initially lower permeability

(see also results of niche experiments in Figure 7.5-1). This would indicate that for mechanically-induced increasing permeability (e.g., by unloading near a drift), a larger increase in zones with an initially lower permeability would result in a more homogeneous permeability field. On the other hand, for mechanically induced decreasing permeability (e.g., by thermal stress), the permeability would become more heterogeneous. However, the overall results from the niche experiments show that while the changes in mean permeability are about one order of magnitude, the standard deviation of the heterogeneous permeability field change much less (BSC 2004 [DIRS 170004], Table 6.1.2-1). This is further illustrated in Figure 6.10.5-1, which shows the permeability distribution before and after excavation of the niches during the niche experiments. In Figure 6.10.5-1a, which shows the composite excavation response for three niches located in the Tptpmn unit, the excavation induced changes in permeability shift the permeability distribution, while the spread (standard deviation of log permeability) remains approximately constant. Figure 6.10.5-1b, which shows the excavation response for one niche in the Tptpll unit, indicates a smaller shift in relation to its distribution. Figure 6.10.5-1 indicates that the main impact of THM is a change in the mean permeability, even for an initially heterogeneous permeability field. Therefore, it is appropriate to apply the mean permeability changes calculated in this model report to a seepage analysis that considers either the homogenous or heterogeneous permeability field.

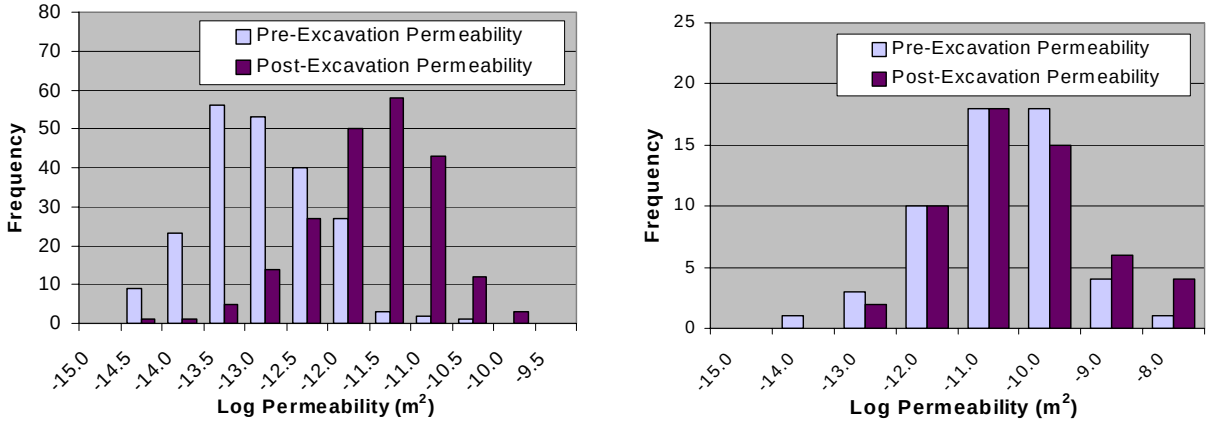

(a) Measurements in Tptpmn unit **(b) Measurements in Tptpll unit**

DTN (measured): LB0310AIRK0015.001 [DIRS 168564]; Output DTN (Histogram plot): LB0306DSTTHMVL.002.

NOTE: Conducted in several boreholes in the crown of three niches (Niche 3107, 3569 and 4788 in the Tptpmn unit, and Niche 1620 in the Tptpll unit).

Figure 6.10.5-1. Histogram of Permeability Distribution Derived from Permeability Measurements

6.11 DISCUSSION OF AN ALTERNATIVE CONCEPTUAL MODEL

As mentioned in Section 6.2, a continuum model was selected for the analysis in this model report for the following reasons:

1. It is consistent with the continuum approaches used in all other UZ models, including the drift-scale TH and THC models, which all have been extensively validated for TH processes (e.g., BSC 2001 [DIRS 157330], Section 6).

2. Previous analyses of TM processes at SHT and DST have indicated that a continuum approach with a linear elastic or nonlinear elastic material model is sufficient to capture observed displacements (Sobolik et al. 1998 [DIRS 162049]; Sobolik et al. 1999 [DIRS 163202], p. 735).

3. Previous comparison of a continuum conceptualization with an alternative discrete fracture conceptualization for TM analysis has shown minor differences in the calculated rock mass deformations (BSC 2001 [DIRS 155957], p. 125).

For an alternative, discrete-fracture approach could be used to calculate similar type of results (mechanically induced changes in permeability and capillary pressure) as with the continuum model approach used in this model report. For the results of these two analyses to agree, a similar stress aperture function would be required for both modeling approaches. This would include a similar residual fracture aperture and fracture normal deformability that provides the upper and lower limits of possible changes in fracture permeability. Thus, a correctly calibrated stress-aperture function should limit the permeability changes to about one order of magnitude for both a continuum and an alternative discrete-fracture approach. The continuum approach used in this model report is adequate because it captures the relevant THM processes at various in situ tests at Yucca Mountain (Section 7) and is sufficient for performing bounding predictions of THM-induced changes in permeability and its impact on the flow field (the bounding concept is described in Section 6.4.2). For the case of yielding around a stable drift (Section 6.8.1), the permeability changes calculated based on the result of the discontinuum mechanical analysis in the *Drift Degradation Analysis* (BSC 2004 [DIRS 166107], Appendix R) are consistent with permeability changes calculated with the continuum model in Section 6.7.2. For the case of a collapsed drift (Section 6.8.2), the discontinuum analysis leads to larger changes caused by block separation in a zone of loose blocks around the drift. Even in this case of severe yielding, a continuum analysis generates useful results if changes in hydrologic properties are tied to strain rather than stress, or if the stress-versus-permeability function is corrected for changes in plastic strain. If significant rock mass yielding occurs, hydrologic properties should be corrected for plastic strain emanating from inelastic fracture opening.

7. MODEL VALIDATION

The drift scale coupled thermal-hydrological-mechanical (THM) process model is used to evaluate the impact of THM processes on permeability and flow in the near-field of the emplacement drifts. The results are used to assess the importance of THM processes on seepage and to support related FEP screening arguments. Consistent with this use, the *Technical Work Plan for: Near-Field Environment and Transport: Near-Field Coupled Processes (TH Seepage and THM) Model Report Integration* (BSC 2004 [DIRS 170236]) indicates that Level I validation is adequate for the drift scale THM model.

7.1 SPECIFICS OF THE DRIFT SCALE THM MODEL VALIDATION

The following subsections describe the specifics of the drift scale THM model validation including confidence building during and after model development, validation steps and validation criteria in accordance with Section 2.2.2 of the TWP (BSC 2004 [DIRS 170236]).

7.1.1 Confidence Building During Model Development to Establish Scientific Basis and Accuracy for Intended Use

For Level I validation of the drift scale THM model, Section 2.2.2.2 of the TWP (BSC 2004 [DIRS 170236]) specifies the following requirements for *Confidence Building During Model Development*. The development of the model should be documented in accordance with the requirements of Section 5.3.2(b) of AP-SIII.10Q, *Models*. The development of the drift scale THM model has been conducted according to these criteria, as follows:

1. *Selection of input parameters and/or input data, and a discussion of how the selection process builds confidence in the model. [AP-SIII.10 Q 5.3.2(b) (1) and AP-2.27Q Attachment 3 Level I (a)].*

   The direct inputs to the drift scale THM model have all been obtained from controlled sources (see Section 4.1 and Tables 4.1-1a and b), including discussion about selection of input and design parameters. The THM properties used as direct input into the drift scale THM model and their sources are summarized in Section 4.1.1.1. A more in-depth discussion of the appropriateness of the selected THM properties for the drift scale THM model is given in Section 6.4. Appendix D contains a discussion of the impact of updated thermal properties. Model assumptions are described in Section 5. Thus, this requirement has been satisfied.

2. *Description of calibration activities, and/or initial boundary condition runs, and/or run convergences, simulation conditions set up to span the range of intended use and avoid inconsistent outputs, and a discussion of how the activity or activities build confidence in the model. Inclusion of a discussion of impacts of any non-convergence runs [(AP-SIII.10Q 5.3.2(b)(2) and AP-2.27Q Attachment 3 Level I (e)].*

   Detailed discussion of initial and boundary conditions for the drift scale THM model can be found in Sections 4.1.1.2, 4.1.1.3, 6.2 and 6.3. Sections 6.5 and 6.6 provide detailed discussion of various model results for the Tptpmn and the Tptpll units respectively (i.e., those of convergence runs). Additional simulation conditions are covered in sensitivity

cases for low quality rock in the Tptpll in Section 6.7 and for drift collapse in Section 6.8. Discussion of nonconvergence runs is not relevant for this model report. Thus, this requirement has been satisfied.

3. *Discussion of the impacts of uncertainties to the model results including how the model results represent the range of possible outcomes consistent with important uncertainties. [(AP-SIII.10 Q 5.3.2(b)(3) and AP-2.27Q Attachment 3 Level 1 (d) and (f)]*.

   Discussion of model uncertainties and their impacts on model results is provided in Section 6.10. A summary discussion on uncertainties and their impact is given in Section 8.2.

4. *Formulation of defensible assumptions and simplifications. [AP-2.27Q Attachment 3 Level I (b)]*.

   Discussion of assumptions and simplifications is provided in Sections 5, 6.1, and 6.2. Additional discussions of simplifications are found in Section 6.10.

5. *Consistency with physical principles, such as conservation of mass, energy, and momentum. [AP-2.27Q Attachment 3 Level I (c)]*.

   Consistency with physical principles is demonstrated by the conceptual and mathematical formulations in Section 6.2 and the selection and use of the TOUGH2 and FLAC3D codes in Sections 3 and 6.2

7.1.2 Confidence Building After Model Development to Support the Scientific Basis of the Model

For confidence building after model development, Section 2.2.2 of the TWP (BSC 2004 [DIRS 170236]), "Confidence Building After Model Development," imposes the following requirements for model validation:

1. *AP-SIII.10Q, Section 5.3.2(c), Method 1: Corroboration of model results with data acquired from the Drift Scale Test (DST).*

   Comparison of model results with experimental data is the main method of validation for the drift scale THM model. The remainder of Section 7 explains the respective validation and modeling activities in detail, and discusses explicitly how the criteria for this validation method, as defined in Section 2.2.2.4 of the TWP (BSC 2004 [DIRS 170236]), have been met.

2. *AP-SIII.10Q, Section 5.3.2(d), Technical review through publication in a refereed professional journal.*

   The validation criterion is that a technical review is conducted through at least one publication in a refereed professional journal, as stipulated in Section 2.2.2.4 of the TWP (BSC 2004 [DIRS 170236]). The publication needs to describe the modeling activity for the models in this model report. Section 7.9 addresses this criterion.

7.1.3 Validation Steps

In accordance with model validation methods, the drift scale THM model is first tested by a coupled THM simulation of the Yucca Mountain Drift Scale Test (DST) and a coupled hydrological-mechanical (HM) simulation of the Yucca Mountain niche experiments. This tests the underlying conceptual model for representing fractured rock and demonstrates that the drift scale THM model appropriately captures all THM processes relevant to the performance of the repository at Yucca Mountain. Additional validation is conducted by corroboration with observation of sidewall fracturing in tunnels at Yucca Mountain, results of an alternative conceptual model (method 2), and through publication in peer-reviewed journals. Multiple lines of evidence are provided from natural analogues in the geothermal field and from other heater tests.

In accordance with the original *Technical Work Plan for: Performance Assessment Unsaturated Zone* (BSC 2004 [DIRS 167969], Section I-3-3-1, p. 45), and as updated in *Technical Work Plan for: Near-Field Environment and Transport: Near-Field Coupled Processes (TH Seepage and THM) Model Report Integration* (BSC 2004 [DIRS 170236], Section 2.2.2), the validation of the drift scale THM model is conducted in three steps (Figure 7.1.3-1):

- Validation of TM aspects
- Validation of HM aspects
- Validation of THM aspects.

As shown in Figure 7.1.3-1, each of these steps represents part of or the entire path for calculating THM-induced changes in permeability and their impact on hydrological processes.

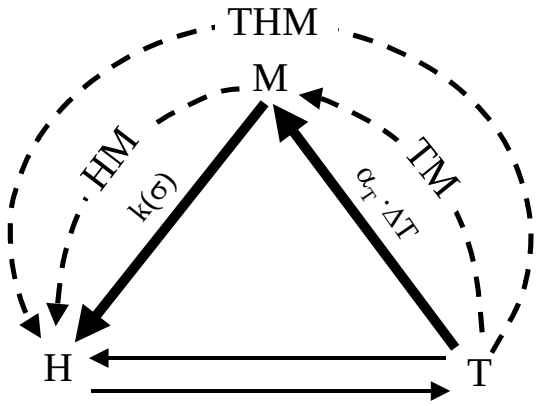

Figure 7.1.3-1. Illustration of Coupling Paths for Validation of TM, HM and THM Aspects of the Drift Scale THM Model

The model's ability to capture these TM, HM, and THM processes is tested by corroboration with experimental data from the DST, including:

- Rock mass displacement measured by multipoint extensometers (MPBXs) installed in boreholes
- Air-permeability measurements conducted at periodic intervals through the duration of the DST.

The drift scale THM model's ability to capture the general TM responses is tested by comparison of model results to observations from MPBX extensometers at the DST. The relative displacements between grid points located at respective measurement points and the borehole collar are compared to the model. Agreement of general displacement responses confirms the appropriateness of the underlying conceptual model for representing TM responses in the fractured rock mass at Yucca Mountain.

For the purpose of this report, the validation for TM processes emphasizes the effect of thermal stress on permeability. However, because there are no direct measurements of thermal stress at the DST, the validation of the TM model is conducted by comparison of simulation results to measured TM-induced displacements. If the TM induced displacements are well predicted, then TM-induced stresses are also expected to be well predicted. Both TM-induced stress and TM-induced displacement depend on the in situ rock thermal expansion coefficient. There is also another potential impact of thermal stress on permeability. If the thermal stress is sufficiently high, the thermal stress may induce inelastic deformation as discussed in Section 6.10.2. Such inelastic deformations and failure near the surface of the drift wall can result in additional changes in permeability. The drift scale THM model is capable of simulating moderate inelastic behavior near the drift wall as discussed in Sections 6.7 and 6.8. Model validation should also assure that the predicted thermal stresses are within reasonable limits so that the potential for inelastic behavior near the drift wall is predicted with sufficient accuracy.

The drift scale THM model capability to capture HM responses (mechanically-induced changes in permeability) is tested by comparison of simulated versus measured changes in air-permeability. Air-permeability changes at the DST arise from (1) fracture opening or closure (that is, HM processes) and (2) thermally-induced changes in water saturation, (that is, TH processes). The two effects may either reinforce or offset each other. To determine the contributions of these processes in the DST it is necessary to investigate air-permeability measurements in different regions around the heated drift. For example, for measurements conducted in the boreholes farthest away from the heat source, the saturation-induced changes are expected to be negligible, and HM effects dominate. Further confirmation of the model capability to represent HM responses (mechanically induced permeability changes) is provided by corroboration with excavation-induced permeability changes observed near four excavated niches in the Tptpmn and Tptpll unit. Agreement of the general responses of simulated and measured air-permeability at various regions around the DST, as well as in the excavated disturbed zone of niche experiments, confirms the appropriateness of the adopted model for relating permeability to changes in the three-dimensional stress field.

It should be noted that both the DST and niche experiments were used to derive the stress-versus-aperture relationship used in this analysis (Section 6.4.4). Two points of measured permeability changes were abstracted, one from the DST giving an estimate of the residual permeability and one from the niche experiment representing the mean increase in permeability in the crown of a drift at one specific initial permeability value. Thus, the validation of the HM part is conducted following the intent of comparing observed data with model predictions made largely independent of test results.

As illustrated in Figure 7.1.3-1, the THM aspect represents the full path from T to H, which is the sum of the TM and HM couplings. In the DST, representation of the full THM path depends on both TM and HM couplings. In the DST, the full THM path consists of (1) thermally induced stress (TM coupling) and (2) stress-induced permeability changes (HM coupling). Thus, first the increased temperature induces thermal stresses that change the in situ stress field. These changes in the in situ stress field act upon preexisting fractures, which may open or close, resulting in changes in fracture permeability. A misrepresentation of either TM or HM processes in the simulation process will propagate as a misrepresentation of the full THM path. The drift scale THM model capability to capture this chain of processes is tested by comparison of simulated versus measured changes in air-permeability. This is the most relevant validation for the purpose of this report.

The validity of the conceptual model for simulating TH processes (TH coupling in Figure 7.1.3-1) at the Yucca Mountain is been demonstrated through model-data comparison using data from various in situ tests (BSC 2004 [DIRS 170338], Section 7). The drift scale THM model uses a continuum model consistent with the overlapping-continuum (matrix and fracture continuum) approach applied in *Drift-Scale Coupled Processes (DST and TH Seepage) Models* (BSC 2004 [DIRS 170338], Section 6.2.1). Thus, a formal validation of all the TH processes is not performed in this model report, which is focused on THM effects. However, it is emphasized that the simulated temperature field at the DST is in reasonable agreement with the measured one, because temperature changes are the driving force for THM coupling (Figure 7.1.3-1). Validation of the drift scale THM model against the DST is conducted in the following steps:

1. Check that the simulated temperature field is in reasonable agreement with the observed temperature field to ensure that the THM model is properly implemented in terms of thermal behavior.

2. Check that simulated rock mass displacements capture the general trends and average magnitudes of observed displacements (validation of TM processes).

3. Check that the simulated changes in air permeability capture the general trends and magnitudes observed in the field (validation of THM processes).

A validation of the drift scale THM model is also conducted against measurement of excavation-induced changes in air permeability in the crown of four niches. This validation investigates the validity of the stress-permeability model and the stress-aperture function over a range of initial permeability values. Validation against the niche experiments was not explicitly included as an item in *Technical Work Plan for: Performance Assessment Unsaturated Zone*

(BSC 2004 [DIRS 167969], Section I-3-3-1), but was added since it provided a test of the model for an experiment conducted in the Tptpll unit. This test is used to confirm the model capability to capture stress-induced changes in both the Tptpmn and Tptpll unit and confirm the observation that the stress-induced permeability changes are generally smaller in the Tptpll unit than in the Tptpmn unit.

The mechanical model and in situ strength properties of lithophysal rock are further validated by corroboration against observations of minor damage in the sidewalls of the ESF Main Drift and ECRB Cross Drift. The validation is checked in two ways: (a) against field observations of Tptpll and Tptpul units and (b) against an alternative model of the *Drift Degradation Analysis* (BSC 2004 [DIRS 166107], Section 7.6.5.2). The mechanical properties derived for the low quality lithophysal rock are verified by comparison of predicted yielding to minor damage observed in the sidewalls of the ESF Main drift and ECRB Cross Drift (BSC 2004 [DIRS 166107], Section 7.6.5.2).

The validation of the drift scale THM model against the DST, niche excavation experiments, and side-wall fracturing in the ECRB is complemented by evidence from other heater tests, from comparison to an alternative conceptual model, and from publication in peer-reviewed journals.

7.1.4 Validation Criteria

Because the main output from this report is thermal-mechanically-induced changes in the permeability field during heating of the rock mass, it is particularly important to validate that the model can predict changes in the permeability field with sufficient accuracy for its intended use. The relevant criterion for validation of the complete THM path considers the chain of TM and HM links as shown in Figure 7.1.3-1. For THM processes, the validation criterion is to find general, qualitative agreement with air-permeability measurements and trends during the heating phase. The predicted changes in air permeability are in the correct direction and correct within an order of magnitude; that is, log (k/k_i) simulated and measured differ by less than 1. Observed trends (e.g., k/k_i decreases followed by increases, or the reverse) are matched by model predictions (BSC 2004 [DIRS 170236], Section 2.2.2). The quantitative criterion of simulation results within one order of magnitude is reasonable considering the natural variability of permeability at Yucca Mountain, and considering the variability of permeability used in the seepage models for development of drift seepage probabilities. At Yucca Mountain, the permeability generally spans over four orders of magnitude in each rock unit, and the mean permeability is varied over four orders of magnitude in the seepage analysis. A prediction of TM-induced permeability changes within one order of magnitude is sufficient for the intended use of evaluating THM effects on the seepage models. In Section 2.2.2 of the TWP (BSC 2004 [DIRS 170236]), the validation criteria for TM processes are as follows: The average magnitude of relative displacements and the trends of displacement evolution should be captured in the numerical model, and the average displacements for the rock mass as a whole, taken over the entire heating sequence, should be within 50 percent. A prediction of the rock mass thermal expansion (which is measured by extensometer displacements in the DST) within 50 percent of

measured values ensures that the thermal expansion coefficient, and thermal stress, are within 50 percent of actual conditions. The 50 percent criterion for displacements is motivated by two reasons:

1) If the model predicts thermally-induced stresses and displacements within 50 percent, it signifies that the evolution and extent of thermal stresses and their impact on permeability changes are reasonably well predicted. Limiting the error in the prediction of thermal stress to 50 percent assures that the error in the predicted permeability changes as a result of elastic changes in fracture aperture is within an order of magnitude.

2) If the model predicts thermally-induced stresses and displacements within 50 percent, it signifies that the evolution and extent of any inelastic zone near the drift wall and its impact on permeability changes near the drift wall are reasonably well predicted. Limiting the error to 50 percent assures that error in the predicted permeability changes near the drift wall is within an order of magnitude.

The 50 percent limit for the first reason can be derived considering the following: if the thermal stress increases so much that the fracture permeability reaches close to its residual value, then the permeability can decrease at most to a factor of 0.03 of its original value in the Tptpmn model (Section 6.9). If the simulated thermal stress under predicted the in situ thermal stress by 50 percent, then the predicted permeability correction factor could be estimated at about 0.06 or less. The fact that a 50 percent under prediction of stress would lead to a permeability factor of 0.06 or less can be understood from the stress-versus-permeability function shown in Figure 6.4.4-1. The model results summarized in Section 6.9 show that permeability decreases at most to 0.03 of its original value at peak thermal stress. In Figure 6.4.4-1, this would represent going from point 1 to point 2. Underestimating the stress by 50 percent implies going from point 1 to half way between point 1 and 2. This would lead to a permeability correction factor of about 0.06 or less. Thus, the permeability change factor would still be predicted with the accuracy well within one order of magnitude.

The 50 percent limit for the second reason can be derived considering the stress evolution at the drift wall as discussed in Section 6.10.2. In Section 6.10.2 it was concluded that the current drift scale THM model for the Tptpmn model domain predicts a maximum compressive stress of about 31 MPa in the crown of the drift, whereas the rock mass compressive strength is estimated at about 60 to 70 MPa. Therefore, a prediction of the TM-induced thermal stress within 50 percent provides a sufficient margin assuring that compressive stress could not exceed 60 MPa at the drift crown, so that the results indicating that no significant failure will occur for a drift in the Tptpmn unit are valid. For the Tptpll unit, a low quality lithophysal rock unit, inelastic (nonseismic) behavior is expected to occur during the excavation of the drift, whereas TM-induced stresses are expected to be small and therefore not important in the Tptpll unit (Section 6.7).

It is noted that the measured displacements at the DST generally span a range of ±50 percent for various but equivalently located monitoring points (Section 7.4.2). Thus, if the average displacements are predicted within 50 percent, then the local variability in displacement and hence the local variability in TM processes will be within 50 percent of those predicted.

Validation criteria for calculation of excavation-induced permeability changes in the niche experiments are equivalent to the criteria for predictions of permeability changes in the DST. The predicted changes in permeability are in the correct direction and correct within an order of magnitude; that is, log (k/k_i) simulated and measured differ by less than 1. Observed trends (e.g., k/k_i decreases followed by increases, or the reverse) are matched by model predictions.

Finally, the corroboration against observations of minor damage in the sidewalls of the ESF Main Drift and ECRB Cross Drift are judged qualitatively since there are no quantitative measurements for comparison. However, if the calculated pattern of yielding (fracturing) around the drifts agrees with that observed, it indicates that the mechanical model and the rock mass strength properties are appropriate.

In summary, the following validation criteria derived from Section 2.2.2.4 of the TWP (BSC 2004 [DIRS 170236]) for corroboration against field observations are used:

- The predicted changes in air permeability at the DST and niche excavations are in the correct direction and match the average of the observed changes within an order of magnitude; that is, log (k/k_i) simulated and measured differ by less than 1.

- Observed trends of air permeability (e.g., k/k_i decreases followed by increases, or the reverse) at the DST and niche excavations are matched by model predictions.

- The predicted displacements at the DST are within 50 percent of the measured average displacement, for the rock mass as a whole, taken over the entire heating sequence.

- The observed pattern of yielding (minor-fracturing) observed in lithophysal rock around the ECRB Cross Drift is matched qualitatively by the model simulation.

Of these criteria, the first two, related to prediction of permeability changes, are most relevant for the purpose of this model report.

7.2 THE DRIFT SCALE TEST

7.2.1 Design and Geometry

The DST is a large-scale, long-term thermal test designed to investigate coupled thermal-mechanical-hydrological-chemical behavior in a fractured, welded tuff rock mass (CRWMS M&O 1998 [DIRS 111115]). The test block is located in one of the alcoves of the Exploratory Studies Facility (ESF) in the Tptpmn unit. Figure 7.2.1-1 shows a plan view of the test block, and Figure 7.2.1-2 shows a three-dimensional perspective of the DST, showing electrical heaters and many of the approximately 150 instrumented boreholes for measuring thermal, hydrological, mechanical, and chemical processes. The DST test block centers around the Heated Drift, which is 47.5 m long. Heating is provided by nine floor canister heaters within

the Heated Drift, as well as 50-rod heaters, referred to as "wing heaters," placed into horizontal boreholes emanating from the Heated Drift. Each wing heater is composed of two equal-length segments (4.44 m) separated by a 0.66 m gap. The distance between the Heated Drift wall and the tip of the first heater segments is 1.66 m. Dimensions of the Heated Drift and canister heaters are similar to the current design of waste emplacement drifts. The heaters of the DST were activated on December 3, 1997. The heating phase continued for approximately four years, until January 14, 2002. Currently, the DST is in the midst of a planned four-year cooling period.

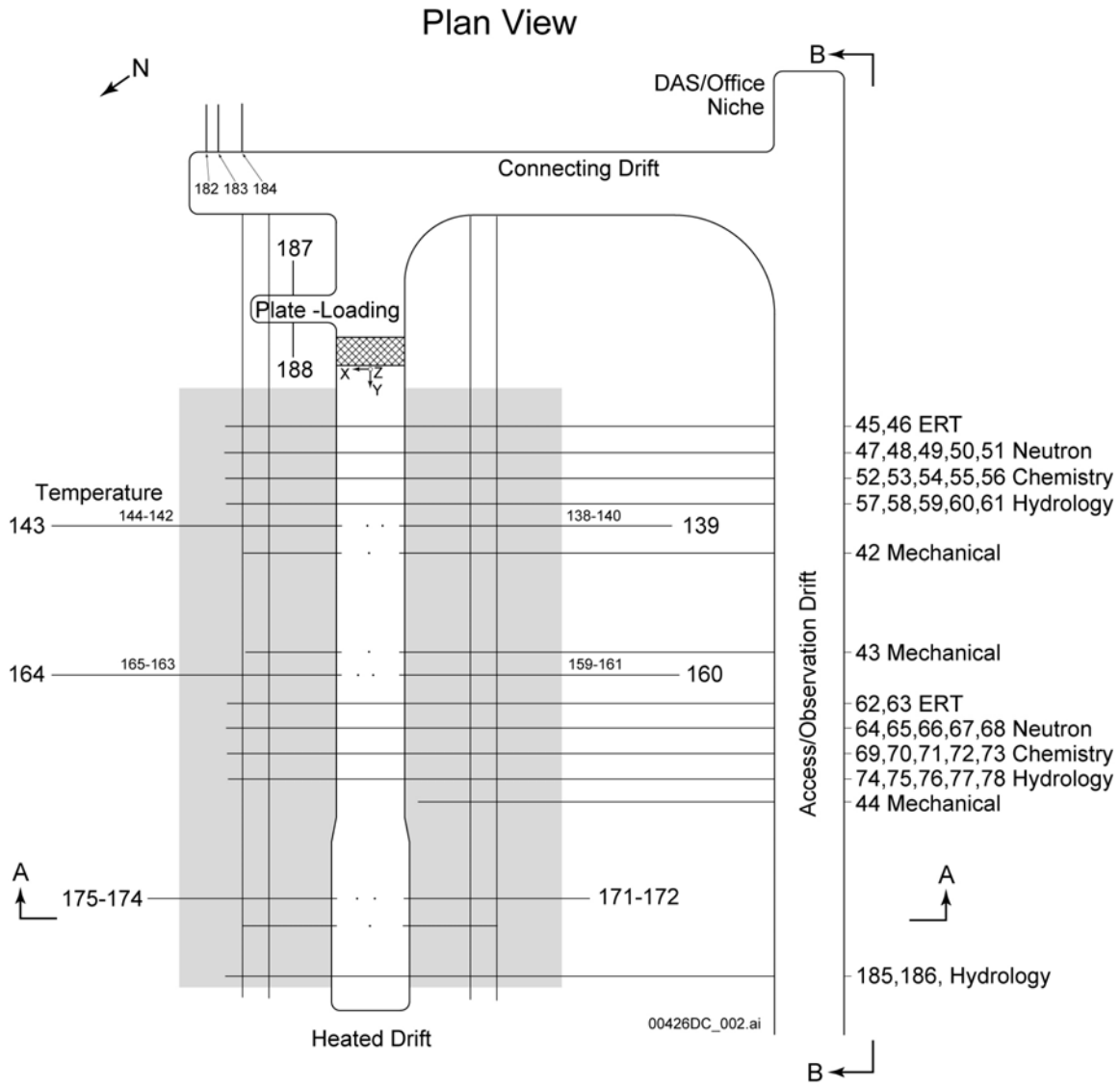

Source: Birkholzer and Tsang 1997 [DIRS 100597], Figure 3.1-1.

Figure 7.2.1-1. Plan View of DST Block

7.2.2 Measurements to Probe Coupled THM Processes

Measurements in the DST include laboratory and field characterization of the test block prior to the activation of heaters and, passive monitoring, and active testing during the heating and subsequent cooling phases. Preheat laboratory characterization included measurements of thermal properties, hydrological properties, mechanical properties, mineralogy-petrology studies, and pore-water chemical and isotopic analyses using rock core. Preheat field characterization of the thermal test block involved rock mass classification, fracture mapping, video logging of the boreholes, geophysical measurements, and air-permeability testing.

Measurements during the heating and cooling phases of the DST are divided into two categories: continuous passive monitoring data, and active testing data, which are acquired periodically. The DST test block has been instrumented with thousands of sensors to monitor the thermal, mechanical, hydrological, and chemical processes on at least an hourly basis. In Figure 7.2.1-2, the instrumented boreholes are color-coded according to their functions. For the purpose of this model report, the focus is on boreholes designed to measure thermal (yellow), hydrological (blue), and mechanical (green) behavior, as extracted in Figures 7.2.2-1 to 7.2.2-3. Radial arrays of 20 m long boreholes emanating from the heated drift monitor the temperature evolution, as do longitudinal boreholes parallel to and extending over most of the length of the heated drift. Temperature sensors in each borehole are installed at approximately 30-cm intervals. Most boreholes labeled as “hydrological” originate from the observation drift. These are clusters of 40-m long boreholes forming vertical fans that bracket the Heated Drift and the wing heaters. These boreholes are used for periodic active testing of air-permeability changes to track the time evolution and spatial distribution of drying, condensation and changes in intrinsic permeability in the test block. Deformation of the rock mass is being monitored with an array of multiple-point borehole extensometer (MPBX) systems. In the radial MPBX boreholes, there are four anchors attached to the borehole wall at distances of about 1, 2, 4, and 15 m from the drift wall. The displacements of each anchor, relative to the drift wall, are continuously monitored.

The DST design and geometry are described in the following reports: *Drift Scale Test Design and Forecast Results* (CRWMS M&O 1997 [DIRS 146917]) and *Drift Scale Test As-Built Report* (CRWMS M&O 1998 [DIRS 111115]). The results of preheat characterization of the test block are contained in *Ambient Characterization of the Drift Scale Test Block* (CRWMS M&O 1997 [DIRS 101539]). Comprehensive documentation of DST measurements for the four-year heating period is given in *Thermal Testing Measurements Report* (BSC 2004 [DIRS 169900]). This latter report elaborates on the testing methods, gives representative results, and discusses measurement uncertainties. The comparison of simulated and measured DST results below primarily uses data described in the thermal testing report.

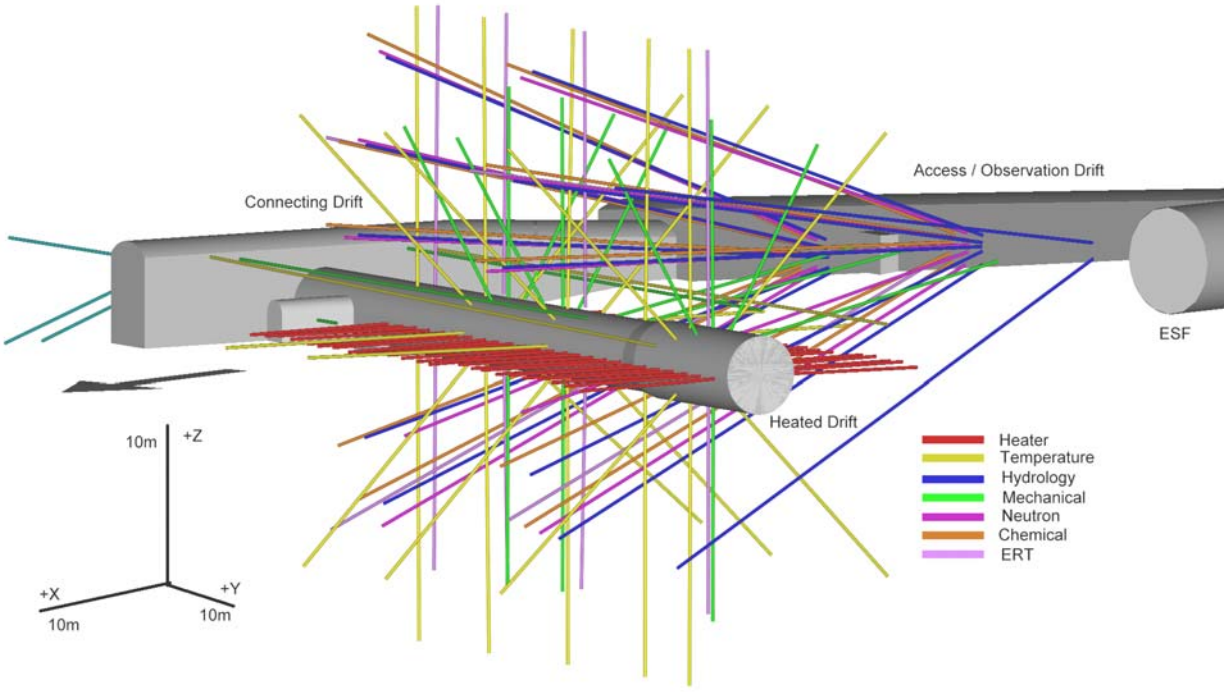

Source: BSC 2004 [DIRS 169900], Figure 6.3-2.

Figure 7.2.1-2. Three-Dimensional Perspective of the As-Built Borehole Configuration of the DST

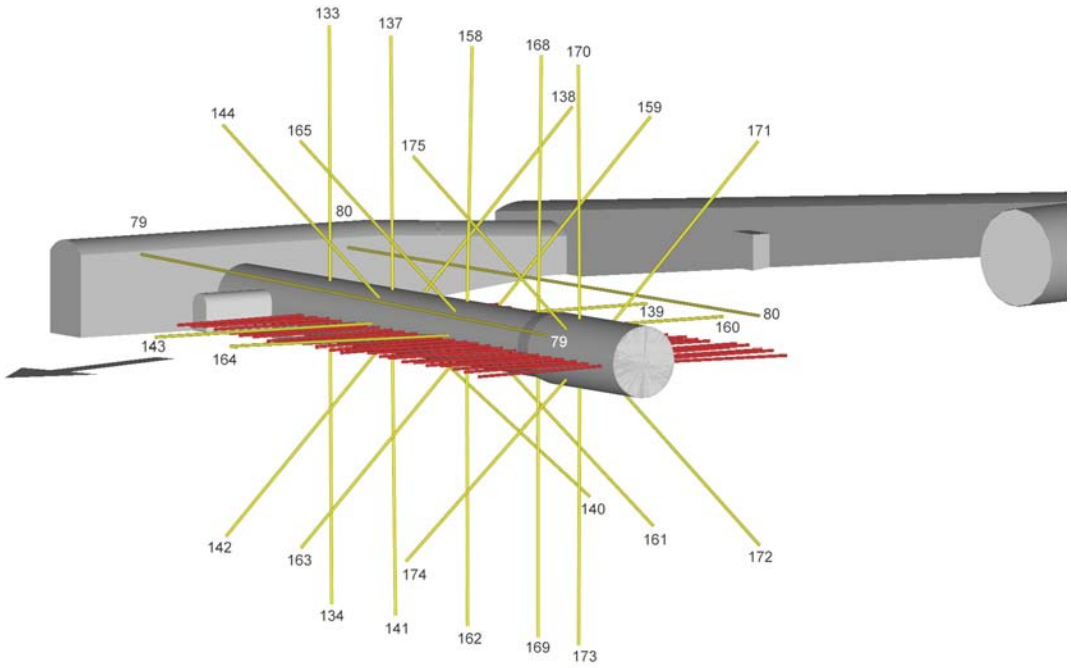

Source: BSC 2004 [DIRS 169900], Figure 6.3-3.

Figure 7.2.2-1. Three-Dimensional Perspective of Wing Heaters and Temperature Boreholes in the DST

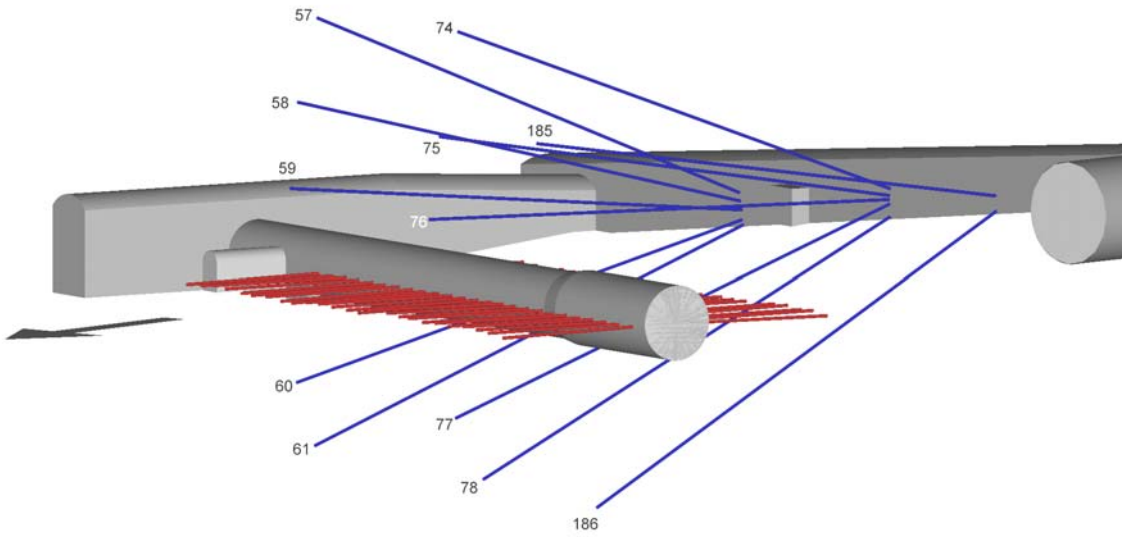

Source: BSC 2004 [DIRS 169900], Figure 6.3-4.

Figure 7.2.2-2. Three-Dimensional Perspective of Wing Heaters and Hydrology Boreholes in the DST

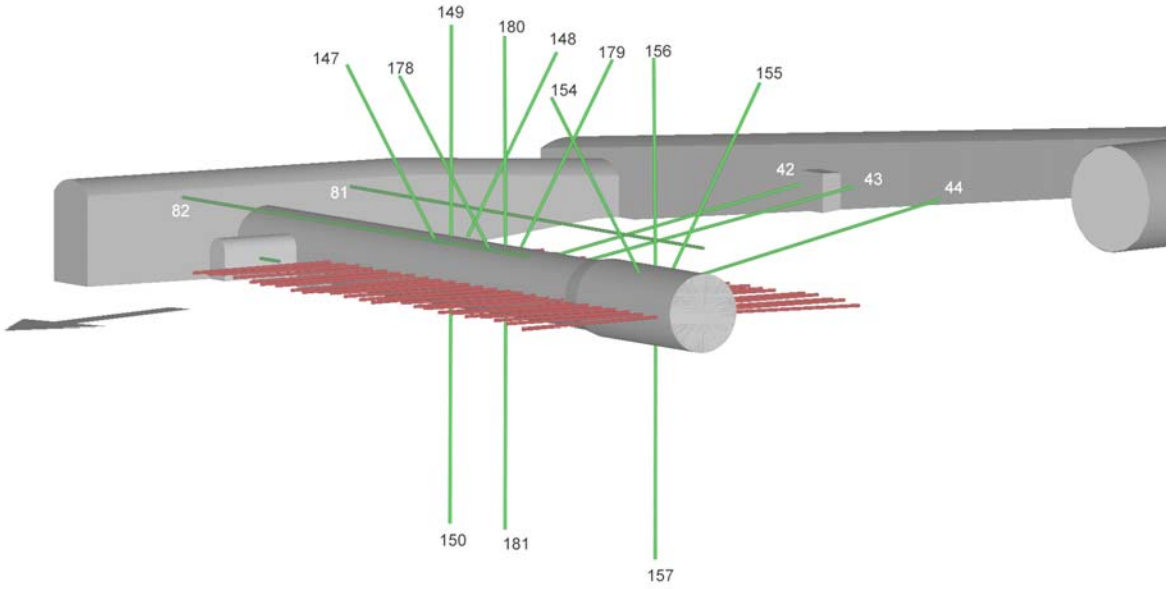

Source: BSC 2004 [DIRS 169900], Figure 6.3-5.

Figure 7.2.2-3. Three-Dimensional Perspective of Wing Heaters and Boreholes for Mechanical Measurements in the DST

7.3 DST MODEL DOMAIN

The DST model domain is a two-dimensional representation of the DST in a section crossing the heated drift perpendicular to its axis (Figure 7.3-1a). The two-dimensional model is half-symmetric with a vertical symmetry plane along the center axis of the Heated Drift. The model domain extends vertically 250 m from the top of the Tptpul stratigraphic unit (z = 100) down to the bottom of the Tptpll stratigraphic unit (z = -150 m) (The stratigraphy of the geological units is extracted from the nearby borehole USW SD-9.). The lateral model boundary is placed at a distance of 100 m from the center of the Heated Drift. Model components include three geological units (Tptpul, Tptpmn, and Tptpll); the Heated Drift, the concrete invert, and wing heaters. The Heated Drift is represented by a gridblock that is assigned a large permeability and thermal conductivity to represent advective, conductive, and radiative transport of heat. An extra grid element is added to simulate loss of heat and vapor through the bulkhead at the end of the Heated Drift. A heat loss coefficient for the bulkhead was determined through model calibration of early temperature data (Section 7.4.1). In addition, a constant pressure boundary is applied outside the simulated bulkhead, and a high permeability is assigned to simulate loss of vapor from the heated drift.

The mechanical, hydrologic, and thermal boundary and initial conditions are presented in Figures 7.3-1b to d. The initial vertical stress is estimated using an average density of $2.2 \cdot 10^3$ kg/m^3 for the overlying rock units, leading to a vertical compressive stress of about 5.8 MPa at the depth of the Heated Drift (for a depth of 267.5 m according to Rutqvist 2002 [DIRS 162047], p. 123). The average density of $2.2 \cdot 10^3$ kg/m^3 is based on values of saturated rock density and thickness of layers, as described in Section 6.3 and Section 5, Assumption 2. The magnitudes of maximum and minimum principal compressive horizontal stresses are 0.6 and 0.5 of the vertical stress, with the maximum horizontal stress oriented normal to the drift axis (CRWMS M&O 1997 [DIRS 103564], Table 3-2, pp. 3–23). The stress normal to the top boundary (representing the stress produced from the overlying rock mass) and the right lateral boundary (representing the remote maximum principal compressive stress) are fixed throughout the simulation. The mechanical boundary condition on the right lateral boundary is a stress boundary condition rather than the zero displacement restrictions adopted in the predictive simulation (compare Figures 6.3-1b and 7.3-1b). The zero-displacement restriction applied on lateral boundaries of the Tptpmn and Tptpll model domains (Section 6.3) is justified by repetitive symmetry conditions arising from simultaneous heating of the rock mass from multiple emplacement drifts. The stress boundary condition used on the right lateral model boundary of the DST model is justified because it involves a single heat source (i.e., floor and wing heaters), relatively short heating time, and small volume of the rock affected by temperature change.

The top and bottom TH model boundary conditions are identical to the ones used in the *Thermal Tests Thermal-Hydrological Analyses/Model Report* (BSC 2001 [DIRS 157330], Section 6.1.2). The fixed hydrologic and thermal boundary conditions on the top and bottom of the model were obtained from an independent TH simulation of a one-dimensional model domain extending from the ground surface to the water table (BSC 2001 [DIRS 157330], Section 6.1.2). The TH boundary condition at the right lateral boundary condition is no heat and no fluid flow across the boundary. However, this boundary is located sufficiently far away to preclude any boundary effects on TH simulation results near the heated drift during the four-year heating period.

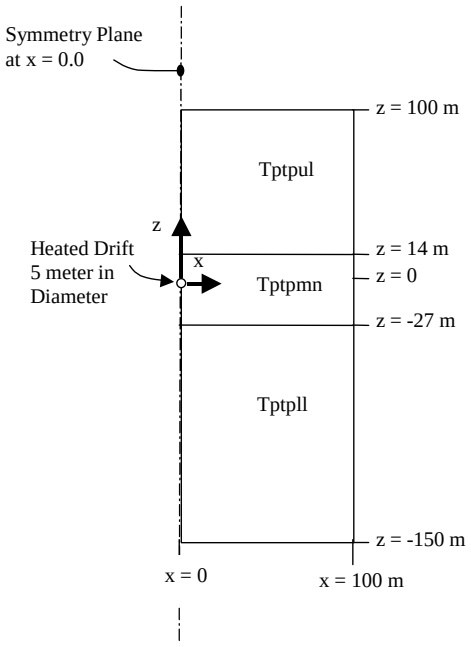

(a) Geometry

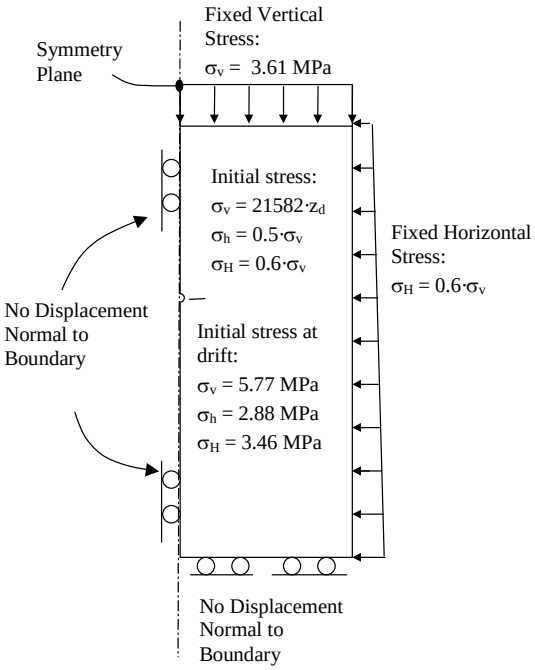

(b) Mechanical boundary conditions

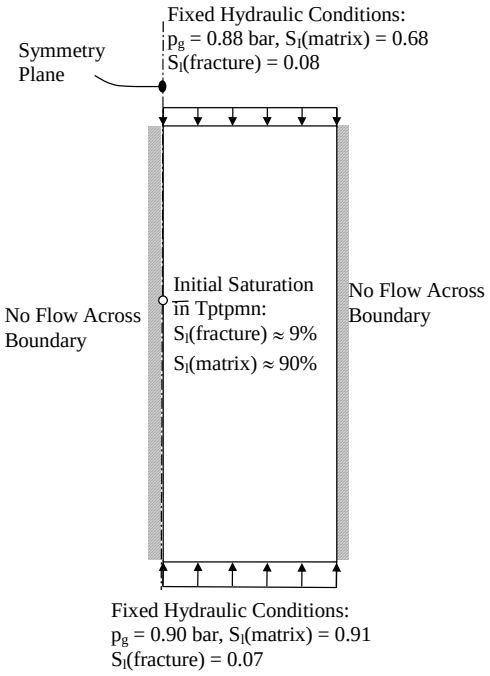

(c) Hydrological boundary conditions

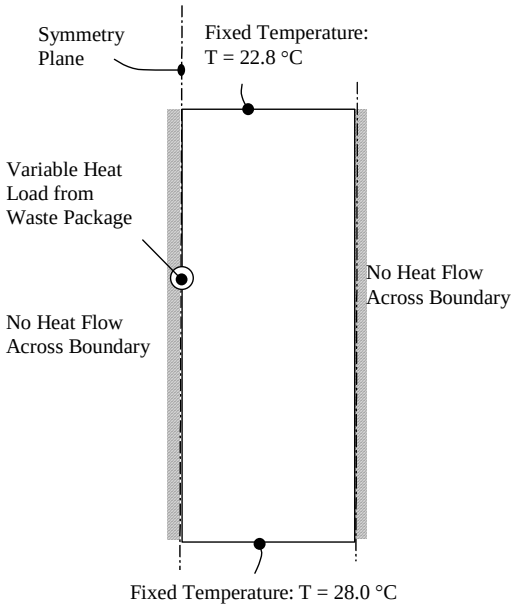

(d) Thermal boundary conditions

NOTES: Presented with (a) Geometry, (b) Mechanical, (c) Hydrological and (d) Thermal Boundary Conditions.
P_g = gas pressure, S_l = liquid saturation, z_d = depth below ground surface.

Figure 7.3-1. Two-Dimensional Representation of the DST in a Section Crossing the Heated Drift Perpendicular to Its Axis

The total heating power applied to the DST model domain reflects average values of the actual heating power. Average values were calculated for various time periods in *Drift-Scale Coupled Processes (DST and TH Seepage) Models* (BSC 2004 [DIRS 170338], Table 7.3.4-1). The periods of identical average power output, as applied to the model, are given in Table 7.3-1 separately for the drift heaters and wing heaters. The heater power for the two-dimensional model was calculated from the total heat power in Table 7.3-1, divided by 47.5 m (the length of the heat source along the Heated Drift). In addition, the heat power for the drift heater in the half-symmetric model is divided by two, and the power of the wing heaters is distributed with 43.1 percent to the inner wing heaters and 56.9 percent to the outer wing heaters. This is in accordance with a ratio of heat power between the outer and inner wing heaters of 1.3188, as given in DTN: MO9912SEPDOIHP.000 [DIRS 129272].

Table 7.3-1. Total Average Heater Power at Various Times of Heating in the DST

Time	Drift Heaters (kW)	Wing Heaters (kW)
12/03/1997-05/31/1999	52.1	132.1
06/01/1999-03/02/2000	50.0	125.1
03/02/2000-05/02/2000	47.9	120.4
05/02/2000-08/15/2000	45.8	114.6
08/15/2000-03/31/2001	43.3	106.4
04/01/2001-05/02/2001	43.4	106.7
05/02/2001-08/22/2001	41.4	101.6
08/22/2001-09/30/2001	39.4	96.3
10/01/2001-01/14/2002	39.4	96.8

Source: BSC 2004 [DIRS 170338], Table 7.3.4-1.

The properties utilized in the DST model domain are summarized in Table 4.1.4. TH properties are taken from the site-specific rock-property set DKM-TT99, which is also used in the DST TH model in *Drift-Scale Coupled Processes (DST and TH Seepage) Models* (BSC 2004 [DIRS 170338], Table 4.1.2). Mechanical properties, Young's modulus and Poisson's ratio for TSw1 and TSw2 TM units, are identical to those in the predictive drift scale THM analysis (Section 4.1.1.1). These properties were developed in the Microsoft Excel spreadsheet entitled *THM rock mass modulus v1.xls* (submitted to TDMS under DTN: LB0306DRSCLTHM.001), based on intact rock properties and field mapping in the ESF. These elastic parameters, which represent the bulk rock mass (including the effect of fractures), have been estimated using an empirical method based on the Geological Strength Index. The adopted rock mass Young's modulus is about 50 percent lower than the Young's modulus of intact rock determined on core samples from the site.

The TM and HM properties of the rock mass were developed in Section 6.4 of this model report. The parameters for these properties are given in Table 7.3-2. In Figure 7.3-2, the function for a temperature-dependent thermal expansion coefficient is compared to measured thermal expansion coefficients on intact rock samples from the DST block. The adopted thermal expansion coefficient is close to the site-specific values of the intact-rock thermal expansion coefficient (Figure 7.3-2) for temperature up to 200°C. Values close to the intact-rock thermal expansion coefficient were adopted in Section 6.4.3 based on TM simulation results by Sobolik et al. (1999 [DIRS 163202], p. 741) and results presented in *Coupled*

Thermal-Hydrologic-Mechanical Effects on Permeability Analysis and Models Report (BSC (2001 [DIRS 155957], pp. 21 and 115 through 125), which showed that measured TM responses are well predicted by assigning the rock mass an intact rock thermal expansion coefficient.

Table 7.3-2. Summary of TM and HM Parameters and Properties of the Rock Mass Developed in This Model Report for the DST Model Domain

Geologic Unit >		Tptpul (tsw33)	Tptpmn (tsw34)	Tptpll (tsw35)	Source
Initial hydraulic aperture	b_i (μm)	167	52	153	Calculated using Equation 6.4-4 and frequency and permeability given in Table 4.1-4.
Parameters b_{max} and α for the stress-aperture function	b_{max} (μm) α (1/MPa)	200 0.52	200 0.52	200 0.52	Developed in Section 6.4.4 of this model report.
Thermal expansion coefficient	α_T (10^{-6}/°C)	5.0+0.0583×T	5.0+0.0583×T	5.0+0.0583×T	Derived from intact rock thermal expansion coefficient in Section 6.4.3 of this model report.
Young's Modulus	E (GPa)	19.40	14.77	14.77	Extracted from Excel spreadsheet entitled *THM rock mass modulus v1.xls* (Submitted to TDMS under DTN: LB0306DRSCLTHM.001) in which these properties were derived from the qualified sources listed in Table 4.1-1b under items about intact rock properties and field mapping.
Poisson's Ratio	ν (-)	0.23	0.21	0.21	

T = Temperature in °C.

7.4 DST VALIDATION RESULTS

The drift scale THM model is validated for measurements taken during the 49.5-month heating phase of the DST. The results are presented by comparing the calculated THM responses to measurements, which have been grouped into equivalent categories based on their location relative to the Heated Drift. Such grouping of the field data is conducted to display typical trends of the field data and their variability.

7.4.1 Modeling of Temperature Field

In modeling the DST, agreement between the calculated and measured temperature was obtained if heat loss through the bulkhead was simulated. A bulkhead heat-loss coefficient of 0.4375 W/ºK was determined by calibrating the model for a drift wall temperature of 150°C at 12 months (Rutqvist 2004 [DIRS 170509], p. 60). Without considering the heat loss through the bulkhead, the temperature at the drift wall would be overestimated, and consequently TM forces and displacements would also be overestimated.

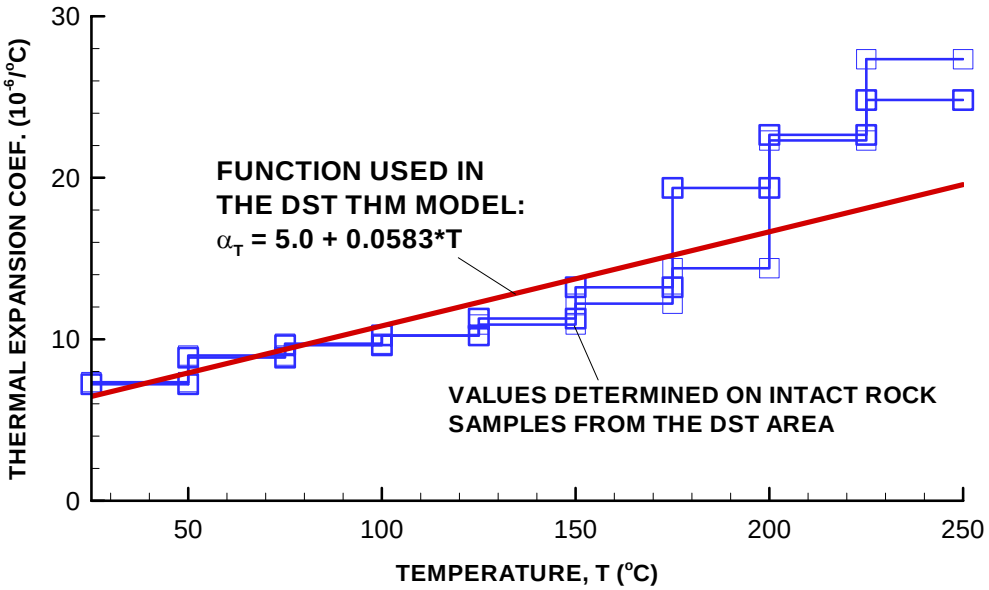

DTN: MO0004RIB00035.001 [DIRS 153848], Tables 9 and 11.

NOTE: Laboratory values were determined on core samples from the DST block during two cycles of heat-up.

Figure 7.3-2. Temperature-Dependent Thermal Expansion Coefficient Used in the DST Model Domain and Comparison to Laboratory-Determined Values on Intact Rock

Figure 7.4.1-1 shows the calculated temperature after 12 months of heating and the location of thermal boreholes used for validation of the temperature calculation. Figures 7.4.1-2 and 7.4.1-3 show the comparison of measured and simulated temperature profiles. The measured temperature includes data from four borehole arrays located at y ≈ 12, 23, 32, and 39 m along the Heated Drift. These borehole arrays are located well inside the axial extensions of the Heated Drift and wing heaters. In Figures 7.4.1-2 and 7.4.1-3, the calculated temperatures are well within the range of measured values. The measured temperature profiles along most boreholes show a characteristic plateau at about 100°C, indicating two-phase boiling conditions with so-called heat-pipe effects (for an in-depth discussion refer to BSC 2004 [DIRS 170338], Section 7.4.3.1). The model also shows a “kink” in the temperature profiles; however, it appears to be smeared, probably because of model discretization. These local deviations in the temperature profiles are not relevant for studying TM-induced responses at the DST. Overall, it is concluded from Figures 7.4.1-2 and 7.4.1-3 that good agreement is achieved between simulated and measured temperatures. Furthermore, the similarity in temperature profiles at various locations along the axis of the tunnel (y ≈ 12, 23, 32, and 39 m) shows that two-dimensional and half-symmetric model approximation is justified and accurate for predicting temperatures in boreholes located well within the extension of the Heated Drift.

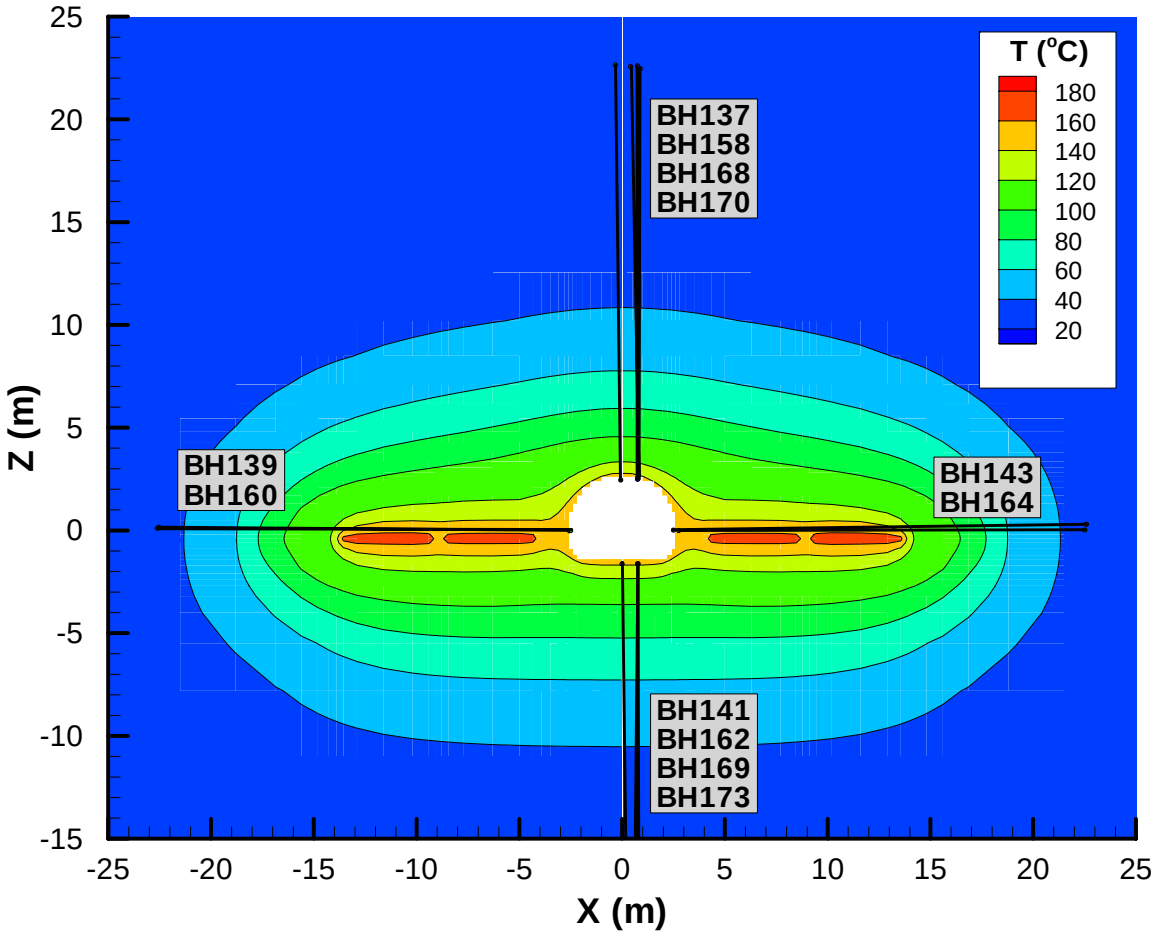

DTN (borehole locations): MO0002ABBLSLDS.000 [DIRS 147304].

Output DTN (simulated contour): LB0306DSTTHMVL.002.

Figure 7.4.1-1. Calculated Temperature Distribution after 12 Months of Heating and Location of Thermal Boreholes for Comparison of Simulated and Measured Temperature Profiles

7.4.2 Validation for TM Processes

The TM part of the drift scale THM model is validated by comparing calculated and measured displacements in radial MPBX boreholes. Such comparison validates the drift scale THM model for the thermal expansion process, as well as for the values of the thermal expansion coefficient.

Figure 7.4.2-1 shows calculated displacements relative to the drift axis and the locations of radial MPBX boreholes and their anchors, which are used for validation of the calculated thermal expansion. Measured data include displacements from MPBX borehole arrays located at $y \approx 41.1$, 21.0, and 13.7 m. All these arrays are within the axial extensions of the Heated Drift, with the one at $y \approx 41.1$ being farthest out, located about 4.6 m from the edge of the heated area. In general, the measured displacements show a larger spread than temperature measurements. This reflects the fact that mechanical displacements are more sensitive to local heterogeneities in

the rock mass, such as fractures. In addition, there are a few anchors in which the measured data are erratic, unreasonable, or missing, and therefore excluded from this analysis. Unreasonable results are a few measurements giving displacements that can not be physically explained as a measure of displacements in the rock mass, but must be caused by measurements error or, for example, slip in anchors. The quality of displacements measured at the various anchors is documented in *Thermal Testing Measurements Report* (BSC 2004 [DIRS 169900], Section 6.3.3.1.1).

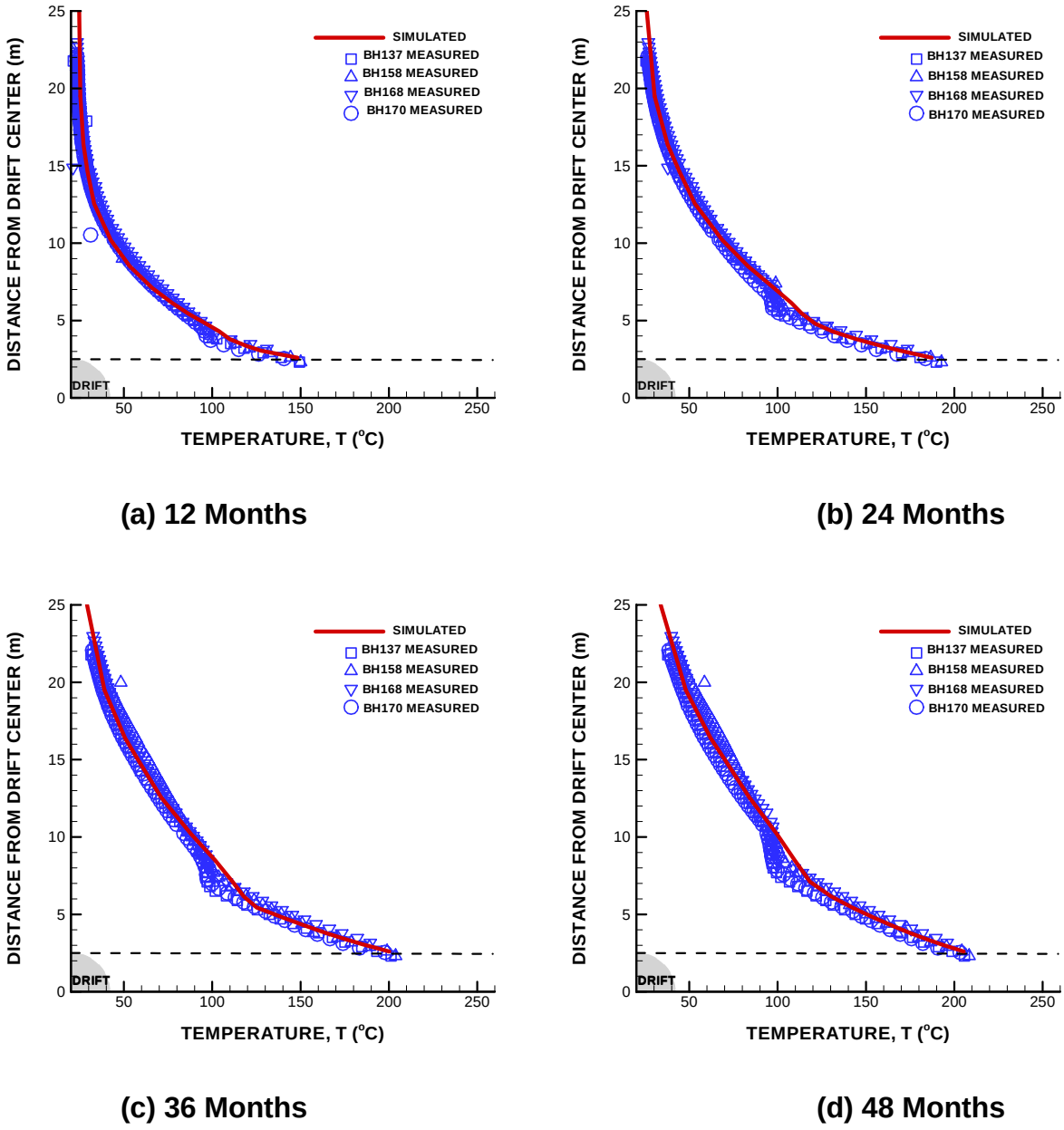

DTN (measured): MO0208RESTRDST.002 [DIRS 161129]; Output DTN (simulated): LB0306DSTTHMVL.002.

Figure 7.4.1-2. Measured and Simulated Temperature Profiles along Vertically-up Boreholes at the Drift Crown

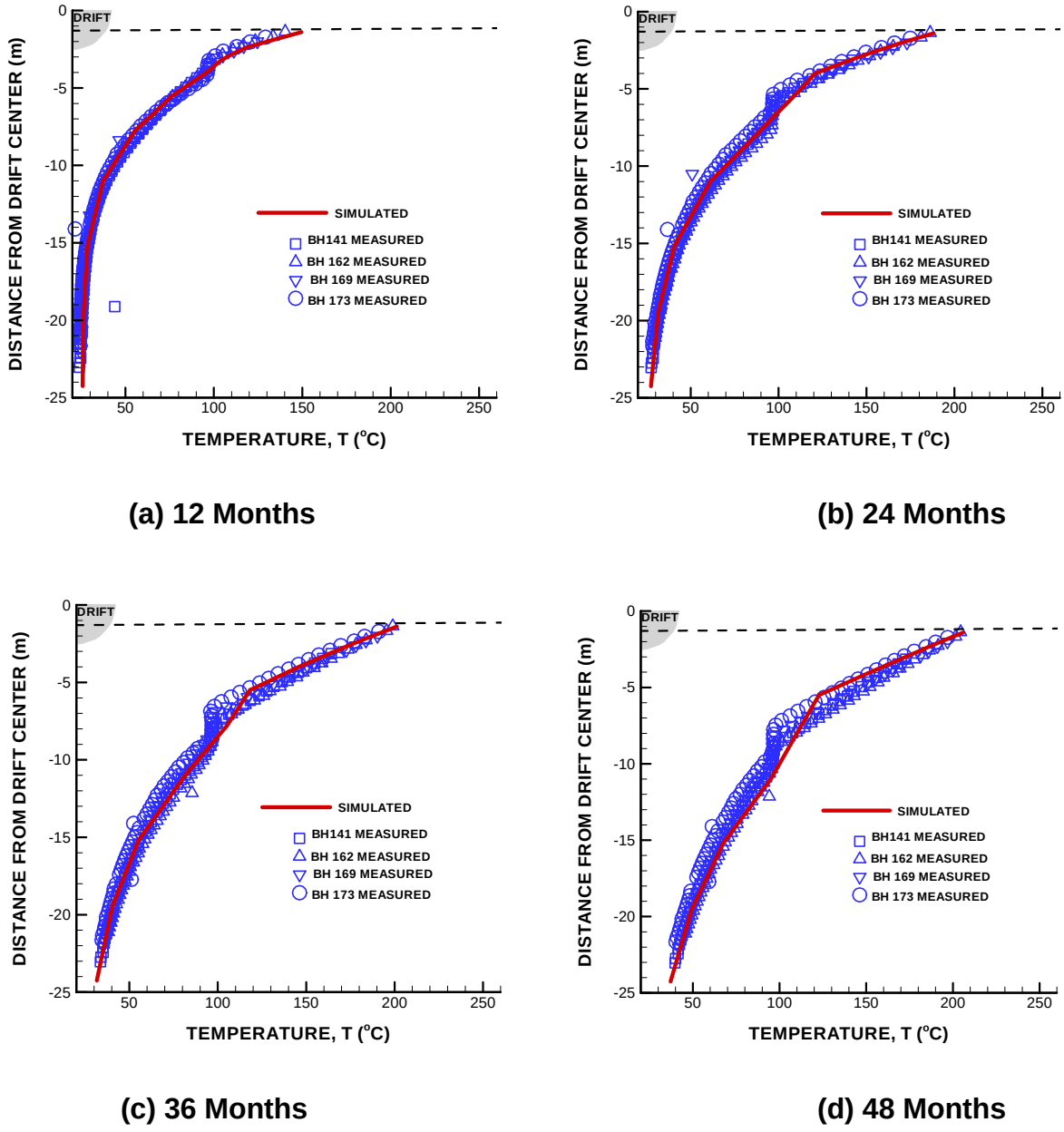

DTN (measured): MO0208RESTRDST.002 [DIRS 161129]; Output DTN (simulated): LB0306DSTTHMVL.002.

Figure 7.4.1-3. Measured and Simulated Temperature Profiles along Vertically-down Boreholes Extending Downward from the Drift Floor

The measured displacements at various points in the rock mass are grouped according to their radial distance from the drift wall. That is, measurements taken at Anchors 1, 2, 3, and 4, respectively, located at 1, 2, 4, and 15 m from the drift wall, are compiled into four groups regardless of their angular direction and axial location along the Heated Drift. The measured and simulated displacements for each group are compared in Figure 7.4.2-2. With the exception of data from early time, the simulated displacements are within the range of measured displacement. Agreement is best for Anchors 2 and 3, whereas the calculated displacement at

Anchor 1 is a lower-bound prediction. At Anchor 4, the displacement is slightly under predicted during the first half the heating period, whereas better agreement is obtained at the end of the heating period. The calculated and measured displacements in the lower vertical boreholes are generally greater (green lines in Figure 7.4.2-2) than in the inclined and upper vertical boreholes. This is because the incremental displacements in the lower vertical borehole are impacted by an additional displacement, caused by the expansion of the concrete invert. The extensometers in the lower vertical boreholes have their borehole-collar anchor placed in the concrete invert rather than at the drift wall (Figure 7.4.2-1).

A quantitative evaluation of model predictions is provided by statistical measures according to Wagner et al. (2001 [DIRS 163532]). Three statistical measures are considered in the quantitative evaluations: root-mean-square-difference (RMSD), mean-difference (MD), and normalized-absolute mean difference (NAMD). The three statistical measures are a function of simulated ($V_{sim,\ i}$) and measured ($V_{meas,\ i}$) variables that, in this case, are the simulated and measured displacements.

The RMSD, for a specific time is described as:

$$RMSD = \left[\frac{\sum_{i=1}^{N} \left(V_{sim,i} - V_{meas,i} \right)^2}{N} \right]^{1/2} \qquad \text{(Eq. 7.4.2-1)}$$

RMSD is a classic statistical measure with a bias towards larger differences between measured and simulated responses. The smaller the RMSD, the better the agreement between simulated and measured responses. N is the number of measurements for a specific time.

The MD for a specific time is described as:

$$MD = \frac{\sum_{i=1}^{N} \left[V_{sim,i} - V_{meas,i} \right]}{N} \qquad \text{(Eq. 7.4.2-2)}$$

A positive MD indicates a general overestimation of the measured variable, whereas the converse applies for a negative MD.

The NAMD for a specific time is described as:

$$NAMD = \sum_{i=1}^{N} \left| \frac{V_{sim,i} - V_{meas,i}}{V^{0}_{meas,i}} \right| \cdot \frac{1}{N} \qquad \text{(Eq. 7.4.2-3)}$$

where $V^{0}_{meas,i}$ in this case, is measured displacement. NAMD provides a percentage of the absolute difference between measured and simulated variables relative to the measured variable.

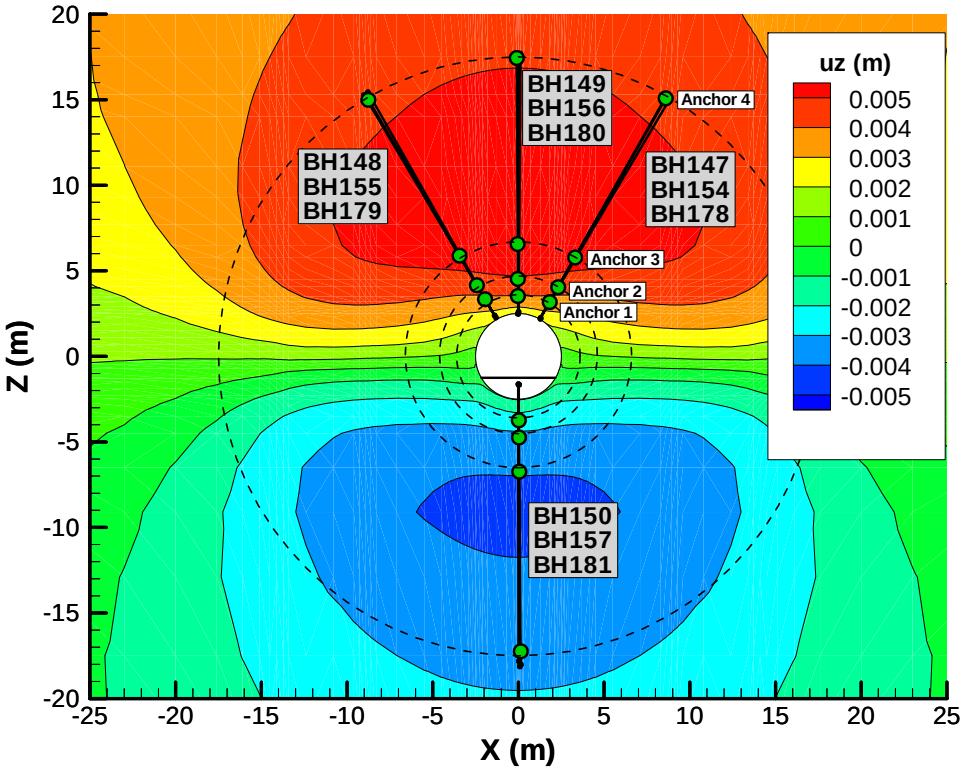

DTN (borehole locations): MO0002ABBLSLDS.000 [DIRS 147304]; Output DTN: LB0306DSTTHMVL.002.

Figure 7.4.2-1. Simulated Vertical Displacement (UZ) after 12 Months of Heating and Location of Mechanical MPBX Boreholes for Comparison with Measured Displacement

Figure 7.4.2-3 presents the RMSD, MD, and NAMD for all simulated and measured displacements shown in Figure 7.4.2-2. The curves in Figure 7.4.2-3 were calculated using an Microsoft Excel spreadsheet as described in detail in Appendix B. In Figure 7.4.2-3a, the RMSD increases from about 1 mm at 6 months to about 2 mm at the end of the heating. The increasing RMSD with time reflects increasing variability in measured displacement. The MD shows that the overall displacement field during the first 30 months is underestimated by about 1 mm, a number that is reduced to about 0.5 mm at the end of the heating period (Figure 7.4.2-3b). The NAMD is about 45 percent at 6 months, but gradually reduces to less than 25 percent after 24 months of heating. Thus, as a whole, the displacements are clearly within the validation criterion of ±50 percent discussed in Section 7.1.4. As discussed in Section 7.1.4, prediction of TM-induced displacements within 50 percent also implies that TM-induced stresses are within 50 percent of those predicted (since the rock mass response is elastic), and that the error on the evolution of the permeability will be limited to within one order of magnitude.

The general agreement in the magnitude of displacement over the entire heating period confirms the findings by Sobolik et al. (1999 [DIRS 163202], p. 741) and those reported in *Coupled Thermal-Hydrologic-Mechanical Effects on Permeability Analysis and Models Report* (2001 [DIRS 155957], pp. 21 and 115 through 125), suggesting that the intact-rock thermal expansion coefficient is an appropriate representation of the in situ thermal expansion coefficient

at the DST. Also, the SHT was simulated using the intact-rock thermal expansion coefficient and showed generally good agreement with measured results (CRWMS M&O 1999 [DIRS 129261], pp. 9-10).

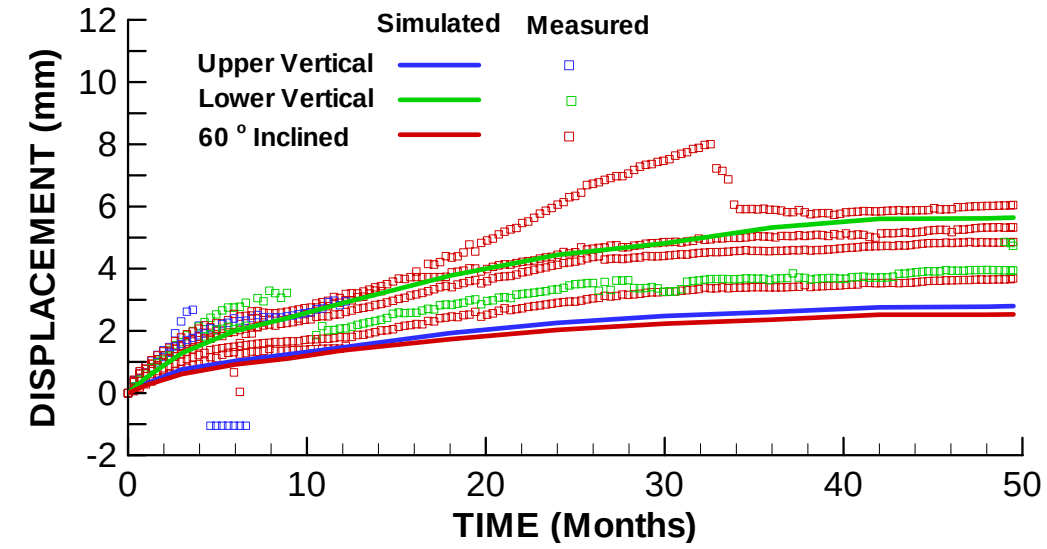

(a) Anchor 1

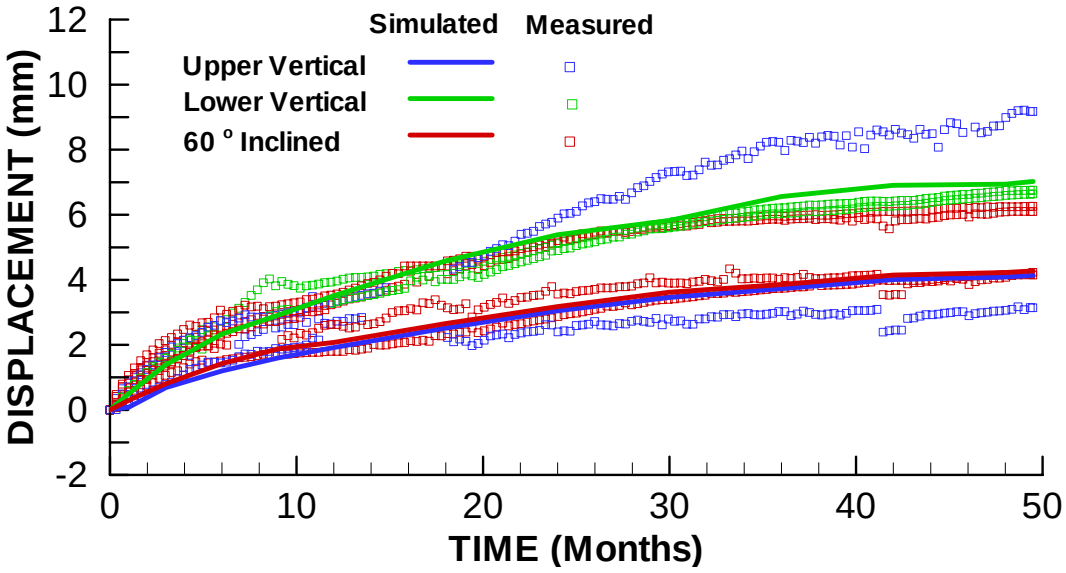

(b) Anchor 2

DTN (measured): SN0207F3912298.037 [DIRS 162046]; Output DTN (simulated): LB0306DSTTHMVL.002.

NOTE: Measured values are from borehole numbers shown in Figure 7.4.2-1.

Figure 7.4.2-2. Measured and Simulated Evolution of Displacement in MPBX Boreholes

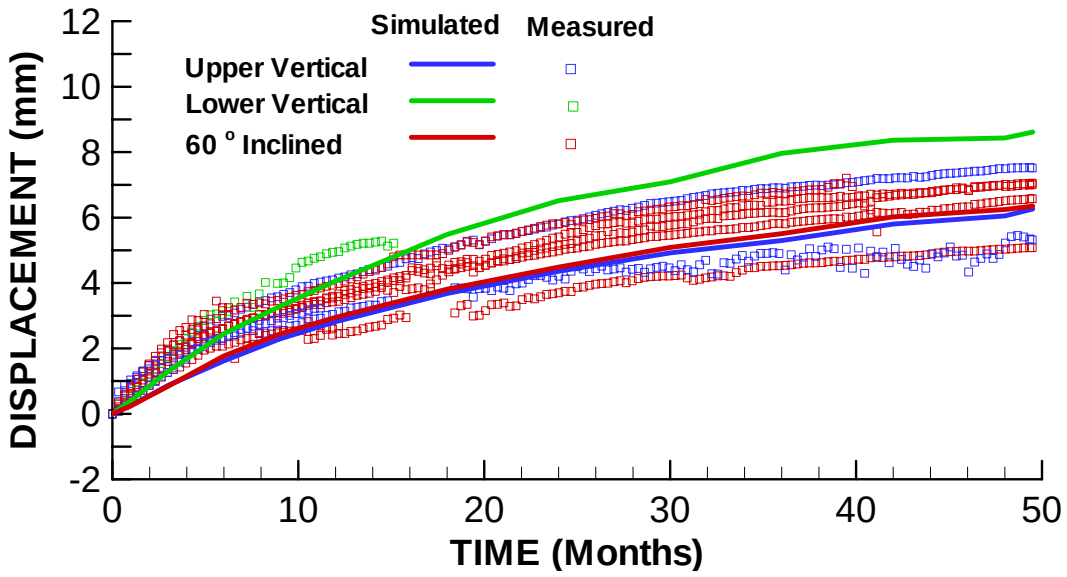

(c) Anchor 3

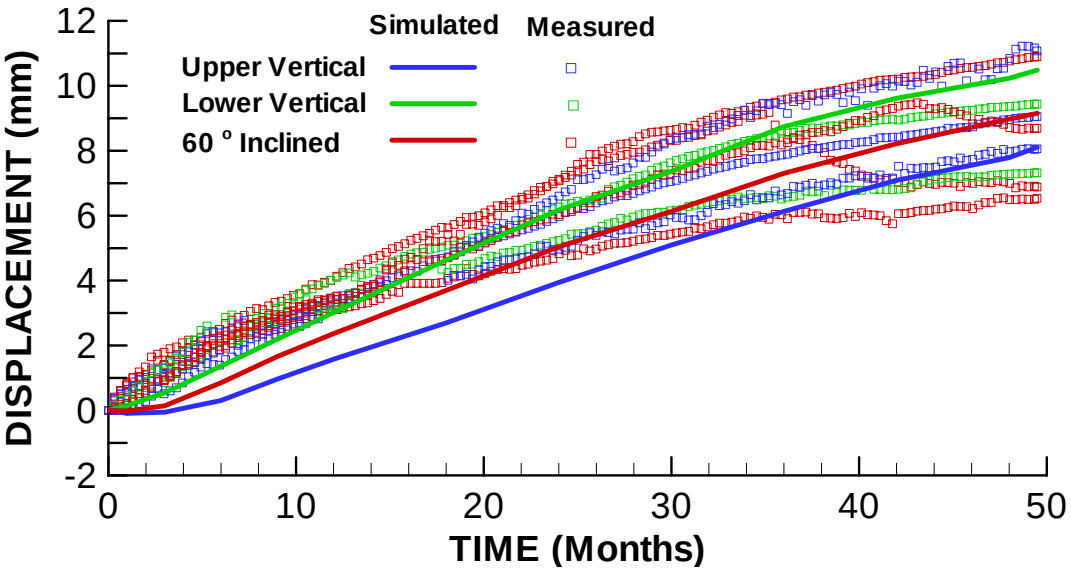

(d) Anchor 4

DTN (measured): SN0207F3912298.037 [DIRS 162046]; Output DTN (simulated): LB0306DSTTHMVL.002.

NOTE: Measured values are from borehole numbers shown in Figure 7.4.2-1.

Figure 7.4.2-2. Measured and Simulated Evolution of Displacement in MPBX Boreholes (Continued)

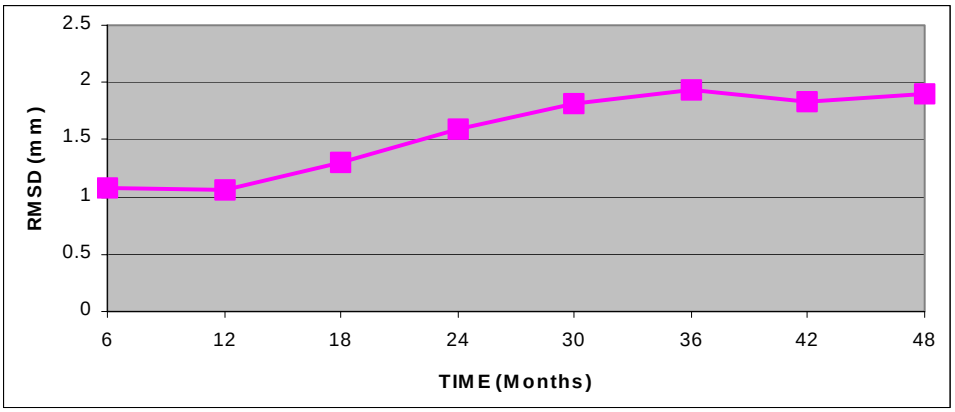

(a) Root-mean-square-difference (RMSD)

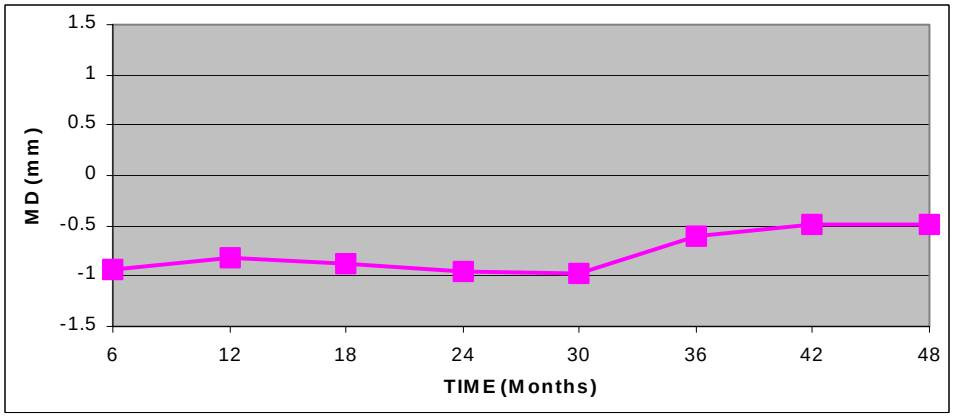

(b) Mean-difference (MD)

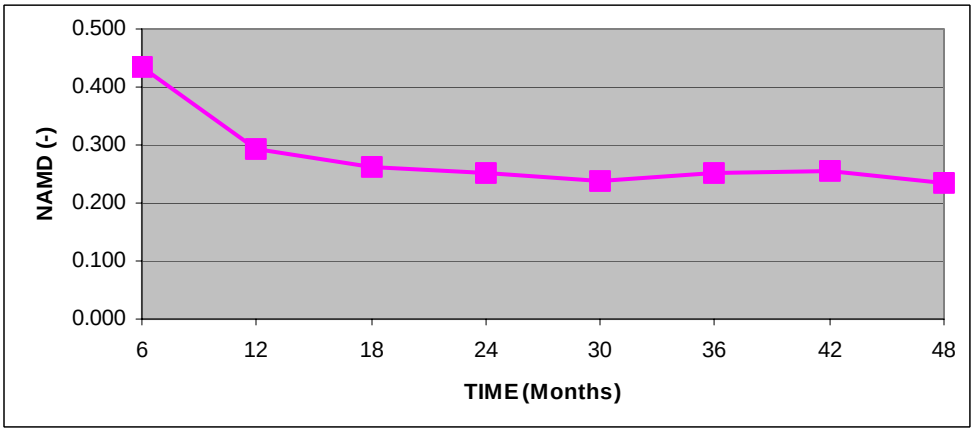

(c) Normalized-absolute mean difference (NAMD)

Output DTN (Statistical analysis): LB0306DSTTHMVL.002.

NOTE: Statistical analyses leading to the curves presented in this figure are described in Appendix B.

Figure 7.4.2-3. Statistical Measures for Displacement Comparative Analysis

The analysis by Sobolik et al. (1999 [DIRS 163202]) compares pre-test prediction of TM responses to measurements in the early part of the heater test. The agreement between the calculated and predicted displacement was generally good over the entire time period. However, toward the end of the period evaluated, the predicted displacements were overestimated because the temperature predictions at that time did not consider a step-wise reduction of heating power to limit the wall temperature at 200°C. In the other analysis (BSC 2001 [DIRS 155957], Section 6.4), simulated and measured results of displacements are compared for the first 18 months of heating. A comparison of displacements predicted in *Coupled Thermal-Hydrologic-Mechanical Effects on Permeability Analysis and Models Report* (BSC 2001 [DIRS 155957], Section 6.4) with those predicted in this report is presented in Section 7.7. No pre-test prediction of TM-responses at the DST was conducted with the current drift scale THM model because the coupled THM simulator (TOUGH-FLAC) was not developed before commencement of the DST.

The finding that the intact rock thermal expansion coefficient is appropriate seems to contradict results from separate determinations of what is described as a "rock-mass thermal expansion coefficient" at the SHT and DST (CRWMS M&O 1999 [DIRS 129261], pp. 9-11, and BSC 2004 [DIRS 169900], Section 6.3.3.6.3). In that case, the in situ thermal expansion coefficient was back-calculated directly from measured deformations and temperature changes along certain extensometers at the SHT and DST. It was found that the in situ thermal expansion coefficient determined by this method is about 50 percent lower than the intact-rock thermal expansion coefficient. The 50 percent lowering of the in situ thermal expansion coefficients was attributed to some of the displacements being accommodated by closure of fractures. The apparent contradiction between the results of numerical modeling (which generally shows that the intact-rock thermal expansion coefficient is appropriate) and the direct back calculated in situ thermal expansion (which indicates that a 50 percent lower thermal expansion coefficient would be appropriate) can have two contributing causes:

1) The in situ back analyzed thermal expansion coefficients at SHT and DST were determined from measurements in horizontal boreholes, whereas the comparison of measured and simulated displacements in this model report was conducted for vertical or subvertical boreholes. The in situ thermal expansion coefficient along horizontal boreholes may be lower because vertical fractures are most abundant at the site (The horizontal boreholes at the DST are located along the axis of the heated drift and could not be included in the two-dimensional model.).

2) The in situ back-analyzed thermal expansion coefficient at the SHT and DST is impacted by simultaneous increases in temperature and thermal stress, and may therefore be different from the basic thermal expansion coefficient that is part of the input to a numerical model. The basic thermal expansion coefficient, by definition, is a measure of the expansion of the rock for a temperature increase under a stress-free condition. If the thermal expansion coefficient is determined under confinement, some of the rock expansion will be prevented and the thermal expansion coefficient would be underestimated.

Nevertheless, the in situ back-analyzed thermal expansion provides a lower bound for the basic in situ thermal expansion coefficient, whereas the intact-rock thermal expansion coefficient

provides an upper bound. In this study, it was shown that in the vertical direction at the DST, the intact-rock thermal expansion coefficient is appropriate.

7.4.3 Validation for THM Processes

The drift scale THM model is validated for THM processes by comparing calculated against measured changes in absolute air permeability. The measured change in air permeability reflects two simultaneous processes: TM-induced changes in intrinsic permeability and TH-induced changes in relative permeability for air flow. TM-induced changes in intrinsic permeability result from thermal stresses associated with the heating of the rock mass. Thermal stresses act upon existing fractures, changing their aperture, that may either increase or decrease the intrinsic fracture permeability. TH-induced changes are associated with thermally driven changes of moisture content in fractures. Wetting and drying in fractures (in other words, increase and decrease of liquid saturation) give rise to changes in relative permeability for air flow.

Figure 7.4.3-1 presents the simulated liquid fracture saturation after 12 months of heating and the location of boreholes for air-permeability measurement. The figure shows that a dryout zone has formed around the Heated Drift and wing heaters. Just outside the dryout zone, a zone of higher-than-ambient saturation forms because the produced vapor condenses in cooler areas. The dryout zone and the condensation zone progressively move away from the heated drift over time. This movement is controlled by the flow of vapor away from the heat source along the thermal gradient and a reversed liquid flow along the capillary gradient toward the inner, dryer regions. The increased temperature near the heat source causes boiling of liquid water (which resides primarily in the matrix rock). The vapor first moves from the matrix to the fractures and then through the permeable fractures, driven primarily by pressure increases caused by boiling. Vapor generally flows away from the drift towards cooler regions, but a portion of the vapor also flows towards the drift and out through the bulkhead. This is possible because the bulkhead acts as an open boundary with a constant pressure. In addition, there is a gravity-driven liquid flow that tends to drain the condensation zone above the heated drift.

Air-injection tests performed in the condensate zone should reflect a decrease in moisture-induced changes in relative gas permeability, whereas measurements performed in the dryout zone should reflect an increase in moisture-induce changes in relative gas permeability. Corresponding moisture-induced changes in relative permeability caused by the wetting and drying of fractures are shown in Figure 7.4.3-2a. This figure shows that the increased fracture liquid saturation in the condensate zone causes a reduction in relative permeability to about 30 percent of its original value. In the dryout zone, the relative permeability has increased slightly from its original value because fractures in this zone are completely dry.

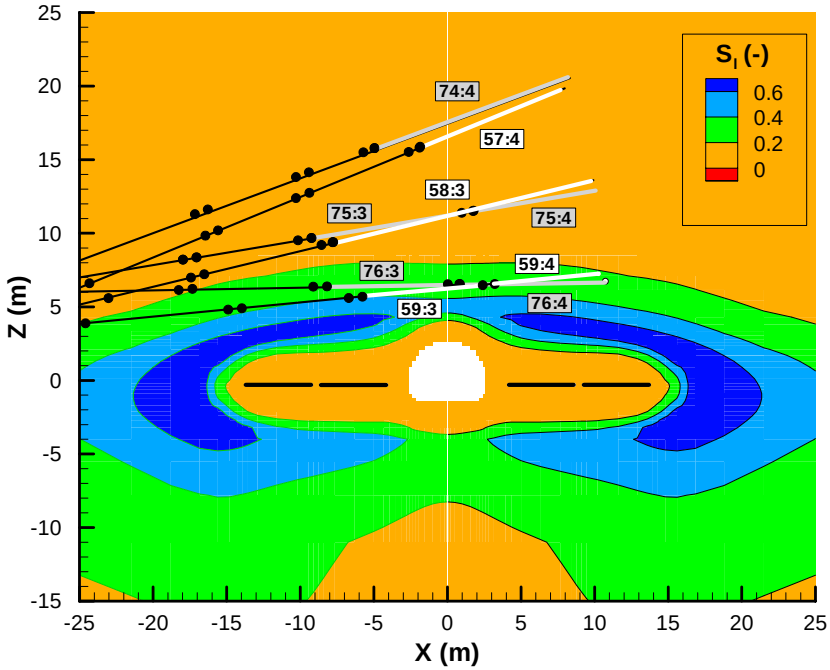

DTN (borehole locations and sensors): MO0002ABBLSLDS.000 [DIRS 147304]; Output DTN: LB0306DSTTHMVL.002.

NOTE: Initial fracture liquid saturation is approximately 0.09.

Figure 7.4.3-1. Simulated Distribution of Fracture Liquid Saturation (S_l) after 12 Months of Heating and Location of Borehole Sections Where Simulated and Measured Air Permeability Are Compared

Figure 7.4.3-2b shows the total permeability changes, combining TH-induced relative permeability changes with TM-induced changes in intrinsic permeability. The figure shows that TM effects cause the permeability to decrease around the drift and wing heaters, including the inner dryout zone and outer condensate zone. In the condensate zone, the permeability has now decreased to about 10 percent of its original value. In Figure 7.4.3-2b, a zone of increased permeability appears above the Heated Drift at about z = 20 m. This zone of increased permeability is caused entirely by TM effects, which are caused by open vertical fractures. Vertical fractures open in this area because of a reduction in horizontal stresses. This reduction causes the redistribution of horizontal stresses towards the Heated Drift to balance high thermal stresses near the heat source.

The calculated permeability changes are compared to air-permeability measurements in Figure 7.4.3-3. The comparisons between calculated and measured responses are made at three locations about 6, 12, and 18 m above the center of the drift. The air-permeability measurements at these three locations were selected for comparison because they represent typical air-permeability responses for measurements performed near the heat source (at z = 6 m), far away from the heat source (z = 18 m), and at a mid-distance (z = 12 m). Also, the measured data at these locations are the most complete, with few failures of the packer system throughout the 4-year heating period. At z = 6 m, four boreholes sections (76:3, 76:4, 59:3, and 59:4) are

located symmetrically around x = 0 (see Figure 7.4.3-1). In these sections, the air permeability first decreases with time to reach a minimum at about 24 months. Thereafter, the permeability increases slightly in three borehole sections and more in the fourth (Figure 7.4.3-3a). The figure compares measured changes in air permeability at the four borehole sections with calculated changes in permeability. The solid line indicates the calculated changes in air permeability, which are the product of the intrinsic permeability (TM effect) and gas relative permeability (TH effect). The figure shows that the solid line representing the combined TH and TM effects matches three of four measurements best. In the fourth borehole section, 59:3, the measured changes match a pure TH response the best. Note that the last data point in borehole Section 59:4 was used for calibration of the stress-versus-permeability function in Section 6.4.4.

At about z = 12, three borehole sections (75:3, 75:4, and 58:3) are located symmetrically around x = 0 and between z =10 and 14 m. Measured responses in these three boreholes are consistent, with an initial increase in air permeability during the first 9 months, followed by a gradual decrease with time until the end of heating. The decrease in permeability can be interpreted either as a change in intrinsic permeability (TM), or as a change in relative permeability (TH), or a combination of the two (THM). However, the initial increase during the first 9 months can only be explained as a TM response.

For the measurements located farthest away from the drift, (74:4 and 57:4 at z ≈ 18 m), there is an increase in air permeability caused solely by TM-induced changes in intrinsic permeability (TM in Figure 7.4.3-3c). At this location, far away from the Heated Drift, no effect from TH-induced changes appears until about 36 months, when a slight wetting starts to take place.

The results in Figure 7.4.3-3 are calculated with the parameters b_{max} = 200 μm and α = 0.52 MPa^{-1} as developed in Section 6.4.4 of this report. The overall simulated changes in air permeability using those parameters are in agreement with the measured changes, and the validation criterion discussed in Section 7.1 is met. That is, the predicted changes in air permeability are in the correct direction and correct within an order of magnitude: log (k/k_i) simulated and measured differ by less than 1. Observed trends (e.g., k/k_i decreases followed by increases, or the reverse) are matched by model predictions. The predicted THM responses are on average stronger than the measured ones and hence the stress-aperture function defined by the parameter b_{max} = 200 μm and α = 0.52 MPa^{-1} can be considered a bounding estimate that emphasizes the effect of thermal stress on permeability. Note that the predicted permeability increases at 74:4 and 57:4, at z ≈ 18 m, do not show a bounding behavior, but rather show a reasonable good agreement with the measured permeability change. This is consistent with the calibration of the stress-versus-permeability function against the mean permeability changes for excavation (decreasing stress) effects.

The conclusion that the stress-versus-permeability function provides a bounding estimate of thermally induced permeability changes also holds for comparison to air-permeability measurements conducted at borehole sections other than those depicted in Figure 7.4.3-1. Indeed, the parameters b_{max} = 200 μm and α = 0.52 MPa^{-1} were determined by model calibration for the strongest reduction in air-permeability measured out of 46 boreholes sections surrounding the DST (Section 6.4.4). As a sensitivity case, a second simulation is conducted with a more moderate stress-aperture function defined by b_{max} = 150 μm and α = 0.6 MPa^{-1}. The results of

this simulation show a better agreement with the “average” observed HM behavior at the DST (Figure 7.4.3-4).

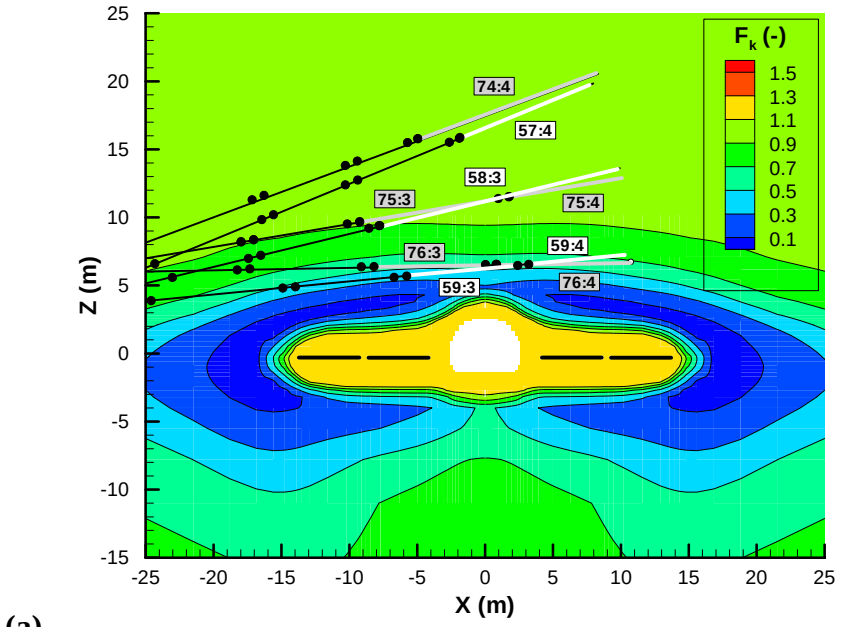

(a)

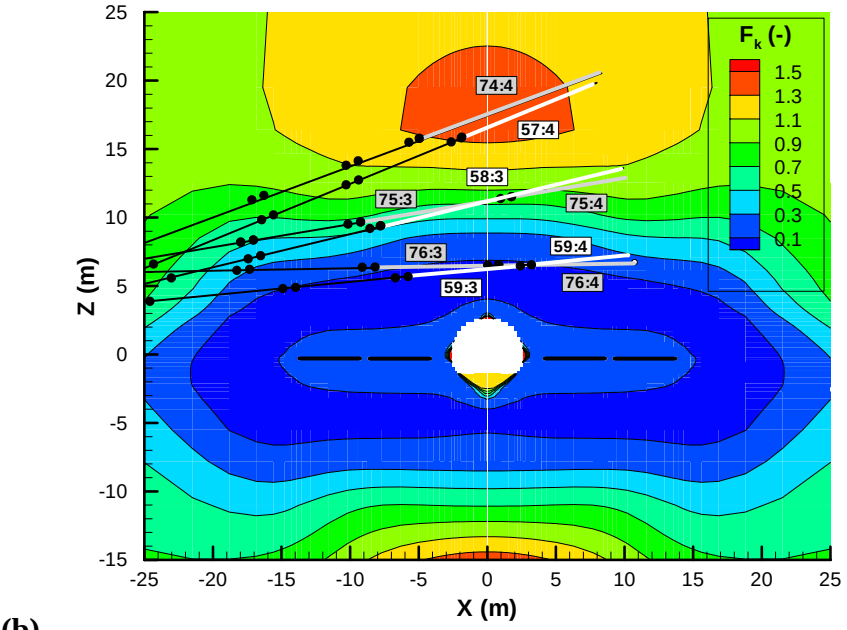

(b)

DTN (borehole locations and sensors): MO0002ABBLSLDS.000 [DIRS 147304]; Output DTN: LB0306DSTTHMVL.002.

NOTES: (a) Changes in relative air permeability caused by TH-induced moisture redistribution.

(b) Change in absolute air permeability caused by the combined effect of moisture redistribution and stress-induced changes in intrinsic permeability.

Figure 7.4.3-2. Simulated Changes in Air Permeability at the Drift Scale Test after 12 Months of Heating Expressed in Terms of Permeability Correction Factor ($F_k = k/k_i$) Relative to Preheating Permeability (k_i)

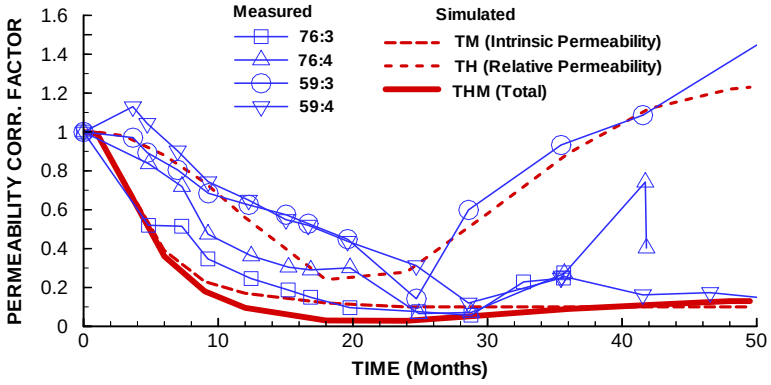

(a) Group located at z ≈ 6 m

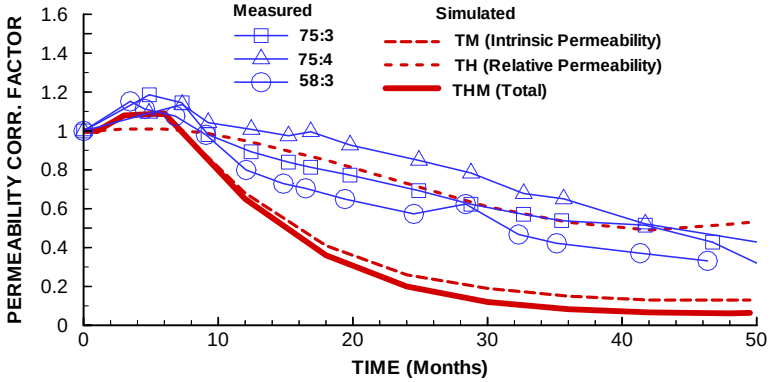

(b) Group located at z ≈12 m

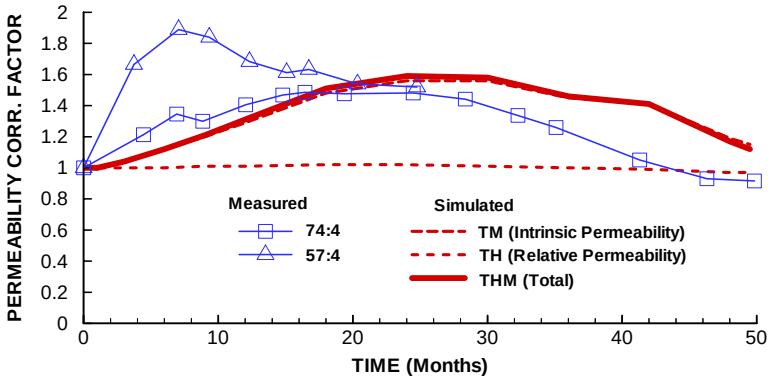

(c) Group located at z ≈18 m

DTN (measured): LB0208AIRKDSTH.001 [DIRS 160897]; Output DTN (simulated): LB0306DSTTHMVL.002.

Figure 7.4.3-3. Measured and Simulated Evolution of Permeability Correction Factors ($F_k = k/k_i$) for Three Groups Located at Various Distances above the Heated Drift (b_{max} = 200 μm, α = 0.52 MPa^{-1})

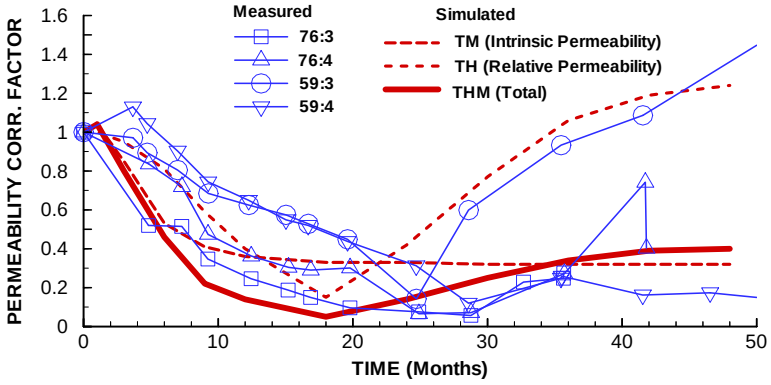

(a) Group located at z ≈ 6

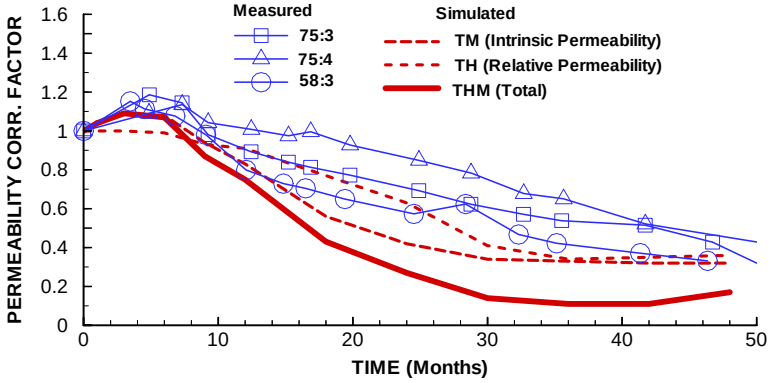

(b) Group located at z ≈12 m

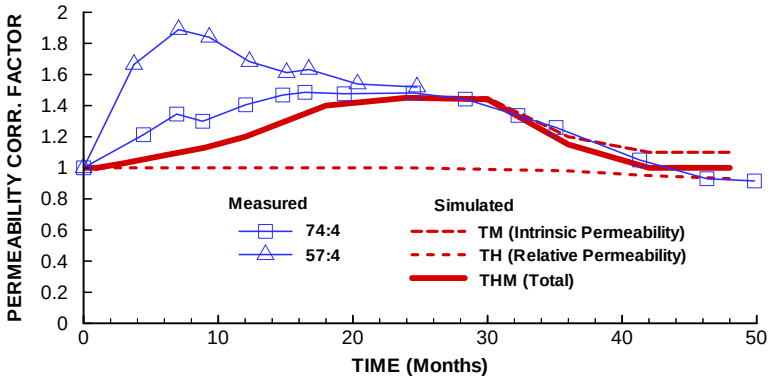

(c) Group located at z ≈ 18 m

DTN (measured): LB0208AIRKDSTH.001 [DIRS 160897]; Output DTN (simulated): LB0306DSTTHMVL.002.

Figure 7.4.3-4. Measured and Simulated Evolution of Permeability Correction Factors (F_k = k/k_i) for Three Groups Located at Various Distances above the Heated Drift (b_{max} = 150 μm, α = 0.6 MPa^{-1})

Figure 7.4.3-5 presents a comparison of predicted and measured air-permeability changes with permeability correction factor in log scale. This gives a different perspective of the permeability changes near the heated drift. Note that the vertical axis spans over four orders of magnitude, which roughly corresponds to the natural range of permeability in the Tptpmn unit. Included in the picture is the predicted permeability correction factor (solid line) and upper and lower limits of the validation criterion (dashed lines) defined in Section 7.1.3. The dashed lines represent the criterion that the predicted changes in permeability should be correct within an order of magnitude; that is, log (k/k_i) simulated and measured differ by less than 1. The figure shows that: (1) the simulated permeability changes are within the validation criterion, (2) the simulated and measured permeability changes are small compared to the natural permeability range, and (3) the simulated changes for the bounding case truly represent a bounding case that emphasizes the effect of THM coupling on permeability.

It should also be noted that the overall good agreement between simulated and measured permeability changes is even more satisfactory considering that some of the disagreements may be a result of uncertainties in measurement. However, whereas relatively large uncertainties are expected in the measured values of permeability, the uncertainty in the permeability change factor should be smaller. The permeability of the rock is estimated using some conceptual model for fluid flow (e.g. radial flow), and the measured value of permeability depends on which conceptualization is used. However, for determining the permeability change factor, there are fewer uncertainties because regardless of which conceptual model is used, the permeability change factor is proportional to the ratio of flow rates between two tests. The uncertainties in the measured permeability correction factor can be evaluated by examining the measured variability in permeability change factor at the site. For example, Figure 7.4.3-3b shows that, at 20 months, the permeability change factor varies between 0.7 to 1.0 for the three different boreholes located about 12 meters from the drift. This variation can be caused by measurement uncertainties but is more likely caused by heterogeneities in the rock mass. There are heterogeneities in both fracture and intact rock properties as well as in the degree of fracturing, which all produce different responses at different locations. Nevertheless, the good agreement between measurements at three different boreholes in Figure 7.4.3-3b indicates that the uncertainty in the measured permeability change factor is less than 30 percent. This is also supported by a relatively smooth and consistent decrease in permeability as a function of time (a more erratic behavior of permeability change factor would indicate greater measurement uncertainty). Individual measurements that show distinctly different behavior from other measurements have been evaluated. For example, borehole Section 59:3 shows a trend of increasing permeability from 25 to 50 months, which is not seen in other measurements at similar locations. At about 50 months, the packers for this particular section failed and it is possible that earlier measurements were affected by leaking packers.

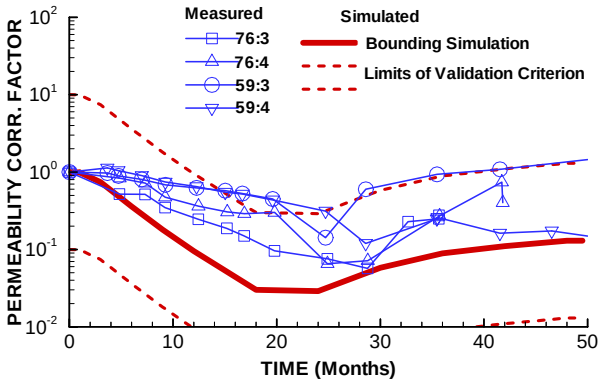

(a) Bounding case at z ≈ 6

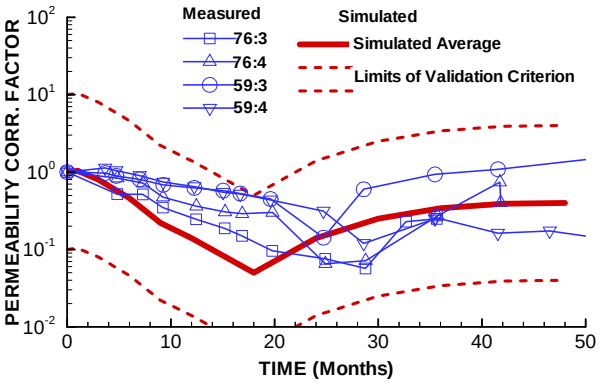

(d) Average case at z ≈ 6

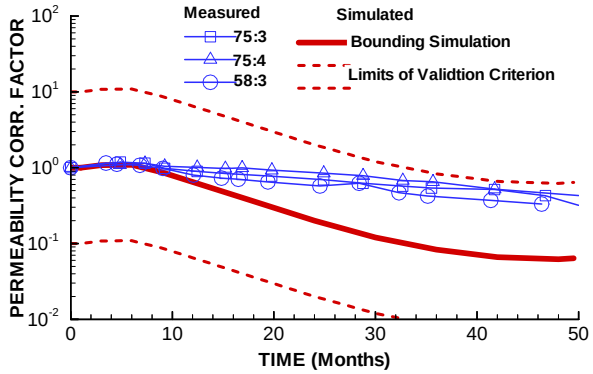

(b) Bounding case at z ≈ 12

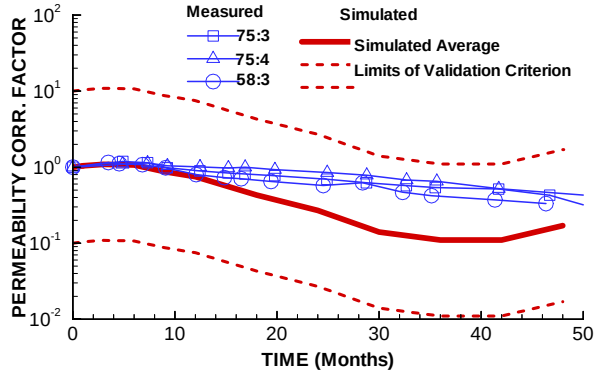

(e) Average case at z ≈ 12

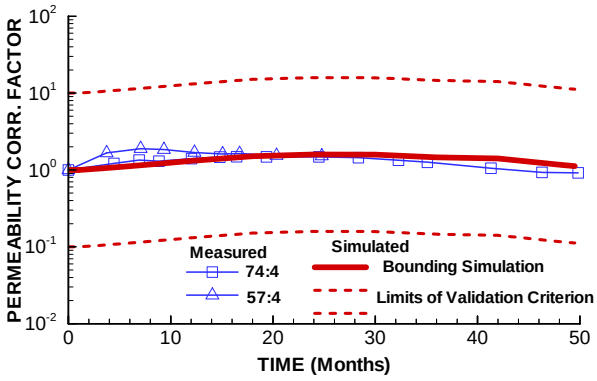

(c) Bounding case at z ≈ 18

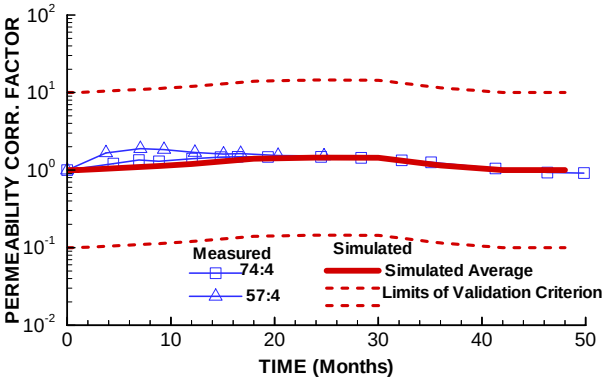

(f) Average case at z ≈ 18

DTN (measured): LB0208AIRKDSTH.001 [DIRS 160897]; Output DTN (simulated): LB0306DSTTHMVL.002.

Figure 7.4.3-5. Measured and Simulated Evolution of Permeability Correction Factors (F_k = k/k_i) Presented in a Log Scale with Comparison to Validation Criteria Limits of Predictions According to Section 7.1-4

7.5 COMPARISON AGAINST NICHE TESTS

An additional validation of the drift scale THM model is conducted against air-permeability measurements conducted at three excavated niches located in the Tptpmn unit and one excavated niche located in the Tptpll unit. These tests were conducted to study permeability changes near a drift wall caused by excavation effects (i.e., mechanical unloading of the rock mass near the drift wall, causing fracture opening and consequent permeability increase). In the Tptpmn unit, the air permeability was measured before and after excavation in 0.3 m packer-isolated sections along three boreholes located about 0.65 m above the niches (BSC 2004 [DIRS 170004], Section 6.1). The boreholes are denoted UM (Upper Middle), UL (Upper Left), and UR (Upper Right). All these boreholes are located at the same elevation, with UM located above the centerline of the drift and UR and UL located about 1 m to the right and left of the centerline, respectively. In Section 6.4.4 of this model report, one data point of the permeability-change ratio was extracted from this data set to determine the parameters b_{max} and α. The validation performed in this section aims to investigate the validity of the stress-permeability model and the stress-aperture function over a range of initial permeability values. The calculated changes in permeability presented in this section were derived using an MS Excel spreadsheet as described in Appendix C.

In this study, the niche excavations were modeled using the FLAC3D V2.0 code to calculate changes in the stress field. A model of the niches is described by Rutqvist (2002 [DIRS 162047], p. 14). Based on the calculated stress field, new fracture apertures for each fracture set can be calculated from Equation 6.2-9. The new apertures are then inserted into Equation 6.2-5 to calculate the excavation permeability correction factors F_{kxe}, F_{kye}, and F_{kze} in the x, y, and z direction. Finally, the geometric mean of the excavation permeability correction factors is calculated from Equation 6.4-5. This calculation is repeated for different initial permeability values to cover a range from k = 1e – 15 m^2 to k = 1e – 9 m^2 (see Appendix C for details).

Figure 7.5-1 compares the calculated and measured geometric mean of pre- to post-excavation ratios for the four niches. In the measured data, the geometric mean of the change ratio was calculated for individual preexcavation permeability intervals (bins). Figure 7.5-1a shows the composite results of data collected from boreholes at three niches located in the Tptpmn unit. Data from several boreholes (UL, UM, and UR), with packer sections located within the axial extension of the niches, are selected, leading to a total of 213 measurements. Figure 7.5-1b shows data from the only niche excavation experiment performed in the Tptpll unit, with a total of 54 measurements. Figure 7.5-1 shows that (1) the simulated and measured permeability changes are in good agreement, (2) the calculation correctly captures the observed trend that permeability generally changes more in initially lower-permeability sections, and (3) the calculation correctly captures the observation of smaller changes in permeability in the Tptpll unit than in the Tptpmn unit.

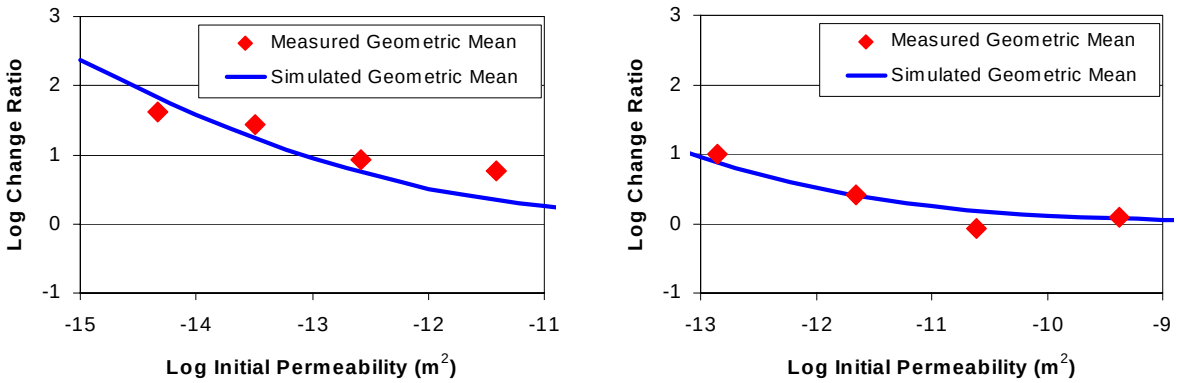

(a) Tptpmn unit (Niches 3107, 3560, and 4788) **(b) Tptpll unit (Niche 1620)**

DTN (measured): LB0310AIRK0015.001 [DIRS 168564]; Output DTN (calculated): LB0306DSTTHMVL.002.

NOTES: Calculation is conducted with b_{max} = 200 μm and α = 0.52 MPa^{-1}, and calculated results represent the mean permeability change factor F_k defined in Equation 6.2-7. The calculation of the lines for UM calculated is described in Appendix C. In DTN: LB0310AIRK0015.001 [DIRS 168564], the measured Log Change Ratio for Niches 3107, 3560, 4788, and 1620 is found in filename "Plots of pre and post holes N2 N3 N4 N5 N5AK-reformated N4 corrected reviewed.xls." In this file, data for Niches 3107, 3560, 4788, and 1620 are found under sheets denoted N3, N2, N4, and N5, respectively.

Figure 7.5-1. Measured and Calculated Permeability Change Ratio at Niches 3107, 3560, and 4788 in the Tptpmn Unit and Niche 1620 in the Tptpll Unit

Although Figure 7.5-1 shows that mean permeability changes are well predicted using the homogenous rock mass model, individual measurements generally show a scatter between a factor of 1 and 1,000 (Figure 7.5-2). Scatter of the measured data over orders of magnitude is not surprising, considering that a very short packer spacing of 0.3 units was used in a heterogeneous rock mass. This can be compared to measurements of air permeability at the DST shown in Figure 7.4.3-3, which indicates permeability reduction changes, but with much less scatter between individual measurement points. Part of the reason for a smaller variability in measured permeability change factor at the DST is that these measurements were taken over several meter-long borehole sections in which the effect of local heterogeneities was averaged out in the measured pressure and flow responses. For the niche test, the measurements were taken using a shorter packer spacing (0.3 m), which is on the order of fracture spacing. The variability in pre- to postexcavation ratios in the niche experiments can be explained by mechanical responses in fractures belonging to different fracture sets (Figure 7.5-2a). The largest permeability increases can occur as a result of opening of fractures in Set 3, which is a horizontal fracture set. Such large permeability increases could occur for the extreme case of a borehole interval connected only to horizontal fractures. Another extreme is the case where the borehole is connected to a fracture of Set 2, in which the fractures are vertical, striking along the drift. Theoretically, this could give a significant reduction in permeability. However, the Tptpmn unit is highly fractured and, therefore a strong reduction in permeability caused by fracture closure in only one fracture set is unlikely. Although fractures in Set 2 would be close to their residual value, it is likely that they are connected to horizontal fractures that are kept open. Fracture Set 1 is oriented perpendicular to the borehole axis and is, therefore the most likely to intersect the borehole. Figure 7.5-2b illustrates the calculated permeability changes in different directions (x, y, and z, where x is horizontal and normal to the niche tunnel axis, y is

horizontal parallel to the niche tunnel axis, and z is vertical). The figure shows that permeability increases in all directions with most changes occurring in the horizontal permeability.

In summary, the observed scatter in the pre- to postexcavation ratio observed at the niches is likely caused by local heterogeneities in the fracture network and in the characteristics of individual fractures. In addition, some of the measured results are affected by measurement uncertainties. For example, the packers are deflated, removed, and then inserted and inflated again for another test.

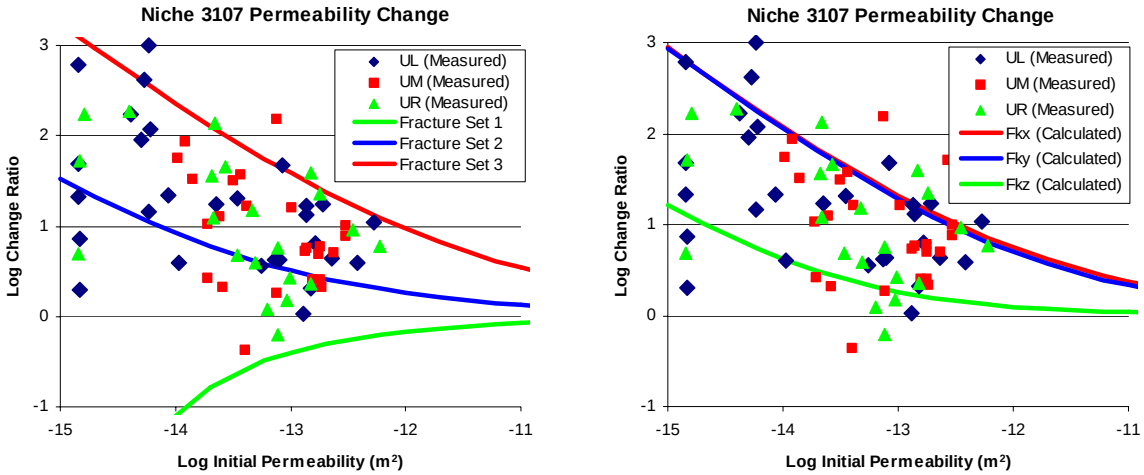

(a) **(b)**

DTN: LB0310AIRK0015.001 [DIRS 168564]; Output DTN: (calculated) LB0306DSTTHMVL.002.

NOTE: In the simulation, the niche is oriented with its cross-section in the x, z-plane, with x being horizontal and z vertical, and y is parallel to the niche tunnel axis. The fracture plane in fracture Sets 1, 2 and 3 is oriented normal to x, y, and z directions, respectively. Thus, Set 1 is vertical striking along the niche tunnel axis, Set 2 is vertical striking normal to the niche tunnel axis, and Set 3 is horizontal.

Calculation is conducted with b_{max} = 200 μm and α = 0.52 MPa^{-1}. The calculations resulting in the three lines (blue, red and green) in (a) and (b) are described in Appendix C.

Figure 7.5-2. Comparison of Measured Permeability-Change Ratio for Individual Measurements at Niche 3107 to (a) Simulated Permeability-Change Ratio in the Three Fracture Sets, and to (b) Permeability Correction Factors in x, y, and z Direction

Figure 7.5-3 presents a comparison of simulated and measured data taken from both the Tptpmn and Tptpll units (Niches 3107, 3560, 4788, and 1620) consolidated into one single data set. The figure presents the geometric mean of both simulated and measured data, standard deviation of measured data, and the limits of the validation criterion defined in Section 7.1-4. The agreement between calculated mean values and trends in the Tptpmn unit and Tptpll unit shows that the stress-versus-permeability model of the drift scale THM model is applicable for both Tptpmn and Tptpll units over their entire range of initial permeability values. For the air permeability test conducted in the Tptpll unit, some extreme permeability changes occur (even at high initial permeability), which is reflected by a large standard deviation. The presence of lithophysae may have impacted the measurements. In general, the measurements conducted at one-foot borehole lengths are difficult in the Tptpll unit, since the unit contains lithophysal cavities that can be

larger than one foot in diameter. Figure 7.5-3 shows that most of the measured permeability changes are within the limits defined by the validation criterion, even considering variability reflected by the standard deviation of the log change ratio. However, it should be emphasized that the only validation requirement is that the measured mean permeability change ratio be within the limits of the validation criterion, because this is what the model is designed to predict.

As discussed in Section 6.10.5, for the purpose of this report, it is sufficient to predict changes in mean permeability for the excavation effect. As shown in Figure 6.10.5-1, the mechanically induced changes in permeability at the niches cause a change in mean permeability while the distribution (standard deviation) of the permeability does not change significantly. A heterogeneous permeability field is an important feature considered in *Seepage Model for PA Including Drift Collapse* (BSC 2004 [DIRS 167652], Section 6). The mechanically induced changes in permeability predicted in this report can be factored in as a change in mean permeability on such heterogeneous permeability field.

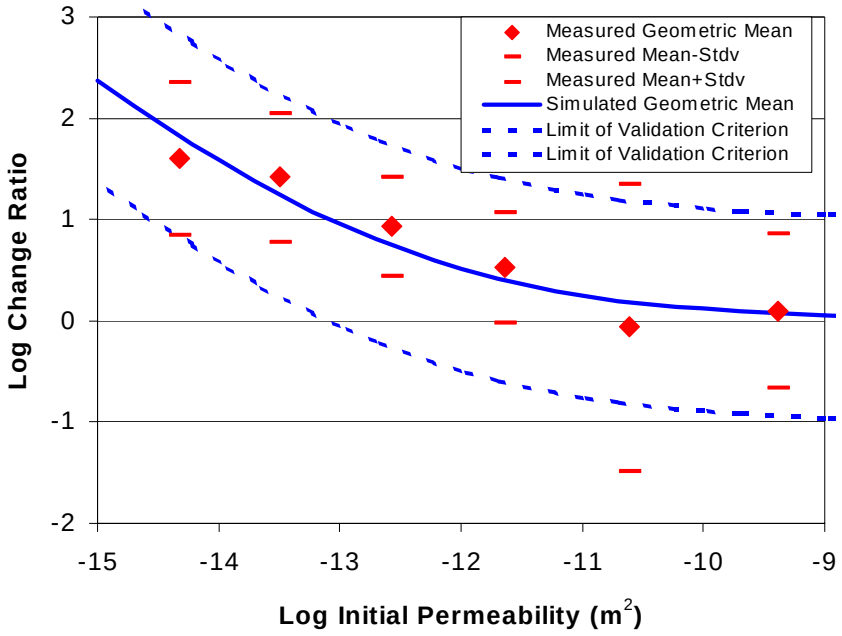

DTN (measured): LB0310AIRK0015.001 [DIRS 168564]; Output DTN (calculated): LB0306DSTTHMVL.002.

Figure 7.5-3. Measured and Calculated Permeability Change Ratio at Niches 3107, 3560, and 4788 in the Tptpmn Unit and Niche 1620 in the Tptpll Unit with Comparison of Mean Values and Standard Deviation of Measurements and Mean Value of Simulation and Limits of Validation Criterion Shown

7.6 VALIDATION AGAINST OBSERVATIONS OF SIDEWALL FRACTURING IN THE ECRB CROSS DRIFT

This section presents the validation of the mechanical model and in situ strength properties of lithophysal rock against observations of minor damage in the sidewalls of the ESF Main Drift and ECRB Cross Drift (BSC 2004 [DIRS 166107], Section 7.6.5.2). The lithophysal rock properties were extracted from *Drift Degradation Analysis* (BSC 2004 [DIRS 166107], Appendix E, Table E-10). In that report, the mechanical properties of the lithophysal units were divided into several categories ranging from low quality (Category 1) to high quality (Category 5) lithophysal rock. The mechanical properties for Categories 1 and 5 lithophysal rock are listed in Table 7.6-1 below.

7.6.1. Validation Method

The validation is checked in two ways: (a) against field observations of Tptpll and Tptpul units and (b) against an alternative model of the *Drift Degradation Analysis*. The mechanical properties derived for the low quality lithophysal rock are verified by comparison of predicted yielding to minor damage observed in the sidewalls of the ESF Main drift and ECRB Cross Drift (BSC 2004 [DIRS 166107], Section 7.6.5.2). The consistency of this analysis with field observation and the alternative model provides confidence in the mechanical model and mechanical properties derived for the low quality lithophysal rock.

7.6.2 Summary of Field Observations

Tunnels in all rock units at Yucca Mountain are stable after excavation, regardless of depth or rock quality. However, some damage in the form of wall parallel fractures (opening of existing fracture fabric) at the springline, the point of highest shearing stress, can be observed in the sidewalls of the tunnels at greater depth in the Tptpll (BSC 2004 [DIRS 166107], Section 7.6.5.2). Figure 7.6.2-1 shows formation/opening of wall parallel fractures observed in 12-inch diameter boreholes drilled for geomechanical sampling in the sidewalls of the ESF Main Drift and ECRB Cross Drift at the tunnel springline. The wall parallel fractures are typical of stress-induced yield in tunnels. Boreholes drilled in the relatively low quality Tptpll at depths of 300 to 350 m show sidewall fracturing to depths of approximately 0.5 to 0.6 m. Holes drilled into relatively high quality Tptpul at depths of approximately 200 to 250 m show no fracturing (BSC 2004 [DIRS 166107], Section 7.6.5.2). The presence of these fractures and their depth into the drift wall, observed in large-hole drilling, are convenient features from which to estimate the rock mass strength properties and validation of the model. Additionally, no sidewall damage is observed in drifts in the higher quality Tptpul at shallower depths.

7.6.3 Calculation Results for Tptpll and Tptpul units

Similar to an analysis made in *Drift Degradation Analysis* (BSC 2004 [DIRS 166107], Section 7.6.5.2), a parametric study of rock yield depth was conducted using FLAC3D for Category 1 (low quality lithophysal rock) and Category 5 (high quality lithophysal rock). The analysis was conducted for an imposed overburden depth of between 244 and 364 m. A Mohr-Coulomb material model was used with material parameters for low and high quality lithophysal rock given in Table 7.6-1. As seen in Figure 7.6.3-1, the model reproduces the

approximate depth of observed underground sidewall damage for Category 1. The model results indicate that the rock adjacent to the drift wall yields in a state of uniaxial compression because the minimum stress at or near the drift wall is zero or small (since the radial stress component is zero). The models also show that, for the range of potential lithophysal rock properties, there is no drift wall yield at the depth of the Tptpul from Category 1. Some of the yield seen in Figure 7.6.3-1 (e.g., for Category 5 above and below the springline) may be caused by the discretization of the circular drift shape, using square elements.

7.6.4 Comparison with Alternative Model of Drift Degradation Analysis

The results of this analysis are consistent with simulation results presented in *Drift Degradation Analysis* (BSC 2004 [DIRS 166107], Section 7.6.5.2), using an alternative modeling approach. In both models, inelastic deformation and yielding take place on the side of the drift and not on the top of the drift. Furthermore, both models predict a yielding of about 0.5 m at the springline (compare Figure 7.6.2-1 in this report with BSC 2004 [DIRS 166107], Section 7.6.5.2, Figures 7-26 and 7-27).

Table 7.6-1. Mechanical Properties Used for Model Validation Against Observations of Sidewall Fracturing in the ECRB Cross Drift

	Category 1	Category 5	Source
Young's Modulus E (GPa)	1.9	19.7	BSC (2004 [DIRS 166107]), Appendix E, Table E-10
Bulk Modulus (GPa)	1.07	10.95	BSC (2004 [DIRS 166107]), Appendix E, Table E-10
Shear Modulus (GPa)	0.80	8.21	BSC (2004 [DIRS 166107]), Appendix E, Table E-10
Cohesion (MPa)	2.33	7.00	BSC (2004 [DIRS 166107]), Appendix E, Table E-10
Friction Angle (Degrees)	40	40	BSC (2004 [DIRS 166107]), Appendix E, Table E-10
Tensile strength (MPa)	0.8	0.8	BSC (2004 [DIRS 166107]), Figure 7-21

NOTE: Category 1 properties are also listed in Table 4.1-3b for direct input to predictive analysis. The tensile strength of 0.8 was obtained from the x-intercept of Figure 7-21 in *Drift Degradation Analysis* (BSC 2004 [DIRS 166107]), to be consistent with the drift degradation analysis.

7.7 COMPARISON TO AN ALTERNATIVE CONCEPTUAL MODEL

An additional validation of the drift scale THM model is conducted by comparing this model to the results of a previous analysis of the DST (BSC 2001 [DIRS 155957], Section 6.4.2). In the previous analysis (BSC 2001 [DIRS 155957], Section 6.4.2), the first 18 months of the DST were simulated by two separate three-dimensional analyses, one using a continuum-based model and one using a discrete-fracture model (see Section 1 for a brief description of the alternative discrete-fracture model). In both simulations, the thermal expansion coefficient was set to $9.73°C^{-1}$. In Figure 7.7-1, the simulated results of the previous analysis (BSC 2001 [DIRS 155957], Section 6.4.2) are compared to a separate simulation using the drift scale THM model for displacement at Anchor 4 (located about 15 m from the drift wall) in borehole 148. In this analysis, the drift scale THM model was applied using an equivalent value of the thermal

expansion coefficient ($9.73°C^{-1}$). The mechanical properties of the discrete-fracture model (a distinct element model) include properties of the intact rock between fractures, and fracture properties such as normal stiffness, shear stiffness and shear strength, whereas the mechanical properties of the continuum models implicitly account for the effect of fracturing. The mechanical properties for all the models were developed to represent the in situ rock mass properties at the site. However, for the thermal expansion leading to displacements in extensometers at the DST, the thermal expansion coefficient is the most important, whereas mechanical properties such as Young's modulus are of secondary importance.

It can be concluded that the three separate models analyzing the DST—the two continuum-based (one drift scale THM, one reported in BSC 2001 [DIRS 155957], Section 6.4.2) and one discrete-element model—all provided similar results in magnitude and trend, even taking into account differences in model discretization and calculation of temperature. The good agreement between the drift scale THM model and the alternative discrete-fracture approach shown in Figure 7.7-1 is typical for comparisons made at several anchors around the DST. The good agreement between the independent numerical models provides additional confidence for the validation of the TM part of the drift scale THM model. Moreover, the results in Figure 7.7-1 support the determination that a continuum approach is sufficient to model the thermal expansion of the rock mass in this particular case.

7.8 MULTIPLE LINES OF EVIDENCE

The general results of a number of THM experiments conducted at the Nevada Test Site and other fractured rock sites are described below for multiple lines of evidence in support of the drift scale THM model.

7.8.1 Nevada Test Site THM Experiments

Four TM/THM experiments relating to high level nuclear waste research were conducted at the G-tunnel in Rainier Mesa. These tests included a single borehole heater test, small-diameter heater test, heated block test, and prototype engineered barrier system field test. One objective of the heated block test was to measure rock mass mechanical and TM properties of welded ash-flow tuff under controlled thermal- and stress-loading conditions. The block was subjected to maximum temperatures ranging from 76° to 130°C, and equal biaxial stresses with magnitudes up to 10.6 MPa (Zimmerman et al. 1986 [DIRS 145625]). The effective modulus of deformation ranged from 0.4 to 0.83 times the intact-rock measurements, depending on the number of joints included and their apertures. A slight dependence of modulus on stress was indicated, but no significant temperature effects on modulus were identified.

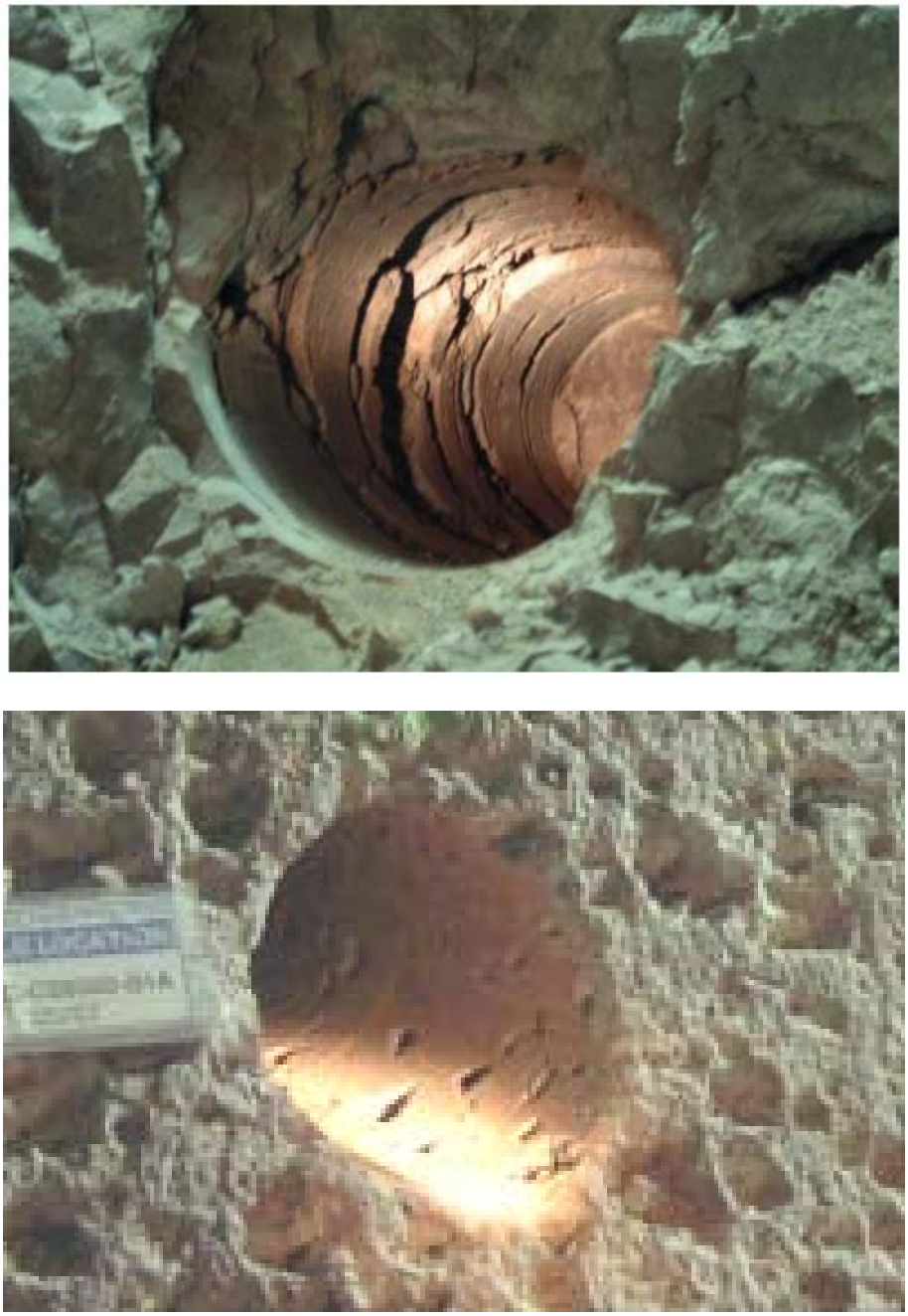

Source: BSC 2004 [DIRS 166107], Figure 7-25.

NOTES: Top photo shows sidewall fracturing/opening of preexisting wall parallel fractures in a 12-inch diameter horizontal borehole drilled in the springline of the ESF in low quality Tptpll (approximately Category 1). Overburden depth is approximately 325 m. Depth of fracturing is approximately 1.5 to 2 ft. The bottom photo shows a horizontal, 12-inch diameter borehole drilled in the springline in high quality Tptpul (approximately Category 5) in the ESF showing no sidewall damage. The depth of overburden is approximately 250 m.

Figure 7.6.2-1. Observed Rock Mass Conditions at the Tunnel Springline in Lithophysal Rock in the ESF

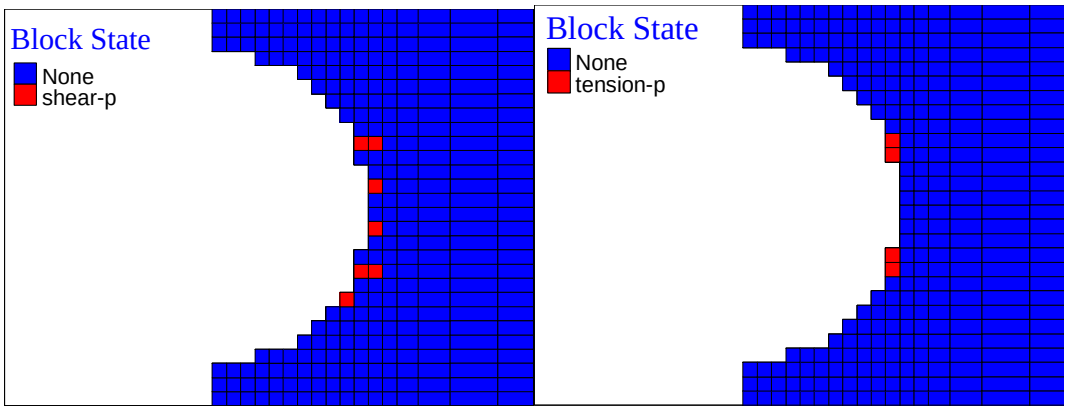

(a) Category 1 rock at 244 m depths **(b) Category 5 rock at 244 m depths**

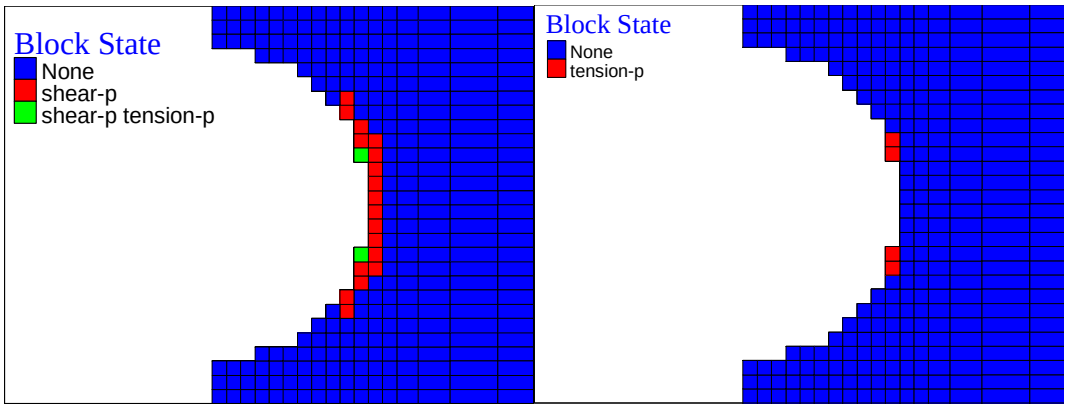

(c) Category 1 rock at 298 m depths **(d) Category 5 rock at 298 m depths**

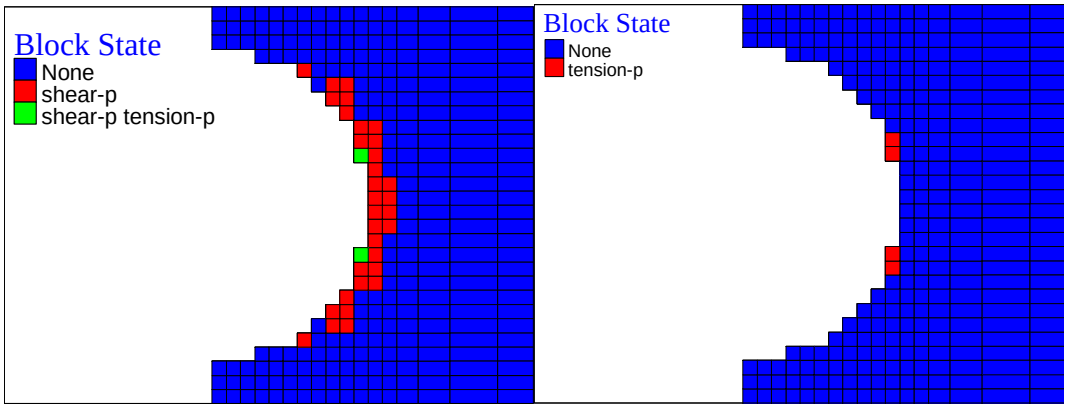

(e) Category 1 rock at 364 m depths **(f) Category 5 rock at 364 m depths**

Output DTN: LB0308DSTTHMVL.001.

NOTE: For Category 1 rock, the yield zone at the sidewall extends about 0.25 to 0.5 m (1 to 2 feet) into the sidewall when the depth increases from 298 and 364 m. At Yucca Mountain, fracturing was observed to extend about 1 to 2 feet into the sidewall in a section of the ECRB cross drift located in low quality rock at a depth of 325 m.

Figure 7.6.3-1. Extent of Yield Zone for a Drift Located at 244, 298, and 364 m for Category 1 Rock (Low Quality Tptpll) and Category 5 Rock (High Quality Tptpll and Tptpul)

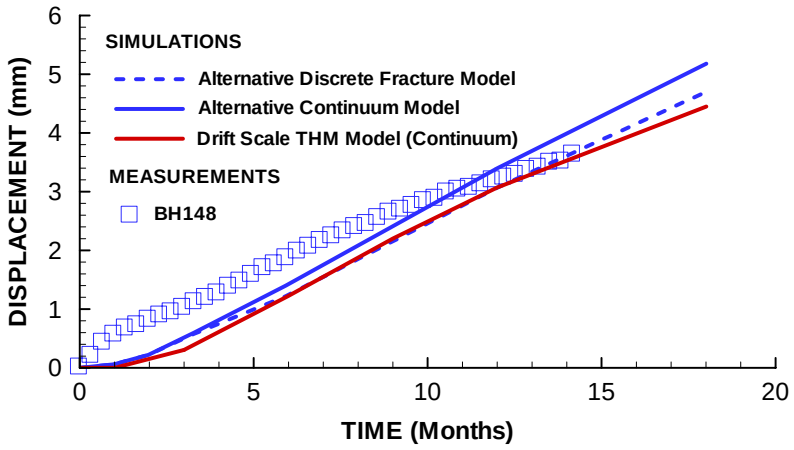

Output DTN: LB0306DSTTHMVL.002.

NOTE: The simulation results of alternative discrete fracture model and alternative continuum model have been extracted from *Coupled Thermal-Hydrologic-Mechanical Effects on Permeability Analysis and Models Report* (BSC 2001 [DIRS 155957], Figure 6.4.2-12, p. 121). Simulation results using the drift scale THM model are compared to the simulation results of this same report (BSC 2001 [DIRS 155957]). The measured values were extracted from DTN: SN0207F3912298.037 [DIRS 162046].

Figure 7.7-1. Simulated and Measured Evolution of Displacements at Anchor 4 in MPBX Borehole 148

A second objective of the heated block test was to determine the effects of excavation, stress, and temperature changes on the permeability of a single joint. The permeability of a single near vertical fracture was measured using three vertical boreholes in a linear array. The largest changes in permeability were associated with excavation of the block when the apparent permeability increased from 76 to 758 microdarcies (i.e about one order of magnitude). Subsequent compressive loading decreased the permeability but did not completely reverse the unloading conditions, and the apparent permeability ranged from 252 to 332 microdarcies over a compressive stress range of 3.1 to 10.6 MPa (Hardin and Chesnut 1997 [DIRS 100534], pp. 4 to 6). Increased temperature under biaxial confinement decreased the fracture aperture, lowering the apparent permeability from 234 to 89 microdarcies during heating caused by rock thermal expansion. These observations are consistent (i.e., of the same order of magnitude) with the Yucca Mountain THM modeling and field studies described earlier. That is, fracture permeability increases about one order of magnitude as a result of near surface unloading during excavation, and decreases by less than one order of magnitude during heating.

7.8.2 Underground Testing at Stripa

Over 20 years ago, a time-scaled heater test was performed at Stripa to investigate the long-term TM response to thermal loading (Chan et al. 1980 [DIRS 154672]). Analysis showed that, in the full-scale and time-scale heater tests, heat flow conformed to the linear conduction theory and was not affected by fractures or other discontinuities. Thermoelastic deformation of the rock mass was nonlinear and less than expected. Early in the tests, measured displacements were much less than predicted by linear thermoelasticity. Later, the displacements increased uniformly, but in fixed proportions to predicted levels. This was likely a result of fracture closure in response to thermal expansion. Fracture closure was confirmed by observation of

diminished water inflow to the heater and instrument boreholes (Nelson et al. 1981 [DIRS 150092], p. xi) and by increased compressional wave velocity during heating (Paulsson et al. 1980 [DIRS 154570], p. 4). The closing of fractures (and resulting changes in fracture permeability due to thermal input) is consistent with the results of the Yucca Mountain studies described in this report.

7.8.3 DECOVALEX Findings at Fanay-Augères and Kamaishi Mine Heater Tests

The results in this model report can also be compared to findings in the international cooperative project DECOVALEX (DEvelopment of COupled models and their VALidation against EXperiments in nuclear waste isolation). Model validation against in situ tests, such as Fanay-Augères (Rejeb 1996 [DIRS 162589]), and Kamaishi Mine (Rutqvist et al. 2001 [DIRS 162586]) demonstrates that the temperature field can be predicted with confidence because it is mainly governed by heat conduction through rock masses with little influence from discrete fractures. Rock mass deformation measured along extensometers between anchors placed several meters apart can also be predicted reasonably well in trends and magnitudes. This is because the bulk thermal expansion of the rock is dominated by the thermal expansion of the matrix rock, while fractures have a secondary effect that appears as a reduction of the rock mass thermal expansion coefficient. It can also be concluded from these two heater tests that the general thermal expansion of the rock mass is essentially elastic for measurements conducted over several meters of fractured rock. However, although the bulk thermal expansion of the rock mass is essentially elastic and reversible, the displacement and aperture changes measured over individual fractures are generally irreversible. That is, there is a remaining change in fracture aperture after the rock mass has cooled down to ambient conditions. Furthermore, it is more difficult to predict the responses of individual fractures than to predict the overall rock mass thermal expansion. This might be important for predicting changes in hydraulic permeability, which critically depends on the aperture changes of fractures.

7.8.4 Geothermal Reservoir Temperature-Permeability Correlation

In addition to field studies of coupled THM processes that provide direct evidence of how a potential repository at Yucca Mountain would perform, corroborative results for coupled THM effects may be found in the geothermal literature. A survey of geothermal reservoir properties worldwide (Björnsson and Bodvarsson 1990 [DIRS 154606], pp. 19 to 21) showed a correlation between permeability and temperature for various geothermal systems (Figure 7.8.4-1). The values are scattered, but they indicate a trend toward decreasing permeability with increasing temperatures. The low permeability at temperatures around 300°C and above is more likely caused by geochemical effects. THM effects may be present at lower temperatures.

7.8.5 Coupled THM Analyses of the Yucca Mountain Drift Scale Test within DECOVALEX III

The TM and THM responses of the Yucca Mountain DST are independently analyzed by the participants of the DECOVALEX III project, which is an international research project for development of coupled models and their validation against experiments. The outcome of the analyses by DECOVALEX participants, generally corroborative of the contents of this model report, was presented in the international GeoProc2003 conference held in Stockholm, Sweden, in October 2003 (Datta et al. 2003 [DIRS 170398]; Rutqvist et al. 2003 [DIRS 170400]; Hsiung et al. 2003 [DIRS 170402]; Green and Painter 2003 [DIRS 170403]; Olivella et al. 2003 [DIRS 170405]; and Millard and Rutqvist 2003 [DIRS 170406]).

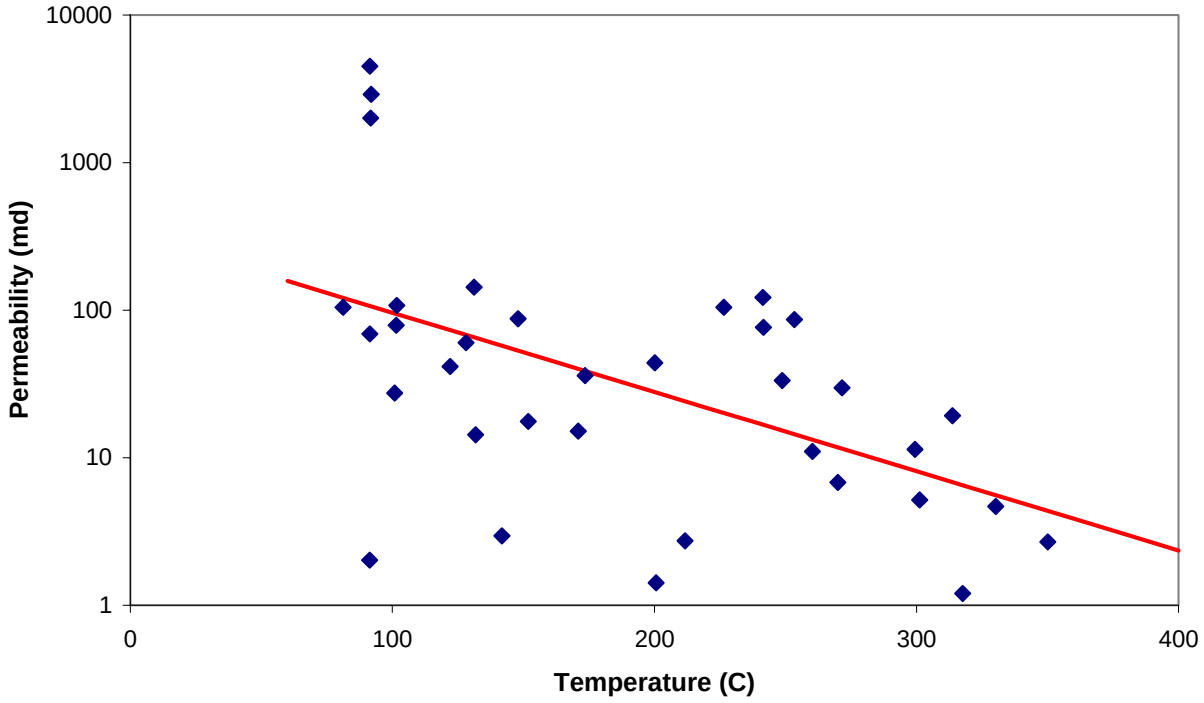

Source: Björnsson and Bodvarsson 1990 [DIRS 154606], Figure 1.

Figure 7.8.4-1. Correlation Between Permeability and Temperature for Geothermal Reservoirs Worldwide

Three independent analyses presented by Rutqvist et al. (2003 [DIRS 170400]), Green and Painter (2003 [DIRS 170403]), and Olivella et al. (2003 [DIRS 170405]) show good agreement in the results of moisture redistribution around the drift. The formation of a dryout zone and its extent at various times are consistent for these three independent analyses.

In Millard and Rutqvist (2003 [DIRS 170406]), the predictions of mechanical displacement using the Yucca Mountain coupled THM process model is compared to an independent model analysis conducted by a research team from the Commissariat a l′Energie Atamique de Cadarache in France. It was concluded that the displacement predicted by the two independent analyses compared reasonably well to the measured ones, both in trends and average magnitude. Both analyses showed that the in situ rock mass thermal expansion coefficient is appropriately represented by a temperature-dependent thermal expansion coefficient derived from intact rock samples. And finally, the two analyses indicate that rock behavior is essentially elastic, although a few instances of inelastic behavior can be observed near the drift wall. The displacements calculated by the two models, as presented by Millard and Rutqvist (2003 [DIRS 170406]), also agree with displacements calculated by a third model, presented by Hsiung et al. (2003 [DIRS 170402]).

Permeability changes calculated using the Yucca Mountain coupled THM process model (Rutqvist et al. 2003 [DIRS 170400]) are generally in agreement with permeability changes calculated with two other models (Olivella et al. 2003 [DIRS 170405]; Hsiung et al. 2003 [DIRS 170402]). The analysis by Rutqvist et al. (2003 [DIRS 170400]) and Hsiung et al. (2003 [DIRS 170402]) consistently shows that fracture aperture change caused by changes in stress normal to fractures is the dominating mechanism of permeability changes. Thus, permeability changes caused by shear slip appear to be small compared to changes caused by normal stress.

Finally, all four analyses of the DST were conducted using the continuum approach. The four research teams each concluded that a continuum approach is appropriate for modeling of coupled THM processes in the fractured Tptpmn rock at the DST.

The papers from the GeoProc2003 conference will be published in the Elsevier Sciences Book Series on Engineering Geology. Furthermore, the results of DECOVALEX III are to be published in an upcoming special issue of the *International Journal of Rock Mechanics*.

7.9 PUBLICATION IN PEER-REVIEWED JOURNALS

The TOUGH2-FLAC3D simulator was presented in the *International Journal of Rock Mechanics & Mining Sciences* in 2002 (Rutqvist et al. 2002 [DIRS 162048]). This paper includes the fundamental theories and underlying conceptual models for the TOUGH2 code, the FLAC3D code, and the coupling functions between the two codes. An application of the simulator for a drift scale THM analysis of the repository at Yucca Mountain has been published in a special issue of the *Journal of Contaminant Hydrology* (Rutqvist and Tsang 2003 [DIRS 162584]). This published analysis is similar to the one conducted in this report, but does not include the recent extensive validation against the DST. The results and the general conclusions of the published analysis are consistent with the results presented in this report. An application of the TOUGH2-FLAC3D code to problems related to HM processes in the

geological sequestration of greenhouse gases has also been published (Rutqvist and Tsang 2002 [DIRS 162587]).

7.10 EVALUATION OF CRITERIA AND SUMMARY

In Section 7 of this model report, confidence in the drift scale THM model has been achieved by corroboration with several in situ tests and in situ observations at the Yucca Mountain, by comparison to alternative models, by publications in peer-review journals, through multiple lines of evidence provided from natural analogues in the geothermal field and from other heater tests, and from corroboration with several other independent analysis models within the international code comparison project DECOVALEX. The validation criteria defined in Section 2.2.2 of the TWP (BSC 2004 [DIRS 170236]) have been met. Specifically:

- The predicted changes in air permeability at the DST and niche excavations are in the correct direction and correct within an order of magnitude; that is, log (k/k_i) simulated and measured differ by less than 1 (see Figures 7.4.3-3 and 4, and 7.5-1).

- Observed trends of air permeability (e.g., k/k_i decreases followed by increases, or the reverse) at the DST and niche excavations are matched by model predictions (see Figures 7.4.3-3 and 4, and 7.5-1).

- The predicted displacements at the DST are within 50 percent of the measured average displacement, for the rock mass as a whole, taken over the entire heating sequence (see Figure 7.4.2-3c).

- The observed pattern of yielding (minor-fracturing) observed in lithophysal rich rock around the ECRB Cross Drift is matched by the model simulation (Section 7.6.3).

In addition to meeting the formal validation criteria listed above, the general comparison of the coupled THM model results against DST heating phase data supports the contention that relevant THM processes are well represented by the model. In general, calculated responses are within the range of measurements. Only a few minor aspects of the model validation could be improved. One of those is the calculated displacement during the first few months of heating, which disagrees slightly with measurement results. More precise matching of calculated and measured air-permeability changes might be possible. However, the present analysis of the DST heating phase shows that the drift scale THM model is adequate for the analysis of coupled THM processes, and that:

1) The underlying conceptual model is sound.

2) The continuum representation of the fractured rock mass using average properties is adequate.

3) The average parameters derived for the continuum model are representative of the temporal and spatial discretizations considered in the model.

Furthermore, the analysis shows that the conceptual model for HM coupling is adequate. This validation indicates that fracture opening and closing caused by changes in normal stress is the

dominant mode of permeability change. Mechanical responses in the DST indicates that no significant shear slip occurs, except possibly in isolated instances such as the displacements of Anchor 1 as shown in Figure 7.4.2-2a (see upper red line in Figure 7.4.2-2a for a 2 mm reduction of displacements from 32 to 34 months). The measured change in air permeability at the DST does not show any widespread increase. Although a few increases in permeability have been observed, they appear to be isolated to one packed-off section, while no such increases are noted in neighboring sections. Thus, even if the above-discussed displacement reduction in Figure 7.4.2-2a is caused by a fracture slip, there is no indication that such an event induced any significant increase in the fracture permeability. This observation provides further evidence that shear-induced permeability enhancement is not significant, and that fracture opening or closure by changes in normal stress is the dominant mode of permeability change.

The findings here in Section 7 of this report are generally supported by studies of similar heater tests such as Stripa Mine, Fanay-Augères, and Kamaishi Mine (Section 7.8). In particular, the temperature field and the bulk thermal expansion of the rock can be predicted with confidence using a simple thermoelastic model. Analyses of Fanay-Augères and Kamaishi Mine experiments indicate that predicting the magnitude of displacements at individual points of the rock mass and over individual fractures can be difficult (Section 7.8). However, the rock mass characteristics at Yucca Mountain differ from those at these other heater tests: The rock mass of the repository units at Yucca Mountain is heavily fractured volcanic tuff, while the other experiments have been conducted in sparsely fractured granitic rock. In relation to other fractured rock sites, the rock mass at Yucca Mountain is relatively homogenous (ubiquitously fractured), with much less spatial variability in rock mass mechanical and hydrological properties. This is especially evident for hydraulic permeability, which at sparsely fractured sites generally ranges over six orders of magnitude, whereas the permeability at each rock unit at Yucca Mountain generally spans less than four orders of magnitude. The conceptual model in Figure 6.2-1, combined with a continuum model approach, is shown to be appropriate for the analysis of THM processes, because the rock mass at Yucca Mountain is ubiquitously fractured, forming a dense, well-connected fracture network for fluid flow. This is the main reason why the drift scale THM model consistently captures relevant THM responses at Yucca Mountain.

In summary, the overall validation process documented in this report has demonstrated the drift scale THM model to be sufficiently accurate and adequate for its intended use: to provide changes in hydrological properties (permeability and capillary strength) for the seepage models and to evaluate the impact of coupled THM processes on the flow field around an emplacement drift. Model data comparison shows overall agreement of calculated and measured THM responses. The model adequately captures relevant drift scale THM processes at Yucca Mountain, and that the analysis in Section 6 of this model report provides a bounding estimate of changes in hydrological properties for an emphasized effect of THM coupling. Activities and requirements for confidence building during model development have also been satisfied. The model development activities and the described post-development validation activities establish the scientific bases for the drift scale THM model. Through the multitude of model validations and the substantial evidence documented in this report, the required level of confidence of the drift scale THM model has been achieved.

INTENTIONALLY LEFT BLANK

8. CONCLUSIONS

8.1 SUMMARY AND CONCLUSIONS

This model report documents the results obtained from numerical simulation of the coupled thermal-hydrological-mechanical (THM) processes in the vicinity of a waste emplacement drift at the nuclear waste repository at Yucca Mountain. One of the main objectives for the drift-scale coupled simulations is to investigate the impact of coupled processes on the potential for water entering an emplacement drift (seepage). Coupled THM processes can impact the potential for seepage in several ways because the heat generated by the decay of radioactive waste results in rock temperature elevated from ambient for thousands of years after emplacement. Heating the rock will cause thermal expansion, which in turn will change the stress field around the emplacement drift. Thermally induced changes in the stress field will act upon preexisting fractures, that generally tend to tighten to smaller apertures, with the result of changing the hydrological properties of the rock mass. The purpose of the drift scale THM model is to provide changes in permeability around the drift to be used to assess the importance of THM processes on seepage and support in the model reports *Seepage Model for PA Including Drift Collapse* (BSC 2004 [DIRS 167652]) and *Abstraction of Drift Seepage* (BSC 2004 [DIRS 169131]), and to support arguments for exclusion of features, events, and processes (FEPs) in the analysis reports *Features, Events, and Processes in Unsaturated Zone Flow and Transport* (BSC 2004 [DIRS 170012]) and *Features, Events, and Processes: Disruptive Events* (BSC 2004 [DIRS 170017]). The TSPA calculations do not use any output from this report. In addition to estimating the changes in permeability distribution-caused THM effects, the model report also assesses the impact of such changes on the flow field around the vicinity of an emplacement drift.

Information on the following parameters are propagated to the seepage models:

- Estimates of THM induced changes in fracture permeability around an intact and fully collapsed drift

- Estimates of THM induced changes in capillary pressure around an intact and fully collapsed drift.

These parameters are estimated through a bounding analysis that brackets the potential impact of THM processes on hydrologic properties (including permeability) and the flow field. The bounding case is realized by adopting parameter values that emphasize the effect of coupling (Section 6.4.5). This includes a bounding estimate of the thermal expansion coefficient (that emphasizes thermal stress) and a bounding estimate of a stress-versus-permeability function (that emphasizes effect of thermal stress on permeability). In addition, the results of THM analyses are compared to TH analyses with no effect of THM coupling.

The drift scale THM model was applied to analyze the impact of coupled THM processes in the case of an emplacement drift located either in the Tptpmn unit (Tptpmn model domain) or in the Tptpll unit (Tptpll model domain). Results from the drift scale THM model are presented in Sections 6.5 (Tptpmn model domain), 6.6 (Tptpll model domain), and 6.7 (low quality Tptpll rock), and have been submitted to the Technical Data Management System (TDMS) as output

under DTNs listed in Section 9.4. In addition, Section 6.8 estimates potential changes in hydrologic properties around a degraded and collapsed drift in the Tptpll unit. A brief summary and discussion of the results are given in Section 6.9. The following main conclusions are drawn from Section 6 of this model report:

- The hydrological properties will change around an emplacement drift, first as a result of excavation of the drift and later as a result of heating of the rock mass surrounding the drift. The excavation of the drift is predicted to induce a maximum one-order-of-magnitude increase in the horizontal permeability at the drift crown; whereas the vertical permeability at the same location is predicted to increase by much less.

- The maximum THM effects will occur around 100 to 1,000 years after emplacement of the waste, when the temperature in the rock mass at the repository level reaches its maximum. The primary THM effects are thermally induced and excavation-induced changes in the stress field that act on preexisting fractures, causing fracture closure or opening with accompanying changes in fracture permeability and capillary pressure. These effects will last well over 10,000 years because of elevated temperature.

- Thermal stresses in the horizontal direction will increase significantly; whereas the vertical stresses will remain almost unchanged through the thermal period. The analysis indicates that horizontal compressive stresses can increase by more than 10 MPa at the repository level away from the drift (Figure 6.5.3-1), and by more than 25 MPa at the drift wall (Figures 6.5.3-3 and 6.5.3-4). As a result, the vertical intrinsic permeability will decrease in a zone extending several hundred meters above and below the repository (Figure 6.5.4-1). Using a bounding estimated stress-versus-permeability relationship that emphasizes the effect of stress on permeability, the vertical permeability in the Tptpmn unit is predicted to decrease by at most a factor of 0.03 from the original permeability (Figure 6.5.4-3). In the Tptpll unit, vertical permeability is predicted to decrease by at most a factor of 0.5 from the original value (Figure 6.6.1-5).

- The maximum principal compressive stress will occur at the drift crown at around 100 to 500 years after the emplacement and is not expected to exceed 35 MPa (Figures 6.5.3-4 and 6.7.1-1a). An analysis of the observed rock scaling at the crown of the DST shows that a maximum principal compressive stress of about 60 MPa would be required to initiate limited rock scaling in the Tptpmn unit. Thus, the drift scale THM model shows that thermal stress is not likely to induce failure at an emplacement drift located in the Tptpmn unit. For an emplacement drift located in the Tptpll unit, a limited yielding at the sidewalls of the drift is expected during excavation, but only for a drift located in the low quality lithophysal rock.

- The analysis indicates that the impact of stress-induced changes in hydrological properties on the flow field is small, with the strongest impact occurring for a repository located in the Tptpmn model domain. While the liquid vertical flux distribution in the fracture continuum is slightly affected, the main impact appears to be on the dryout zone near the emplacement drift. When stress-induced changes in hydrological properties are considered, the extent of the dryout zone is slightly smaller, and resaturation of the rock

will reach the drift wall in a shorter time (Figure 6.5.5-4). In the longer term, at around 10,000 years, vertical permeability is still significantly decreased, especially just above the emplacement drift. The impact of this reduction in permeability is small, but tends to prevent vertical flux from reaching the drift wall at the drift crown (Figure 6.5.5-5).

- The impact of stress-induced changes in hydraulic properties on the flow field around a stable emplacement drift in the Tptpll unit is similar to those for a repository in the Tptpmn unit, but the magnitude of impact is much smaller. The reason is that both the initial stresses and initial fracture permeability are higher in the Tptpll unit than in the Tptpmn unit. Higher initial stresses imply that fractures are initially already compressed to a higher stiffness and closer to their residual aperture value, which prevents further closure during the thermal period. Higher initial fracture permeability results in a larger residual fracture aperture and, therefore the possible relative reduction in permeability is smaller.

- For a collapsed emplacement drift, changes in hydrological properties are larger than for a stable drift. The permeability in the host rock outside a rubble-filled collapsed drift is estimated to increase by 1 to 2 orders of magnitude in the drift crown and by 2 to 3 orders of magnitude near the sidewalls (Figure 6.8.4-1). The capillary pressure is estimated to decrease by less than a factor of 0.5 in the drift crown and by less than one order of magnitude on the side of the drift (Figure 6.8.4-1).

The THM-induced changes in hydrological properties (permeability and capillary strength) are outputs from this model report. In addition, it is concluded from the analysis conducted in this model report that the calculated changes in hydrological properties have a minor impact on the flow field. A minor impact on the flow field supports the exclusion of FEPs related to TM effects on fracture characteristics (permeability and capillarity) near the repository but does not provide conclusive evidence for the impact of THM processes on seepage. For estimating the impact of THM processes on seepage, the output from this model report (changes in permeability and capillary strength) is provided to the *Seepage Model for PA Including Drift Collapse* (BSC 2004 [DIRS 167652]), where such impact analysis is documented. The overall importance of THM effects on drift seepage is abstracted in *Abstraction of Drift Seepage* (BSC 2004 [DIRS 169131]).

8.2 MODEL VALIDATION AND UNCERTAINTIES

The drift scale THM model is validated against the DST and other field experiments and observations at Yucca Mountain, as described in Section 7 of this model report. Through the substantial information provided, the required level of confidence of the drift scale THM model is achieved. The analysis of the DST heating phase shows that the drift scale THM model captures relevant THM processes and that the underlying conceptual model is sound. In particular, analysis of the DST shows that the conceptual model for stress-versus-permeability

coupling is valid and capable of capturing the observed changes in permeability. Based on the simulations and observations at the DST and other field experiments at Yucca Mountain, the following conclusion is drawn regarding fundamental rock mass THM behavior:

- The dominant mode of stress-induced permeability change is elastic fracture opening or closing caused by changes in stress normal to the fractures. This conclusion is supported by the good agreement between measured and simulated air permeability changes in the DST (Section 7.4.3) and the ability of the model to capture mean permeability changes at niche experiments (Section 7.5). Furthermore, no sign of significant permeability enhancement by shear slip has been observed at the DST (Section 7.4.3).

The fracture normal stress-versus-permeability relationship is the most important aspect of this analysis. This relationship (discussed in Section 6.10.4) is the key for an accurate assessment of the possible stress-induced changes in hydraulic properties at the repository. The relationship provides limits for how much permeability can decrease or increase from stress change. Other aspects, or sources of uncertainties, such as conceptualization of the fracture network (Section 6.10.1) or possible inelastic mechanical responses near the drift wall (Section 6.10.2) and even possible shear slip (Section 6.10.3), are of minor importance compared to the limits of the stress-versus-permeability relationship. In this study, a bounding estimate of the normal stress-versus-permeability function was developed and validated against field experiments at a relevant drift-scale. The stress-permeability function adopted for predictive analysis with the drift scale THM model is a bounding one that emphasizes TM-induced changes in permeability, and hence, emphasizes the impact of THM coupling. In addition, the results of THM analyses with maximum effect of coupling are compared to TH analyses with no THM coupling.

Because of the limited number of field experiments in the Tptpll unit, there are larger uncertainties regarding predicted THM behavior in this unit. However, for a stable drift, stress-induced permeability changes are expected to be bounded within one to two orders of magnitude for both the Tptpmn and Tptpll units. For a collapsed drift, the permeability changes are bounded by a 1 to 2 order-of-magnitude increase in the drift crown and a 2 to 3 order-of-magnitude increase on the side of the drift. Because these bounds were obtained for bounding estimates of input THM properties (thermal expansion coefficient, stress-versus-permeability function, and strain-versus-permeability function that emphasizes the effect of TM induced changes in hydrologic properties), the possible impact of THM processes on percolation flux is adequately bounded in concurrence with YMRP acceptance criteria, as discussed in Section 4.2.

8.3 MODEL LIMITATIONS

The limitations of the drift scale THM model, as for all predictive models, are defined by the conceptual model and by the uncertainties and validity ranges of input data. The following model limitations are identified:

- The drift scale THM model is a continuum model with average properties and, therefore, is meant to represent overall changes in space and time. Hence, the analysis does not provide local changes occurring at the scale of an individual fracture, but rather their impact on the overall average changes.

- The coupled THM analysis was conducted in two-dimensional vertical sections rather than with a full three-dimensional representation. However, the two-dimensional approach has been tested by model validation against several three-dimensional field experiments (e.g. DST).

- Rather than a sensitivity study with variation of each input parameter over a wide range of values, a bounding analysis was conducted that brackets the potential impact of thermal-hydrological-mechanical processes on hydrologic properties (including permeability) and the flow field (Section 6.2.4 describes the bounding strategy).

- The drift scale THM analysis is conducted with homogenous properties that vary for different rock units. Therefore, the analysis provides mean changes in hydrological properties, but does not explicitly provide potential changes in the distribution (e.g. standard deviation) of hydrological properties.

- The heater experiment used for model validation, the DST, is located in the Tptpmn repository unit. Because no heater test has been performed in the Tptpll unit, the calculated effects of THM processes (and estimated changes in permeability) are more uncertain for the Tptpll unit (Section 8.2).

In summary, the coupled THM process model provides a bounding estimate of mean changes in hydrologic properties (permeability and capillary strength) that emphasizes the effect of THM on hydrologic properties, as a function of time and space at the drift scale.

8.4 SATISFACTION OF ACCEPTANCE CRITERIA

In Section 4.2, several U.S. Nuclear Regulatory Commission acceptance criteria were identified. This section discusses how they are satisfied in this model report. The satisfaction of Acceptance Criteria 1 and 2 for *Quantity and Chemistry of Water Contacting Engineered Barriers and Waste Forms* are described as follows:

Acceptance Criterion 1, **System Description and Model Integration Are Adequate:**

> **AC1(1)** Total system performance assessment adequately incorporates important design features, physical phenomena, and couplings, and uses consistent and appropriate assumptions throughout the quantity and chemistry of water contacting engineered barriers and waste forms abstraction process.

Response: The results supplement thermal seepage results from TH simulations reported in the model report entitled *Drift-Scale Coupled Processes (DST and TH Seepage) Models* (BSC 2004 [DIRS 170338]), which feeds the model report *Abstraction of Drift Seepage* (BSC 2004 [DIRS 169131]), where probability distributions of ambient and thermal seepage are developed for use in the TSPA. To ensure consistency between the present model report and the TH study (BSC 2004 [DIRS 170338], Section 6.2), the same conceptual model and TH properties are used (Section 1). The drift scale THM model used hydrological, thermal, and mechanical properties consistent with current UZ analyses and coupled processes analyses (Section 4.1). Because of the high density and connectivity of the fracture network, the conceptual model used is a dual-permeability continuum model with interacting fractured and matrix continua, consistent with the UZ flow model and other coupled analyses (Section 6.2.1).

> **AC1(2)** The abstraction of the quantity and chemistry of water contacting engineered barriers and waste forms uses assumptions, technical bases, data, and models, that are appropriate and consistent with other related U.S. Department of Energy abstractions. For example, the assumptions used for the quantity and chemistry of water contacting engineered barriers and waste forms are consistent with the abstractions of "Degradation of Engineered Barriers" (Section 2.2.1.3.1); "Mechanical Disruption of Engineered Barriers (Section 2.2.1.3.2); "Radionuclide Release Rates and Solubility Limits" (Section 2.2.1.3.4); "Climate and Infiltration" (Section 2.2.1.3.5); and "Flow Paths in the Unsaturated Zone" (Section 2.2.1.3.6). The descriptions and technical bases provide transparent and traceable support for the abstraction of quantity and chemistry of water contacting engineered barriers and waste forms.

Response: The assumptions (described in Section 5), computational model with underlying conceptual model (described in Section 6.2), input data (described in Sections 4, 6.3 and 6.4), are consistent with models associated with related to abstractions. In particular, assumptions, model and input data for thermal and hydrological processes are consistent with other models for unsaturated flow and transport, as well as with models drift seepage at Yucca Mountain (Sections 1, 4.1.1, 5, 6.2.1, and 6.2.2). Moreover, the assumptions, model and input data for mechanical processes are consistent with related geomechanical analyses at Yucca Mountain, including analyses of engineered barrier system design and ground control as well as analysis of drift degradation (Sections 4.1.1, 6.2.1, 6.4.2, and 6.4.3).

> **AC1(3)** Important design features, such as waste package design and material selection, backfill, drip shield, ground support, thermal loading strategy, and degradation processes, are adequate to determine the initial and boundary conditions for calculations of the quantity and chemistry of water contacting engineered barriers and waste forms.

Response: The design parameters of including drift geometry (drift diameter and spacing) and thermal load strategy are selected according to current design (Sections 4.1.1, and 6.3). The mechanical data for the near-field are consistent analyses of engineered barrier system design and ground control as well as analysis of drift degradation and drift degradation processes is adequately considered (Sections 4.1.1, 6.2.1, 6.4.2, 6.4.3, and 6.8).

> **AC1(4)** Spatial and temporal abstractions appropriately address physical couplings (thermal-hydrologic-mechanical-chemical).

Response: Adequate spatial and temporal variability of model parameters and boundary conditions is employed in process-level models to estimate the impact of THM processes on hydrologic properties around an emplacement drift and its effect on drift seepage. A bounding analysis is conducted that brackets the potential impact of THM processes on hydrologic properties (including permeability) and the potential impact on the flow field (bounding approach described in Section 6.2.4). The bounding case is realized by adopting parameter values that emphasize the effect of THM coupling (Sections 6.4.3, 6.4.4, and 6.4.5). This includes a bounding estimate of the thermal expansion coefficient (that emphasizes thermal stress) and a bounding estimate of a stress-versus-permeability function (that emphasizes the effect of thermal stress on permeability). In addition, the results of THM analyses with maximum coupling effect are compared to TH analyses with no THM coupling effect (Sections 6.6 through 6.8). This includes temporal variability in hydraulic properties caused by THM effects and temporal variability in infiltration flux. The impact of drift degradation on permeability is analyzed for several scenarios, including scenarios from an expected scenario of an intact drift and an extreme scenario of a completely collapsed drift (Section 6.8). Uncertainties related to spatial heterogeneities are discussed in Section 6.10.5.

> **AC1(8)** Adequate technical bases are provided, including activities such as independent modeling, laboratory or field data, or sensitivity studies, for inclusion of any thermal-hydrologic-mechanical-chemical couplings and features, events, and processes.

Response: A bounding analysis is conducted that brackets the potential impact of THM processes on hydrologic properties (including permeability) and the flow field (Sections 1, 6.2.4, 6.4, 6.5, and 6.6). The bounding case is realized by adopting parameter values that maximize the effect of coupling (Section 6.4.5). This includes a reasonable bounding estimate of the thermal expansion coefficient (that emphasizes thermal stress) and a bounding estimate of a stress-versus-permeability function (that emphasizes permeability change). Uncertainties related to spatial heterogeneity are discussed in Section 6.10.5. Uncertainties related to the most important input parameter, the stress-versus-permeability relationship, are discussed in Section 6.10.4. The estimated permeability changes using the bounding analysis that maximizes the effect of THM coupling are provided to the seepage models, which in turn feed seepage abstraction (Section 8.1).

> **AC1(12)** Guidance in NUREG–1297 and NUREG–1298 (Altman, et al., 1988 [DIRS 103597], [DIRS 103750]), or other acceptable approaches, is followed.

Response: The Quality Assurance Requirements Document commits to NUREGs 1297 and 1298 and procedures have been adopted to implement that commitment. Adherence to these procedures is determined by QA audits and other oversight activities.

Acceptance Criterion 2, **Data Are Sufficient for Model Justification:**

> **AC2(2)** Sufficient data were collected on the characteristics of the natural system and engineered materials to establish initial and boundary conditions for conceptual models of thermal-hydrologic-mechanical-chemical coupled processes, that affect seepage and flow and the engineered barrier chemical environment.

Response: The drift scale THM model is described and justified in Section 6.2, and establishment of initial and boundary conditions for the conceptual models in the various model domains are described in Sections 6.3 and 7.3.

> **AC2(3)** Thermo-hydrologic tests were designed and conducted with the explicit objectives of observing thermal-hydrologic processes for the temperature ranges expected for repository conditions and making measurements for mathematical models. Data are sufficient to verify that thermal-hydrologic conceptual models address important thermal-hydrologic phenomena.

Response: The Yucca Mountain DST, described in Section 7.2, was designed to observe coupled THMC processes for the temperature ranges expected for repository conditions. The drift scale THM model was validated against measurements at the DST (Section 7.3), and a good agreement between simulated and measured results shows that the thermal-hydrological conceptual model used in the drift scale THM model addresses important thermal-hydrologic phenomena (Section 7.10).

> **AC2(4)** Sufficient information to formulate the conceptual approach(es) for analyzing water contact with the drip shield, engineered barriers, and waste forms is provided.

Response: The coupled THM model and the conceptual approach for analyzing coupled THM processes are extensively described and justified in Section 6.2. The model validation in Section 7 shows that the underlying conceptual model is sound, and that a continuum representation of the fractured rock mass, using average properties, is adequate (Section 7.10).

Acceptance Criterion 3, **Data Uncertainty Is Characterized and Propagated Through the Model Abstraction:**

> **AC3(1)** Models use parameter values, assumed ranges, probability distributions, and bounding assumptions that are technically defensible, reasonably account for uncertainties and variabilities, and do not result in an under-representation of the risk estimate.

Response: A bounding analysis is conducted that brackets the potential impact of THM processes on hydrologic properties (including permeability) and the flow field (Sections 1, 6.2.4, 6.4, 6.5, and 6.6). The bounding case is realized by adopting parameter values that emphasize the effect of coupling (Section 6.4.5). This includes a reasonable bounding estimate of the thermal expansion coefficient (that emphasizes thermal stress) and a bounding estimate of a stress-versus-permeability function (that emphasizes effect of stress on permeability). Uncertainties related to spatial heterogeneity are discussed in Section 6.10.5. Uncertainties related to the most important input parameter, which is the stress-versus-permeability relationship, are discussed in Section 6.10.4. The estimated changes in hydrological properties using the bounding analysis that emphasizes the effect of THM coupling are provided to the seepage models (Section 8). Thus, the model parameter used does not result in an under-representation of the risk estimate.

> **AC3(4)** Adequate representation of uncertainties in the characteristics of the natural system and engineered materials is provided in parameter development for conceptual models, process-level models, and alternative conceptual models. The U.S. Department of Energy

may constrain these uncertainties using sensitivity analyses or conservative limits. For example, the U.S. Department of Energy demonstrates how parameters used to describe flow through the engineered barrier system bound the effects of backfill and excavation-induced changes.

Response: A bounding analysis is conducted that brackets the potential impact of THM processes on hydrologic properties (including permeability) and the flow field (Sections 1, 6.2.4, 6.4, 6.5, and 6.6). The bounding case is realized by adopting parameter values that emphasize the effect of coupling (Section 6.4.5). Uncertainties related to the most important input parameter, which is the stress-versus-permeability relationship, are discussed in Section 6.10.4.

Acceptance Criterion 4, Model Uncertainty Is Characterized and Propagated Through the Model Abstraction:

AC4(1) Alternative modeling approaches of features, events, and processes are considered and are consistent with available data and current scientific understanding, and the results and limitations are appropriately considered in the abstraction.

Response: The choice of model approach and discussion of alternative model approaches are provided in Sections 6.2.1 and 6.2.3. For example, in Section 6.2.1, the adopted continuum model approach versus the alternative distinct element approach is discussed. The model and the modeling results are compared to independent mathematical models in Sections 6.8.1, 7.6.4, 7.7, and 7.8.5. In Sections 6.8.1, 7.6.4, and 7.7, the drift scale THM model is compared to an alternative distinct element model for various simulation cases. In Section 7.8.5, comparison of the drift scale THM model to four independent mathematical models is discussed.

AC4(2) Alternative modeling approaches are considered and the selected modeling approach is consistent with available data and current scientific understanding. A description that includes a discussion of alternative modeling approaches not considered in the final analysis and the limitations and uncertainties of the chosen model is provided.

Response: The choice of model and discussion of alternative model approaches are provided in Sections 6.2.1 and 6.2.3. The model validation in Section 7 shows that the underlying conceptual model is sound, and that a continuum representation of the fractured rock mass using average properties is adequate and consistent with available data (Section 7.10). The uncertainties of the chosen model are discussed in Sections 6.10 and 8.2, and the model limitations are given in Section 8.3.

AC4(3) Consideration of conceptual model uncertainty is consistent with available site characterization data, laboratory experiments, field measurements, natural analog information and process-level modeling studies; and the treatment of conceptual model uncertainty does not result in an under-representation of the risk estimate.

Response: A bounding case analysis is performed by adopting parameter values that emphasize the effect of coupling (Section 6.4.5). This includes a reasonable bounding estimate of the thermal expansion coefficient (that emphasizes thermal stress) and a bounding estimate of a stress-versus-permeability function (that emphasizes effect of stress on permeability). Uncertainties related to simplification of naturally fractured system and spatial heterogeneity are

discussed in Sections 6.10.1 and 6.10.5, respectively. Uncertainties related to the most important input parameter, which is the stress-versus-permeability relationship, are discussed in Section 6.10.4. The estimated changes in hydrological properties using the bounding analysis that emphasizes the effect of THM coupling are provided to the seepage models (Section 8). Thus, conceptual model uncertainty does not result in an under-representation of the risk estimate.

> **AC4(5)** If the U.S. Department of Energy uses an equivalent continuum model for the total system performance assessment abstraction, the models produce conservative estimates of the effects of coupled thermal-hydrologic-mechanical-chemical processes on calculated compliance with the postclosure public health and environmental standards.

Response: A bounding analysis is conducted that brackets the potential impact of THM processes on hydrologic properties (including permeability) and the flow field (Sections 1, 6.2.4, 6.4, 6.5, and 6.6). The bounding case is realized by adopting parameter values that emphasize the effect of coupling (Section 6.4.5). This includes a reasonable bounding estimate of the thermal expansion coefficient (that emphasizes thermal stress) and a bounding estimate of a stress-versus-permeability function (that emphasizes effect of stress on permeability). The estimated changes in hydrological properties using the bounding analysis that emphasizes the effect of THM coupling are provided to the seepage models, which in turn feed seepage abstraction (Section 8).

Acceptance Criterion 5, **Model Abstraction Output is Supported by Objective Comparison:**

> **AC5(2)** Abstracted models for coupled thermal-hydrologic-mechanical-chemical effects on seepage and flow and the engineered barrier chemical environment, as well as on the chemical environment for radionuclide release, are based on the same assumptions and approximations demonstrated to be appropriate for process level models or closely analogous natural or experimental systems. For example, abstractions of processes, such as thermally induced changes in hydrological properties, or estimated diversion of percolation away from the drifts, are adequately justified by comparison to results of process-level modeling, that are consistent with direct observations and field studies.

Response: The drift scale THM model has been extensively tested against field observations, in particular against field measurements at the Yucca Mountain DST (Section 7.2). The model validation against field observations in Section 7 shows that the drift scale THM model is adequate for simulating and predicting thermally induces changes in hydrological properties (Section 7.10 and 8.2).

> **AC5(3)** Accepted and well-documented procedures are used to construct and test the numerical models that simulate coupled thermal-hydrologic-mechanical-chemical effects on seepage and flow, engineered barrier chemical environment, and the chemical environment for radionuclide release. Analytical and numerical models are appropriately supported. Abstracted model results are compared with different mathematical models, to judge robustness of results.

Response: The procedures for constructing the numerical model are given in Sections 6.3 and 6.4. The procedures for testing the numerical model are given in Section 7.1. A comprehensive model validation documented in Section 7 demonstrates that the drift scale THM model adequately captures relevant THM processes that may affect abstraction output (Section 7.10). The model and the modeling results are compared to independent mathematical models in Sections 6.8.1, 7.6.4, 7.7, and 7.8.5. In Section 6.8, the calculated changes in hydrologic properties for different numerical models and modeling approaches are compared.

8.5 OUTPUT DTNS

All the simulation cases presented in this model report have, without exception, been submitted to the TDMS. For all simulation cases, all computer files that needed to reproduce the model results using the qualified software have been submitted. The input and output files for each simulation case and the developed data are presented in separate DTNs as presented below:

Drift Scale THM Model Predictions for Tptpmn and Tptpll Model Domains	Simulations: LB0306DRSCLTHM.001
	Summary plots: LB0306DRSCLTHM.002
Drift Scale THM Model Predictions for Low Quality Rock in Tptpll Unit	Simulations: LB0308DRSCLTHM.001
	Summary plots: LB0308DRSCLTHM.002
Impact Analysis of Updated Thermal Properties	Simulations: LB0403DRSCLTHM.001
	Summary plots: LB0403DRSCLTHM.002
DST and Niche THM Model Validation	Simulations: LB0306DSTTHMVL.001
	Summary plots: LB0306DSTTHMVL.002
ECRB Sidewall Model Validation	Simulations: LB0308DSTTHMVL.001

Reproducibility by a qualified individual is possible by consulting this model report and the pertinent scientific notebook pages listed in Table 6-1.

INTENTIONALLY LEFT BLANK

9. INPUTS AND REFERENCES

The following is a list of references cited in this document. Column 2 represents the unique six-digit numerical identifier (the Document Input Reference System [DIRS] number), which is placed in the text following the reference callout (e.g., BSC 2004 [DIRS 167969]). The purpose of these numbers is to assist the reader in locating a specific reference. Within the reference list, multiple sources by the same author (e.g., BSC 2002) are sorted alphabetically by title.

9.1 DOCUMENTS CITED

Altman, W.D.; Donnelly, J.P.; and Kennedy, J.E. 1988. *Peer Review for High-Level Nuclear Waste Repositories: Generic Technical Position.* NUREG-1297. Washington, D.C.: U.S. Nuclear Regulatory Commission. TIC: 200651. 103597

Altman, W.D.; Donnelly, J.P.; and Kennedy, J.E. 1988. *Qualification of Existing Data for High-Level Nuclear Waste Repositories: Generic Technical Position.* NUREG-1298. Washington, D.C.: U.S. Nuclear Regulatory Commission. TIC: 200652. 103750

Alvarez, T.A., Jr.; Cording, E.J.; and Mikhail, R.A. 1995. "Hydromechanical Behavior of Rock Joints: A Re-Interpretation of Published Experiments." *Rock Mechanics, Proceedings of the 35th U.S. Symposium, University of Nevada, Reno, 5-7 June 1995.* Daemen, J.J.K. and Schultz, R.A., eds. Pages 665-671. Brookfield, Vermont: A.A. Balkema. TIC: 225160. 170495

Birkholzer, J.T. and Tsang, Y.W. 1997. *Pretest Analysis of the Thermal-Hydrological Conditions of the ESF Drift Scale Test.* Milestone SP9322M4. Berkeley, California: Lawrence Berkeley National Laboratory. ACC: MOL.19971201.0810. 100597

Bjornsson, G. and Bodvarsson, G. 1990. "A Survey of Geothermal Reservoir Properties." *Geothermics, 19,* (1), 17-27. New York, New York: Pergamon Press. TIC: 249741. 154606

Boitnott, G.N. 1991. *Mechanical and Transport Properties of Joints.* Ph.D. dissertation. New York, New York: Columbia University. TIC: 256276. 170529

Brodsky, N.S.; Riggins, M.; Connolly, J.; and Ricci, P. 1997. *Thermal Expansion, Thermal Conductivity, and Heat Capacity Measurements for Boreholes UE25 NRG-4, UE25 NRG-5, USW NRG-6, and USW NRG-7/7A.* SAND95-1955. Albuquerque, New Mexico: Sandia National Laboratories. ACC: MOL.19980311.0316. 100653

BSC (Bechtel SAIC Company) 2001. *Coupled Thermal-Hydrologic-Mechanical Effects on Permeability Analysis and Models Report.* ANL-NBS-HS-000037 REV 00. Las Vegas, Nevada: Bechtel SAIC Company. ACC: MOL.20010822.0092. 155957

BSC 2001. *Ground Control for Emplacement Drifts for SR.* ANL-EBS-GE-000002 REV 00 ICN 01. Las Vegas, Nevada: Bechtel SAIC Company. ACC: MOL.20010627.0028. 155187

BSC 2001. *Multiscale Thermohydrologic Model.* ANL-EBS-MD-000049 REV 00 ICN 02. Las Vegas, Nevada: Bechtel SAIC Company. ACC: MOL.20020123.0279. 158204

BSC 2001. *Thermal Tests Thermal-Hydrological Analyses/Model Report.* ANL-NBS-TH-000001 REV 00 ICN 02. Las Vegas, Nevada: Bechtel SAIC Company. ACC: MOL.20011116.0025. 157330

BSC 2001. *UZ Flow Models and Submodels.* MDL-NBS-HS-000006 REV 00 ICN 01. Las Vegas, Nevada: Bechtel SAIC Company. ACC: MOL.20020417.0382. 158726

BSC 2002. *Repository Design, Repository/PA IED Subsurface Facilities Plan Sht. 1 of 5, Sht. 2 of 5, Sht. 3 of 5, Sht. 4 of 5, and Sht. 5 of 5.* DWG-MGR-MD-000003 REV A. Las Vegas, Nevada: Bechtel SAIC Company. ACC: MOL.20020601.0194. 159527

BSC 2002. *Ventilation Model.* ANL-EBS-MD-000030 REV 01 ICN 01. Las Vegas, Nevada: Bechtel SAIC Company. ACC: MOL.20021106.0055. 160975

BSC 2003. *Subsurface Geotechnical Parameters Report.* 800-K0C-WIS0-00400-000-00A. Las Vegas, Nevada: Bechtel SAIC Company. ACC: ENG.20040108.0001. 166660

BSC 2004. *Abstraction of Drift Seepage.* MDL-NBS-HS-000019, Rev. 01. Las Vegas, Nevada: Bechtel SAIC Company. 169131

BSC 2004. *Analysis of Hydrologic Properties Data.* ANL-NBS-HS-000042, Rev. 00. Las Vegas, Nevada: Bechtel SAIC Company. 170038

BSC 2004. *Calibrated Properties Model.* MDL-NBS-HS-000003, Rev. 02. Las Vegas, Nevada: Bechtel SAIC Company. 169857

BSC 2004. *Conceptual Model and Numerical Approaches for Unsaturated Zone Flow and Transport.* MDL-NBS-HS-000005 REV 01. Las Vegas, Nevada: Bechtel SAIC Company. ACC: DOC.20040922.0006. 170035

BSC 2004. *D&E / PA/C IED Emplacement Drift Configuration and Environment.* 800-IED-MGR0-00201-000-00B. Las Vegas, Nevada: Bechtel SAIC Company. ACC: ENG.20040326.0001. 168489

BSC 2004. *D&E / PA/C IED Typical Waste Package Components Assembly.* 800-IED-WIS0-00204-000-00B. Las Vegas, Nevada: Bechtel SAIC Company. ACC: ENG.20040202.0012. 167369

BSC 2004. *Development of Numerical Grids for UZ Flow and Transport Modeling.* ANL-NBS-HS-000015 REV 02. Las Vegas, Nevada: Bechtel SAIC Company. ACC: DOC.20040901.0001. 169855

BSC 2004. *Drift Degradation Analysis.* ANL-EBS-MD-000027 REV 03. Las Vegas, Nevada: Bechtel SAIC Company. ACC: DOC.20040915.0010. 166107

BSC 2004. *Drift-Scale Coupled Processes (DST and TH Seepage) Models.* MDL-NBS-HS-000015 REV 01. Las Vegas, Nevada: Bechtel SAIC Company. ACC: DOC.20040930.0003. 170338

BSC 2004. *Drift-Scale THC Seepage Model.* MDL-NBS-HS-000001, Rev. 03. Las Vegas, Nevada: Bechtel SAIC Company. 169856

BSC 2004. *Features, Events, and Processes: Disruptive Events.* ANL-WIS-MD-000005, Rev. 02. Las Vegas, Nevada: Bechtel SAIC Company. 170017

BSC 2004. *Features, Events, and Processes in UZ Flow and Transport.* ANL-NBS-MD-000001, Rev. 03. Las Vegas, Nevada: Bechtel SAIC Company. 170012

BSC 2004. *Geologic Framework Model (GFM2000).* MDL-NBS-GS-000002 REV 02. Las Vegas, Nevada: Bechtel SAIC Company. ACC: DOC.20040827.0008. 170029

BSC 2004. *In Situ Field Testing of Processes.* ANL-NBS-HS-000005, Rev. 03. Las Vegas, Nevada: Bechtel SAIC Company. 170004

BSC 2004. *Mountain-Scale Coupled Processes (TH/THC/THM).* MDL-NBS-HS-000007 REV 02. Las Vegas, Nevada: Bechtel SAIC Company. 169866

BSC 2004. *Q-List.* 000-30R-MGR0-00500-000-000 REV 00. Las Vegas, Nevada: Bechtel SAIC Company. ACC: ENG.20040721.0007. 168361

BSC 2004. *Seepage Model for PA Including Drift Collapse.* MDL-NBS-HS-000002 REV 03. Las Vegas, Nevada: Bechtel SAIC Company. ACC: DOC.20040922.0008. 167652

BSC 2004. *Simulation of Net Infiltration for Present-Day and Potential Future Climates.* MDL-NBS-HS-000023, Rev. 00. Las Vegas, Nevada: Bechtel SAIC Company. 170007

BSC 2004. *Technical Work Plan for: Near-Field Environment and Transport: Near-Field Coupled Processes (TH Seepage and THM) Model Report Integration.* TWP-MGR-PA-000015 REV 00. Las Vegas, Nevada: Bechtel SAIC Company. ACC: DOC.20040610.0001. 170236

BSC 2004. *Technical Work Plan for: Performance Assessment Unsaturated Zone.* TWP-NBS-HS-000003 REV 02 Errata 001. Las Vegas, Nevada: Bechtel SAIC Company. ACC: MOL.20030102.0108; DOC.20040121.0001. 167969

BSC 2004. *Thermal Testing Measurements Report.* TDR-MGR-HS-000002 REV 00. Las Vegas, Nevada: Bechtel SAIC Company. ACC: DOC.20040928.0005. 169900

BSC 2004. *UZ Flow Models and Submodels.* MDL-NBS-HS-000006, Rev. 02. Las Vegas, Nevada: Bechtel SAIC Company. 169861

BSC 2004. *Ventilation Model and Analysis Report.* ANL-EBS-MD-000030, Rev. 04. Las Vegas, Nevada: Bechtel SAIC Company. 169862

Canori, G.F. and Leitner, M.M. 2003. *Project Requirements Document.* TER-MGR-MD-000001 REV 02. Las Vegas, Nevada: Bechtel SAIC Company. ACC: DOC.20031222.0006. 166275

Chan, T.; Binnall, E.; Nelson, P.; Stolzman, R.; Wan, O.; Weaver, C.; Ang, K.; Braley, J.; and McEvoy, M. 1980. *Thermal and Thermomechanical Data from In Situ Heater Experiments at Stripa, Sweden.* LBL-11477. Berkeley, California: Lawrence Berkeley Laboratory. TIC: 211543. 154672

CRWMS (Civilian Radioactive Waste Management System) M&O (Management and Operating Contractor) 1997. *Ambient Characterization of the Drift Scale Test Block.* BADD00000-01717-5705-00001 REV 01. Las Vegas, Nevada: CRWMS M&O. ACC: MOL.19980416.0689. 101539

CRWMS M&O 1997. *Drift Scale Test Design and Forecast Results.* BAB000000-01717-4600-00007 REV 01. Las Vegas, Nevada: CRWMS M&O. ACC: MOL.19980710.0155. 146917

CRWMS M&O 1997. *Yucca Mountain Site Geotechnical Report.* B00000000-01717-5705-00043 REV 01. Two volumes. Las Vegas, Nevada: CRWMS M&O. ACC: MOL.19971017.0736; MOL.19971017.0737. 103564

CRWMS M&O 1998. *Drift Scale Test As-Built Report.* BAB000000-01717-5700-00003 REV 01. Las Vegas, Nevada: CRWMS M&O. ACC: MOL.19990107.0223. 111115

CRWMS M&O 1998. *Drift Scale Test Progress Report No. 1.* BAB000000-01717-5700-00004 REV 01. Las Vegas, Nevada: CRWMS M&O. ACC: MOL.19990209.0240. 108306

CRWMS M&O 1998. *Geology of the Exploratory Studies Facility Topopah Spring Loop.* BAB000000-01717-0200-00002 REV 01. Las Vegas, Nevada: CRWMS M&O. ACC: MOL.19980415.0283. . 102679

CRWMS M&O 1999. *Single Heater Test Final Report.* BAB000000-01717-5700-00005 REV 00 ICN 1. Las Vegas, Nevada: CRWMS M&O. ACC: MOL.20000103.0634. 129261

CRWMS M&O 2000. *Calculation of Permeability Change Due to Coupled Thermal-Hydrological-Mechanical Effects.* CAL-NBS-MD-000002 REV 00. Las Vegas, Nevada: CRWMS M&O. ACC: MOL.20000711.0192. 149040

CRWMS M&O 2000. *Geologic Framework Model (GFM3.1).* MDL-NBS-GS-000002 REV 00 ICN 01. Las Vegas, Nevada: CRWMS M&O. ACC: MOL.20000121.0115. 138860

CRWMS M&O 2000. *Statistical Analysis of Empirical Rock Properties by Lithostratigraphic Units.* CAL-GCS-GE-000001 REV 00. Las Vegas, Nevada: CRWMS M&O. ACC: MOL.20000317.0486. 168569

da Cunha, A.P. 1993. "Research on Scale Effects in the Determination of Rock Mass Mechanical Properties – The Portuguese Experience." *Scale Effects in Rock Masses 93, Proceedings of the Second International Workshop on Scale Effects in Rock Masses, Lisbon, Portugal, 25 June 1993.* da Cunha, A.P., ed. Pages 285-291. Brookfield, Vermont: A.A. Balkema. TIC: 255893. 168515

da Cunha, A.P. 1993. "Scale Effects in Rock Engineering – An Overview of the Loen Workshop and Other Recent Papers Concerning Scale Effects." *Scale Effects in Rock Masses 93, Proceedings of the Second International Workshop on Scale Effects in Rock Masses, Lisbon, Portugal, 25 June 1993.* da Cunha, A.P., ed. Pages 3-14. Brookfield, Vermont: A.A. Balkema. TIC: 255893. 168514

Datta, R.; Barr, D.; and Boyle, W. 2003. "Measuring Thermal, Hydrological, Mechanical, and Chemical Responses in the Yucca Mountain Drift Scale Test." *GeoProc 2003, International Conference on Coupled T-H-M-C Processes in Geo-Systems: Fundamentals, Modelling, Experiments & Applications, Stockhom, Sweden, 13-15 October 2003.* Stehpansson, O.; Hudson, J.A.; and Jing, L., eds. Pages 141-146. Stockholm, Sweden: Royal Institute of Technology. TIC: 256086. 170398

de Marsily, G. 1986. *Quantitative Hydrogeology: Groundwater Hydrology for Engineers.* San Diego, California: Academic Press. TIC: 208450. 100439

Doughty, C. 1999. "Investigation of Conceptual and Numerical Approaches for Evaluating Moisture, Gas, Chemical, and Heat Transport in Fractured Unsaturated Rock." *Journal of Contaminant Hydrology, 38,* (1-3), 69-106. New York, New York: Elsevier. TIC: 244160. 135997

Green, R.T. and Painter, S. 2003. "Numerical Simulation of Thermal-Hydrological Processes Observed at the Drift-Scale Heater Test at Yucca Mountain, Nevada." *GeoProc 2003, International Conference on Coupled T-H-M-C Processes in Geo-Systems: Fundamentals, Modelling, Experiments & Applications, Stockhom, Sweden, 13-15 October 2003.* Stehpansson, O.; Hudson, J.A.; and Jing, L., eds. Pages 161-166. Stockholm, Sweden: Royal Institute of Technology. TIC: 256088. 170403

Hardin, E.L. and Chesnut, D.A. 1997. *Synthesis Report on Thermally Driven Coupled Processes.* Milestone SPL8BM4. Livermore, California: Lawrence Livermore National Laboratory. ACC: MOL.19980113.0395. 100534

He, J. 1993. "A Case Review of the Deformation Modulus of Rock Mass: Scale Effect." *Scale Effects in Rock Masses 93, Proceedings of the Second International Workshop on Scale Effects in Rock Masses, Lisbon, Portugal, 25 June 1993.* da Cunha, A.P., ed. Pages 87-91. Brookfield, Vermont: A.A. Balkema. TIC: 255893. 168516

Hillel, D. 1998. *Environmental Soil Physics.* San Diego, California: Academic Press. TIC: 254422. 165404

Hoek, E. and Brown, E.T. 1997. "Practical Estimates of Rock Mass Strength." *International Journal of Rock Mechanics and Mining Science & Geomechanics Abstracts, 34,* (8), 1165-1186. Oxford, England: Pergamon. TIC: 256245. 170501

Hoek, E.; Carranza-Torres, C.; and Corkum, B. 2002. "Hoek-Brown Failure Criterion – 2002 Edition." 5th North American Rock Mechanics Symposium and 17th Tunnelling Association of Canada Conference: NARMS-TAC 2002, July 7-10, University of Toronto. Toronto, Ontario, Canada: Rocscience. Accessed March 17, 2003. TIC: 253954. http://www.rocscience.com/Anon/ResearchPapers/NARMS.pdf 162204

Hsiung, S.M.; Chowdhury, A.H.; and Nataraja, M.S. 2003. "Thermal-Mechanical Modeling of a Large-Scale Heater Test." *GeoProc 2003, International Conference on Coupled T-H-M-C Processes in Geo-Systems: Fundamentals, Modelling, Experiments & Applications, Stockhom, Sweden, 13-15 October 2003.* Stehpansson, O.; Hudson, J.A.; and Jing, L., eds. Pages 153-159. Stockholm, Sweden: Royal Institute of Technology. TIC: 256090. 170402

Itasca Consulting Group 1998. *3DEC, 3 Dimensional Distinct Element Code, User's Guide (Version 2.00).* Minneapolis, Minnesota: Itasca Consulting Group. TIC: 247503. 148865

Itasca Consulting Group. 1997. *FLAC^{3D}, Fast Lagrangian Analysis of Continua in 3 Dimensions.* Version 2.0 Five volumes. Minneapolis, Minnesota: Itasca Consulting Group. TIC: 251273. 156788

Jackson, C.P.; Hoch, A.R.; and Todman, S. 2000. "Self-Consistency of a Heterogeneous Continuum Porous Medium Representation of a Fractured Medium." *Water Resources Research, 36,* (1), 189-202. Washington, D.C.: American Geophysical Union. TIC: 247466. 141523

Jury, W.A.; Gardner, W.R.; and Gardner, W.H. 1991. *Soil Physics.* 5th Edition. New York, New York: John Wiley & Sons. TIC: 241000. 102010

LBNL (Lawrence Berkeley National Laboratory) 1998. *YMP-LBNL-QIP-S1.0 (Attachment 2), Form A, Attachment A.* SCMS Identifier: EXT v1.0, DI: EXT v1.0 DFA R00. Berkeley, California: Lawrence Berkeley National Laboratory. ACC: MOL.19990526.0364. 170774

LBNL 2000. *Software Baseline Request, 2KGRIDV1.F V1.0.* Software Tracking Number: 10244-1.0-00. Berkeley, California: Lawrence Berkeley National Laboratory. ACC: MOL.20010730.0061. 170773

LBNL 2002. *Requirements Document (RD) for FLAC3D Version 2.0.* Document Identifier: 10502-RD-2.0-00. Berkeley, California: Lawrence Berkeley National Laboratory. ACC: MOL.20031031.0302. 170766

LBNL 2002. *Software Management Report (SMR) for Delb.dat v1.0.* Document Identifier: 10507-SMR-1.0-00. Berkeley, California: Lawrence Berkeley National Laboratory. ACC: MOL.20020923.0117. 170772

LBNL 2002. *Software Management Report (SMR) for Gpzones.dat v1.0.* Document Identifier: 10509-SMR-1.0-00. Berkeley, California: Lawrence Berkeley National Laboratory. ACC: MOL.20020923.0120. 170770

LBNL 2002. *Software Management Report (SMR) for tin v1.1.* Document Identifier: 10899-SMR-1.1-00. Berkeley, California: Lawrence Berkeley National Laboratory. ACC: MOL.20030409.0082. 170771

LBNL 2002. *Software Validation Test Report (VTR) for FLAC3D Version 2.0.* Document Identifier: 10502-VTR-2.0-00. Berkeley, California: Lawrence Berkeley National Laboratory. ACC: MOL.20020416.0062. 170767

LBNL 2002. *Users Manual (UM) for FLAC3D Version 2.0.* Document Identifier: 10502-UM-2.0-00. Berkeley, California: Lawrence Berkeley National Laboratory. ACC: MOL.20020416.0061. 170769

LBNL 2002. *Users Manual (UM) for TOUGH Version 1.6.* Document Identifier: 10007-UM-1.6-00. Berkeley, California: Lawrence Berkeley National Laboratory. ACC: MOL.20020925.0042. 170765

LBNL 2003. *Validation Test Report (VTR) for TOUGH V1.6.* Document Identifier: 10007-VTR-1.6-02. Berkeley, California: Lawrence Berkeley National Laboratory. ACC: MOL.20030312.0199. 170764

Leverett, M.C. 1941. "Capillary Behavior in Porous Solids." *AIME Transactions, Petroleum Development and Technology, Tulsa Meeting, October 1940. 142*, 152-169. New York, New York: American Institute of Mining and Metallurgical Engineers. TIC: 240680. 100588

Lin, M.; Hardy, M.P.; and Bauer, S.J. 1993. *Rock Mass Mechanical Property Estimations for the Yucca Mountain Site Characterization Project.* SAND92-0450. Albuquerque, New Mexico: Sandia National Laboratories. ACC: NNA.19921204.0013. 104585

Liu, H.H.; Doughty, C.; and Bodvarsson, G.S. 1998. "An Active Fracture Model for Unsaturated Flow and Transport in Fractured Rocks." *Water Resources Research, 34,* (10), 2633-2646. Washington, D.C.: American Geophysical Union. TIC: 243012. 105729

Manteufel, R.D.; Ahola, M.P.; Turner, D.R.; and Chowdhury, A.H. 1993. *A Literature Review of Coupled Thermal-Hydrologic-Mechanical-Chemical Processes Pertinent to the Proposed High-Level Nuclear Waste Repository at Yucca Mountain.* NUREG/CR-6021. Washington, D.C.: U.S. Nuclear Regulatory Commission. TIC: 207771. 100776

Millard, A. and Rutqvist, J. 2003. "Comparative Analyses of Predicted and Measured Displacements During the Heating Phase of the Yucca Mountain Drift Scale Test." *GeoProc 2003, International Conference on Coupled T-H-M-C Processes in Geo-Systems: Fundamentals, Modelling, Experiments & Applications, Stockhom, Sweden, 13-15 October 2003.* Stehpansson, O.; Hudson, J.A.; and Jing, L., eds. Pages 173-178. Stockholm, Sweden: Royal Institute of Technology. TIC: 256089. 170406

Nelson, P.H.; Rachiele, R.; Remer, J.S.; and Carlsson, H. 1981. *Water Inflow into Boreholes During the Stripa Heater Experiments.* LBL-12574. Berkeley, California: Lawrence Berkeley Laboratory. TIC: 228851. 150092

NRC (U.S. Nuclear Regulatory Commission) 2003. *Yucca Mountain Review Plan, Final Report.* NUREG-1804, Rev. 2. Washington, D.C.: U.S. Nuclear Regulatory Commission, Office of Nuclear Material Safety and Safeguards. TIC: 254568. 163274

Olivella, S.; Gens, A.; and Gonzalez, C. 2003. "THM Analysis of a Heating Test in a Fractured Tuff." *GeoProc 2003, International Conference on Coupled T-H-M-C Processes in Geo-Systems: Fundamentals, Modelling, Experiments & Applications, Stockhom, Sweden, 13-15 October 2003.* Stehpansson, O.; Hudson, J.A.; and Jing, L., eds. Pages 167-172. Stockholm, Sweden: Royal Institute of Technology. TIC: 256091. 170405

Paulsson, B.N.P.; King, M.S.; and Rachiele, R. 1980. *Ultrasonic and Acoustic Emission Results from the Stripa Heater Experiments.* Parts I & II. LBL-10975. Berkeley, California: Lawrence Berkeley National Laboratory. TIC: 211547. 154570

Peters, R.R.; Klavetter, E.A.; Hall, I.J.; Blair, S.C.; Heller, P.R.; and Gee, G.W. 1984. *Fracture and Matrix Hydrologic Characteristics of Tuffaceous Materials from Yucca Mountain, Nye County, Nevada.* SAND84-1471. Albuquerque, New Mexico: Sandia National Laboratories. ACC: NNA.19900810.0674. 121957

Pruess, K.; Oldenburg, C.; and Moridis, G. 1999. *TOUGH2 User's Guide, Version 2.0.* LBNL-43134. Berkeley, California: Lawrence Berkeley National Laboratory. TIC: 253038. 160778

Pruess, K.; Wang, J.S.Y.; and Tsang, Y.W. 1990. "On Thermohydrologic Conditions Near High-Level Nuclear Wastes Emplaced in Partially Saturated Fractured Tuff, 2. Effective Continuum Approximation." *Water Resources Research, 26,* (6), 1249-1261. Washington, D.C.: American Geophysical Union. TIC: 224854. 100819

Rejeb, A. 1996. "Mathematical Simulations of Coupled THM Processes of Fanay-Augères Field Test by Distinct Element and Discrete Finite Element Methods." *Developments in Geotechnical Engineering, 79,* 341-368. New York, New York: Elsevier. TIC: 254247. 162589

Rutqvist, J. 2002. YMP-LBNL-JR-1 UZ AMRs for SR - Thermal-Hydrological-Mechanical Effects. Scientific Notebook SN-LBNL-SCI-204-V1. ACC: MOL.20020701.0135; MOL.20020724.0607. 162047

Rutqvist, J. 2004. YMP-LBNL-JR-2 UZ AMRs for SR - Thermal-Hydrological-Mechanical Effects. Scientific Notebook SN-LBNL-SCI-204-V2. ACC: MOL.20040513.0119. 170509

Rutqvist, J. and Stephansson, O. 2003. "The Role of Hydromechanical Coupling in Fractured Rock Engineering." *Hydrogeology Journal, 11,* (1), 7-40. New York, New York: Springer-Verlag. TIC: 254245. 162583

Rutqvist, J. and Tsang, C-F. 2002. "A Study of Caprock Hydromechanical Changes Associated with CO{subscript 2}-Injection into a Brine Formation." *Environmental Geology, 42,* (2-3), 296-305. New York, New York: Springer-Verlag. TIC: 254244. 162587

Rutqvist, J. and Tsang, C-F. 2003. "Analysis of Thermal-Hydrologic-Mechanical Behavior Near an Emplacement Drift at Yucca Mountain." *Journal of Contaminant Hydrology, 62-63,* 637-652. New York, New York: Elsevier. TIC: 254205. 162584

Rutqvist, J.; Börgesson, L.; Chijimatsu, M.; Nguyen, T.S.; Jing, L.; Noorishad, J.; and Tsang, C.-F. 2001. "Coupled Thermo-Hydro-Mechanical Analysis of a Heater Test in Fractured Rock and Bentonite at Kamaishi Mine — Comparison of Field Results to Predictions of Four Finite Element Codes." *International Journal of Rock Mechanics & Mining Sciences, 38,* (1), 129-142. New York, New York: Pergamon. TIC: 254246. 162586

Rutqvist, J.; Tsang, C.-F.; and Tsang, Y. 2003. "Analysis of Stress- and Moisture-Induced Changes in Fractured Rock Permeability at the Yucca Mountain Drift Scale Test." *GeoProc 2003, International Conference on Coupled T-H-M-C Processes in Geo-Systems: Fundamentals, Modelling, Experiments & Applications, Stockhom, Sweden, 13-15 October 2003.* Stehpansson, O.; Hudson, J.A.; and Jing, L., eds. Pages 147-152. Stockholm, Sweden: Royal Institute of Technology. TIC: 256087. 170400

Rutqvist, J.; Wu, Y.-S.; Tsang, C.-F.; and Bodvarsson, G. 2002. "A Modeling Approach for Analysis of Coupled Multiphase Fluid Flow, Heat Transfer, and Deformation in Fractured Porous Rock." *International Journal of Rock Mechanics and Mining Sciences, 39,* (4), 429-442. New York, New York: Pergamon. TIC: 253953. 162048

Serafim, J.L. and Pereira, J.P. 1983. "Considerations on the Geomechanical Classification of Bieniawski." *Proceedings of the International Symposium on Engineering Geology and Underground Construction, Lisbon, Portugal, 1983. 1,* II.33-II.44. Lisbon, Portugal: Sociedade Portuguesa de Geotecnia, Laboratório Nacional de Engenharia Civil. TIC: 226267. 101711

Sobolik, S.R.; Finley, R.E.; and Ballard, S. 1998. "Post-Test Comparison of Thermal-Mechanical Measurements vs. Analyses for the In-Situ Single Heater Test, Yucca Mountain, Nevada." *International Journal of Rock Mechanics and Mining Sciences, 35,* (4-5), 649. New York, New York: Pergamon. TIC: 253944. 162049

Sobolik, S.R.; Finley, R.E.; and Ballard, S. 1999. "Thermal-Mechanical Measurements in the Drift Scale Test, Yucca Mountain, Nevada." *Rock Mechanics for Industry, Proceedings of the 37th U.S. Rock Mechanics Symposium, Vail, Colorado, USA, 6-9 June, 1999.* Amadei, B.; Kranz, R.L.; Scott, G.A.; and Smeallie, P.H.; eds. *2,* 735-742. Brookfield, Vermont: A.A. Balkema. TIC: 245246. 163202

Tsang, Y.W. and Birkholzer, J.T. 1999. "Predictions and Observations of the Thermal-Hydrological Conditions in the Single Heater Test." *Journal of Contaminant Hydrology, 38,* (1-3), 385-425. New York, New York: Elsevier. TIC: 244160. 137577

Van Golf-Racht, T.D. 1988. *Fundamentals of Fractured Reservoir Engineering.* Developments in Petroleum Science, 12. New York, New York: Elsevier. TIC: 239220. 170723

Wagner, R.A.; Ballard, S.; Blair, S.C.; and Mukhopadhyay, S. 2001. "A Methodology for Validation of Process Models Used to Simulate Thermal Tests at Yucca Mountain." *Rock Mechanics in the National Interest, Proceedings of the 38th U.S. Rock Mechanics Symposium, DC Rocks 2001, Washington, D.C., USA, 7-10 July 2001.* Elsworth, D.; Tinucci, J.P.; and Heasley, K.A.; eds. Volume 1. Pages 631-636. Exton, Pennsylvania: A.A. Balkema. TIC: 250864. 163532

Wang, J.S. 2004. "Scientific Notebooks Referenced in Model Report U0250 Drift-Scale THM Model MDL-NBS-HS-000017 REV 01." Memorandum from J.S. Wang (BSC) to File, April 5, 2004, with attachments. ACC: MOL.20030505.0160; MOL.20030805.0188; MOL.20030929.0055; MOL.20040416.0319; MOL.20040714.0062; MOL.20040719.0213. 170508

Williams, N.H. 2001. "Contract #: DE-AC08-01NV12101 - Drift Scale Test (DST) White Paper: Scaling Along the Roof of the Heated Drift." Letter from N.H. Williams (BSC) to S.P. Mellington (DOE/YMSCO), May 15, 2001, PROJ.05/01.033, with enclosure. ACC: MOL.20010622.0252. 159516

Witherspoon, P.A.; Wang, J.S.Y; Iwai, K.; and Gale, J.E. 1980. "Validity of Cubic Law for Fluid Flow in a Deformable Rock Fracture." *Water Resources Research, 16,* (6), 1016-1024. Washington, D.C.: American Geophysical Union. TIC: 220088. 123506

Zhao, J. and Brown, E.T. 1992. "Hydro-Thermo-Mechanical Properties of Joints in the Carnmenellis Granite." *Quarterly Journal of Engineering Geology, 25,* 279-290. London, England: Geological Society. TIC: 256243. 170499

Zimmerman, R.M.; Blanford, M.L.; Holland, J.F.; Schuch, R.L.; and Barrett, W.H. 1986. *Final Report, G-Tunnel Small-Diameter Heater Experiments.* SAND84-2621. Albuquerque, New Mexico: Sandia National Laboratories. ACC: HQS.19880517.2365. 145625

9.2 CODES, STANDARDS, REGULATIONS, AND PROCEDURES

10 CFR 63. Energy: Disposal of High-Level Radioactive Wastes in a Geologic Repository at Yucca Mountain, Nevada. Readily available. 156605

AP-2.22Q, Rev. 1, ICN 1. *Classification Analyses and Maintenance of the Q-List.* Washington, D.C.: U.S. Department of Energy, Office of Civilian Radioactive Waste Management. ACC: DOC.20040714.0002.

AP-SV.1Q, Rev. 1, ICN 1. *Control of the Electronic Management of Information.* Washington, D.C.: U.S. Department of Energy, Office of Civilian Radioactive Waste Management. ACC: DOC.20040308.0001.

LP-SI.11Q-BSC, Rev. 0, ICN 0. *Software Management.* Washington, D.C.: U.S. Department of Energy, Office of Civilian Radioactive Waste Management. ACC: DOC.20040225.0007.

YMP-LBNL-QIP-SV.0, Rev. 2, Mod. 1. *Management of YMP-LBNL Electronic Data.* Berkeley, California: Lawrence Berkeley National Laboratory. ACC: MOL.20020717.0319.

9.3 SOURCE DATA, LISTED BY DATA TRACKING NUMBER

GS000308311221.005. Net Infiltration Modeling Results for 3 Climate Scenarios for FY99. Submittal date: 03/01/2000. 147613

GS000608314224.006. Provisional Results: Geotechnical Data for Station 26+00 to 30+00, North Ramp and Main Drift of the ESF, Full-Periphery Geotechnical Maps (Drawings OA-46-222 through OA-46-226) and Rock Mass Quality Ratings Report. Submittal date: 06/28/2000. 152572

GS950508314224.003. Provisional Results: Geotechnical Data - Full Periphery Map Data from North Ramp of the Exploratory Studies Facility, Stations 0+60 to 4+00. Submittal date: 05/24/1995. 107488

GS960908314224.015. Provisional Results: Geotechnical Data for Stations 30+00 to 40+00, Main Drift of the ESF, Full-Periphery Geotechnical Maps and Rock Mass Quality Ratings Report. Submittal date: 09/09/1996. 108372

GS960908314224.016. Provisional Results: Geotechnical Data for Station 40+00 to 50+00, Main Drift of the ESF, Full-Periphery Geotechnical Maps and Rock Mass Quality Ratings Report. Submittal date: 09/09/1996. 108373

GS960908314224.017. Provisional Results: Geotechnical Data for Stations 50+00 to 55+00, Main Drift of the ESF, Full-Periphery Geotechnical Maps and Rock Mass Quality Ratings Report. Submittal date: 09/09/1996. 108376

GS960908314224.020. Analysis Report: Geology of the North Ramp - Stations 4+00 to 28+00 and Data: Detailed Line Survey and Full-Periphery Geotechnical Map - Alcoves 3 (UPCA) and 4 (LPCA), and Comparative Geologic Cross Section - Stations 0+60 to 28+00. Submittal date: 09/09/1996. 106059

GS970108314224.002. Geotechnical Data for Station 55+00 to Station 60+00, Main Drift of the ESF, Full Periphery Geotechnical Maps. Submittal date: 01/31/1997. 107490

GS970208314224.004. Geotechnical Data for Station 60+00 to Station 65+00, South Ramp of the ESF. Submittal date: 02/12/1997. 107492

GS970808314224.009. Provisional Results: Geotechnical Data for Station 65+00 to Station 70+00, South Ramp of the ESF; Full-Periphery Geotechnical Maps (Drawings 0A-46-269 through 0A-46-274) and Rock Mass Quality Ratings Report. Submittal date: 08/18/1997. 107494

GS970808314224.011. Provisional Results: Geotechnical Data for Station 70+00 to Station 75+00, South Ramp of the ESF. Submittal date: 08/25/1997. 107495

GS970808314224.013. Provisional Results: Geotechnical Data for Station 75+00 to Station 78+77, South Ramp of the ESF. Submittal date: 08/25/1997. 107497

LB000300123142.001. Thermal-Hydrological Simulations of the Drift Scale Test. AMR N0000, Thermal Tests Thermal Hydrological Analysis/Model Report. Submittal date: 03/24/2000. 148120

LB0205REVUZPRP.001. Fracture Properties for UZ Model Layers Developed from Field Data. Submittal date: 05/14/2002. 159525

LB0208AIRKDSTH.001. Air Permeability Data for the Heating Phase of the DST. Submittal date: 08/09/2002. 160897

LB0208UZDSCPMI.002. Drift-Scale Calibrated Property Sets: Mean Infiltration Data Summary. Submittal date: 08/26/2002. 161243

LB0210THRMLPRP.001. Thermal Properties of UZ Model Layers: Data Summary. Submittal date: 10/25/2002. 160799

LB03023DKMGRID.001. UZ 3-D Site Scale Model Grids. Submittal date: 02/26/2003. 162354

LB0303THERMSIM.001. UZ Thermal Modeling: Simulations. Submittal date: 03/28/2003. 165167

LB0310AIRK0015.001. Developed Data for Air-K Tests. Submittal date: 10/08/2003. 168564

LB0402THRMLPRP.001. Thermal Properties of UZ Model Layers: Data Summary. Submittal date: 02/20/2004. 168481

LB970600123142.001. Ambient Characterization of the ESF Drift Scale Test Area by Field Air Permeability Measurements. Submittal date: 06/13/1997. 105589

LB980120123142.004. Air Injections in Boreholes 57 through 61, 74 through 78, 185 and 186 in the Drift Scale Test Area. Submittal date: 01/20/1998. 105590

LB980120123142.005. Hydrological Characterization by Air Injections Tests in Boreholes in Heated Drift in DST. Submittal date: 01/20/1998. 114134

LB990501233129.004. 3-D UZ Model Calibration Grids for AMR U0000, "Development of Numerical Grids of UZ Flow and Transport Modeling." Submittal date: 09/24/1999. 111475

LB991131233129.004. Modeling of Thermo-Hydrological Data to Simulate Flow, Transport, and Geothermal Conditions of the UZ Model. AMR U0050, "UZ Flow Models and Submodels." Submittal date: 03/11/2000. 162183

LL000114004242.090. TSPA-SR Mean Calculations. Submittal date: 01/28/2000. 142884

MO0002ABBLSLDS.000. As-Built Borehole Locations and Sensor Locations for the Drift Scale Test Given in Local (DST) Coordinates. Submittal date: 02/01/2000. 147304

MO0004RIB00035.001. Rock Thermal Expansion. Submittal date: 04/07/2000. 153848

MO0208RESTRDST.002. Restructured Drift Scale Test (DST) Heating Phase Power and Temperature Data. Submittal date: 08/06/2002.	161129
MO0306MWDASLCV.001. ANSYS-LA-Coarse Ventilation. Submittal date: 07/01/2003.	165695
MO0306MWDDPPDR.000. Drift Profile Prediction and Degraded Rock Mass Characteristics. Submittal date: 06/18/2003.	164736
MO0307MWDAC8MV.000. Analytical-La-Coarse-800M Ventilation. Submittal date: 07/15/2003.	165395
MO9901MWDGFM31.000. Geologic Framework Model. Submittal date: 01/06/1999.	103769
MO9912SEPDOIHP.000. Determination of Outer/Inner Heater Power Ratio Using Heater Power Data. Submittal date: 12/16/1999.	129272
SN0207F3912298.037. Summary of Smoothed Measurements of Displacement Data for the Heating Phase of the Drift Scale Test (with Results from 12/3/1997 through 1/14/2002). Submittal date: 07/15/2002.	162046
SNL01B05059301.006. Laboratory Thermal Expansion Data for Boreholes UE25 NRG-4, NRG-5; USW NRG-6 and NRG-7/7A. Submittal date: 02/07/1996.	129168
SNL02030193001.001. Mechanical Properties Data for Drillhole USW NRG-6 Samples from Depth 22.2 ft. to 328.7 ft. Submittal date: 05/17/1993.	120572
SNL02030193001.002. Mechanical Properties Data for Drillhole USW NRG-6 Samples from Depth 22.2 ft. to 427.0 ft. Submittal date: 06/25/1993.	120575
SNL02030193001.003. Mechanical Properties Data for Drillhole UE-25 NRG-2 Samples from Depth 150.5 ft. to 200.0 ft. Submittal date: 07/07/1993.	120578
SNL02030193001.004. Mechanical Properties Data for Drillhole USW NRG-6 Samples from Depth 462.3 ft. to 1085.0 ft. Submittal date: 08/05/1993.	108415
SNL02030193001.005. Mechanical Properties Data for Drillhole UE-25 NRG#3 Samples from Depth 15.4 ft. to 297.1 ft. Submittal date: 09/23/1993.	122545
SNL02030193001.006. Mechanical Properties Data for Drill Hole UE-25 NRG#2A Samples from Depth 90.0 ft. to 254.5 ft. Submittal date: 10/13/1993.	120579
SNL02030193001.007. Mechanical Properties Data for Drill Hole UE-25 NRG#3 Samples from Depth 263.3 ft. to 265.7 ft. Submittal date: 10/20/1993.	120582
SNL02030193001.008. Mechanical Properties Data for Drill Hole USW NRG-6 Sample 416.0 ft. Submittal date: 10/20/1993.	120597

SNL02030193001.012. Mechanical Properties Data for Drillhole UE25 NRG-5 Samples from Depth 847.2 ft. to 896.5 ft. Submittal date: 12/02/1993. 108416

SNL02030193001.013. Mechanical Properties Data for Drillhole UE25 NRG-2B Samples from Depth 2.7 ft. to 87.6 ft. Submittal date: 12/02/1993. 120614

SNL02030193001.014. Mechanical Properties Data for Drillhole UE25 NRG-4 Samples from Depth 378.1 ft. to 695.8 ft. Submittal date: 01/31/1994. 109609

SNL02030193001.015. Mechanical Properties Data for Drillhole UE25 NRG-4 Samples from Depth 527.0 ft. Submittal date: 02/16/1994. 120617

SNL02030193001.016. Mechanical Properties Data for Drillhole USW NRG-7/7A Samples from Depth 18.0 ft. to 472.9 ft. Submittal date: 03/16/1994. 120619

SNL02030193001.018. Mechanical Properties Data for Drillhole USW NRG-7/7A Samples from Depth 344.4 ft. Submittal date: 04/11/1994. 109611

SNL02030193001.019. Mechanical Properties Data for Drillhole USW NRG-7/7A Samples from Depth 507.4 ft. to 881.0 ft. Submittal date: 06/29/1994. 108431

SNL02030193001.020. Mechanical Properties Data for Drillhole USW NRG-7/7A Samples from Depth 554.7 ft. to 1450.1 ft. Submittal date: 07/25/1994. 108432

SNL02030193001.021. Mechanical Properties Data (Ultrasonic Velocities, Static Elastic Properties, Triaxial Strength, Dry Bulk Density & Porosity) for Drillhole USW NRG-7/7A Samples from Depth 345.0 ft. to 1408.6 ft. Submittal date: 02/16/1995. 108433

SNL02030193001.022. Mechanical Properties Data for Drill Hole USW NRG-6 Samples from Depth 5.7 ft. to 1092.3 ft. Submittal date: 02/27/1995. 109613

SNL02030193001.023. Mechanical Properties Data (Ultrasonic Velocities, Static Elastic Properties, Unconfined Strength, Triaxial Strength, Dry Bulk Density & Porosity) for Drillhole USW SD-12 Samples from Depth 16.1 ft. to 1300.3 ft. Submittal date: 08/02/1995. 108435

SNL02030193001.024. Elevated Temperature Confined Compression Tests (Ultrasonic Velocities, Static Elastic Properties, Unconfined Strength, Triaxial Strength, Dry Bulk Density & Porosity) for Drillhole USW SD-9 Samples from Depth 52.6 ft. to 2222.9 ft. Submittal date: 09/05/1995. 122530

SNL02030193001.026. Mechanical Properties Data (Ultrasonic Velocities, Elastic Moduli and Fracture Strength) for Borehole USW SD-9. Submittal date: 02/22/1996. 108436

SNL02030193001.027. Summary of Bulk Property Measurements Including Saturated Bulk Density for NRG-2, NRG-2A, NRG-2B, NRG-3, NRG-4, NRG-5, NRG-6, NRG-7/7A, SD-9, and SD12. Submittal date: 08/14/1996. 108410

9.4 OUTPUT DATA, LISTED BY DATA TRACKING NUMBER

LB0306DRSCLTHM.001. Drift Scale THM Model Predictions: Simulations. Submittal Date: 6/26/2003.

LB0306DRSCLTHM.002. Drift Scale THM Model Predictions: Summary Plots. Submittal Date: 6/26/2003.

LB0308DRSCLTHM.001. Drift Scale THM Model Predictions For Poor Quality Rock In Tptpll: Simulations. Submittal Date: 8/29/2003.

LB0308DRSCLTHM.002. Drift Scale THM Model Predictions For Poor Quality Rock In Tptpll: Summary Plots. Submittal Date: 8/29/2003.

LB0306DSTTHMVL.001. DST And Niche THM Model Validation: Simulations. Submittal Date: 6/26/2003.

LB0306DSTTHMVL.002. DST And Niche THM Model Validation: Summary Plots Values. Submittal Date: 6/26/2003.

LB0308DSTTHMVL.001. ECRB Sidewall THM Model Validation: Simulations. Submittal Date: 8/29/2003.

LB0403DRSCLTHM.001. Drift Scale THM Model Predictions: Simulations. Submittal Date: 3/31/04

LB0403DRSCLTHM.002. Drift Scale THM Model Predictions: Summary plots. Submittal Date: 3/31/04.

9.5 SOFTWARE CODES

LBNL 1999. *Software Code: EXT*. V1.0. Sun Ultra Sparc, Sun OS 5.5.1. 10047-1.0-00. 147562

LBNL 2000. *Software Routine: 2KGRIDV1.F*. V1.0. SUN Ultra Sparc, SUN OS 5.5.1. 10244-1.0-00. 147553

LBNL 2002. *Software Code: FLAC3D*. V2.0. PC, Windows 98. STN: 10502-2.0-00. 154783

LBNL 2002. *Software Code: Tin*. V1.1. PC, Windows 98. 10899-1.1-00. 162038

LBNL 2002. *Software Routine: Delb.dat*. V1.0. PC, Windows 98. STN: 10507-1.0-00. 154791

LBNL 2002. *Software Routine: Gpzones.dat.* V1.0. PC, Windows 98. STN: 10509-1.0-00. 154792

LBNL 2003. *Software Code: TOUGH2.* V1.6. PC/MS-DOS Windows 98, Sun UltraSparc/Sun OS 5.5.1, DEC-Alpha OSF1 V4.0. 10007-1.6-01. 161491

INTENTIONALLY LEFT BLANK

APPENDIX A

CALIBRATION OF α AND b_{MAX}

CALIBRATION OF α AND B_{MAX}

The calibration of α and b_{max} in Section 6.4.4 was conducted using Microsoft Excel 97 SR-2 spreadsheets. Two spreadsheets were constructed: (1) a spreadsheet to determine combinations of α and b_{max} satisfying F_{kr} = 0.125 (red line in Figure 6.4.4-2), and (2) a spreadsheet to determine combinations of α and b_{max} satisfying F_{ke} = 9 (blue line in Figure 6.4.4-2).

A.1. SPREADSHEET FOR DETERMINING COMBINATIONS OF α AND B_{MAX} SATISFYING $F_{KR} = 0.125$ (RED LINE IN FIGURE 6.4.4-2)

A spreadsheet was developed in Microsoft Excel 97 SR-2 to calculate F_{kr} for fixed inputs of initial stresses, initial permeability, and fracture frequency, and for variable inputs of α and b_{max}. The spreadsheet has been submitted to TDMS Output DTN: LB0306DSTTHMVL.002 filename: dst_fkr.xls. It performs calculations in the following steps:

1) Calculate initial fracture aperture (b_i) from initial permeability (k_i) and fracture frequency (f) according to Equation 6.4-4:

$$b_i = \sqrt[3]{6 \times k_i / f} \qquad \text{(Eq. A-1)}$$

2) Calculate the residual fracture apertures (b_{1r}, b_{2r}, and b_{3r}) for fractures belonging to set 1, 2, and 3, respectively, according to:

$$b_{1r} = b_i + b_{\max}\left[-\exp\left(\alpha\sigma_{xi}\right)\right] \qquad \text{(Eq. A-2)}$$

$$b_{2r} = b_i + b_{\max}\left[-\exp\left(\alpha\sigma_{yi}\right)\right] \qquad \text{(Eq. A-3)}$$

$$b_{3r} = b_i + b_{\max}\left[-\exp\left(\alpha\sigma_{zi}\right)\right] \qquad \text{(Eq. A-4)}$$

where σ_{ix}, σ_{iy}, and σ_{iz} are initial stresses, in x, y and z direction. Equations A-2 to A-4 are derived from Equation 6.2-9, assuming that the current stress is infinitely high and, hence fractures are compressed to their residual stage.

3) Calculate initial-to-residual permeability correction factors, F_{kxr}, F_{kyr} and F_{kzr} for x, y and z permeability, respectively, according to:

$$F_{kxr} = \frac{b_{2r}^3 + b_{3r}^3}{2b_i^3},\ F_{kyr} = \frac{b_{1r}^3 + b_{3r}^3}{2b_i^3}, F_{kzr} = \frac{b_{1r}^3 + b_{2r}^3}{2b_i^3} \qquad \text{(Eq. A-5)}$$

4) Calculate the geometric mean of the permeability changes as:

$$F_{kr} = \sqrt[3]{F_{kxr} \times F_{kyr} \times F_{kzr}} \qquad \text{(Eq. A-6)}$$

Fixed inputs are: σ_{xi} = -3.46e6 Pa, σ_{yi} = -2.89e6 Pa, σ_{zi} = -5.77e6 Pa, k_i = 1e-13 m^2, and f = 4.32 m^{-1}. Initial stress at DST is according to Figure 7.3-1b, based on Assumption 2 in Section 5. Permeability is the geometric mean of permeability measurements conducted around the DST area (SHT and DST). The geometric of 1e-13 m^2 calculated from LB970600123142.001 [DIRS 105589], LB980120123142.004 [DIRS 105590], and LB980120123142.005 [DIRS 114134], is documented and presented in *Analysis of Hydrologic Properties Data* (BSC 2004 [DIRS 170038], Figure 6-2, SHT+DST). Frequency is extracted from Table 4.1-3a for the Tptpmn unit (as discussed in Sections 6.4.4 and 6.10.4, it is appropriate to use the values k_i = 1e-13 m^2 representing the local permeability at the DST rather than the value of 3.3e-13 m^2 given in Table 4.1-3a).

Variable inputs are α (in Pa^{-1}) and b_{max} (in m).

Final output is F_{kr}, which should be matched to be close to 0.125.

A hard copy of the spreadsheet is provided below. In this case, b_{max} was varied between 1.0e-4 and 2.5e-4 m. For each b_{max}, the α value that gave the closest match of F_{kr} to 0.125 was determined by trial and error. This was conducted by entering different values in the α column until the best possible match of F_{kr} to 0.125 was obtained. The best match was determined for one decimal point of the α value.

Input	Input	Input	Input	Input	Varied	Calibrated
Sig_xi	Sig_yi	Sig_zi	k_i	freq	bmax	alpha
-3.46E+06	-2.89E+06	-5.77E+06	1.00E-13	4.32	1.000E-04	3.40E-07
-3.46E+06	-2.89E+06	-5.77E+06	1.00E-13	4.32	1.500E-04	4.50E-07
-3.46E+06	-2.89E+06	-5.77E+06	1.00E-13	4.32	2.000E-04	5.20E-07
-3.46E+06	-2.89E+06	-5.77E+06	1.00E-13	4.32	2.500E-04	5.80E-07
-3.46E+06	-2.89E+06	-5.77E+06	1.00E-13	4.32	3.000E-04	6.30E-07
-3.46E+06	-2.89E+06	-5.77E+06	1.00E-13	4.32	3.500E-04	6.70E-07
-3.46E+06	-2.89E+06	-5.77E+06	1.00E-13	4.32	4.000E-04	7.10E-07

For visibility, the spreadsheet in filename: dst_fkr.xls is spit into two tables on this page.

Calculated	Calculated	Calculated	Calculated	Calculated	Calculated	Calculated	Matched
b_i	b_r1	b_r2	b_r3	F_krx	F_kry	F_krz	F_ke
5.18E-05	2.09E-05	1.44E-05	3.77E-05	0.203953	0.226403	0.043741	0.1264
5.18E-05	2.02E-05	1.09E-05	4.06E-05	0.245749	0.270601	0.034248	0.1316
5.18E-05	1.87E-05	7.29E-06	4.18E-05	0.264955	0.287107	0.024937	0.1238
5.18E-05	1.82E-05	5.02E-06	4.30E-05	0.286405	0.307592	0.022095	0.1249
5.18E-05	1.79E-05	3.21E-06	4.39E-05	0.30413	0.324547	0.020656	0.1268
5.18E-05	1.73E-05	1.30E-06	4.45E-05	0.316321	0.335048	0.018743	0.1257
5.18E-05	1.75E-05	3.91E-07	4.51E-05	0.331039	0.350322	0.019284	0.1308

The values of b_{max} and α in the above table are plotted as the red line in Figure 6.4.4-2. Note that the units for b_{max} and α are m and Pa^{-1}, in the above table; whereas the units are respectively µm and MPa^{-1} in Figure 6.4.4-2.

The above spreadsheet has been submitted to TDMS Output DTN: LB0306DSTTHMVL.002 filename: dst_fkr.xls.

A.2. COMBINATIONS OF α AND B_{MAX} SATISFYING F_{KE} = 9 (BLUE LINE IN FIGURE 6.4.4-2)

A spreadsheet was developed in MS Excel 97 SR-2 to calculate F_{ke} for fixed inputs of pre-excavation (initial) stresses, post-excavation stresses, initial permeability, and fracture frequency, and for variable inputs of α and b_{max}. The spreadsheet has been submitted to TDMS Output DTN: LB0306DSTTHMVL.002, filename: niche_fke.xls. The spreadsheet performs calculations in the following steps:

1) Calculates initial fracture aperture (b_i) from initial permeability (k_i) and fracture frequency (f) according to Equation A-1.

2) Calculates postexcavation fracture apertures (b_{1e}, b_{2e}, and b_{3e}) for fractures belonging to set 1, 2, and 3, respectively, according to:

$$b_{1e} = b_i + b_{\max}\left[\exp(\alpha\sigma_{xe}) - \exp(\alpha\sigma_{xi})\right] \quad \text{(Eq. A-7)}$$

$$b_{2e} = b_i + b_{\max}\left[\exp(\alpha\sigma_{ye}) - \exp(\alpha\sigma_{yi})\right] \quad \text{(Eq. A-8)}$$

$$b_{3e} = b_i + b_{\max}\left[\exp(\alpha\sigma_{ze}) - \exp(\alpha\sigma_{zi})\right] \quad \text{(Eq. A-9)}$$

where σ_{ix}, σ_{iy}, and σ_{iz} are pre-excavation (initial) stresses and σ_{xe}, σ_{ye}, and σ_{ze} are postexcavation stresses, in x, y and z direction, respectively. Equations A-7 to A-8 are derived from Equation 6.2-9 assuming that the current stress is the stress after excavation.

3) Calculates pre to postexcavation correction factors, F_{kxe}, F_{kye} and F_{kze} for x, y and z permeability, respectively according to:

$$F_{kxe} = \frac{b_{2e}^3 + b_{3e}^3}{2b_i^3},\ F_{kye} = \frac{b_{1e}^3 + b_{3e}^3}{2b_i^3}, F_{kze} = \frac{b_{1e}^3 + b_{2e}^3}{2b_i^3} \quad \text{(Eq. A-10)}$$

4) Calculates the geometric mean of the permeability changes as:

$$F_{ke} = \sqrt[3]{F_{kxe} \times F_{kye} \times F_{kze}} \quad \text{(Eq. A-11)}$$

Fixed inputs are: σ_{xi} = -3.19e6 Pa, σ_{yi} = -2.65e6 Pa, σ_{zi} = -5.31e6 Pa, σ_{xe} = -4.05e6 Pa, σ_{ye} = -1.88e6 Pa, σ_{ze} = -7.50e5 Pa, k_i = 1e-13 m^2, and f = 4.32 m^{-1}. Stress values are given in Rutqvist (2004 [DIRS 170509], p. 125), and were calculated using Assumption 2, Section 5. The initial stress is calculated for a niche located at a depth of 250 m. The air-permeability measurements were conducted at about 0.65 m above the niche, which is 3.25 m high. The initial stresses can then be calculated as σ_{zi} = -(250 - 3.25 - 0.65)×2200×9.81 = -5.31e6 Pa, σ_{yi} = 0.5×(-5.31e6) = -2.65e6 Pa, and σ_{xi} = 0.6×(-5.31e6) = -3.19e6 Pa (negative stress values indicates compressive stress). Initial permeability is 1e-13 m^2 to be consistent with the initial permeability assumed for calibration against F_{kr} above, and fracture frequency is extracted from Table 4.1-3a for the Tptpmn unit.

Variable inputs are α (in Pa^{-1}) and b_{max} (in m).

Final output is F_{ke}, which should be matched to be close to 9.0.

A hard copy of the spreadsheet is provided below. In this case, b_{max} was varied between 1.978e-4 and 2.5e-4 m. For each b_{max}, the α value that gave the closest match of F_{ke} to 9.0 was determined by trial and error. This was conducted by entering different values in the α column until the best possible match of F_{ke} to 9.0 was obtained. The best match was determined for one decimal point of the α value.

Input	Input	Input	Input	Input	Input	Input	Input
Sig_xi	Sig_yi	Sig_zi	Sig_xe	Sig_ye	Sig_ze	k_i	freq
-3.19E+06	-2.65E+06	-5.31E+06	-4.05E+06	-1.88E+06	-7.50E+05	1.00E-13	4.32
-3.19E+06	-2.66E+06	-5.31E+06	-4.05E+06	-1.88E+06	-7.50E+05	1.00E-13	4.32
-3.19E+06	-2.66E+06	-5.31E+06	-4.05E+06	-1.88E+06	-7.50E+05	1.00E-13	4.32
-3.19E+06	-2.66E+06	-5.31E+06	-4.05E+06	-1.88E+06	-7.50E+05	1.00E-13	4.32
-3.19E+06	-2.66E+06	-5.31E+06	-4.05E+06	-1.88E+06	-7.50E+05	1.00E-13	4.32
-3.19E+06	-2.66E+06	-5.31E+06	-4.05E+06	-1.88E+06	-7.50E+05	1.00E-13	4.32
-3.19E+06	-2.66E+06	-5.31E+06	-4.05E+06	-1.88E+06	-7.50E+05	1.00E-13	4.32
-3.19E+06	-2.66E+06	-5.31E+06	-4.05E+06	-1.88E+06	-7.50E+05	1.00E-13	4.32
-3.19E+06	-2.66E+06	-5.31E+06	-4.05E+06	-1.88E+06	-7.50E+05	1.00E-13	4.32
-3.19E+06	-2.66E+06	-5.31E+06	-4.05E+06	-1.88E+06	-7.50E+05	1.00E-13	4.32
-3.19E+06	-2.66E+06	-5.31E+06	-4.05E+06	-1.88E+06	-7.50E+05	1.00E-13	4.32
-3.19E+06	-2.66E+06	-5.31E+06	-4.05E+06	-1.88E+06	-7.50E+05	1.00E-13	4.32
-3.19E+06	-2.66E+06	-5.31E+06	-4.05E+06	-1.88E+06	-7.50E+05	1.00E-13	4.32
-3.19E+06	-2.66E+06	-5.31E+06	-4.05E+06	-1.88E+06	-7.50E+05	1.00E-13	4.32

For visibility, the spreadsheet file niche_fke.xls is split into two tables on this page.

Varied	Calibrated	Calculated	Calculated	Calculated	Calculated	Calculated	Calculated	Calculated	Matched
bmax	alpha	b_i	b_e1	b_e2	b_e3	F_kex	F_key	F_kez	F_ke
2.500E-04	9.20E-07	5.179E-05	4.45E-05	7.43E-05	1.75E-04	20.87	19.71	1.79	9.04
2.200E-04	7.30E-07	5.179E-05	4.18E-05	7.60E-05	1.74E-04	20.70	19.38	1.84	9.04
2.100E-04	6.50E-07	5.179E-05	4.05E-05	7.64E-05	1.74E-04	20.60	19.24	1.84	9.01
2.050E-04	6.00E-07	5.179E-05	3.96E-05	7.66E-05	1.74E-04	20.59	19.20	1.84	8.99
2.040E-04	5.80E-07	5.179E-05	3.92E-05	7.67E-05	1.74E-04	20.74	19.33	1.84	9.04
2.000E-04	5.20E-07	5.179E-05	3.81E-05	7.69E-05	1.75E-04	20.78	19.35	1.83	9.03
1.978E-04	4.60E-07	5.179E-05	3.69E-05	7.69E-05	1.75E-04	20.82	19.37	1.82	9.02
1.978E-04	4.60E-07	5.179E-05	3.69E-05	7.69E-05	1.75E-04	20.82	19.37	1.82	9.02
1.980E-04	4.20E-07	5.179E-05	3.61E-05	7.69E-05	1.75E-04	20.93	19.46	1.81	9.03
2.000E-04	3.70E-07	5.179E-05	3.50E-05	7.68E-05	1.75E-04	21.02	19.54	1.79	9.02
2.040E-04	3.30E-07	5.179E-05	3.42E-05	7.67E-05	1.76E-04	21.15	19.67	1.77	9.02
2.100E-04	2.90E-07	5.179E-05	3.34E-05	7.64E-05	1.76E-04	21.14	19.66	1.74	8.98
2.200E-04	2.50E-07	5.179E-05	3.26E-05	7.61E-05	1.76E-04	21.16	19.70	1.71	8.94
2.500E-04	1.90E-07	5.179E-05	3.12E-05	7.59E-05	1.77E-04	21.68	20.22	1.68	9.03

The values of b_{max} and α in the above table are plotted as the blue line in Figure 6.4.4-2. Note that the units for b_{max} and α are *m* and Pa^{-1}, in the above table; whereas the units are respectively μm and MPa^{-1} in Figure 6.4.4-2.

The above spreadsheet has been submitted to TDMS Output DTN: LB0306DSTTHMVL.002, filename: niche_fke.xls.

APPENDIX B

STATISTICAL ANALYSIS OF DISPLACEMENT DATA

STATISTICAL ANALYSIS OF DISPLACEMENT DATA

A statistical evaluation of the predicted MPBX displacements was conducted using an MS Excel 97 SR-2 spreadsheet. The spreadsheet has been submitted to TDMS Output DTN: LB0306DSTTHMVL.002, filename: u0250_displacement_comparison_statistics.xls. First, the calculated and measured values of displacement were extracted from the x-y plots shown in Figure 7.4.2-2. The values were extracted in TECPLOT V8.0 using the data/probe command for x values of 6, 12, 18, 24, 30, 36, 42, and 48 months. The extracted displacements (in mm) for each anchor were entered into the spreadsheet as shown below. The yellow column shows simulated data for upper vertical (UV), lower vertical (LV), or 60° inclined (INC) extensometers (Figure 7.4.2-1). Blue columns show measured data extracted from Figure 7.4.2-2, with empty cells indicating missing or bad data. Labels 1, 2, 3, and 4 in the table heads indicate Anchors 1, 2, 3, or 4. The numbers in the table below are considered as input to this statistical analysis. Values of displacement in column 2 to 14 are in mm.

	147-1	148-1	149-1	150-1	154-1	155-1	156-1	157-1	178-1	179-1	180-1	SIM UV-1	SIM LV-1	SIM INC-1
	INC-1	INC-1	UV-1	LV-1	INC-1	INC-1	UV-1	LV-1	INC-1	INC-1	UV-1	SIM UV-1	SIM LV-1	SIM INC-1
0														
6	1.98	1.5		2.76		2.53	2.38	2.08	0.51	1.3	1.47	1.03	2.01	0.92
12	2.57	1.8		2.08	2.95	3.12	2.88					1.47	2.9	1.37
18	3.42	2.45		2.83	4.37	3.84						1.93	3.78	1.73
24	4.12	2.9		3.33	6.06	4.45						2.26	4.45	2.03
30	4.41	3.25		3.26	7.48	4.85						2.48	4.82	2.32
36	4.57	3.4		3.66	5.89	5.02						2.61	5.33	2.36
42	4.73	3.54		3.72	5.85	5.09						2.76	5.61	2.52
48	4.84	3.65		3.96	6.02	5.32						2.78	5.62	2.52

	147-2	148-2	149-2	150-2	154-2	155-2	156-2	157-2	178-2	179-2	180-2	SIM UV-2	SIM LV-2	SIM INC-2
	INC-2	INC-2	UV-2	LV-2	INC-2	INC-2	UV-2	LV-2	INC-2	INC-2	UV-2	SIM UV-2	SIM LV-2	SIM INC-2
0														
6	2.51	1.52		2.75	2.02	3.04	2.73			2.32	1.45	1.2	2.33	1.43
12	3.25	1.8	2.68	3.95		3.55	3.32	3.3	2.62			1.92	3.51	2.08
18		2.33		4.4		4.54		4.02	3.16			2.52	4.58	2.66
24	5.14	2.87		5.11		5.2	5.89	4.9	3.57		2.41	3.05	5.38	3.18
30	5.67	3.4		5.75		5.64	7.32	5.6	3.9		2.78	3.46	5.82	3.62
36	5.96	3.74		6.21		5.85	8.12	6.02	4.04		3.02	3.73	6.56	3.86
42	6.1	3.98		6.42		5.73	8.57	6.27	3.54		2.45	4.01	6.9	4.15
48	6.25	4.16		6.75		6.09	8.97	6.6	4.07		3.06	4.09	6.94	4.23

	147-3	148-3	149-3	150-3	154-3	155-3	156-3	157-3	178-3	179-3	180-3	SIM UV-3	SIM LV-3	SIM INC-3
	INC-3	INC-3	UV-3	LV-3	INC-3	INC-3	UV-3	LV-3	INC-3	INC-3	UV-3	SIM UV-3	SIM LV-3	SIM INC-3
0														
6	2.61	2.63	2.99	3.06	3.25	3.13	2.28			2.09	2.34	1.62	2.45	1.77
12	3.56	3.43	4.12	4.95	2.43	3.96	3.08		3.63	2.64		2.82	4.06	2.95
18		4.31	5.05			4.97			4.42			3.68	5.48	3.81
24	5.41	4.98	5.81		3.7	5.81	4.21		5.14			4.36	6.51	4.49
30	6.02	5.46	6.49		4.22	6.33	4.45		5.77			4.92	7.09	5.09
36	6.51	5.81	6.9		4.53	6.73	4.68		6.15			5.3	7.96	5.51
42	6.72	6.14	7.2		4.8		4.91		6.68			5.8	8.36	6.02
48	7.01	6.51	7.49		5.03		5.19		6.96			6.05	8.43	6.25

	147-4	148-4	149-4	150-4	154-4	155-4	156-4	157-4	178-4	179-4	180-4	SIM UV-4	SIM LV-4	SIM INC-4
	INC-4	INC-4	UV-4	LV-4	INC-4	INC-4	UV-4	LV-4	INC-4	INC-4	UV-4	SIM UV-4	SIM LV-4	SIM INC-4
0														
6	2.54	1.9	1.89	2.15		2.22	2.4		2.3	1.97	1.43	0.3	1.36	0.85
12	4.07	3.32	3.45	4.05	3.38	3.08	3.29	3.2	3.49	3.42		1.58	3.01	2.36
18	5.63		4.72	5.08	5.37	4.03		4.28	4.68			2.7	4.63	3.69
24	7.07		5.97	6.27	7.12	4.82	6.6	5.24	6.03		4.97	3.95	6.17	5.04
30	8.32		7.06	7.64	8.64	5.44	8.35	6.16	7.29		6.01	5.6	7.36	6.13
36	8.49		7.88	8.54	9.58	5.98	9.3	6.54	8.21		6.66	6.14	8.74	7.3
42	7.06		8.42	8.95	10.21	5.96	10.1	6.81	9.35		7.41	7.09	9.61	8.2
48	7		8.96	9.37	10.76	6.5	10.82	7.28	8.72		7.98	7.79	10.23	8.97

As described in Section 7.4.2, the three statistical measures considered include: root-mean-square-difference (RMSD), mean-difference (MD), and normalized-absolute mean difference (NAMD). The equations for calculating RMSD, MD, and NAMD are given in Section 7.4.2. The statistical evaluation was made for all anchor categories 1, 2, 3 and 4 separately, as well as for all anchors combined at 6, 12, 18, 24, 30, 36, 42, and 48 months. As an example, the calculations of RMSD, MD, and NAMD at 12 months are given below (simulated and measured values are in mm):

SIM-1-12m	MEA-1-12m	sim-mea	(sim-mea)^2	abs((sim-mea)/mea)
1.47	2.88	-1.410	1.988	0.490
2.9	2.08	0.820	0.672	0.394
1.37	2.57	-1.200	1.440	0.467
1.37	1.8	-0.430	0.185	0.239
1.37	2.95	-1.580	2.496	0.536
1.37	3.12	-1.750	3.063	0.561
		MD	RMSD	NAMD
		-0.925	1.281	0.448
SIM-2-12m	MEA-2-12m	sim-mea	(sim-mea)^2	abs((sim-mea)/mea)
1.92	3.32	-1.400	1.960	0.422
3.51	3.3	0.210	0.044	0.064
3.51	3.95	-0.440	0.194	0.111
2.08	3.25	-1.170	1.369	0.360
2.08	1.8	0.280	0.078	0.156
2.08	3.55	-1.470	2.161	0.414
2.08	2.62	-0.540	0.292	0.206
		MD	RMSD	NAMD
		-0.522	0.933	0.247
SIM-3-12m	MEA-3-12m	sim-mea	(sim-mea)^2	abs((sim-mea)/mea)
2.82	4.12	-1.300	1.690	0.316
2.82	3.08	-0.260	0.068	0.084
4.06	4.95	-0.890	0.792	0.180
2.95	3.56	-0.610	0.372	0.171
2.95	3.43	-0.480	0.230	0.140
2.95	2.43	0.520	0.270	0.214
2.95	3.96	-1.010	1.020	0.255
2.95	3.63	-0.680	0.462	0.187
2.95	2.64	0.310	0.096	0.117
		MD	RMSD	NAMD
		-0.325	0.745	0.185
SIM-4-12m	MEA-4-12m	sim-mea	(sim-mea)^2	abs((sim-mea)/mea)
1.58	3.45	-1.870	3.497	0.542
1.58	3.29	-1.710	2.924	0.520
3.01	4.05	-1.040	1.082	0.257
3.01	3.2	-0.190	0.036	0.059
2.36	4.07	-1.710	2.924	0.420
2.36	3.32	-0.960	0.922	0.289
2.36	3.38	-1.020	1.040	0.302
2.36	3.08	-0.720	0.518	0.234
2.36	3.49	-1.130	1.277	0.324
2.36	3.42	-1.060	1.124	0.310
		MD	RMSD	NAMD
		-1.100	1.056	0.274
		MD-all	RMSD-all	NAMD-all
		-0.809	1.065	0.292

The values for MD-all, RMSD-all, and NAMD-all on the previous page are the outputs for 12 months from this statistical analysis. The complete output from this analysis is listed below:

Time (months)	MD-all	RMSD-all	NAMD-all
6	-0.937	1.086	0.436
12	-0.809	1.065	0.292
18	-0.868	1.307	0.261
24	-0.946	1.597	0.251
30	-0.982	1.812	0.238
36	-0.611	1.928	0.252
42	-0.487	1.830	0.257
48	-0.494	1.898	0.236

Numbers in the table on this page define the curves in Figure 7.4.2-3. As shown in Figure 7.4.2-3, the units for MD-all, RMSD-all, and NAMD-all are mm, mm, and fraction (unitless), respectively.

The entire spreadsheet for this calculation has been submitted to TDMS Output DTN: LB0306DSTTHMVL.002, filename: u0250_displacement_comparison_statistics.xls.

INTENTIONALLY LEFT BLANK

APPENDIX C

CALCULATED PERMEABILITY CHANGE RATIO AT NICHE TESTS

CALCULATED PERMEABILITY CHANGE RATIO AT NICHE TESTS

In Section 7.5 of this model report, the calibrated stress permeability function is tested against air-permeability measurements conducted at several niches over a range of initial permeability values. The UM calculated log permeability change ratio in Figures 7.5.1 and 7.5.2 was calculated using an MS Excel 97 SR-2 spreadsheet similar to the ones developed in APPENDIX A. The spreadsheet for this calculation has been submitted to TDMS Output DTN: LB0306DSTTHMVL.002, filename: u0250_niche_validation.xls.

Inputs for this analysis are preexcavation (initial) stresses, postexcavation stresses, initial permeability, fracture frequency, and the parameters α and b_{max}. The spreadsheet performs the calculations in the following steps:

1) Calculates initial fracture aperture (b_i) from initial permeability (k_i) and fracture frequency (f) according to Equation A-1.

2) Calculates postexcavation fracture apertures (b_{1e}, b_{2e}, and b_{3e}) for fractures belonging to set 1, 2, and 3, respectively, according to Equation A-7, A-8, and A-9, respectively.

3) Calculates pre to postexcavation correction factors F_{ke1}, F_{ke2}, and F_{ke1} for individual fractures belonging to fracture set 1, 2, and 3, respectively, according to:

$$F_{ke1} = \left(\frac{b_{1e}}{b_i} \right)^3 , \; F_{ke2} = \left(\frac{b_{2e}}{b_i} \right)^3 , F_{ke3} = \left(\frac{b_{e3}}{b_i} \right)^3 \qquad \text{(Eq. C-1)}$$

4) Calculates pre to postexcavation correction factors F_{kxe}, F_{kye} and F_{kze} for x, y and z permeability, respectively, according to Equation A-10.

5) Calculates the geometric mean of the permeability changes according to Equation A-11.

Fixed inputs are:

σ_{xi} = -3.19e6 Pa, σ_{yi} = -2.66e6 Pa, and σ_{zi} = -5.31e6 Pa (Rutqvist 2004 [DIRS 170509], p. 125, see also Appendix A)

σ_{xe} = -4.05e6 Pa, σ_{ye} = -1.88e6 Pa, and σ_{ze} = -7.50e5 Pa (Rutqvist 2004 [DIRS 170509], p. 125)

f = 4.32 m^{-1} (extracted from Table 4.1-3a for the Tptpmn unit)

b_{max} = 200e-6 m, α = 0.52e-6 Pa^{-1} (calibrated in Section 6.4.4)

Variable input is the initial permeability, k_i.

A hard copy of the spreadsheet in filename: u0250_niche_validation.xls is provided on the next page.

Input	Input	Input	Input	Input	Input	Input	Input	Input	Varied	Calculated
Sig_xi	Sig_yi	Sig_zi	Sig_xe	Sig_ye	Sig_ze	freq	bmax	alpha	k_i	Log(k_i)
-3.19E+06	-2.65E+06	-5.31E+06	-4.05E+06	-1.88E+06	-7.50E+05	4.32	2.000E-04	5.20E-07	1.00E-08	-8
-3.19E+06	-2.66E+06	-5.31E+06	-4.05E+06	-1.88E+06	-7.50E+05	4.32	2.000E-04	5.20E-07	6.00E-09	-8.221849
-3.19E+06	-2.66E+06	-5.31E+06	-4.05E+06	-1.88E+06	-7.50E+05	4.32	2.000E-04	5.20E-07	2.00E-09	-8.69897
-3.19E+06	-2.66E+06	-5.31E+06	-4.05E+06	-1.88E+06	-7.50E+05	4.32	2.000E-04	5.20E-07	1.00E-09	-9
-3.19E+06	-2.66E+06	-5.31E+06	-4.05E+06	-1.88E+06	-7.50E+05	4.32	2.000E-04	5.20E-07	6.00E-10	-9.221849
-3.19E+06	-2.66E+06	-5.31E+06	-4.05E+06	-1.88E+06	-7.50E+05	4.32	2.000E-04	5.20E-07	2.00E-10	-9.69897
-3.19E+06	-2.66E+06	-5.31E+06	-4.05E+06	-1.88E+06	-7.50E+05	4.32	2.000E-04	5.20E-07	1.00E-10	-10
-3.19E+06	-2.66E+06	-5.31E+06	-4.05E+06	-1.88E+06	-7.50E+05	4.32	2.000E-04	5.20E-07	6.00E-11	-10.22185
-3.19E+06	-2.66E+06	-5.31E+06	-4.05E+06	-1.88E+06	-7.50E+05	4.32	2.000E-04	5.20E-07	2.00E-11	-10.69897
-3.19E+06	-2.66E+06	-5.31E+06	-4.05E+06	-1.88E+06	-7.50E+05	4.32	2.000E-04	5.20E-07	1.00E-11	-11
-3.19E+06	-2.66E+06	-5.31E+06	-4.05E+06	-1.88E+06	-7.50E+05	4.32	2.000E-04	5.20E-07	6.00E-12	-11.22185
-3.19E+06	-2.66E+06	-5.31E+06	-4.05E+06	-1.88E+06	-7.50E+05	4.32	2.000E-04	5.20E-07	2.00E-12	-11.69897
-3.19E+06	-2.66E+06	-5.31E+06	-4.05E+06	-1.88E+06	-7.50E+05	4.32	2.000E-04	5.20E-07	1.00E-12	-12
-3.19E+06	-2.66E+06	-5.31E+06	-4.05E+06	-1.88E+06	-7.50E+05	4.32	2.000E-04	5.20E-07	6.00E-13	-12.22185
-3.19E+06	-2.66E+06	-5.31E+06	-4.05E+06	-1.88E+06	-7.50E+05	4.32	2.000E-04	5.20E-07	2.00E-13	-12.69897
-3.19E+06	-2.66E+06	-5.31E+06	-4.05E+06	-1.88E+06	-7.50E+05	4.32	2.000E-04	5.20E-07	1.00E-13	-13
-3.19E+06	-2.66E+06	-5.31E+06	-4.05E+06	-1.88E+06	-7.50E+05	4.32	2.000E-04	5.20E-07	6.00E-14	-13.22185
-3.19E+06	-2.66E+06	-5.31E+06	-4.05E+06	-1.88E+06	-7.50E+05	4.32	2.000E-04	5.20E-07	2.00E-14	-13.69897
-3.19E+06	-2.66E+06	-5.31E+06	-4.05E+06	-1.88E+06	-7.50E+05	4.32	2.000E-04	5.20E-07	1.00E-14	-14
-3.19E+06	-2.66E+06	-5.31E+06	-4.05E+06	-1.88E+06	-7.50E+05	4.32	2.000E-04	5.20E-07	6.00E-15	-14.22185
-3.19E+06	-2.66E+06	-5.31E+06	-4.05E+06	-1.88E+06	-7.50E+05	4.32	2.000E-04	5.20E-07	2.00E-15	-14.69897
-3.19E+06	-2.66E+06	-5.31E+06	-4.05E+06	-1.88E+06	-7.50E+05	4.32	2.000E-04	5.20E-07	1.00E-15	-15

For visibility, the spreadsheet in filename: u0250_niche_validation.xls is split into two tables on this page; some intermediate calculation columns are not shown.

Calculated	Calculated	Calculated	Calculated	Calculate	Calculated	Calculated
Log(F_k1e)	Log(F_k2e)	Log(F_k3e)	Log(F_kxe)	Log(F_kye)	Log(F_kze)	Log(F_ke)
-0.0075	0.0134	0.0649	0.0399	0.0302	0.0031	0.0244
-0.0089	0.0160	0.0766	0.0474	0.0360	0.0038	0.0290
-0.0128	0.0230	0.1091	0.0682	0.0524	0.0055	0.0420
-0.0161	0.0290	0.1360	0.0858	0.0666	0.0070	0.0531
-0.0191	0.0343	0.1598	0.1015	0.0795	0.0084	0.0631
-0.0277	0.0492	0.2246	0.1457	0.1165	0.0124	0.0915
-0.0350	0.0616	0.2772	0.1826	0.1486	0.0160	0.1157
-0.0416	0.0728	0.3227	0.2155	0.1777	0.0193	0.1375
-0.0604	0.1037	0.4434	0.3059	0.2608	0.0293	0.1987
-0.0766	0.1293	0.5376	0.3798	0.3310	0.0385	0.2498
-0.0914	0.1520	0.6169	0.4439	0.3935	0.0471	0.2948
-0.1339	0.2140	0.8179	0.6134	0.5628	0.0740	0.4167
-0.1711	0.2643	0.9669	0.7444	0.6964	0.0990	0.5133
-0.2055	0.3079	1.0878	0.8535	0.8083	0.1230	0.5949
-0.3078	0.4239	1.3789	1.1235	1.0867	0.1967	0.8023
-0.4013	0.5147	1.5831	1.3177	1.2866	0.2634	0.9559
-0.4916	0.5913	1.7430	1.4716	1.4445	0.3248	1.0803
-0.7868	0.7862	2.1108	1.8299	1.8104	0.4966	1.3790
-1.1030	0.9312	2.3576	2.0725	2.0567	0.6342	1.5878
-1.4730	1.0492	2.5456	2.2582	2.2446	0.7495	1.7508
-4.8940	1.3343	2.9648	2.6738	2.6638	1.0333	2.1236
	1.5351	3.2379	2.9454	2.9369	1.2339	2.3721

Numbers in the orange columns in the two tables on this page define the lines of calculated log change ratio in Figures 7.5-1 and 7.5-2.

The entire spreadsheet for this calculation has been submitted to TDMS Output DTN: LB0306DSTTHMVL.002, filename: u0250_niche_validation.xls.

APPENDIX D

IMPACT OF UPDATED THERMAL PROPERTIES

IMPACT OF UPDATED THERMAL PROPERTIES

Estimates of thermal properties of some nonrepository units were updated during the development of this model report. The simulation results presented in Sections 6.5 to 6.8 are conducted using previous estimates of thermal properties (DTN: LB0210THRMLPRP.001 [DIRS 160799]). To investigate the impact of using previous versus updated estimates of thermal properties, one representative case was chosen for direct comparison of simulation results using updated and previous thermal properties. In this case, the Tptpmn model domain (Section 6.5) was chosen as a representative case. The Tptpmn model domain was chosen because THM-induced changes in hydrological properties were the greatest in that case and, hence any impact from changing thermal properties (and temperature field) would be the greatest. The thermal properties originating from DTN: LB0210THRMLPRP.001 [DIRS 160799] are here denoted as previous properties; whereas the updated properties are taken from DTN: LB0402THRMLPRP.001 [DIRS 168481].

Figures D-1 and D-2 present vertical profiles of calculated temperature and permeability change factors for comparison of simulation results when using both updated and previous thermal properties. Figures D-1b and D-2b present the normalized differences between the two simulation cases, calculated as:

$$ND = \frac{V_{updated} - V_{previous}}{V_{previous}} \qquad \text{(Eq. D-1)}$$

where $V_{updated}$ and $V_{previous}$ are simulated values using updated and previous thermal properties, respectively. Figures D-1b and D-2b show that the difference in calculated values for temperature and vertical permeability factor are within one percent (1%) and five percent (5%), respectively. In the repository unit, changes in vertical permeability are within two percent (2%).

Figure D-3 shows a comparison of the calculated vertical flow distribution around the drift at 10,000 years for simulation results using previous or updated thermal properties. The 10,000-year case was chosen for comparison since Figure D-2b shows that the largest normalized differences in vertical permeability occur at 10,000 years. Figure D-3 shows no observable difference in calculated flow field distribution. This is expected, since changes in temperature and permeability in the repository unit are very small (within two percent) and, hence cannot impact the flow field significantly.

In summary, the differences in the thermal properties in DTN: LB0210THRMLPRP.001 [DIRS 160799] (previous thermal properties) and DTN: LB0402THRMLPRP.001 [DIRS 168481] (update thermal properties) do not have a significant impact on the model results presented in this model report.

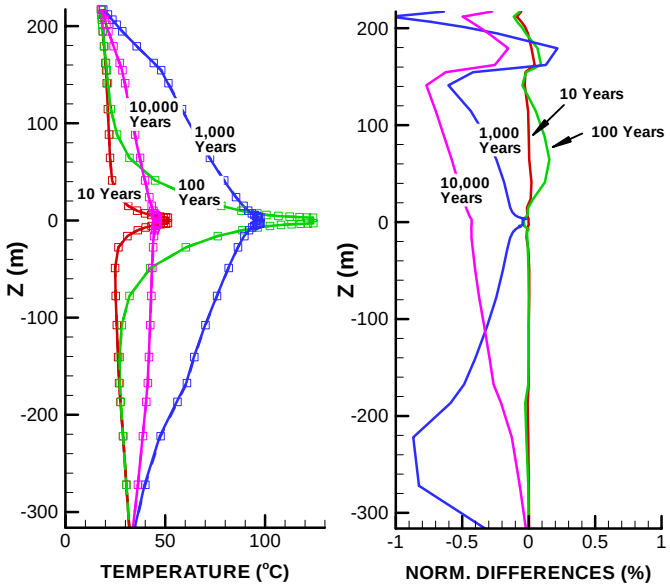

(a) **(b)**

Output DTN: LB0403DRSCLTHM.002.

Figure D-1. Vertical Profiles of: (a) Simulated Temperatures Using Updated (Symbols) and Previous (Lines) Thermal Properties; (b) Normalized Differences Between Simulated Temperature for the Case of Using Updated and Previous Thermal Properties (Tptpmn Model Domain)

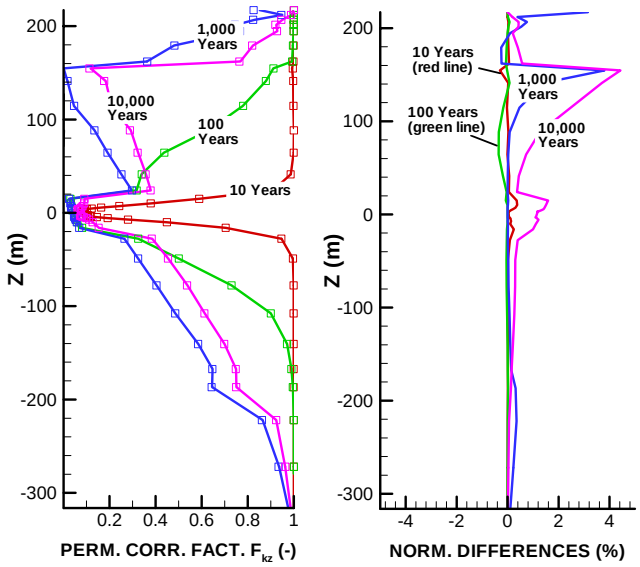

(a) **(b)**

Output DTN: LB0403DRSCLTHM.002.

Figure D-2. Vertical Profiles of: (a) Simulated Vertical Permeability Correction Factor ($F_{kz} = k_z/k_i$) Using Updated (Symbols) and Previous (Lines) Thermal Properties; (b) Normalized Differences Between Simulated Permeability Correction Factor for the Case of Using Updated and Previous Thermal Properties (Tptpmn Model Domain)

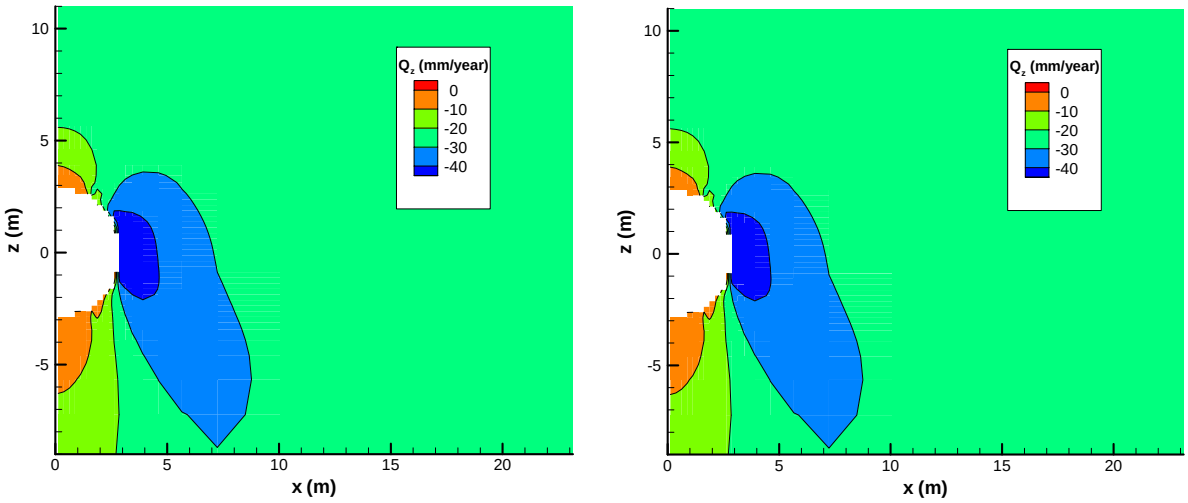

Output DTN: LB0403DRSCLTHM.002.

NOTE: For a Fully Coupled THM Simulation When Using (a) Previous and (b) Updated Estimates of Thermal Properties (Tptpmn Model Domain).

Figure D-3. Comparison of the Distribution of Vertical Percolation Flux (Q_z) in Fractures at 10,000 Years

INTENTIONALLY LEFT BLANK